



UNIVERSITÀ  
DEGLI STUDI  
DI PADOVA

UNIVERSITÀ DEGLI STUDI DI PADOVA  
DIPARTIMENTO DI INGEGNERIA INDUSTRIALE

SCUOLA DI DOTTORATO DI RICERCA IN INGEGNERIA INDUSTRIALE  
INDIRIZZO IN INGEGNERIA Elettrotecnica  
CICLO XXV°

## Vehicle-to-grid (V2G) and grid conditioning systems

**Direttore della Scuola:**

CH.MO PROF. PAOLO COLOMBO .....

**Coordinatore d'indirizzo:**

CH.MO PROF. GIOVANNI MARTINELLI .....

**Supervisore:**

CH.MO PROF. GIUSEPPE BUJA .....

**Dottorando:** NIMA ZABIHI SHEIKHRAJEH

.....

## SOMMARIO

Il termine Vehicle-to-Grid (V2G) si riferisce alla tecnologia che permette uno scambio di potenza bidirezionale tra la rete elettrica e le batterie dei veicoli elettrici di tipo plug-in (PEV). La tecnologia V2G può essere un elemento chiave della rete intelligente, che può utilizzare le batterie dei veicoli come un sistema di accumulo locale. Le batterie dei veicoli possono contribuire alla stabilità della rete e a soddisfare la domanda di energia soprattutto nelle ore di punta. Un PEV ha bisogno di un caricatore bidirezionale per implementare il V2G, e, di conseguenza, gli studi riguardo il loro progetto, la funzionalità e l'efficienza sono del massimo interesse.

Questa tesi descrive lo stato dell'arte di questi caricabatteria e tratta alcuni aspetti di un convertitore bidirezionale e alcuni casi di studio relativi a questo argomento. L'obiettivo principale di questo lavoro è di sviluppare il progetto e gli algoritmi di controllo di un caricabatteria bidirezionale con capacità di caricare la batteria di un veicolo plug-in e contemporaneamente di agire come filtro attivo nei confronti della linea di alimentazione.

Dopo il primo capitolo introduttivo, nel secondo capitolo viene riportata la terminologia usata in questo campo di ricerca. Vengono anche brevemente descritte diverse strategie intelligenti di ricarica, gli approcci per la realizzazione dei caricabatteria dei PEV e gli standard di ricarica. L'analisi dei vari tipi di caricabatteria viene approfondita nel terzo capitolo. Sono considerati il caricabatteria tradizionale (CBC) con front-end costituito da un raddrizzatore a diodi, il caricabatteria dotato di correttore del fattore di potenza (PFC), il caricabatteria bidirezionale (BBC), e il caricabatteria integrale (IBC). Nel capitolo quattro vengono date le definizioni della potenza elettrica in condizioni non sinusoidali assieme ad alcuni esempi delle inadeguatezze della teoria classica della potenza nel descrivere fenomeni non lineari che si verificano durante il funzionamento di un sistema di potenza. Nel quinto capitolo sono presentati i concetti di base della teoria potenza istantanea attiva e reattiva (nota anche come teoria  $pq$ ) applicata alla compensazione di sistemi non sinusoidali. Vengono introdotte le definizioni della potenza reale, immaginaria e di sequenza zero e viene mostrato come questa teoria renda agevole la comprensione dei fenomeni causati da tensioni o correnti non sinusoidali. Essa è particolarmente adatta per il progetto di un caricabatteria quando esso viene visto come un condizionatore di potenza. Il capitolo sei è dedicato ai concetti di base dei filtri attivi di tipo shunt. Essi possono svolgere diversi tipi di funzioni, come la compensazione delle armoniche di corrente generate da carichi non lineari impedendo la loro propagazione nella rete. L'algoritmo di compensazione basato sulle potenze definite nel riferimento  $\alpha\beta$  è molto flessibile e quindi la teoria della potenza istantanea è stata considerata come la base per lo sviluppo del sistema di controllo dei filtri attivi. Alcuni esempi di compensazione descritti nel capitolo precedente sono stati simulati e sono stati riportati i risultati. Nel capitolo sette è considerato il dimensionamento dei dispositivi di potenza che costituiscono il caricabatteria in relazione ai diversi servizi ausiliari che esso può fornire. Sono stati dimensionati in tensione e corrente gli interruttori elettronici di potenza, gli induttori di accoppiamento con la rete e gli altri componenti passivi. Nel capitolo otto viene considerato un caricabatteria che alimenta il proprio carico e contemporaneamente compensa i carichi non lineari connessi nelle vicinanze, costituiti da raddrizzatori. Queste funzionalità aggiuntive in termini di condizionamento della potenza di rete sono state quantificate al fine di determinare la capacità di un caricabatteria costituito da determinati componenti attivi e passivi di supportare la rete svolgendo la funzione di filtro attivo. Nel nono capitolo sono state dimensionate le induttanze di filtro di un caricabatteria per uno specifico caso di studio in cui era richiesta la capacità sia di ricaricare la batteria che di iniettare potenza attiva in rete, sia nel caso di connessione monofase che trifase. La conoscenza dell'ampiezza dell'ondulazione di corrente è un requisito importante per il dimensionamento delle induttanze. Perciò è stato effettuato un calcolo preciso di questa grandezza sia nel caso di un caricabatteria connesso alla rete monofase e operante secondo la tecnica di PWM, sia nel caso di connessione alla rete trifase e adozione della tecnica SVM. Nel capitolo dieci viene considerato un caso di studio riguardo il dimensionamento di un filtro LCL. IL capitolo undici contiene uno studio teorico dei regolatori risonanti. Essi risolvono il problema posto dai convenzionali regolatori PI, che quando sono impiegati per il controllo di grandezze alternate, come accade nel caso delle correnti in un convertitore dc-ac, non sono in grado di annullare l'errore a regime a causa del guadagno finito alla frequenza di funzionamento. Un regolatore risonante presenta invece un guadagno idealmente infinito alla frequenza di funzionamento e quindi garantisce un errore a regime nullo. L'efficacia dei

regolatori risonanti è stata verificata per mezzo di simulazioni. Nel capitolo dodici sono riportate le normative riguardanti i connettori, le modalità di ricarica e la connessione dei caricabatteria dei PEV alla rete elettrica. Esse mirano a definire una procedura di ricarica comune a tutti i PEV e tutte le infrastrutture di ricarica, siano esse pubbliche o private.

## ABSTRACT

The term Vehicle-to-Grid (V2G) refers to the technology that enables a bidirectional power exchange between the electric grid and the batteries of plug-in electric vehicles (PEV). V2G technology can be a key element of the intelligent network, which may use the batteries of the vehicle as a system of local storage. The vehicle battery may contribute to the stability of the grid and to meeting the energy demand, especially in peak hours. A PEV needs a bidirectional charger to implement V2G, and, consequently, the studies regarding their design, functionality and efficiency are of the utmost interest.

This thesis describes the state of art of these chargers and discusses some aspects of a bi-directional converter and some case studies related to this topic. The main objective of this work is to develop the design and the control algorithms of a bidirectional battery charger with capability to charge the battery of a PEV and simultaneously to act as an active filter for the supply line.

After the first introductory chapter, the second chapter reports the terminology used in this field of research. Several smart strategies for charging, approaches for the implementation of the battery chargers for PEVs and the recharging standards are briefly described. The analysis of different types of charger is detailed in chapter three. The conventional battery chargers (CBC) with front-end formed by a diode rectifier, battery chargers with power factor correction (PFC), bi-directional battery chargers (BBC), and integral battery chargers (IBC) are considered. In chapter four, definitions are given of the electrical power in non-sinusoidal conditions, together with some examples of the inadequacies of the classical power theory in describing non-linear phenomena that occur during the operation of a power system. The fifth chapter presents the basic concepts of the theory of instantaneous active and reactive power (also known as p-q theory) applied to the compensation of non-sinusoidal systems. Definition of real, imaginary and zero sequence power are introduced and it is shown how this theory makes it easier to understand the phenomena caused by non-sinusoidal voltages or currents. The theory is particularly suitable for the design of a battery charger when it is seen as a power conditioner. Chapter six is devoted to the basic concepts of shunt active filters. They can perform different types of functions, such as the compensation of current harmonics generated by nonlinear loads to prevent their propagation in the network. The compensation algorithm based on powers defined in reference  $\alpha\beta$  is very flexible and therefore the theory of instantaneous power has been considered as the basis for the development of the control system of active filters. Some examples of compensation described in the previous chapter were simulated and the results have been included. In chapter seven, sizing of the power devices that constitute the battery charger is considered in relation to the various auxiliary services that it can provide. The power electronic switches, the coupling inductors and the other passive components have been sized in voltage and current. In chapter eight it is considered a charger that supplies its load and simultaneously compensates for non-linear loads connected nearby. These additional features in terms of power conditioning were quantified in order to determine the capacity of a battery charger that is formed by given active and passive components to support the network acting as an active filter. In the ninth chapter the filter inductances of a battery charger are sized for a specific case study in which it is required the capability to recharge the battery and to inject active power in the network, both in the case of single-phase and three-phase connection. Evaluation of the ripple current is an important requirement for the design of inductors. Therefore a precise calculation was made of this magnitude both in the case of a battery charger connected to the single phase grid and operating according to the PWM technique, and, in the case of connection to the three-phase grid, operating according to the technique SVM. In chapter ten a case study is considered regarding the design of an LCL filter. Chapter eleven contains a theoretical study of resonant controllers. They solve the problem posed by the conventional PI controllers that, when used for the control of alternate quantities as it occurs for the currents of a DC/AC converter, are not able to cancel the steady state error due to the finite gain at the operating frequency. Instead, a resonant controller has a gain ideally infinite at the operating frequency and thus ensures a zero steady-state error. The effectiveness of the resonant regulators has been verified by means of simulations. Chapter twelve deals with the regulations regarding connectors, charging modes and ways of connecting the PEV chargers to the grid. They are intended to define a charging procedure common to all the PEVs and to all the charging infrastructures, whether public or private.

## **ACKNOWLEDGEMENT**

I would like to express my sincere appreciation to those who made this work possible: Professor, family and friends.

I would like to express my greatest admiration for my parents who constantly motivated and encouraged me to keep working towards this goal. I also thank all my other family members for all the support given during difficult times.

# CONTENTS

<b>Abstract</b> .....	<b>ii</b>
<b>Acknowledgement</b> .....	<b>v</b>
<b>1 Introduction</b> .....	<b>1</b>
<b>2. Vehicle-to-Grid</b> .....	<b>4</b>
2.1. Electric vehicles .....	4
2.1.1. Hybrid electric vehicles .....	5
2.1.2. Fuel cell vehicles .....	5
2.1.3. Vehicle-to-grid capability .....	5
2.2. General electric vehicles configuration .....	5
2.3. Vehicle-to-grid configurations .....	7
2.4. Charger topologies .....	8
2.4.1. Off-board charger .....	8
2.4.2. On-board charger .....	9
2.4.3. Integrated on-board charger .....	9
2.5. Charging Strategies .....	9
2.5.1. Dumb charging .....	10
2.5.2. Dual tariff charging .....	10
2.5.3. Smart charging .....	10
2.5.3.A. Centralized smart charging .....	10
2.5.3.B. Decentralized smart charging .....	10
2.6. Comparing vehicle-to-grid with vehicle-to-home .....	11
<b>3. Battery Charger Topologies</b> .....	<b>13</b>
3.1. Conventional battery chargers .....	14
3.2. Bidirectional battery chargers .....	18
3.2.1. Single-phase topologies .....	18
3.2.2. Three-phase topologies .....	20
3.3. Integral battery chargers .....	21
3.3.1. Single-phase topologies .....	21
3.3.2. Three-phase topologies .....	23
<b>4. Power Definition For Modern Power Systems</b> .....	<b>25</b>
4.1. Voltage and current quantities under non-sinusoidal unbalanced conditions .....	25
4.2. Power definitions .....	27
4.2.1. Apparent power definitions .....	27
4.2.2. Arithmetic apparent power .....	27
4.2.3. Vector apparent power .....	27
4.2.4. Effective apparent power .....	28
4.3. Harmonic pollution and unbalance .....	29
4.4. Fundamental frequency active and reactive power .....	30
4.5. Power factor definitions .....	30

4.6. Examples of the Systems with unbalanced loads .....	31
<b>5. Instantaneous Power Theory .....</b>	<b>36</b>
5.1. The p-q theory .....	38
5.1.1. Basis of the p-q theory .....	38
5.1.2. The clarke transformation .....	38
5.1.3. Three-phase instantaneous active power in terms of $\alpha\beta$ voltage and current components .....	39
5.1.4. Instantaneous p-q powers .....	39
5.2. The p-q theory in three-wire systems .....	40
5.3. The p-q powers in non-sinusoidal cases .....	44
5.3.1. The zero-sequence power in a three-phase system .....	44
5.3.2. Presence of negative-sequence components .....	45
5.3.3. General case including distortions and imbalances in the voltages and in the currents .....	46
<b>6. Compensation .....</b>	<b>50</b>
6.1. Harmonic and reactive power compensation .....	50
6.2. Shunt active filter for harmonic and reactive compensation .....	52
6.3. Unbalanced load .....	53
6.3.1. Using phase-locked-loop in positive-sequence voltage detector .....	55
6.4. MATLAB Simulation results .....	56
<b>7. Design of a Bidirectional Battery Charger .....</b>	<b>63</b>
7.1. DC-link .....	64
7.2. Switch design .....	65
7.2.1. General relationships concerning transistor and diode currents in a switch .....	66
7.2.2. Single phase inverter example .....	68
7.3. Calculation of average and RMS value of the inverter input current .....	73
7.3.1. Switching mode on space vector modulation .....	73
7.3.2. Inverter input current .....	74
7.3.2.1. Average value of the inverter input current .....	75
7.3.2.2. RMS value of the inverter input current .....	76
<b>8. Compensation Capability of a Bidirectional Battery Charger .....</b>	<b>77</b>
8.1. Bidirectional Charger Infrastructure .....	77
8.2. PWM Rectifier/inverter .....	78
8.3. Shunt Active Filter .....	80
8.4. BBC with Active Filtering Function .....	83
8.5. Power capability calculating by Instantaneous reactive power theory .....	85
8.5.1. Stationary reference $\alpha\beta$ –frame .....	85
8.5.2. Synchronous reference $dq$ –frame .....	87
<b>9. L-Filter Design .....</b>	<b>90</b>
9.1. Analysis of ripple current .....	90

9.1.1.	Single phase full-bridge inverter .....	90
9.1.2.	Three phase inverter .....	92
9.1.2.1.	Ripple current due to vector $V_1$ in each switching period ( $\Delta i_{pp1}$ ) .....	95
9.1.2.2.	Ripple current due to vector $V_2$ in each switching period ( $\Delta i_{pp2}$ ) .....	95
9.2.	L minimum value to interface active filter and grid for harmonic compensation ..	97
9.3.	L maximum value to interface active filter and grid for harmonic compensation ..	97
9.4.	Harmonics distortion standards .....	98
9.4.1.	IEEE 519 standards .....	98
9.4.2.	EN 61000-3-2 Standard .....	100
<b>10.</b>	<b>LCL-Filter Design .....</b>	<b>103</b>
10.1.	Design Principles .....	104
10.1.1.	Selection of total inductance ( $L = L_1 + L_2$ ) .....	104
10.1.2.	Selection of inductors $L_1, L_2$ , and capacitor $C_f$ .....	105
10.1.2.1.	Switching harmonic current attenuation .....	106
10.1.2.2.	Fundamental reactive power absorbed by $C_f$ .....	106
10.2.	Control System Considerations .....	107
10.2.1.	Harmonic attenuation of the LCL-filter and choice of the resonance frequency value .....	107
<b>11.</b>	<b>Resonant Controller .....</b>	<b>112</b>
11.1.	Resonant controller .....	113
11.2.	Improved Control Method by Using Proportional Resonant controller .....	118
<b>12.</b>	<b>EV Standards .....</b>	<b>122</b>
12.1.	Charging Infrastructure Standards .....	122
12.1.1.	AC charge levels (defined by SAE J1772) .....	123
12.1.1.1.	AC level 1 .....	123
12.1.1.2.	AC level 2 .....	124
12.1.1.3.	AC level 3 .....	124
12.1.2.	DC fast charging .....	124
12.1.3.	IEC 60309 standard .....	125
12.1.4.	IEC 62196 standard .....	125
12.1.5.	IEC/EN 61851-1 standard; recharging modes .....	125
12.1.5.1.	Mode 1 .....	125
12.1.5.2.	Mode 2 .....	126
12.1.5.3.	Mode 3 .....	126
12.1.5.4.	Mode 4 .....	126
12.1.5.5.	Control pilot .....	126
12.2.	Connectors and Plugs .....	127
12.2.1.	Type 1 (SAE J1772) .....	127
12.2.2.	Type 2 (Mennekes connector) .....	128
12.2.3.	Type 3 (EV Plug Alliance) .....	129
12.2.3.1.	Type 3A .....	130
12.2.3.2.	Type 3C .....	130
12.2.4.	Type 4 (CHAdeMO) .....	131
12.2.4.1.	Interlock of connector .....	132
12.2.4.2.	Protection from electrical shock .....	132
12.2.4.3.	Fail-safe of charging control .....	132



# I. INTRODUCTION

As the number of plug-in electric vehicles (PEV) entering into the market increases, the load of the grid becomes more and more sizeable due to the need of charging the PEV batteries. Electric vehicles (EV) could potentially provide valued services to the power grid when not being driven, reducing ownership costs. Hence, Vehicle-to-Grid (V2G) operation can be a key feature of the smart grid; utilizing vehicle batteries as a local storage becomes meaningful in this frame. Vehicle batteries can help the grid stability and demand especially at peak hours. A bidirectional PEV needs a bidirectional charger to fulfill V2G operation, and accordingly investigations around their design, functionality and efficiency is of at most interest. It is just recently that this topic becomes interesting for both industry and university. This thesis deals with these state of the art chargers in academic level and discusses some aspects of a bidirectional converter and some case studies related to this topic. The main objective of this project is to control and design a bidirectional charger with the aim of charging a plug-in vehicle battery including active power line conditioning capabilities.

In a modern power system, due to broader applications of nonlinear loads such as power electronic equipment, the degree of waveform distorted is increasingly serious now. These loads may cause poor power factors and result a high degree of harmonics. Such cases have brought the power quality as an increasing concern. Moreover, from economical viewpoints, a utility's revenue may get affected at a higher cost. Therefore, efficient solutions for solving these pollution problems have become highly critical for both utilities and customers. Therefore in this thesis, the control of a voltage source converter (VSC) is in focus regarding the power quality problems that could appear at the connection point. The aims have been set to maintain a proper operation of the V2G, in case of network disturbances, and to react in a corrective way during different operating conditions. For this purpose, instantaneous power theory to control the system is implemented and two different line filters as an interface between converter and grid are analyzed and designed; namely an inductance filter (L-filter) and an inductance-capacitance-inductance filter (LCL-filter). LCL-filter becomes more and more attractive as utility interface for grid-connected VSC. Compared to L-filter, LCL-filter can render better switching harmonics attenuation using lower inductance, which makes it suitable for higher power applications. However, LCL-filter design is complex and needs to consider many constraints, such as current ripple through inductors, total impedance of the filter, switching harmonic attenuation, resonance phenomenon and reactive power absorbed by filter capacitors, etc. The forthcoming paragraphs are intended to describe the content of each chapter of the thesis.

In second chapter, before going into the details of power electronics required for the V2G application, the common architectures of PEVs, charging strategies as well as chargers topologies are described to get accustomed with the terminologies. Several smart charging strategies, different approaches for the implementation of chargers in EVs and charging standards are briefly introduced.

In third chapter the various types of battery chargers are reviewed. At first the conventional battery chargers (CBCs) with front-end diode rectifiers are reviewed and then it goes through the power factor corrected (PFC), the bidirectional battery chargers (BBCs) and the integral battery chargers (IBCs). In details, the chapter is organized as follows. Section I describes the CBCs and then dwells on the PFC topologies. Section II illustrates the BBCs; it is divided into two subsections, the first subsection being dedicated to the single-phase topologies and the second one to the three-phase topologies. They are able not only to absorb power but also to reverse the power flow and therefore are termed as BBC. Section III illustrates the IBCs; like Section II, it is divided into two subsections dedicated to the single-phase and three-phase topologies, respectively. In IBCs some or all the power devices of the traction inverter are utilized to set up the battery charger when there is the need of recharging the PEV battery and this can be done since the operating modes “recharge” and “traction” never occur simultaneously. Depending on the reconfiguration, It can be either unidirectional or bidirectional.

In chapter four power definitions under non-sinusoidal conditions are described together with some examples of the inadequacies found in the classical power theory to describe the power phenomena of non-linear power system operation. The electrical engineer requires practical power definitions to analyze a power system. The IEEE published guidelines for the practical definition of electrical quantities and power definitions in non-sinusoidal power systems. These definitions were compiled by an IEEE Working Group on non-sinusoidal situations.

In chapter five the basic concept of the instantaneous power theory (or p-q theory) is presented. The p-q Theory is based on a set of instantaneous powers defined in time domain. It is about compensation of non-sinusoidal systems based on the instantaneous active and reactive power theory. The definitions of real, imaginary and zero-sequence powers are introduced. The physical meanings of each of these powers are explained and some basic compensation examples are shown considering different active power conditioners. It is shown that this theory can be very practical for understanding problems due to non-sinusoidal voltages or currents. It is especially interesting for the design of battery charger as a power conditioner. Some important points that shown in this chapter are: the powers defined in the time domain form are consistent basis for efficient algorithms to be applied in the control of active power conditioners; the undesirable powers to be compensated can be conveniently selected; the instantaneous imaginary power is calculated without time delay (instantaneously) and the compensation algorithm using the a  $\alpha\beta$  transformation can compensate for three phase loads to provide constant instantaneous active power to the source, even if the supply voltages are unbalanced and/or contain harmonics.

Chapter six is dedicated to the basic concept of shunt active filters with different functions. It can compensate current harmonics related to the nearby nonlinear load and hindering its penetration into the system. In fact the battery charger can be considered as an active filter and this chapter is included particularly for designing controllers for active filters for power conditioning. The compensation algorithm based on the powers defined in the  $\alpha\beta$ -reference frame is very flexible, so instantaneous power theory is considered as a base of active filter control system. Some basic compensation examples that mentioned in previous chapter are simulated and the results are shown. For instance it is shown by simulation results that not only the fundamental reactive power but also the harmonic currents caused by the instantaneous imaginary power can be eliminated.

Chapter seven is included sizing of the devices of the BBCs in relation to the different ancillary services that can be executed; this means to find out voltage and current ratings of the semiconductor switches, of the grid-coupling inductor and of the other passive components. This issue has been relied on the DC/AC converter topology. Unfortunately there is no simple analytical relationship between the inverter output current and the current in the diode and IGBT. In fact, the current distribution between diode and IGBT is a function of both power factor ( $\cos \varphi$ ) and modulation index. The average current through the diode and IGBT was approximated by help of some equations that had been derived by computer-aided analysis. Careful study were shown that the average and RMS values calculated for a particular inverter current remained relatively constant when the product of the power factor and the modulation index was held constant for different combinations of PF and M. on the other hand, in the converter circuit, the parameters of the energy storage elements such as

inductors (L) and capacitors (C) are pretty important factor, which affect directly the work of the converter. The DC-link capacitor  $C_{dc}$  provides an intermediate energy storage, which decouples the three phase VSC from the half bridge DC/DC converter. However in this stage the design of the DC/DC converter is outside the scope of this thesis.

In chapter eight a BBC is considered that supplying its own load and in the same time compensating neighborhoods nonlinear loads that is considered a rectifier. These additional capabilities in terms of power grid conditioning have been verified in order to increase the usage of a charger infrastructure. This means for a given system with certain passive component, capabilities to support above mentioned ancillary services are computed. Power capability of BBC is calculated when it has an active filtering function. This is done by computing the BBC current as a function of load power, load power factor and active power which can be delivered by the BBC. This capability should be calculated correctly otherwise a converter will not be able to deliver demanded power to the load or to proper compensation of nonlinear load.

In chapter nine design of the filtering components (L-filter) of a BBC for a specific case of study with the capability of both charging the battery and injecting active power into the grid from both a single-phase and a three-phase utility, are considered. The line filter reduces the high frequency harmonic content of the battery charger line current, caused by the switched operation of the three-phase VSC. Hence, sinusoidal line currents can be obtained. It is included the first order low-pass filter (L-filter) that is the conventional method to interface these converters to the grid. Correct information of maximum switching current ripple is an important parameter for the design of the inductor. Therefore, precise calculation is carried out for both, single-phase grid connected inverter with PWM switching technique and three-phase grid connected inverter with SVM switching technique. The design should satisfy the harmonic current limitations based on standards like IEC (or IEEE 519) and the specification on nearly zero phase displacement of the current with respect to the grid voltage.

Usually, the line filter consists of filter inductors, i.e. L-filter, but by the use of additional capacitors and inductors, other filter combinations such as LC- or LCL-filters can be applied. In chapter ten LCL-filter is considered as a case study. A method for LCL-filter design, which makes the task very convenient, is verified. At first, the total inductance should be determined according to current ripple requirement. With filter capacitor insertion, total inductance is split into two parts. A set of equations is obtained to represent the relationship between the impedances at switching frequency with consideration of switching harmonic attenuation and reactive power constrains. So the overall design can be easily done by solving the equations. Moreover, some considerations about the design of LCL-filters are discussed in this chapter.

Chapter eleven is included the study of the resonant regulators from a theoretical point of view. The resonant regulators are very powerful algorithms since they are able to eliminate the error in the closed-loop control system of alternating currents without the need of executing time-variant transformations of the control signals. When the reference current is a direct signal, as in the DC motor drive, zero steady-state error can be secured by using a conventional proportional-integral (PI) controller. When the reference current is a sinusoidal signal, as in the control of AC currents in an AC/DC converter, however, straightforward use of the conventional PI controller would lead to steady-state error due to finite gain at the operating frequency. A resonant controller guarantees zero steady-state error in a balanced system. The effectiveness of the resonant controller is shown by simulation results.

Chapter twelve is included standards for plugs, charging modes and grid connections of the EV battery chargers. They covers the physical and electrical for conductive and coupling charging and are aimed at defining a common EV charging architecture for the vehicle inlets and for the in-house and public charging infrastructure.

## II. VEHICLE-TO-GRID

The basic concept of vehicle-to-grid (V2G) is that electric vehicles (EV) provide power to the grid while parked. The EV can be a battery-powered electric vehicle (BEV), a fuel cell vehicle (FCV), or a hybrid electric vehicle (HEV). Fuel cell EVs (FCV) generate power from liquid or gaseous hydrogen. BEVs can be charged from the grid during low demand times and discharge when power is needed. HEVs are equipped with batteries; if of a certain capacity, provision is made for the batteries to be charged from the grid (plug-in HEVs, PHEVs). Most FCVs do not have batteries on board; if equipped with them, again provision is made for the batteries to be charged by the grid (plug-in FCVs, PFCVs). BEVs, PHEVs and PFCVs will be hereafter termed PEVs. All of them can function in either mode as BEVs.

Vehicles, in general, are parked over 90 percent of the time [1]. The idea behind V2G operation involves connecting PEVs to the grid while idle, and tapping into their on-board battery packs as sources of stored energy to provide a number of grid services. PHEVs have larger battery packs than HEVs, and unlike BEVs, they have a gasoline tank thus retaining energy capabilities that can still be used to drive the vehicle. V2G is defined as the provision of energy and ancillary services, such as regulation, from an EV to the grid. This can be accomplished by discharging energy through bidirectional power flow. Through V2G, EV owners can produce revenue while their cars are parked which can provide valuable economic incentives for EV ownership. Utilities can also benefit significantly from V2G by having increased system flexibility as well as energy storage for intermittent renewable energy sources such as wind [2]. Many researchers have investigated the various potential benefits and implementation issues of V2G [1]-[10] concept. Kempton and Tomic studied the fundamentals of using EVs/PHEVs for load leveling, regulation, reserve, and other purposes [4], [5].

In this chapter, before going into the details of power electronics required for the V2G application, the common architectures of PEVs, charging strategies as well as chargers topologies are described to get accustomed with the terminologies. Several smart charging strategies, different approaches for the implementation of chargers in EVs and charging standards are briefly introduced.

### 2.1. Electric Vehicles

A typical battery-powered electric vehicle (BEV) has a battery pack connected to an electric motor and provides traction power through the use of a mechanical transmission. The batteries are charged primarily by a battery charger that receives its power from an external source such as the electrical utility. Also during regenerative braking, the motor acts as a generator which provides power back to the batteries and the process slows down the vehicle. The primary advantage of a BEV is that the design is simple and has a low part count. The primary disadvantage is that the driving range of the vehicle is limited to the size of the battery and the time to recharge the battery can range from 8 hours to 15 minutes depending on the battery type, battery charging method and how far the vehicle was driven [1], [3].

### 2.1.1. Hybrid Electric Vehicles

A typical hybrid electric vehicle (HEV) includes a battery pack, motor controller, motor/generator, internal combustion engine, transmission and driveline components. The batteries are charged through an on-board internal combustion engine and a generator. In a plug-in hybrid electric vehicle (PHEV), the batteries can also be charged through a battery charger that receives power from the utility. Some PHEV design will allow the vehicle to operate a certain time on electric power and reduces the amount of time that the engine runs. When the vehicle is not operating, the battery can be charged through a battery charger that is “plugged in” to the electrical utility or other energy sources. A PHEV normally has a larger battery pack than a HEV. The advantage of a PHEV over a HEV is that due to external battery charging, the vehicle can run longer on electric power which in-turn reduces engine fuel consumption.

### 2.1.2. Fuel Cell Vehicles

Most of the prototypal FCVs that are currently under development utilize an on-board tank to store pressurized hydrogen. Hydrogen and conditioned air are fed to a proton exchange membrane (PEM) stack to develop DC power. The traction configuration is the same as a BEV in which an electric motor provides the mechanical power for traction. Some prototypal FCVs are equipped with on-board batteries that allow the energy to be recovered during regenerative braking and provide peak power to the traction motor during vehicle acceleration. The batteries can be kept charged by FC but a plug-in charge from the grid can be arranged (PFCVs). A plug-in fuel cell vehicle (PFCV) has a battery pack and a fuel cell that is connected to an electric motor that provides traction power to the wheels through a transmission. The batteries can be charged by the use of a battery charger that receives its power from the utility but can also be charged by using the fuel cell.

### 2.1.3. Vehicle-to-Grid capability

A PEV can also be designed to provide power for standby power applications, such as back-up power to a home, through its V2G capability. For BEVs, the amount of energy (watt-hours) that can be provided is limited to the size of the on-board energy storage device. For PHEVs and PFCVs, it is limited to not only the battery pack size, but also the amount of fuel that is on-board. The unique aspect of power flow in V2G vehicles is that it is bi-directional, meaning that the vehicle should be able to take power (during charging) and provide power (during discharge) from/to the grid. V2G capability is a promising technology for increasing the amount of distributed generation that can be used during peak hours. On-going demonstrations are being conducted by utilities and customers to evaluate this new technology.

## 2.2. General Electric Vehicles Configuration

According to the Electric Power Research Institute (EPRI), more than 40% of U.S. generating capacity operates overnight at a reduced load, and it is during these off-peak hours that most PHEVs could be recharged. Recent studies show that if PHEVs replace one-half of all vehicles on the road by 2050, only an 8% increase in electricity generation will be required [6].

Most of PEVs utilize on-board battery chargers to recharge the batteries using utility power. The simplest architecture of a PEV is shown in Fig. 2.1. This architecture consists of a battery system and a motor drive that provides power to the motor in a controlled form, which in turn applies the power to the wheels for traction.

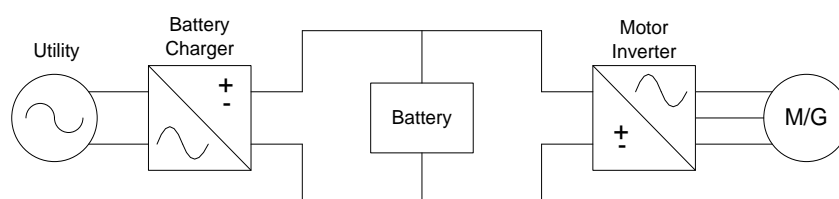


Figure 2.1. Typical PEV architecture

Many of today's EVs use a permanent magnet electric motor that can also act as a generator to recharge the batteries when the brakes are applied. During regenerative braking, the motor acts as a generator that provides power back to the batteries. Friction brakes are used when the vehicle must be stopped quickly or if the batteries are at full charge.

The primary power electronics include a DC-AC converter motor which provides three-phase power to a permanent magnet motor. An example from Toyota Prius HEV configuration is given in Fig. 2.2. In this configuration they use two permanent magnet motors/generator, one of 10kW and the other of 50kW. The battery is connected to a booster and DC-AC converter before feeding to the motor/generators. The power electronics are bidirectional and used for both charging the battery and powering the motors. The motor/generators and gasoline engine feed into a planetary gear set. The system operates in a continuously variable transmission (CVT) mode where the gear ratio is determined by the power transfer between the battery, motor/generators and gasoline engine [7]. The batteries can also be charged using regenerative braking of the motor/generators. In this configuration there is no provision to charge the batteries externally.

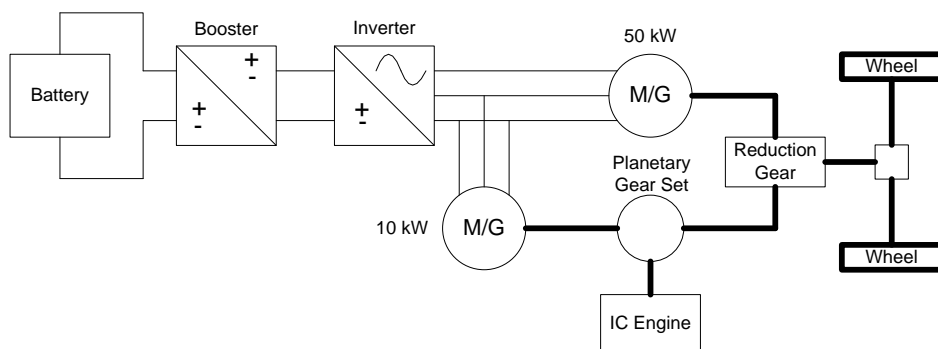


Figure 2.2. Toyota Prius HEV configuration

For PEVs batteries are charged when the vehicles are not being driven. This is normally accomplished through a utility connected AC-DC converter to obtain DC power from the grid. Energy flow is unidirectional as power is taken from the utility to charge the battery pack. A Toyota Prius configuration with PHEV conversion is shown in Fig. 2.3.

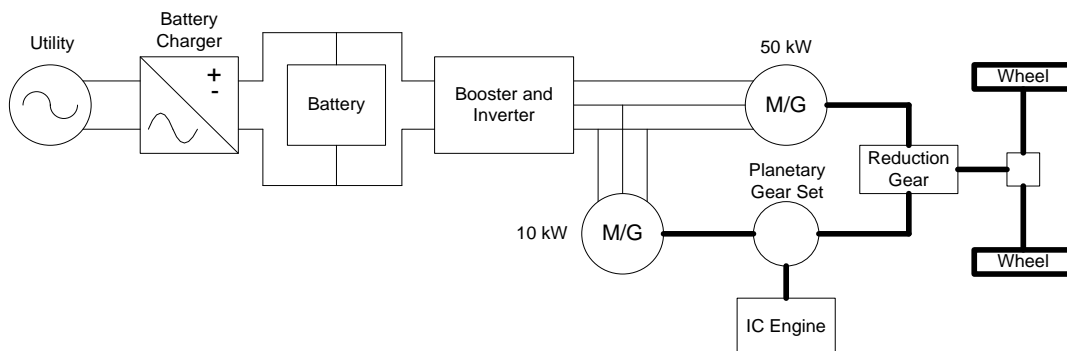


Figure 2.3. Toyota Prius PHEV configuration

The battery voltage for most converted PHEVs are maintained at the same level as the original design (typically 200-500 V) and battery modules are added in parallel to increase the energy capacity of the battery pack, thus allowing the electric motor to run more often than the original HEV design [7].

A FCV configuration with on-board a battery pack is shown in Fig. 2.4. The DC output from the FC stack is fed into a DC-DC converter to a DC power bus. The batteries connected to the DC bus are used to allow the fuel cell stack to operate at more constant operating conditions. Connected to the DC bus there is also the motor supply. The configuration of the traction section is the same as the one of a BEV.

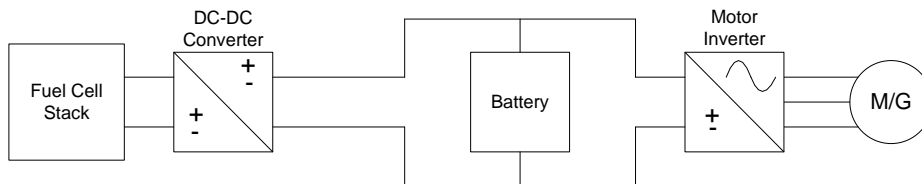


Figure 2.4. FCV configuration

In the PFCV configuration, the batteries are primarily charged using an on-board utility-connected battery charger. This configuration typically uses a larger battery pack than a FCV to give the vehicle a longer driving range under electric power. The configuration shown in Fig. 2.5 uses a PEM fuel cell stack that produces DC power which is then boosted to a higher voltage using a DC-DC converter. An on-board battery charger is connected to the utility to allow the batteries to be recharged when the vehicle is parked.

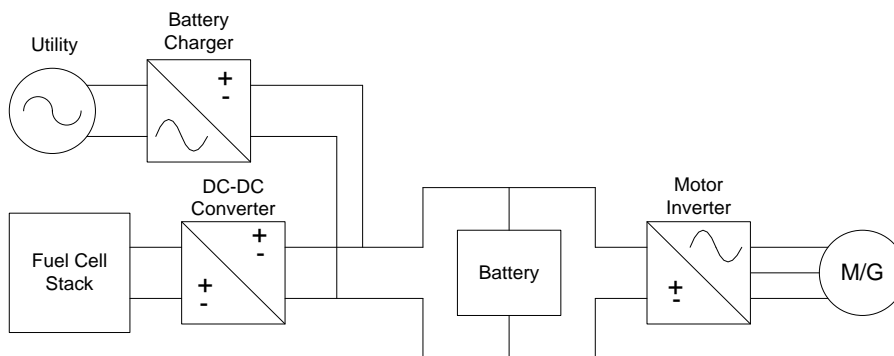


Figure 2.5. Plug-in Fuel cell vehicle configuration (PFCV)

### 2.3. Vehicle-to-Grid Configurations

Today’s PEV can only charge its batteries using AC power typically provided by utility grid. PEV’s can also be designed so that power can be sent back to the grid. A vehicle with this type of technology is defined as being V2G capable (Fig. 2.6). All of the topologies, as discussed in the previous section, utilize a battery pack to store DC energy that must be converted to AC power to be exchanged with the utility for V2G applications. The unique aspect of power electronics for V2G vehicles is that it must be bi-directional, that is capable of both taking power (during charging) and providing power (during discharge) from/to the grid.

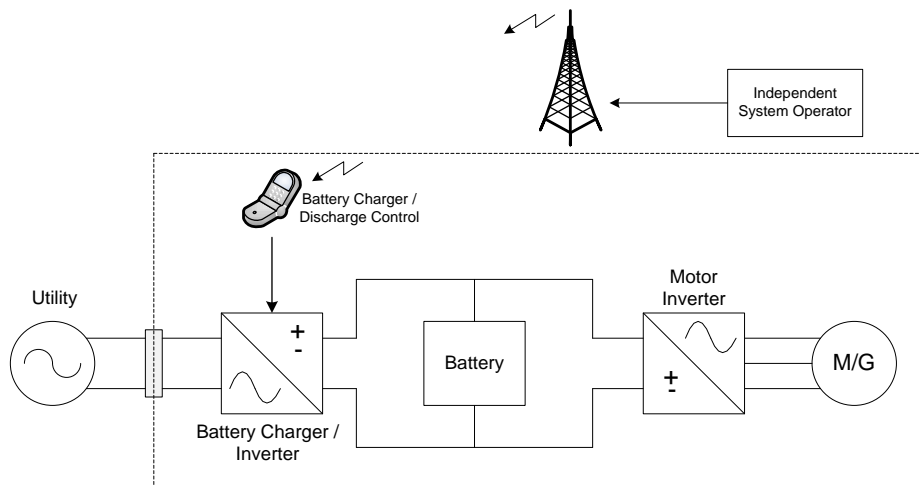


Figure 2.6. PEV with V2G capability

The V2G vehicles for distributed energy applications can provide voltage and frequency regulation, spinning reserves, and electrical demand side management. If used in large numbers, V2G vehicles have the potential to absorb excess electricity produced by renewable sources, such as wind power, when the grid is operated at low load conditions. Studies show that V2G vehicles could be a significant enabling factor for increased penetration of wind energy. Controls can be developed that would allow an operator to dispatch these renewable resources through the use of the battery of the vehicles when they are needed by the utility. A set of fleet vehicles that are parked at a company's facility could potentially be used to provide electricity during periods of high demand to offset the facility's electrical demand charges. A wireless configuration for independent system operator (ISO) to control charge and discharge of a V2G battery is shown in Fig. 2.6.

Each V2G capable vehicle must have three required elements: a power connection to the grid for electrical energy flow, control or logical connection necessary for communication with grid operators, and on-board or off-board (in the infrastructure) precision metering. The configuration depicted in Fig. 2.6 shows that the power electronics being controlled use a wireless cell connection to communicate with the V2G capable vehicles. While these vehicles could provide peak power demand-response resource, their economic values do not generally justify the expense. These services are needed for just a few hours each year, thus the potential revenue from providing these services is limited. It is suggested by some researchers that the most promising markets for V2G are for those services that the electric industry refers to as ancillary services such as voltage and frequency regulation [8].

State-of-charge regulation, battery life, power capacity, energy capacity, and available power connection will be critical factors in the design of these vehicles. The number of battery discharges, charges and state-of-charge control directly effects battery life. Typical V2G vehicles utilize either a Nickel Metal Hydride or Lithium-Ion battery pack.

A promising V2G architecture for supplying battery energy to the grid is the integrated motor inverter shown in Fig. 2.7. This architecture utilizes for the connection to the grid the same power electronics used for the motor supply, thus eliminating the need for a separate battery charger. To this end, the power electronics is reconfigured according to the operation carried out. Generally the charger topologies are categorized in three sections as follow and this architecture is considered as a third topology.

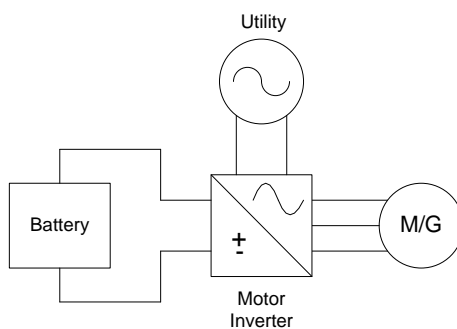


Figure 2.7. integrated PEV architecture for V2G

## 2.4. Charger Topologies

### 2.4.1. Off-board charger

In Fig. 2.8a an off-board charger topology is shown. In this case the charger is an external unit, rather than a component of the EV. Furthermore an off-board charger produces a high DC voltage. The internal Battery Management System (BMS) must be able to charge the battery using this voltage. The major drawback of this topology is that the charger is not integrated in the EV. Hence, it is impossible to charge the battery of an EV without an appropriate charger which provides the needed high DC voltage on-site.



### 2.4.2. On-board charger

Figure 2.8b shows an on-board charger topology. In this case the charger is a component of the EV. The EV can be charged almost everywhere using a single-phase and three-phase supply, respectively. The major drawback of this topology is that this simple on-board charger requires an additional DC/AC converter. One converter enables the V2G capability and the second converter drives the AC propulsion machine.

### 2.4.3. Integrated on-board charger

Finally, in Fig. 2.8c an integrated on-board charger topology is shown. All EVs have to be equipped with a bidirectional on-board charger. A bidirectional charger consists of a combined AC/DC rectifier and DC/AC inverter. This type of charger enables vehicle-to-grid (V2G) capability. Hence, EVs can be used as a distributed energy storage capacity. However, EVs already contain inverters to drive their propulsion machines. Therefore the most efficient approach of implementing a charger in an EV is to integrate the charger in the existing AC propulsion machine inverter.

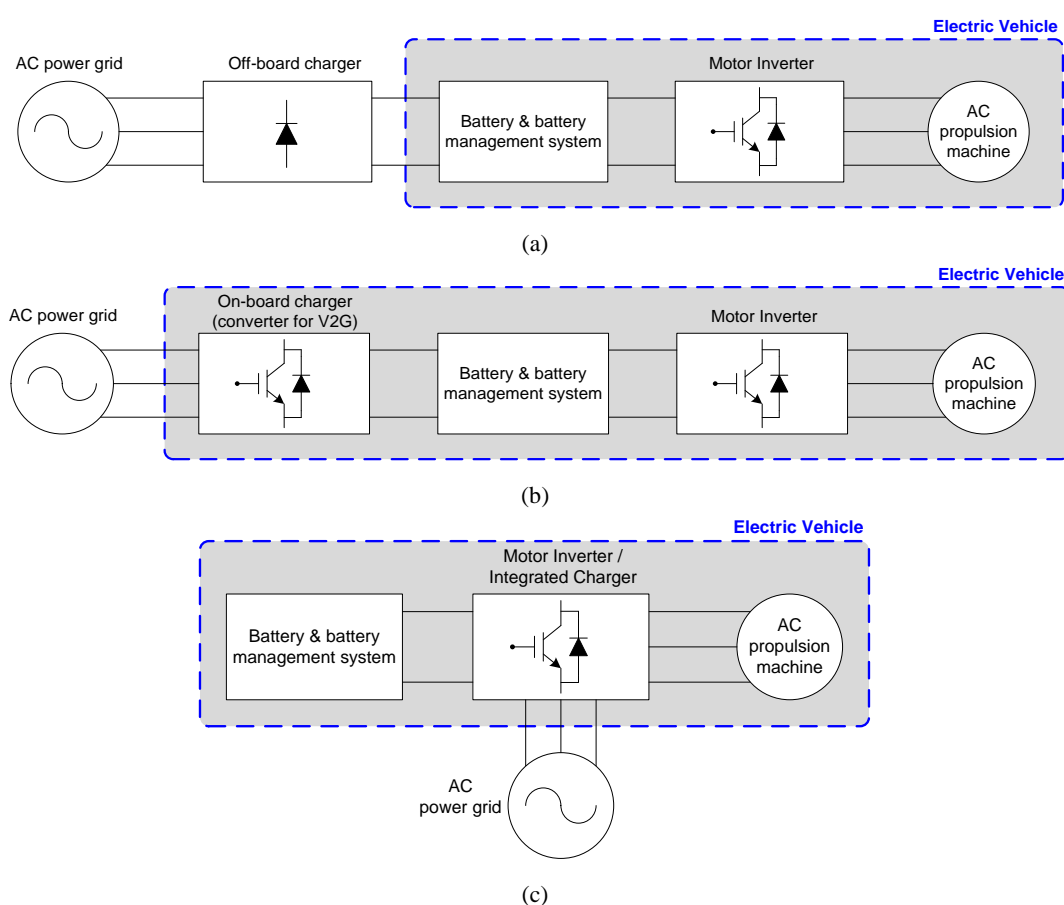


Figure 2.8. Block diagrams of, (a) an off-board charger topology, (b) an onboard charger topology, and (c) an integrated on-board charger topology.

Hence, all power electronics devices are in one unit. This module is called an integrated on-board charger. The major objectives of such an integrated on-board charger are the minimizations of manufacturing costs, maintenance costs and weight of the EV [10].

## 2.5. Charging Strategies

Electric vehicles are new type of additional load on the power grid. The change of the load profile depends on the penetration level of EVs as well as on the used charging strategies. State-of-the-art charging strategies such as dumb charging and dual tariff charging based on simple time-of-use (TOU) pricing are not the appropriate solutions for charging EVs.

### 2.5.1. Dumb charging

Dumb Charging means, that a car starts charging immediately when it arrives somewhere, trying to fully recharge its battery. Strategies based on dumb charging assume that electricity costs are the same during the whole day and therefore people just connect their PHEV to the grid, when they arrive at some location.

### 2.5.2. Dual tariff charging

Dual tariff charging is a well-known approach to shift loads of households from day to night. Therefore the electricity costs are low during the night and high throughout the rest of the day. Understandingly, during night there is much less electricity consumption than during the day. In order to give an incentive to people to shift their consumption (washing machines etc.) to later evening hours, i.e. off-peak hours, the price during the night is low (e.g. from 9pm to 5am) and high throughout the rest of the day.

Several researches have shown that both strategies used for charging EVs causes peak demands such as morning and evening peaks [11]. These demands could lead to violations of power grid constrains. Hence, smart charging is necessary to reduce peak demands and to realize valley-filling. In the majority of cases a novel smart power grid infrastructure is also mandatory. It is more advantageous to upgrade already existing power grids to smart grids, rather than to more powerful grids.

### 2.5.3. Smart charging

A smart power grid mainly consists of an advanced metering infrastructure (AMI) with a distributed control and data communication infrastructure. Both infrastructures together enable smart EV charging capability as well as V2G capability. Furthermore all EVs can be used as a distributed energy storage capacity. Smart charging and smart grids enable the minimization of consumer's electricity costs as well as the cost-efficient update of the existing power grid infrastructure. Several energy control strategies for the minimization of peak demands in the load profile have been proposed by a number of research groups [11].

#### 2.5.3.A. Centralized smart charging

Also there are many ways to perform smart charging. One way to do it would be to give more control to the utilities, owning the grid. The utilities would receive information from car owners, such as how long they will remain parked somewhere and information regarding their energy consumption for the rest of the day. Based on this, the grid could send signals to the PHEVs when to charge and when not. In case of V2G, the grid will also tell the PHEVs when to discharge. The electricity rates could be based on a contract between utilities and PHEV owners, which delivers cheaper energy to PHEV owners which can adhere to the planned duration for staying connected to the grid. Also staying longer connected to the grid could result in lower electricity prices for PHEV owners, as the PHEVs could be used as a storage for buffering electricity. This approach where a central entity, possessing network-, load- and generation information, is able to decide charging and discharging is called *centralized smart charging* [12].

#### 2.5.3.B. Decentralized smart charging

A second way to implement smart charging would be that the utility owners publish prices for charging and discharging, based on time and location. Software in the PHEVs could then decide whether to charge or discharge. An algorithm used for making such decisions would depend on similar data, as needed in the first case: the duration the car will remain parked and the location of the next activity. This approach, where the PHEV owner can decide, when to charge and when not, is called *decentralized smart charging* [12].

Which of these two above mentioned general approaches will be used or even a mixture of the two, depends on many factors such as legislation, utility policy, car manufacturing and smart grid evolution. Furthermore, smart charging can be divided in two types as follow:

- *Smart charging at home:*

The scenario of smart charging at home also considers other loads such as washing machines and refrigerator. Loads are divided in critical loads, shift-able loads and interruptible loads. EVs are classified as shift-able loads. Therefore smart EV charging at home should be carried out slowly during off-peak time. The main objective of smart charging at home is to achieve low electricity costs [10].

- *Public smart charging:*

On the other hand the scenario of public smart charging is based on quick charging during the day. In this case electricity costs are high and depend on the moment of charging, the duration of charging and the amount of consumed energy. The setup and maintenance of additional public charging infrastructure also increases the costs for consumers. Hence, new and additional infrastructure should be avoided whenever possible. The main objective of public smart charging is to charge the batteries of the EVs with the needed amount of energy during a defined time window [10].

## 2.6. Comparing Vehicle-to-grid with Vehicle-to-home

Vehicle-to-home (V2H) avoids the infrastructure and tariff problems associated with vehicle-to-grid. V2H would be used to level the house electricity demand profile; sharp power increases associated with running high power appliances for short periods would be controlled. The resulting smoother demand from the grid would give electric suppliers a more manageable load. With energy storage in place the peak demands could be shifted such that electric load remains more constant throughout the day. This would allow more efficient and cost effective electricity generation to be used. Vehicle-to-home would improve the effectiveness of renewable energy sources; excess generation can be stored and used when generation is low. Vehicle-to-grid (V2G) is parallel i.e. within a grid any car can be used to power any house by feeding its power back to the grid. In contrast, vehicle-to-home is more limited; a single vehicle is used to supply a single house. The trade-off is simplicity versus flexibility; more vehicles working together offer flexible storage but will be more difficult to control. A further discussion point is locality. V2G and V2H are a form of distributed generation; the electrical load is geographically close to the electrical source. Transmission is therefore minimal compared to centralized generation so costs of transmission infrastructure and transmission losses are reduced. V2H represents the simplest case with regards to infrastructure and transmission. A single house operating V2H will have simple infrastructure requirements and negligible transmission losses. V2G can vary in infrastructure complexity and transmission distance depending on the number of vehicles involved and the geographical area serviced. A group of vehicles acting in a group as an electrical source is a more technically challenging situation than V2H and opens up the possibility of larger transmission distances [6].

Vehicle-to-Building (V2B) or V2H operation is a concept that is practically viable today being far simpler than V2G, and it may be implemented on a 3-5 year time horizon while V2G is based on the assumption of large-scale penetration of PEVs, which is envisioned on a 10-15 year time horizon in the most optimistic scenarios [3].

## References

- [1] S.G. Wirasingha, N. Schofield, and A. Emadi, "Plug-in hybrid electric vehicle developments in the US: Trends, barriers, and economic feasibility", Proc. of on Vehicle Power and Propulsion Conf. (VPPC), 2008, pp.1-8.
- [2] E. Sortomme and M. A. El-Sharkawi, "Optimal Scheduling of Vehicle-to-Grid Energy and Ancillary Services", *IEEE Transactions On Smart Grid*, vol. 3, no. 1, March 2012.
- [3] C. Pang, P. Dutta, and M. Kezunovic, "BEVs/PHEVs as Dispersed Energy Storage for V2B Uses in the Smart Grid", *IEEE Transactions On Smart Grid*, vol. 3, no. 1, March 2012
- [4] W. Kempton and J. Tomić, "Vehicle-to-grid implementation: From stabilizing the grid to supporting large-scale renewable energy," *J. Power Source*, vol. 144, no. 1, pp. 280–294, 2005.
- [5] W. Kempton and J. Tomić, "Vehicle-to-grid power fundamentals: Calculating capacity and net revenue," *J. Power Source*, vol. 144, no. 1, pp. 268–279, 2005.

- [6] G. Haines, A. McGordon, and P. Jennings, “The Simulation of vehicle to home systems-Using electric vehicle battery storage to smooth domestic electricity demand”, Ecological Vehicles and Renewable Energies Conference (EVER), Monaco 2009.
- [7] Electric Power Research Institute (EPRI) Report, “Technology primer: the plug-in hybrid electric vehicle,” pp. 1-2, 2007.
- [8] B. Kramer, S. Chakraborty, and B. Kroposki, “A review of plug-in vehicles and vehicle-to-grid capability”, Proc. of IEEE Int. Conf. on Industrial Electronics (IECON), 2008, pp. 2278 – 2283.
- [9] J. Tomic and W. Kempton, “Using fleets of electric-drive vehicles for grid support,” *Elsevier J. of Power Sources*, vol. 168, no. 2, pp. 459–468, June 2007.
- [10] G. Glanzer, T. Sivaraman, J. I. Buffalo, M. Kohl, and Hubert Berger, “Cost-efficient Integration of Electric Vehicles with the Power Grid by Means of Smart Charging Strategies and Integrated On board Chargers”, Environment and Electrical Engineering Int. Conf. (EEEIC), 2011, pp. 1-4.
- [11] H. Makkonen, J. Partanen, P. Silventoinen, “Concept of battery charging and discharging in automotive applications,” International Symposium on Power Electronics Electrical Drives Automation and Motion (SPEEDAM), June 2010.
- [12] R. A. Waraich, M. D. Galus, M. Balmer, G. Andersson, K. W. Axhausen, “Plug-in Hybrid Electric Vehicles and Smart Grid: Investigations Based on a Micro-Simulation,” [http://www.eeh.ee.ethz.ch/uploads/tx\\_ethpublications/galus\\_iatbr2009\\_PHEVs.pdf](http://www.eeh.ee.ethz.ch/uploads/tx_ethpublications/galus_iatbr2009_PHEVs.pdf)

### III. BATTERY CHARGER TOPOLOGIES

Battery chargers play a critical role in the development of electric and hybrid vehicles. Plug-in Electric Vehicles (PEV) batteries are recharged from the utility by help of either a house connection or a recharging bollard [1]. In Europe, the house connection provides electric energy from a single-phase 230V outlet whilst the recharging bollard does it from a three-phase 400V outlet. Almost all the PEVs are fitted with battery chargers that comply with both the outlets.

The conventional battery chargers (CBCs) only absorb power from the utility; for this reason, they are often termed unidirectional battery chargers (UBCs). Early CBCs utilized thyristor rectifiers. They adjusted the battery supply voltage by controlling the thyristor firing angle at the pace of the utility frequency so that a large ripple was superimposed on the battery charging current unless abating it with a bulky inductor. To lessen the ripple of the battery charging current, today's CBCs are set up with front-end diode rectifiers cascaded by choppers. Whether using thyristor or diode rectifiers, CBCs exhibit a poor power factor due to the high distortion and/or the low displacement factor of the current drawn from the utility. Further to the concern on the quality of the utility service under the proliferation of the CBCs, UBCs with higher power factor have been developed. The improvement is achieved by suitably shaping and phasing the current thanks to front-end diode rectifiers made active by the insertion of a transistor. The relevant battery chargers are termed as semi-active UBCs or power factor corrected (PFC) UBCs or simply PFC [2].

Battery chargers that really draw a nearly sinusoidal, voltage-in-phase current from the utility rely on front-end AC/DC converters [3]. They are able not only to absorb power but also to reverse the power flow and therefore are termed as bidirectional battery chargers (BBCs).

Recently, the concept of Vehicle-to-Grid (V2G) has gained an increasing interest as an opportunity for the grid. This scenario is expected to become practical as soon as a large number of PEVs will be marketed as explained in chapter two. It is evident that the PEVs equipped with BBCs are able to implement the V2G concept because of the bidirectional power flow capability of their battery chargers. Therefore, BBCs enabled to execute V2G have two operating modes, namely the "recharge" mode when they absorb energy from the grid and the "generation" mode when they deliver energy to the grid [4]. Modern PEVs are propelled by AC traction motors fed by inverters that are merely DC/AC converters. In the latest years, the idea has arisen to utilize some or all the power devices of the traction inverter to set up the battery charger when there is the need of recharging the PEV battery. Clearly, this can be done since the operating modes "recharge" and "traction" never occur simultaneously [5], [6]. The resultant battery chargers are termed as integral battery chargers (IBCs) and have the merit of reducing the power electronics onboard the PEVs. Depending on the reconfiguration, IBCs can be either unidirectional or bidirectional.

In this chapter the various types of battery chargers mentioned above are reviewed. It starts from the CBCs with front-end diode rectifiers and then goes through the PFCs, the BBCs and the IBCs. In details, the chapter is organized as follows. Section I describes at first the CBCs and then dwells on the PFC topologies. Section II illustrates the BBCs; it is divided into two Subsections, the first

Subsection being dedicated to the single-phase topologies and the second one to the three-phase topologies. Section III illustrates the IBCs; like Section II, it is divided into two Subsections dedicated to the single-phase and three-phase topologies, respectively. Throughout the chapter the conventions are pursued of naming as: i) “converter”, a conversion circuitry with a bidirectional power flow, ii) “rectifier” and “chopper”, AC/DC and DC/DC conversion circuitries with unidirectional power flow, iii) “inverter”, a DC/AC converter when it converts power from DC to AC side, and iv) “inverse inverter” a DC/AC converter when it converts power from AC to DC side.

### 3.1. Conventional Battery Chargers

CBCs with front-end diode rectifiers can include two or three conversion stages as outlined in Fig. 3.1. The first stage is a diode rectifier with a capacitor load that levels the rectified voltage. The successive stage is a chopper usually of buck type since the voltage of the PEV batteries is typically less compared to the rectified utility voltage. Otherwise, a chopper of boost type is used. At the beginning of the charge, the chopper operates in current control mode; when the battery voltage approaches its nominal value, the chopper enters into voltage control mode and completes the charging process.

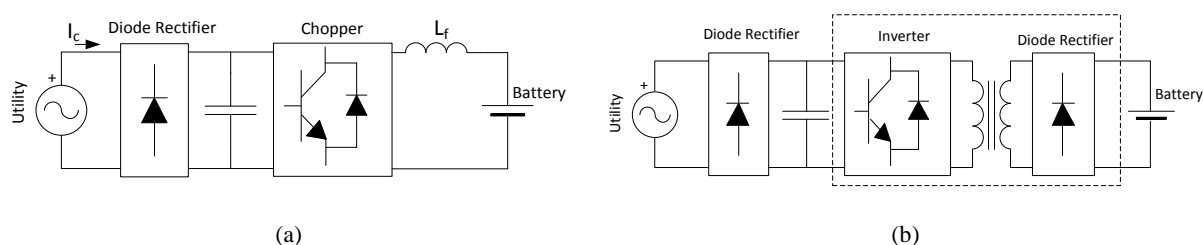


Figure 3.1. Schematic of CBC with front-end diode rectifier; a) CBC for voltage gain close to one, and b) CBC for voltage gain much different from one.

For chopper voltage gains close to one, the output of the chopper is directly connected to the battery through inductor  $L_f$ , as outlined in Fig. 3.1(a); the inductor is mandatory to smooth the current ripple produced by the high-frequency switching of the chopper. For chopper voltage gains much different from 1, f.i. when a 48V battery is charged from a 230V utility, the efficiency of the chopper would become low. To cope with the loss of efficiency, the chopper is replaced with a circuitry composed by the cascade of a single-phase inverter, a high-frequency transformer and a diode rectifier, as shown in the dashed block of Fig. 3.1(b). The circuitry behaves like a chopper with voltage gain determined by the turn ratio of the transformed.

Because of the front-end diode rectifier, the current drawn by a CBC from the utility is highly distorted and the resulting power factor is poor. Figure 3.2 shows the simulation result of a diode rectifier with its parameters in table 3.1.

The CBC inconvenience of a poor power factor is overcome by having recourse to the PFCs. Two basic PFC topologies have been developed, according to the controlled quantity (voltage or current).

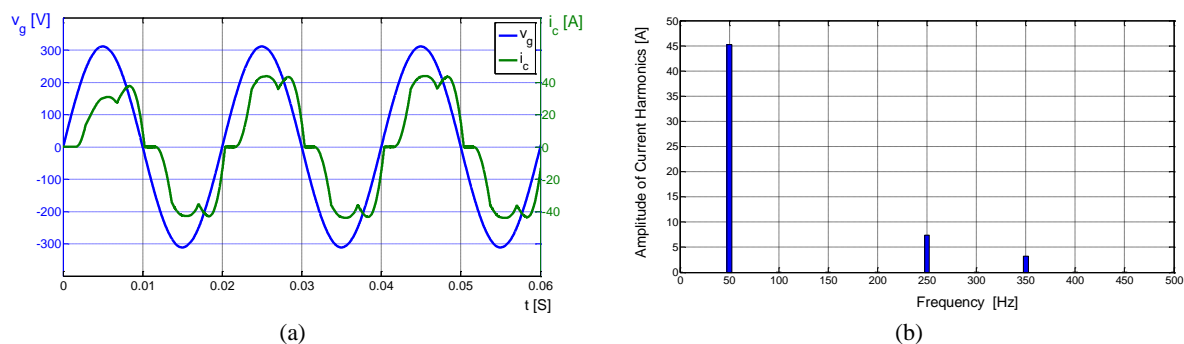
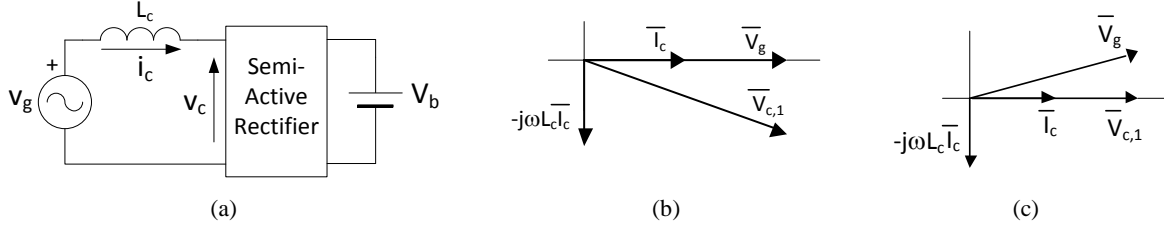


Figure 3.2. Current drawn by CBC from utility, a) Grid voltage and current waveform, b) Spectrum of current “ $I_c$ ”

Table 3.1. Parameters of front-end diode rectifier connected to the grid as a battery charger

$V_{g\phi}$ [V]	$I_c$ [A]	$L_c$ [mH]	$C$ [ $\mu$ F]	$R_b$ [ $\Omega$ ]	$V_b$ [V]
220	32	4.3	330	0.26	448

A voltage controlled (VC) PFC is made of a semi-active rectifier and a line inductor  $L_c$ , as given in Fig. 3.3. The active rectifier controls the AC voltage  $v_c$  at its input in a PWM fashion. Besides decoupling the PFC input from the utility, the inductor plays the role of filtering the high-frequency harmonics of current injected into the utility by the PWM voltage impressed at the PFC input.


 Figure 3.3. a) Schematic of VC PFC, b) Phasor diagram for PFC when  $i_c$  is in phase with  $v_g$ , and c)  $i_c$  is in phase with  $v_{c,1}$ .

Let the fundamental component of  $v_c$  be designated with  $v_{c,1}$ . In order that the PFC draws a sinusoidal current  $i_c$  in phase with the utility voltage  $v_g$ , magnitude and phase of  $v_{c,1}$  must have appropriate values. By representing the fundamental components of voltages and current in the input mesh of Fig. 3.3(a) with phasor quantities, the voltage equation of the mesh is

$$\bar{V}_{c,1} = \bar{V}_g - j\omega L_c \bar{I}_c \quad (3.1)$$

and the relevant phasor diagram is traced in Fig. 3.3(b). The diagram shows that the requirements for  $i_c$  to be in phase with  $v_g$  are as follows: i) the phasor of  $v_{c,1}$  must be behind the phasors of both  $v_g$  and  $i_c$ , and ii) the magnitude of  $\bar{V}_{c,1}$  must be higher than  $\bar{V}_g$  [7].

The semi-active rectifier of a VC PFC has the topology of Fig. 3.4(a), with the front-end diode rectifier cascaded by transistor T, diode D and capacitor C. The capacitor prevents the pulsating component of current produced by the switching of T from entering into the battery, provided that the capacitor impedance is lower than the equivalent series resistance (ESR) of the battery. Otherwise, a small inductor is inserted in series with battery. From Fig. 3.4(a), it emerges that, during the positive flow of  $i_c$ , the voltage  $v_c$  at the input of the semi-active rectifier is equal to the battery voltage  $V_b$  when T is off and to zero when T is on; likewise, during the negative flow of  $i_c$ , the voltage at the input of the active rectifier is equal to the opposite of the battery voltage  $-V_b$  when T is off and to zero when T is on. By properly selecting the on/off times of T,  $v_c$  can be modulated in a sinusoidal way. Nevertheless, the phasor requirement in point i) is not met all along the utility period [8]. Indeed, in the fraction of the utility period where  $i_c$  is positive and  $v_c$  is negative and, likewise, where  $i_c$  is negative and  $v_c$  is positive,  $v_c$  can take only values of the same sign of  $i_c$  or, at the most, can be kept at zero. With regards the magnitude requirement in point ii), it is met when, for any state of charge of the battery,  $V_b$  is higher than the peak value  $V_g$ , peak of the utility voltage. In the opposite case, the requirement can be met by cascading the active rectifier with a buck chopper, as outlined in Fig. 3.4(b). As a consequence of the non-complete fulfillment of the phasor requirement,  $i_c$  still suffers from a certain degree of distortion. The voltage and current waveforms related to the configuration of Fig. 3.4(a) are shown in Fig. 3.4(c-g) and the system parameters used in this simulation are given in table 3.2.

Table 3.2. Parameters of VC PFC and CC PFC (Fig. 3.4a).

$V_{g\phi}$ [V]	$I_c$ [A]	$L_c$ [mH]	$C$ [ $\mu$ F]	$f_{sw}$ [kHz]	$R_b$ [ $\Omega$ ]	$L_f$ [mH]	$V_b$ [V]
230	16	4.3	330	10	0.15	0.24	345

The capacitor embedded in the active rectifier of Fig. 3.4(b) must be pre-charged to the peak value of the utility voltage through the diodes of the rectifier before enabling switching of T. During pre-charge, a device, e.g. a resistor, must be connected in series to the capacitor to limit the current inrush. The residual current distortion existing in the PFCs controlled as in Fig. 3.3(b) is eliminated by setting  $i_c$  to be in-phase with  $v_{c,1}$ , as traced in Fig. 3.3(c). The power factor, however, is still less than 1 because now a phase displacement occurs between the current drawn from the utility and the utility voltage.

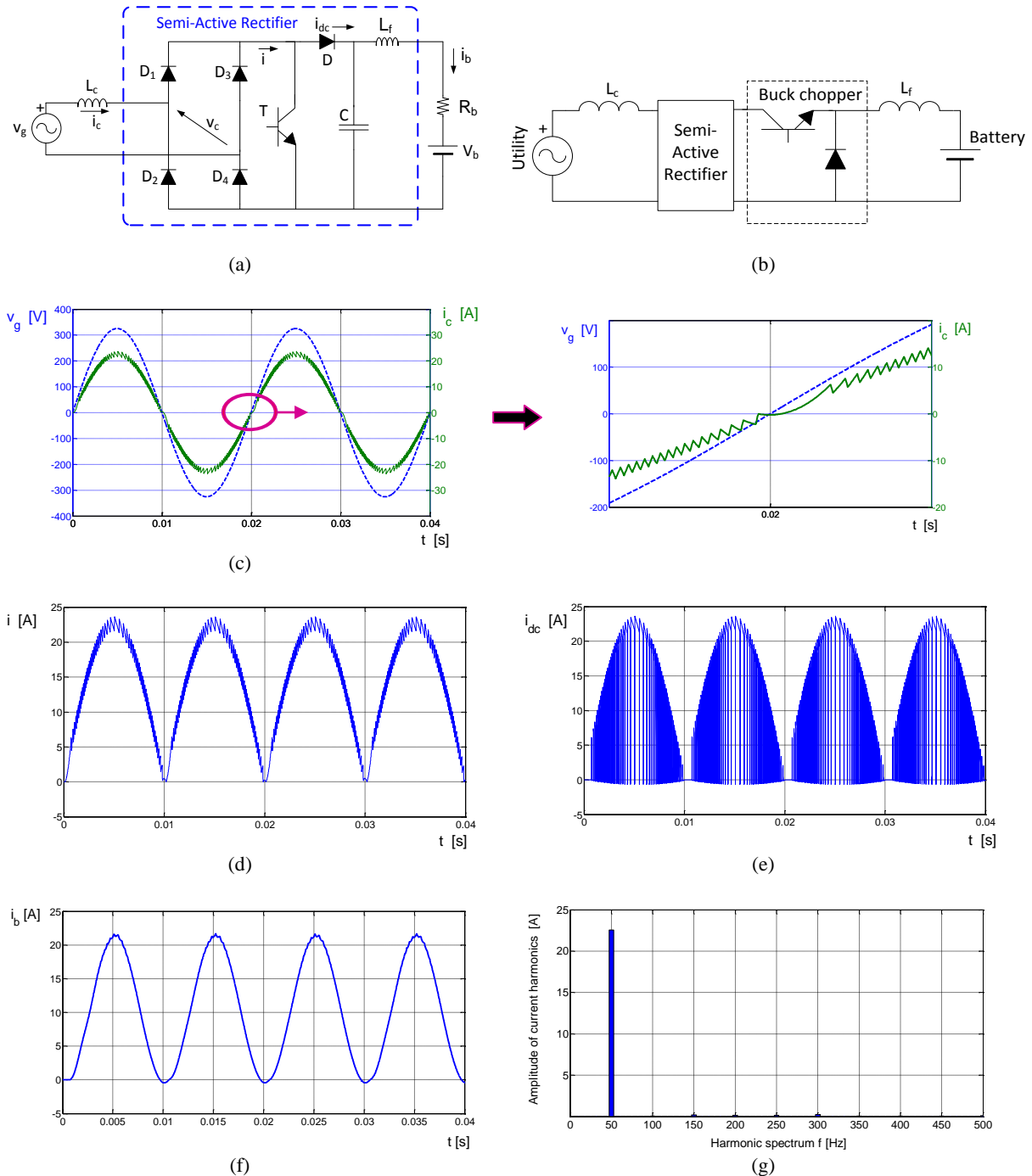


Figure 3.4. a) Topology of VC PFC, b) VC PFC with cascaded buck chopper, c) grid voltage and current, d) output current of rectifier, e) DC bus current, f) battery current, and g) spectrum of grid side current “ $i_c$ ”.

A current controlled (CC) PFC has the topology of Fig. 3.5. Differently from a VC PFC, inductor  $L_c$  is here inserted in the DC side of the front-end diode rectifier and, together with transistor T, diode D



and capacitor  $C$ , constitutes a boost chopper. By changing the duty-cycle of transistor  $T$  in the opposite way to the instantaneous magnitude of the utility voltage, the current drawn by the utility is forced to be sinusoidal and in-phase with the voltage, flowing through diodes  $D1$  and  $D4$  during the positive half period of the utility voltage and through diodes  $D2$  and  $D3$  during the negative one. As for a VC PFC, a CC PFC does not fully eliminate the distortion of the utility current. Indeed, at the zero crossings of the utility voltage there is no enough voltage to shape the current in the sinusoidal way; this is shown in Fig. 3.4(c) and Fig. 3.5(b) [9], [10]. The voltage and current waveforms related to the configuration of Fig. 3.5(a) are shown in Fig. 3.5(b-f) and the system parameters used in this simulation are the same given in table 3.2.

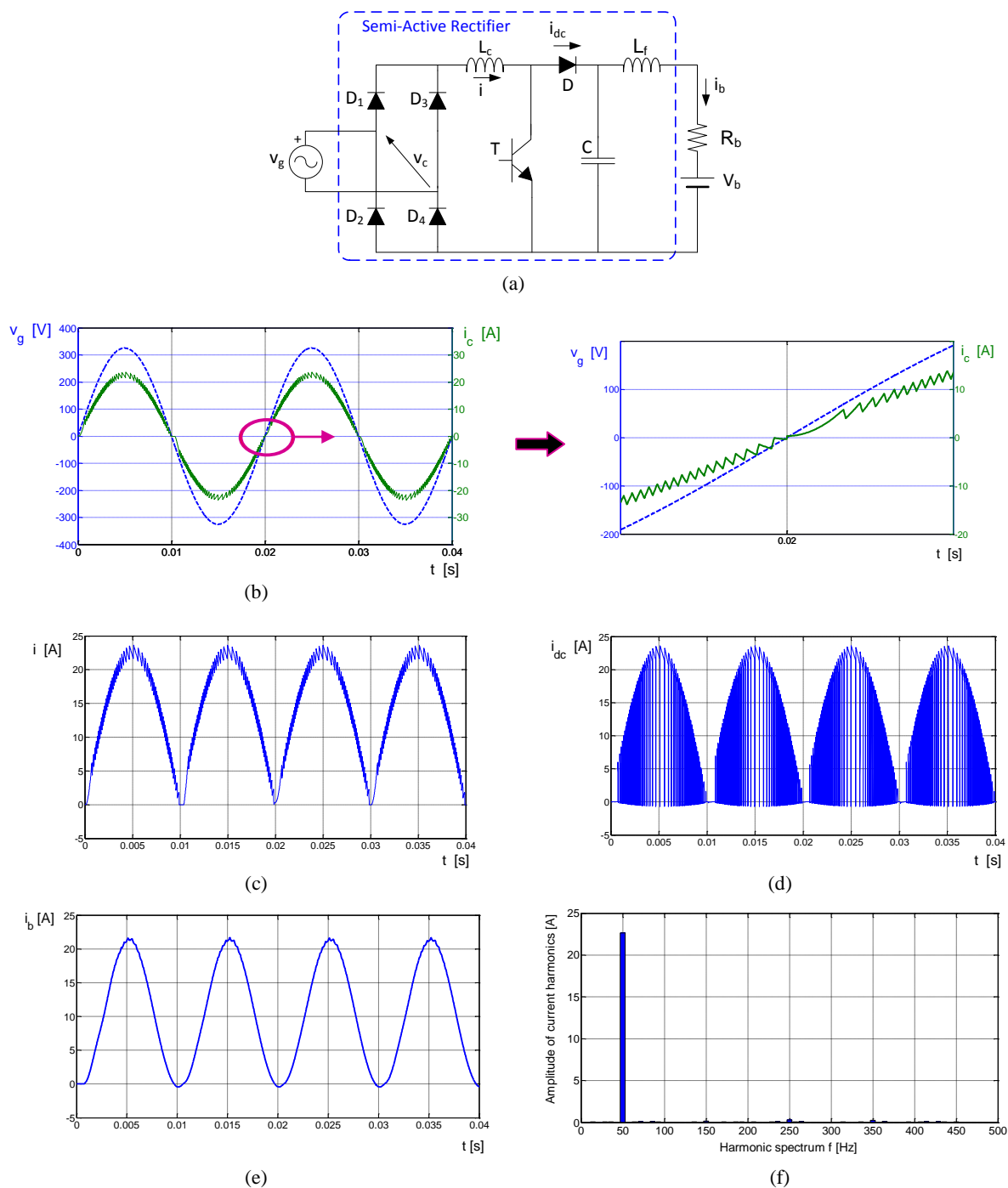


Figure 3.5. a) Topology of CC PFC, b) grid voltage and current, c) output current of rectifier, d) DC bus current, e) battery current, and g) spectrum of grid side current “ $I_c$ ”.

Straightforward extension of the PFC topologies to a three-phase utility does not allow the achievement of a better power factor. In fact, each phase of the front-end three-phase diode rectifier conducts for two intervals during the utility period, the maximum length of each being one third of the utility period, and hence the current drawn from the utility phases is discontinuous. Furthermore, during the conduction interval of any phase of the diode rectifier, that phase shares the current with one of the other two phases for the first half of the conduction interval and with the remaining phase for the second half. Then the current drawn from the utility phases can be not sinusoidal even along the conduction intervals of the phases of the diode rectifier.

### 3.2. Bidirectional Battery Chargers

BBCs can be set up for both single-phase and three-phase utility. They use an AC/DC converter as a front stage and line inductors to decouple the AC/DC converter from the utility [11]. The schematic of a single-phase BBC is given in Fig. 3.6. The AC/DC converter applies a PWM voltage at its input and, as before, inductor  $L_c$  comes useful to filter the current harmonics injected into the utility by the PWM voltage impressed at the input of the AC/DC converter.

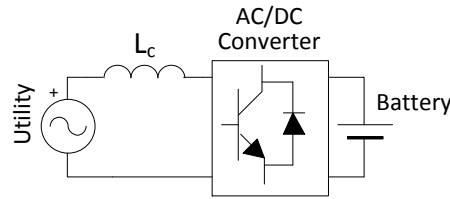


Figure 3.6. Schematic of single-phase BBC.

#### 3.2.1. Single-phase topologies

A single-phase BBC can utilize a half-bridge or a full bridge AC/DC converter [12]. A BBC with half-bridge AC/DC converter has the topology of Fig. 3.7. It contains transistors  $T_1$  and  $T_2$  with respective freewheeling diodes  $D_1$  and  $D_2$ , and two equal capacitors  $C_1$  and  $C_2$ . Besides splitting the battery voltage into two equal parts, the capacitors offer a low impedance path to the high frequency harmonics of current flowing in the DC side of the AC/DC converter so as to avoid their circulation into the battery. The fundamental component  $\bar{V}_{c,1}$  of the voltage  $v_c$  at the input of the AC/DC converter can be displaced of any angle from  $\bar{V}_g$ . Therefore, provided that  $\bar{V}_{c,1}$  is greater than  $\bar{V}_g$ , a unity displacement factor can be truly obtained whilst the current distortion is minimized by the filtering action of  $L_c$ . This raises the power factor of the BBC up to be nearly unity. According to the phasor diagram of Fig. 3.3(b), the BBC operates in the “recharge” mode when  $\bar{V}_{c,1}$  lags  $\bar{V}_g$  and in the “generation” mode in the opposite case.

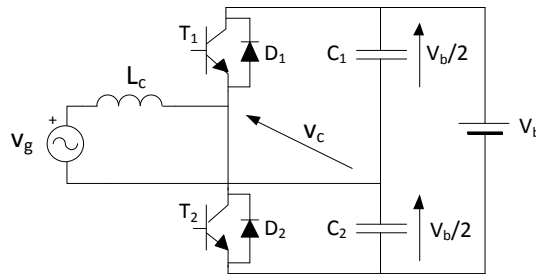


Figure 3.7. Topology of single-phase half-bridge BBC.

The peak value of  $\bar{V}_{c,1}$  ranges from 0 to half the battery voltage. When the battery voltage is not enough to meet the magnitude requirement for  $\bar{V}_{c,1}$ , a DC/DC converter of buck type is inserted between the AC/DC converter and the battery and adapts the voltage across the capacitor embedded in the AC/DC converter to that of the battery. The DC/DC converter can be either bidirectional or not, depending on whether the PEV is intended or not intended to support the V2G services. The topology

of a bidirectional DC/DC converter is shown in Fig. 3.8 and comprises transistors  $T_5$  and  $T_6$  with respective freewheeling diodes  $D_5$  and  $D_6$ , and inductor  $L_f$ . When  $T_5$  is commanded,  $T_6$  is left open; the electric energy goes from the AC/DC converter to the battery and the DC/DC converter operates in buck mode. When  $T_6$  is commanded,  $T_5$  is left open; the electric energy goes from the battery to the AC/DC converter and the DC/DC converter operates in boost mode. Differently from Fig. 3.4(b), here inductor  $L_f$  plays the twofold action of smoothing the current ripple in the buck mode and of acting as an electric energy storage element in the boost mode.

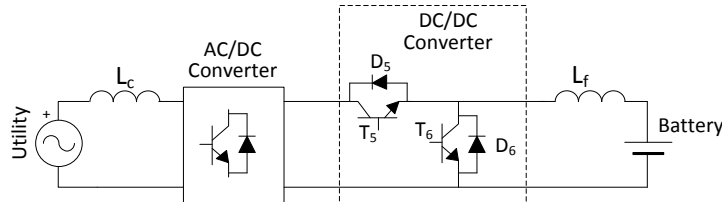


Figure 3.8. BBC with bidirectional DC/DC converter.

The main weaknesses of the half-bridge topology are as follows: i) the peak value of the fundamental component of  $v_c$  is equal only to half the battery voltage, and ii) a control action is needed to balance the charge across the two capacitors.

A BBC with full-bridge AC/DC converter has the topology of Fig. 3.9. It delivers twice the voltage of the single-phase counterpart for a given battery voltage and does not need any balancing action of the capacitor charge [13]. On the other side, the topology includes two more transistors  $T_3$  and  $T_4$  with respective free-wheeling diodes  $D_3$  and  $D_4$ , and requires double voltage ratings for the transistors. As for the half-bridge topology, the direction of the energy flow is dictated by the phase of  $\bar{V}_{c,1}$  with respect to  $\bar{V}_g$ . In Fig. 3.9(a,b), voltage and current of AC/DC side of full-bridge BBC in both operating mode “recharge” and “generation” are shown. The system parameters used for simulation are given in table 3.3.

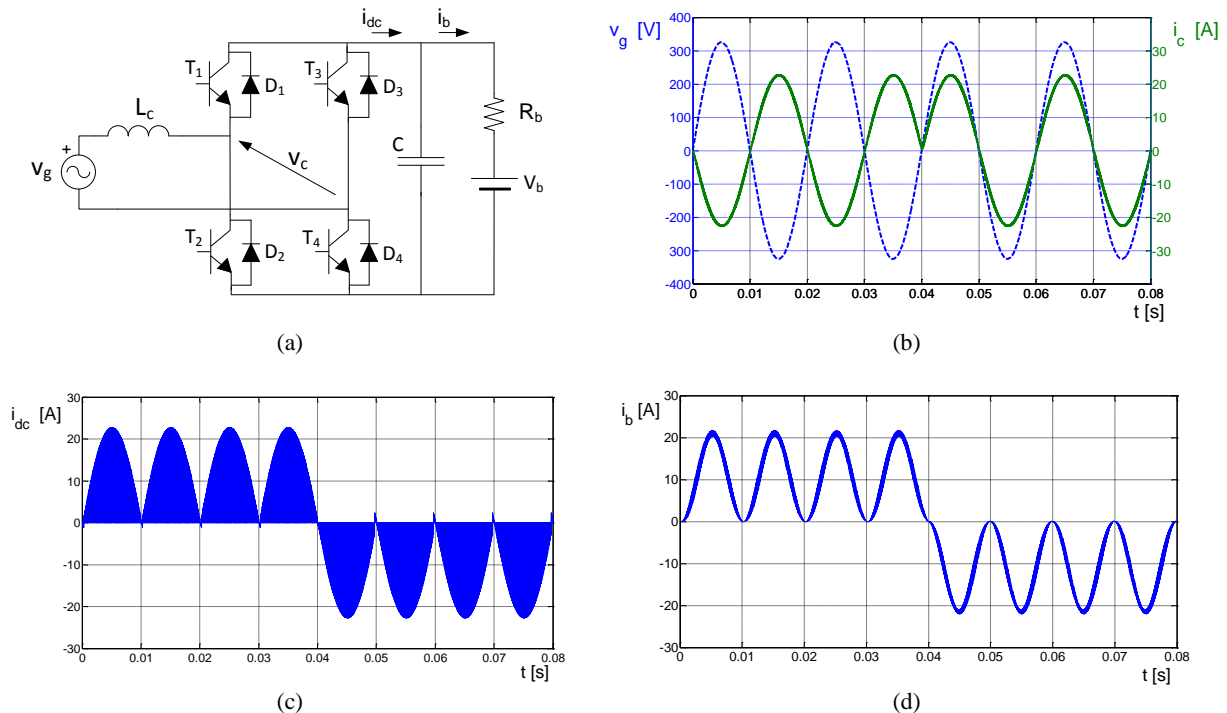


Figure 3.9. a) Topology of single-phase full-bridge BBC, b) grid voltage and current, c) DC bus current, and d) battery current

### 3.2.2. Three-phase topologies

A three-phase connection is characterized by supply voltages and currents higher than a single-phase connection and hence a three-phase BBC is rated for larger values of voltage and current. The topology of a three-phase BBC together with voltages and currents in both operating mode (recharge and generation) are shown in Fig. 3.10 and the system parameters used for simulation are given in table 3.3 [14], [15]. The voltages at the inputs of the three-phase AC/DC converter are of PWM type and are shifted of  $2\pi/3$  each from the other. As in the single-phase case, the inputs are decoupled from the utility by means of line inductors  $L_c$ . To draw sinusoidal currents from a three-phase utility, the peak value of the fundamental component of the line-to-line voltages at the AC/DC converter inputs must exceed the peak value of the utility line-to-line voltages. Under linear voltage modulation, this entails that  $V_b$  must be higher than  $\sqrt{3}V_{g,peak}$ . If this constraint is not met, a DC/DC converter is inserted between the AC/DC converter and the battery as in single-phase BBCs.

Table 3.3. Parameters of single-phase and three-phase BBC.

	$V_{g\phi}$ [V]	$I_c$ [A]	$L_c$ [mH]	$C$ [ $\mu$ F]	$f_{sw}$ [kHz]	$R_b$ [ $\Omega$ ]	$V_b$ [V]
<b>Single-phase</b>	230	16	4.3	330	10	0.15	345
<b>Three-phase</b>	230	32	2.3	330	10	0.26	600

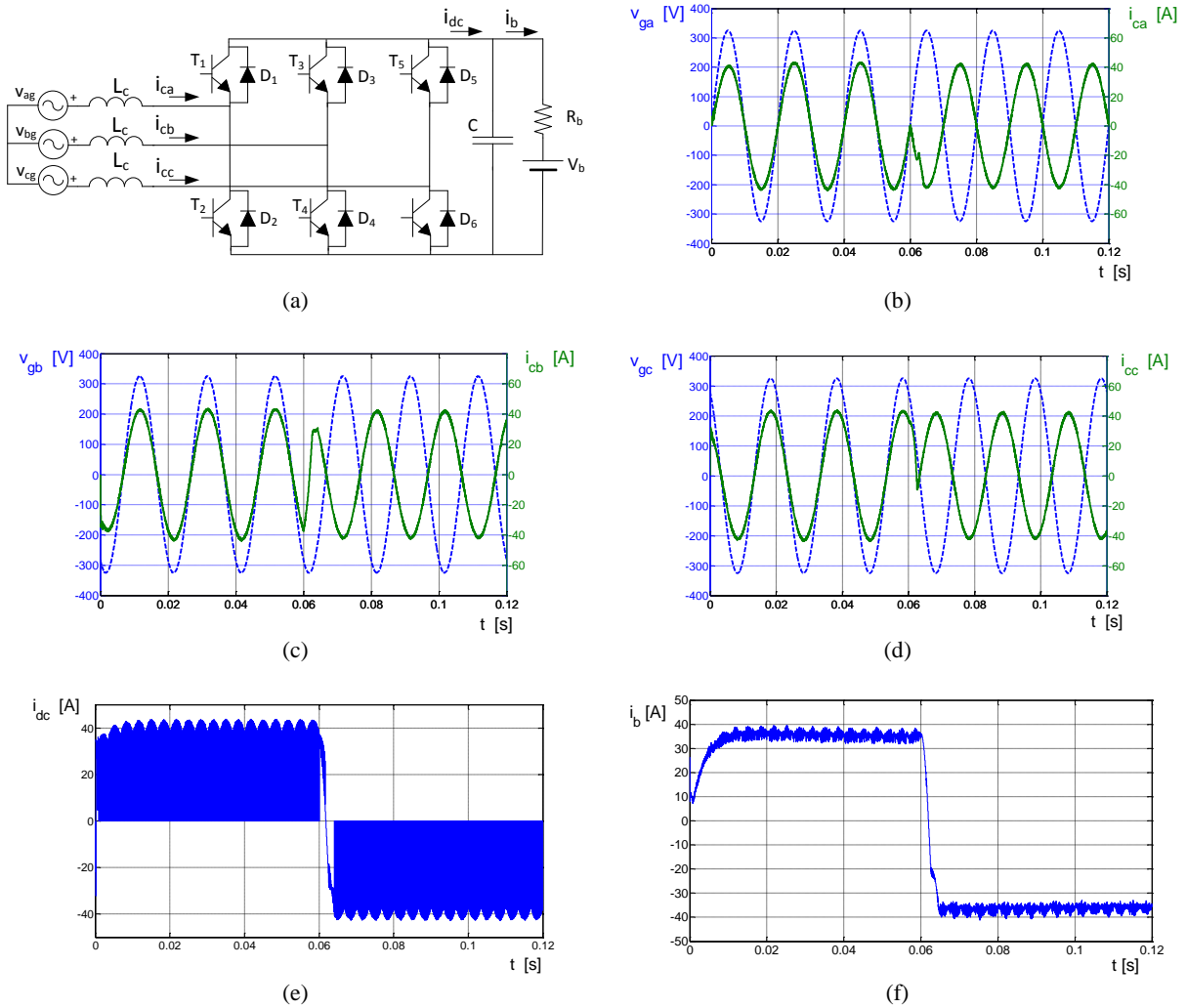


Figure 3.10. a) three-phase BBC topology, grid voltage and current: b) phase “a”; c) phase “b”; d) phase “c”, e) DC bus current, and f) battery current.

Let the phase currents be sinusoidal and in phase with the utility voltages. The power absorbed by a three-phase BBC is

$$P_{3\phi} = 3V_{g,rms}I_{c,rms} \quad (3.2)$$

where  $V_{g,rms}$  is the rms value of the phase voltages of the utility and  $I_{c,rms}$  the rms value of the phase currents. A single-phase BBC connected between two phases of the same utility and drawing the same current absorbs a power of

$$P_{1\phi} = \sqrt{3}V_{g,rms}I_{c,rms} \quad (3.3)$$

which is  $\sqrt{3}$  times lower than  $P_{3\phi}$ . Therefore, despite their higher cost due to the larger component count, the three-phase BBCs are preferred for a fast battery charging.

In USA, houses are supplied by distribution transformers that have a single-phase primary and a center-tapped secondary (Fig. 3.11). Between center tap and terminals of the secondary, two supply voltages with RMS value of 120V and phase displacement of  $\pi$  are available. Lighter home loads are connected between the center tap and one of the two terminals of the secondary whilst heavier loads are connected between the two terminals of the secondary, thus having a 240V supply.

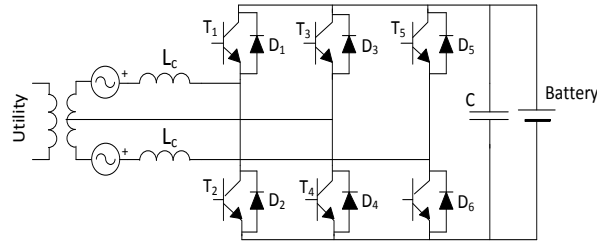


Figure 3.11. Split-phase BBC.

A BBC that complies with this utility has the topology of Fig. 3.11 and is termed as split-phase BBC. It is built up around a three-phase AC/DC converter and charges the battery from both the 120V and 240V supplies [16], [17]. When the BBC is connected to the 120V outlet, the transistors of the middle leg and of one of the two side legs of the AC/DC converter are commanded whilst the transistors of the third leg are left off. Instead, when the BBC is connected to the 240V outlet, the transistors of the two side legs of the AC/DC converter are commanded whilst the transistors of the middle leg are left off. In both the cases, the BBC operates as a single-phase full-bridge topology.

### 3.3. Integral Battery Chargers

IBCs are commonly obtained by a suitable reconfiguration of the traction inverter, aimed at turning the traction inverter into a battery charger. The reconfiguration is activated by opening or closing one or more switches, often of electromechanical type, at the time of changing the operating mode from “traction” to “recharge” or vice versa. IBCs dispense with the demand of an on-purpose battery charger with benefits in terms of cost, weight and space for the PEVs. To reduce even more the need of additional components, also the phase windings of the traction motor are often utilized for filtering or electric energy storage purposes while the PEVs are in the “recharge” mode.

#### 3.3.1. Single-phase topologies

A single-phase IBC can have the topology of Fig. 3.12(a) [18], where  $K_1$  is a relay, and  $K_2$  and  $K_3$  the contacts of a switchover relay. During the “traction” mode,  $K_1$  is closed whilst  $K_2$  and  $K_3$  are open, and the motor, represented by its phase inductances  $L_1$ ,  $L_2$ , and  $L_3$ , is supplied by the AC/DC converter operated as an inverter. During the “recharge” mode,  $K_1$  is open and  $K_2$  and  $K_3$  are closed. In this mode, transistors  $T_1$  and  $T_2$  and the transistors of one of the other two legs of the AC/DC converter, for example  $T_3$  and  $T_4$ , are commanded in the way of operating as a single-phase full-bridge BBC. The transistors of the third leg, in this case  $T_5$  and  $T_6$ , are kept open. Motor inductances  $L_1$  and  $L_2$  are connected in series and constitute the line inductor of the BBC. If the motor

inductances are too small to perform the filtering task, an additional inductor is inserted in series to them. Note that the resulting IBC is bidirectional and hence can operate in the “generation” mode too. To comply with a battery voltage lower than the utility peak voltage, the topology of Fig. 3.12(a) can be rearranged as in Fig. 3.12(b), where the third leg of the AC/DC converter is used as a DC/DC buck converter and a three-contact switchover relay is added. In the “traction” mode, contacts  $K_4$  and  $K_6$  are closed whilst contact  $K_5$  is open; in the “recharge” mode, the opposite occurs. Should the neutral point of the motor is accessible,  $L_f$  can be replaced by  $L_3$ .

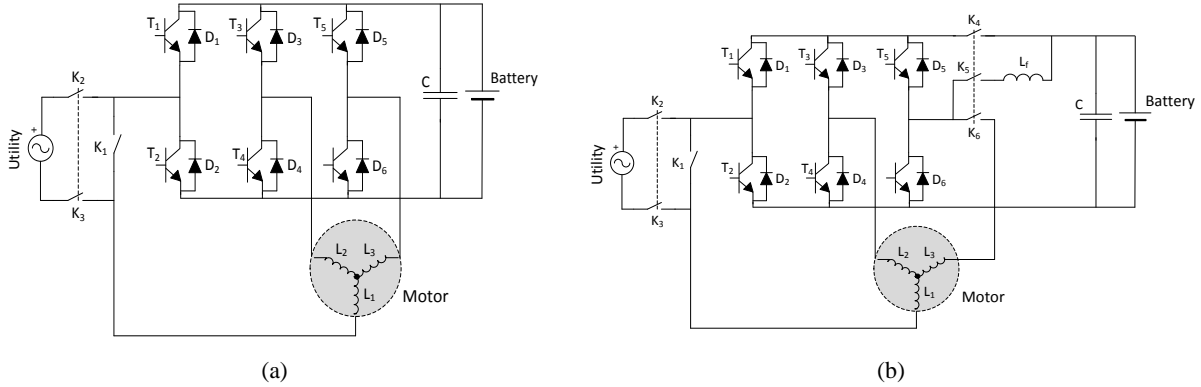


Figure 3.12. Topology of single-phase IBC; a) without and b) with built-in DC/DC converter.

A unidirectional IBC is shown in Fig. 3.13. This topology has been proposed for electric scooters, where the limited battery capacity does not make it convenient to reconfigure the traction inverter as a BBC [19], [20]. The IBC utilizes an additional front-end diode rectifier and works as follows. During the “traction” mode, relay  $K_1$  is kept open; the AC/DC converter is operated as an inverter and supplies the traction motor. During the “recharge” mode,  $K_1$  is kept closed; the IBC is supplied by the utility through the diode rectifier and the AC/DC converter is operated as a CC PFC with three interleaved stages. To this end, the lower transistors of the three legs of the AC/DC converter are commanded while the upper transistors are left off. Each stage of the IBC utilizes one phase winding of the motor as electric energy storage element. By this IBC, the ripple of the current charging the battery is greatly diminished; as a return, the IBC is affected by the distortion of the current utility inherent to any PFC topology and requires the accessibility of the neutral point of the motor.

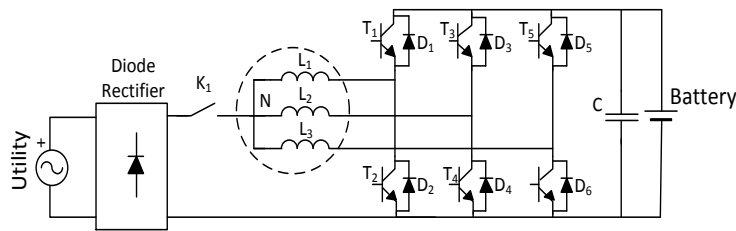


Figure 3.13. Topology of single-phase IBC with front-end diode rectifier.

In [21] a PEV with two traction drives is considered and the IBC topology of Fig. 3.14 is proposed. In the “recharge” mode, the utility is plugged between the neutral points of the two motors. The three legs of the two traction inverters are commanded in a parallel fashion to alleviate the current burden of each phase and the IBC behaves like a full-bridge BBC. As an alternative, the three legs can be commanded in an interleaved way with the aim of improving the waveform of the current charging the battery. To lessen the switching losses, it is also possible to command only the lower transistors of the three legs of the two traction inverters leaving the upper ones off [22]. Under this command, the IBC behaves like a VC UBC and is again affected by some distortion of the current utility.

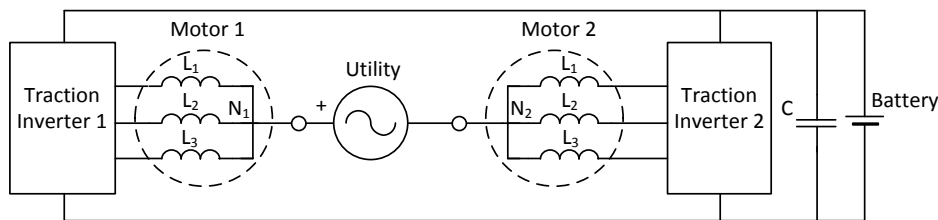


Figure 3.14. Schematic of single-phase IBC with two traction drives

### 3.3.2. Three-phase topologies

Figure 3.15 shows the topology of a three-phase IBC [24]. Differently from the single-phase IBC of Fig. 3.12, here the terminals of the motor windings connected to the neutral point must be accessible in order to form a three-phase system of line inductors, one for each phase of the IBC. To change the winding connection from “traction” to “recharge” mode, a changeover relay with three contacts  $K_1$ ,  $K_2$  and  $K_3$  is necessary. The resultant IBC operates as a three-phase BBC.

An interesting arrangement able to match the rectified voltage with any value of the battery voltage without needing a cascade buck or boost DC/DC converter is shown in Fig. 3.16 [25]. The arrangement consists in splitting the motor windings into two sections, denoted with  $a$  and  $b$ , to implement an in-set transformer. The two sections are suitably connected according to the operating mode by help of three changeover relays, each of them with three contacts. In the “traction” mode all the three relays are set to the lower position so that the two sections of each motor winding are connected in series and the neutral point  $N$  of the motor is created. In the “recharge” mode the relays are set to the upper position and the motor windings are split into two sections, each of them with its neutral point. The two sections constitute a three-phase transformer with the section  $a$  supplied from the utility and the section  $b$  having an induced voltage with magnitude determined by the turn ratio. As in Fig. 3.15, the resultant IBC operates as a three-phase BBC.

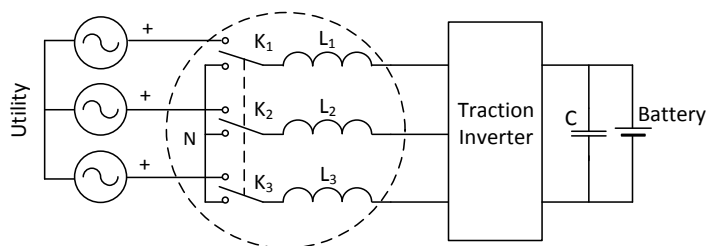


Figure 3.15. Schematic of a three-phase IBC.

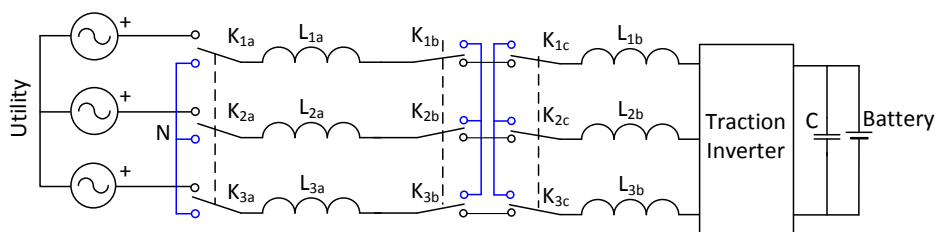


Figure 3.16. Three-phase IBC with in-set transformer.

### References

- [1] C.C.Chan and K.T.Chau, “An overview of power electronics in electric vehicles”, *IEEE Transactions on Industrial Electronics*, vol. 44, no. 1, pp. 3-13, February 1997.
- [2] A.Emadi, Y.J.Lee and K.Rajashekara, “Power electronics and motor drives in electric, hybrid electric, and plug-in hybrid electric vehicles”, *IEEE Transactions on Industrial Electronics*, vol. 55, no. 6, pp. 2237-2243, June 2008.

- [3] B.Singh, B.N.Singh, A.Chandra, K.AI-Haddad, A.Pandey and D.P. Kothari, "A Review of Three-Phase Improved Power Quality AC–DC Converters", *IEEE Transactions on Industrial Electronics*, vol. 51, n. 3, pp. 641-660, June 2004.
- [4] B. Kramer, S.Chakraborty and B.Kroposki, "A review of plug-in vehicles and vehicle-to-grid capability", Proc. of 34th IEEE Industrial Electronics Conf., 2008, pp. 2278-2283.
- [5] D.Wu, H.Chen, T.Das and D.C.Aliprantis, "Bidirectional power transfer between HEVs and grid without external power converters", Proc. of IEEE Energy 2030 Conf., 2008, pp. 1-6.
- [6] S.Hagbini, K.Khan, S.Lundmark, M.Alakula, O.Carlson, M.Leksell and O.Wallmark, "Integrated chargers for EV's and PHEV's: examples and new solutions", Proc. of Int. Conf. on Electrical Machines, 2010, pp. 1-6.
- [7] M.C.Kisacikoglu, B.Ozpineci and L.M.Tolbert, "Examination of a PHEV bidirectional charger system for V2G reactive power compensation", Proc. of IEEE Applied Power Electronics Conf. and Exposition, 2010, pp. 458-464.
- [8] Y.K.Lo, S.Y.Ou and H.J.Chui, "On evaluating the current distortion of the single-phase switch-mode rectifiers with current slope maps", *IEEE Transactions on Industrial Electronics*, vol. 49, no. 5, pp. 1120-1137, October 2002.
- [9] J.W.Kolar and T.Friedli, "The essence of three-phase PFC rectifier systems", Proceedings of the IEEE 33rd International Telecommunications Energy Conference (INTELEC), 2011, pp. 1-27.
- [10] Y.L.Lee, A.Khaligh and A.Emadi, "Advanced integrated bidirectional AC/DC and DC/DC converter for plug-in hybrid electric vehicles", *IEEE Transactions on Vehicular Technology*, vol. 58, no. 8, pp. 3970-3980, October 2009.
- [11] J.R.Rodriguez, J.W.Dixon, J.R.Espinoza, J.Pontt and P.Lezana, "PWM regenerative rectifiers: state of the art", *IEEE Transactions on Industrial Electronics*, vol. 52, no. 1, pp. 5-22, Feb. 2005.
- [12] J.Salaet, J.Bordonau and J.Peracaula, "SVM based control of a single-phase half bridge boost rectifier under power factor correction and balanced operation", Proc. of IEEE Int. Symposium on Industrial electronics, 2000, pp.130-134.
- [13] D.Dong, T.Thacker, R.Burgos, D.Boroyevich, F.Wang and B.Giewont, "Control design and experimental verification of a multi-function single-phase bidirectional PWM converter for renewable energy systems", Proc. of 13th European Power Electronics and Applications Conference, 2009, pp.1-10.
- [14] M.Bojrup, P.Karlsson, M.Alakula and B.Simonsson, "A dual purpose battery charger for electric vehicles", Proc. of 29th IEEE Power Electronics Specialists Conference, 1998, vol. 1, pp. 565-570.
- [15] J. Gallardo-Lozano, M.I.Milanes-Montero, M.A.Guerrero-Martinez and E. Romero-Cadaval, "Three-phase bidirectional battery charger for smart electric vehicles", Proc. of 7th Int. Conf. on Compatibility and Power Electronics (CPE), 2011, pp. 371-376.
- [16] X.Zhou, G.Wang, S.Lukic, S.Bhattacharya and A.Huang, "Multi-function bidirectional battery charger for plug-in hybrid electric vehicle application", Proc. of IEEE Energy Conversion Congress and Exposition, 2009, pp. 3930-3936.
- [17] X.Zhou, S.Lukic, S.Bhattacharya and A.Huang, "Design and control of grid-connected converter in bi-directional battery charger for plug-in hybrid electric vehicle application", Proc. of IEEE Vehicle Power and Propulsion Conf., 2009, pp. 1716-1721.
- [18] L.Shi, A.Meintz and M.Ferdowsi, "Single-phase bidirectional AC-DC converters for plug-in hybrid electric vehicle applications", Proc. of IEEE Vehicle Power and Propulsion Conference, 2008, pp. 1-5.
- [19] L.Solero, "Nonconventional on-board battery charger for electric vehicle propulsion batteries", *IEEE Transactions on Vehicular Technology*, vol. 50, no 1, pp. 144-149, January 2001.
- [20] G.Pellegrino, E.Armando and P.Guglielmi, "An integral battery charger with power factor correction for electric scooter", *IEEE Transactions on Power Electronics*, vol. 25, no 3, pp. 751-759, March 2010.
- [21] L.Tang and G.J.Su, "A low-cost, digitally-controlled charger for plug-in hybrid electric vehicles", Proc. of IEEE Energy Conversion Congress and Exposition, 2009, pp. 3923-2929.
- [22] R.Martinez and P.N.Enjeti, "A high-performance single-phase rectifier with input power factor correction", *IEEE Transactions on Power Electronics*, vol.11, n°2, pp. 311-317, Mar. 1996
- [23] S.K.Li and S.J.Lee, "An integral battery charger for four-wheel drive electric vehicle", *IEEE Transactions on Industry Applications*, vol. 31, no. 5, pp. 1096-1099, Sept/Oct. 1995.
- [24] S.Kinoshita, "Electric System for Electric Vehicle", United States patent US5504410, Fuji Electric Co LTD, 1996.
- [25] S.Hagbini, M.Alakula, K.Khan, S.Lundmark, M.Leksell, O.Wallmark and O.Carlson, "An integrated charger for plug-in hybrid electric vehicles based on a special interior permanent magnet motor" Proc. of IEEE Vehicle Power and Propulsion Conf., 2010, pp. 1-6.
- [26] M. Bertoluzzo, N. Zabihi, and G. Buja, "Overview on Battery Chargers for Plug-in Electric Vehicles", The 15th International Power Electronics and Motion Control Conference, EPE-PEMC 2012 ECCE Europe.



## IV. POWER DEFINITIONS FOR MODERN POWER SYSTEMS

The modern three-phase power system has to be considered as a self-contained entity when studying power phenomena. Formulations have to be carried out in this domain or in an equivalent transformed domain. Power definitions based on quantities formulated in a single-phase domain are only valid for three-phase systems under perfectly balanced three phase conditions. Application of classical power theory in modern power systems containing distorted waveforms and asymmetry in supply or loading has created many pitfalls and unsatisfactory performance is widely demonstrated in the literature [1-6].

The inadequacies found in the classical power theory to describe the power phenomena of non-linear power system operation were highlighted in 1922 by Bucholz. The well-known Budeanu formulation followed in 1927. Fryze reinterpreted Budeanu's definitions in 1932. Many other attempts followed thereafter when it became increasingly important for a power theory to describe power under non-sinusoidal conditions. The need to reach a conclusion on power definitions were again emphasized from the middle 1980s [1-4]. For example, Czarnecki communicated this deficiency clearly in an IEEE Transactions paper entitled 'What is wrong with the Budeanu Concept of Reactive Power and Distortion Power and why it should be abandoned' [2]. Even today there is disagreement over several aspects and definitions in non-sinusoidal power theory. The need for universally accepted power definitions has come to the fore now, like never before.

The electrical engineer requires practical power definitions to analyze a power system. The IEEE published guidelines for the practical definition of electrical quantities and power definitions in non-sinusoidal power systems in 1996 [5]. These definitions were compiled by an IEEE Working Group on Non-sinusoidal Situations chaired by Professor Alexander Emanuel [6].

### 4.1. Voltage and Current Quantities under Non-sinusoidal Unbalanced Conditions

Customers expect utilities to generate and distribute perfectly sinusoidal voltage waveforms at the fundamental frequency. The power definitions that are proposed in [5] separate the ideal situation of only fundamental frequency components from the polluting components. Only three-phase power systems with non-sinusoidal waveforms with unbalanced conditions (either because the supply voltage is asymmetrical or because the load elements are not balanced) are considered below. Single-phase, sinusoidal and balanced conditions are easily introduced with these definitions as a simplification of non-sinusoidal unbalanced three phase power systems. Assuming that the non-sinusoidal line-neutral voltages and line currents are defined as follows (similarly for phases b and c):

$$v_a(t) = \sqrt{2} \sum_{h \neq 0}^{\infty} V_{ah} \sin(h\omega_1 t + \alpha_{ah}) \quad (4.1)$$

$$i_a(t) = I_{a0} + \sqrt{2} \sum_{h \neq 0}^{\infty} I_{ah} \sin(h\omega_1 t + \beta_{ah}) \quad (4.2)$$

The DC components in the voltage,  $V_{a0}$ ,  $V_{b0}$  and  $V_{c0}$ , should always be zero. The DC values in the line currents  $I_{a0}$ ,  $I_{b0}$  and  $I_{c0}$  could be non-zero depending on the nature of the load. The RMS line-neutral voltage  $V_a$  and line current  $I_a$  (similarly for phases b and c) are related to the harmonic components by

$$V_a^2 = V_{a1}^2 + \sum_{h \neq 2}^{\infty} V_{ah}^2 = V_{a1}^2 + V_{aH}^2 \quad \left( V_{aH}^2 = \sum_{h \neq 2}^{\infty} V_{ah}^2 \right) \quad (4.3)$$

$$I_a^2 = I_{a1}^2 + \sum_{h \neq 2}^{\infty} I_{ah}^2 = I_{a1}^2 + I_{aH}^2 \quad \left( I_{aH}^2 = \sum_{h \neq 2}^{\infty} I_{ah}^2 \right) \quad (4.4)$$

The above formulations of voltage and current distinguish clearly between the fundamental frequency and the non-fundamental frequency (harmonic frequencies grouped) components. The effective three-phase voltage and current are written as

$$V_e^2 = V_{e1}^2 + V_{eH}^2 \quad (4.5)$$

$$I_e^2 = I_{e1}^2 + I_{eH}^2 \quad (4.6)$$

Because there is no neutral current in a three-wire power system, the expression for effective three-phase voltage and current is calculated as

$$V_e = \sqrt{\frac{V_a^2 + V_b^2 + V_c^2}{3}} \quad (4.7)$$

$$I_e = \sqrt{\frac{I_a^2 + I_b^2 + I_c^2}{3}} \quad (4.8)$$

If an artificial neutral point in a three-conductor, three-phase system is not used to find the line-neutral voltage values, the effective three-phase voltage can be calculated from the RMS phase-phase voltage values as

$$V_e = \sqrt{\frac{V_{ab}^2 + V_{bc}^2 + V_{ca}^2}{9}} \quad (4.9)$$

The fundamental frequency and non-fundamental frequency components of the effective voltage and current in a three-wire, three-phase power system are defined as

$$V_{e1} = \sqrt{\frac{V_{ab1}^2 + V_{bc1}^2 + V_{ca1}^2}{9}} \quad (4.10)$$

$$V_{eH} = \sqrt{\frac{V_{abH}^2 + V_{bcH}^2 + V_{caH}^2}{9}} \quad (4.11)$$

$$I_{e1} = \sqrt{\frac{I_{a1}^2 + I_{b1}^2 + I_{c1}^2}{3}} \quad (4.12)$$

$$I_{eH} = \sqrt{\frac{I_{aH}^2 + I_{bH}^2 + I_{cH}^2}{3}} \quad (4.13)$$

The effective three-phase non-fundamental voltage and current values are defined as

$$V_{eH} = \sqrt{\frac{\sum_{h \neq 1}^{\infty} (V_{ah}^2 + V_{bh}^2 + V_{ch}^2)}{3}} \quad (4.14)$$

$$I_{eH} = \sqrt{\frac{\sum_{h \neq 1}^{\infty} (I_{ah}^2 + I_{bh}^2 + I_{ch}^2)}{3}} \quad (4.15)$$

## 4.2. Power Definitions

### 4.2.1. Apparent power definitions

Apparent power definitions, widely used, can be recognized to be either the arithmetic or vector apparent power approach. IEEE 1459-2000 [5] formulates and then demonstrates that the concept of effective (or system) apparent power is the preferred approach. Power definitions used in industrial metering equipment do not in general recognize the importance of the latter definition. Most metering equipment even wrongfully uses the Budeanu definition of reactive power and some report the existence of a distortion power that cannot be physically explained. The different apparent power approaches are summarized below.

### 4.2.2. Arithmetic apparent power

The Budeanu power definition for single-phase power systems is applied on a per phase basis:

$$S_a = \sqrt{P_a^2 + Q_{Ba}^2 + D_{Ba}^2} \quad (4.16)$$

$$S_b = \sqrt{P_b^2 + Q_{Bb}^2 + D_{Bb}^2} \quad (4.17)$$

$$S_c = \sqrt{P_c^2 + Q_{Bc}^2 + D_{Bc}^2} \quad (4.18)$$

where  $S_a$  is the apparent power in phase a (similarly for phases b and c);  $Q_{Ba}$  is Budeanu's reactive power, i.e.

$$Q_{Ba} = \sum_{h=1}^{\infty} V_{ah} I_{ah} \sin(\alpha_{ah} - \beta_{ah}) = \sum_{h=1}^{\infty} Q_{ah} \quad (4.19)$$

(similarly for phases b and c); and  $D_{Ba}$  is Budeanu's 'distortion' power

$$D_{Ba} = \sqrt{S_a^2 - P_a^2 - Q_{Ba}^2} \quad (4.20)$$

(similarly for phases b and c). The three-phase arithmetic apparent power ( $S_A$ ) follows:

$$S_A = S_a + S_b + S_c \quad (4.21)$$

### 4.2.3. Vector apparent power

The active, Budeanu's reactive and distortion power over all three phases can be calculated:

$$P_{\Sigma 3\phi} = P_a + P_b + P_c \quad (4.22)$$

$$Q_{B,3\phi} = Q_{Ba} + Q_{Bb} + Q_{Bc} \quad (4.23)$$

$$D_{B,3\phi} = D_{Ba} + D_{Bb} + D_{Bc} \quad (4.24)$$

where  $P_{\Sigma 3\phi}$  is the three-phase total (or joint) active power, including the fundamental frequency component. The three-phase vector apparent power ( $S_V$ ) follows:

$$S_V = \sqrt{P_{\Sigma 3\phi}^2 + Q_{B,3\phi}^2 + D_{B,3\phi}^2} \quad (4.25)$$

A geometrical interpretation of  $S_V$  and  $S_A$  is presented in Fig. 4.1(a). The Budeanu's expanded approach to three-phase systems i.e. in the case of distortion is shown in Fig. 4.1(b). The method can be easily understood from the three-dimensional representation that vector apparent power  $S_V$  is the diagonal of the box with the sides  $P$ ,  $Q_B$ , and  $D_B$ .

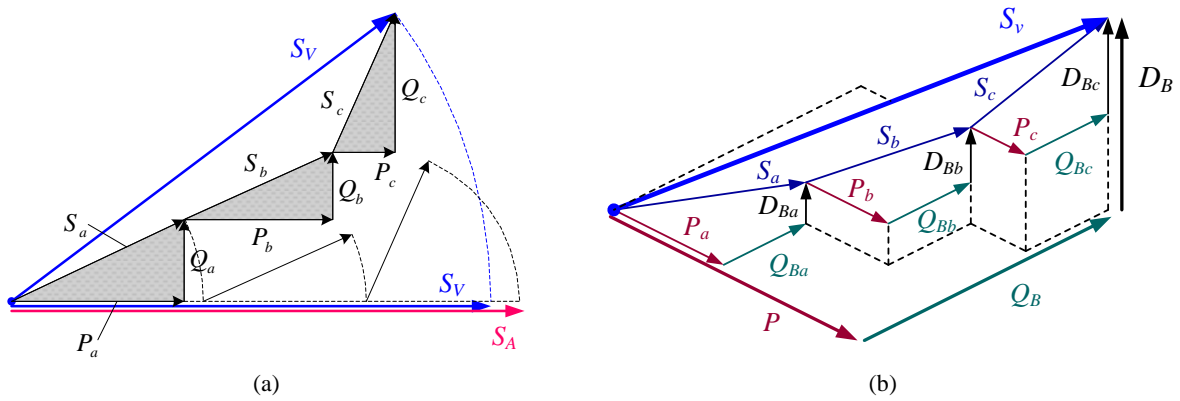


Figure 4.1. a) Arithmetic and vector apparent powers (VA), b) vector apparent power

#### 4.2.4. Effective apparent power

The three-phase or system effective apparent power  $S_e$  can be written in terms of the contribution of the fundamental and non-fundamental frequency voltage and current components:

$$S_e^2 = (V_e I_e)^2 = (V_{e1} I_{e1})^2 + (V_{e1} I_{eH})^2 + (V_{eH} I_{e1})^2 + (V_{eH} I_{eH})^2 \quad (4.26)$$

The three-phase effective apparent power contains a fundamental frequency apparent power  $S_{e1}$  and a non-fundamental frequency apparent power  $S_{eN}$ :

$$S_e^2 = S_{e1}^2 + S_{eN}^2 \quad (4.27)$$

The non-fundamental frequency apparent power is defined so as to consist of three distorting components<sup>1</sup>:

$$S_{eN}^2 = (V_{e1} I_{eH})^2 + (V_{eH} I_{e1})^2 + (V_{eH} I_{eH})^2 = D_{eI}^2 + D_{eV}^2 + S_{eH}^2 \quad (4.28)$$

The three components above are termed:

- $(V_{e1} I_{eH})$  : The current distortion power,  $D_{eI}$
- $(V_{eH} I_{e1})$  : The voltage distortion power,  $D_{eV}$
- $(V_{eH} I_{eH})$  : The effective harmonic apparent power,  $S_{eH}$

<sup>1</sup> IEEE 1459-2000 used the symbol 'e' to indicate that these distortion powers are based on 'effective' three-phase values.

The effective harmonic apparent power  $S_{eH}$  relates to the harmonic distortion power  $D_{eH}$  and the effective harmonic active power  $P_H$ :

$$S_{eH}^2 = P_H^2 + D_{eH}^2 \quad (4.29)$$

where effective harmonic active power  $P_H$  is

$$P_H = \sum_{h \neq 1} (V_{ah} I_{ah} \cos(\varphi_{ah}) + V_{bh} I_{bh} \cos(\varphi_{bh}) + V_{ch} I_{ch} \cos(\varphi_{ch})) \quad (4.30)$$

where  $\varphi_{ih} = \alpha_{ih} - \beta_{ih}$  for  $(i = a, b, c)$

The level of distortion in a three-phase power system is respectively defined by the voltage total harmonic distortion factor  $THD_{eV}$  and the current total harmonic distortion factor  $THD_{eI}$ :

$$THD_{eV} = \frac{V_{eH}}{V_{e1}} \quad (4.31)$$

$$THD_{eI} = \frac{I_{eH}}{I_{e1}} \quad (4.32)$$

The equivalent total harmonic distortion factors can be used to find  $S_{eN}$  (non-fundamental frequency apparent power),  $D_{eI}$ ,  $D_{eV}$ ,  $S_{eH}$ :

$$S_{eN} = S_{e1} \sqrt{(THD_{eI})^2 + (THD_{eV})^2 + (THD_{eI} \cdot THD_{eV})^2} \quad (4.33)$$

$$D_{eI} = S_{e1} \cdot THD_{eI} \quad (4.34)$$

$$D_{eV} = S_{e1} \cdot THD_{eV} \quad (4.35)$$

$$S_{eH} = S_{e1} \cdot THD_{eI} \cdot THD_{eV} \quad (4.36)$$

### 4.3. Harmonic Pollution and Unbalance

The normalized non-fundamental apparent power  $S_{eN}/S_{e1}$  relates to the total harmonic distortion factors:

$$\left(\frac{S_{eN}}{S_{e1}}\right)^2 = (THD_{eI})^2 + (THD_{eV})^2 + (THD_{eI} \cdot THD_{eV})^2 \quad (4.37)$$

Unbalanced loading can cause the three-phase fundamental frequency apparent power to increase without an increase in the transfer of fundamental frequency active power and is isolated by IEEE 1459-2000 as follows:

$$S_{u1} = \sqrt{S_{e1}^2 - S_{+1}^2} \quad (4.38)$$

$$S_{+1} = 3V_{+1}I_{+1} \quad (4.39)$$

The component  $S_{+1}$  is the positive-sequence fundamental apparent power calculated from the RMS values of the fundamental frequency positive-sequence voltage  $V_{+1}$  and fundamental frequency positive-sequence current  $I_{+1}$ . The term  $S_{u1}$  is the unbalanced contribution termed the unbalanced fundamental frequency apparent power:

- A quantitative measure of the level of harmonic pollution is contained in Eq. (4.37). A zero value indicates that no harmonic pollution is present. The ratio  $S_{eN}/S_{e1}$  progressively relates to the level of harmonic pollution.
- Similarly, the ratio  $S_{u1}/S_{e1}$  furnishes a progressive measure of the level of unbalance (it includes both the effect of voltage asymmetry and unbalance in loading).

#### 4.4. Fundamental Frequency Active and Reactive Power

The fundamental frequency apparent power, active power and the fundamental reactive power for a three-phase non-sinusoidal unbalanced power system should be based on positive-sequence quantities [5]:

$$S_{+1}^2 = P_{+1}^2 + Q_{+1}^2 \quad (4.40)$$

$$P_{+1} = 3V_{+1}I_{+1} \cos(\varphi_{+1}) \quad (4.41)$$

$$Q_{+1} = 3V_{+1}I_{+1} \sin(\varphi_{+1}) \quad (4.42)$$

where  $S_{+1}$  is the fundamental frequency apparent power in the positive-sequence quantities;  $P_{+1}$  is the fundamental frequency active power in the positive-sequence quantities; and  $Q_{+1}$  is the fundamental frequency reactive power in the positive-sequence quantities.

The components and the subcomponents discussed in this section are summarized in Fig. 4.2.

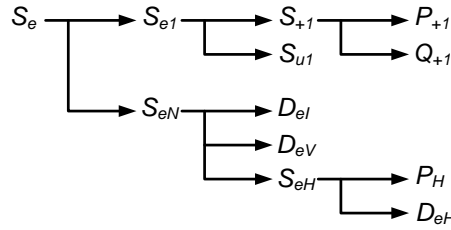


Figure 4.2. The powers' tree (IEEE Std. 1459–2010).

#### 4.5. Power Factor Definitions

The power factor<sup>1</sup> to be used is defined as

$$PF_e = \frac{P_{\Sigma 3\phi}}{S_e} = \frac{P_1 + P_H}{S_e} \quad (4.43)$$

where  $P_1$  is the fundamental frequency active power. The utilization of energy in fundamental frequency components is defined by the positive sequence components as

$$PF_{+1} = \frac{P_{+1}}{S_{+1}} \quad (4.44)$$

where  $PF_{+1}$  is the power factor formulation based on fundamental frequency positive sequence components. The three-phase total (or joint) active power<sup>2</sup>  $P_{\Sigma 3\phi}$  contains both the three-phase fundamental active power  $P_1$  and the three-phase total harmonic active power  $P_H$  :

$$P_{\Sigma 3\phi} = \sum_{h=0}^{\infty} P_h = P_1 + \sum_{h \neq 1}^{\infty} P_h = P_1 + P_H \quad (4.45)$$

The arithmetic or vector apparent power ( $S_A$  or  $S_V$ ) should not be used in the power factor formulation when the three-phase power system is non-sinusoidal and unbalanced:

$$PF_A = \frac{P_{\Sigma 3\phi}}{S_A} \quad (\text{arithmetic power factor}) \quad (4.46)$$

$$PF_V = \frac{P_{\Sigma 3\phi}}{S_V} \quad (\text{vector power factor}) \quad (4.47)$$

<sup>1</sup> The subscript 'e' is used to indicate that this power factor formulation makes use of effective apparent power.

<sup>2</sup> The three-phase joint active power is exactly the same concept as the three-phase joint real power.

When the power system is balanced and sinusoidal,  $PF_A = PF_V = PF_e$ . IEEE 1459-2000 demonstrate that if the power system is unbalanced and non-sinusoidal,  $PF_e < PF_A < PF_V$ , and propose the effective power factor formulation to be used. The above formulations are easy to implement when waveform data is available.

#### 4.6. Examples of the Systems with unbalanced loads

The following illustrations show transformer ( $I^2$ ) when applying 1000 watts of total resistive load, in various combinations, to a 120/208 V “Y” transformer bank.

Loss factors are calculated using two methods:

$$a) \text{ Transformer bank loss factor} = \frac{\text{actual bank } I^2}{\text{balanced bank } I^2}$$

$$b) \text{ Loss factor} = \frac{1}{PF^2} \quad PF = \frac{\text{Watts}}{\text{Volt Amperes}}$$

Powers are calculated using the following three methods:

- A. Arithmetic
- B. Vectorial
- C. Effective

**Case 1.** “Y” Transformer connected to balanced three phase star load (Fig. 4.3).

Total power load that applied are 1000 watts, it means there is  $1000/3 = 333.33w$  in each phase. So load current in each phase is equal to:

$$I_{L,a} = I_{L,b} = I_{L,c} = \frac{P_{1\phi}}{V_\phi} = \frac{333.3}{120} = 2.7 \text{ A}$$

Where  $P_{1\phi}$  is the power of each phase and  $V_\phi$  is the phase voltage of transformer and  $I_{L,a}, I_{L,b}, I_{L,c}$  are load phase currents. In this configuration load currents and transformer currents are equal.

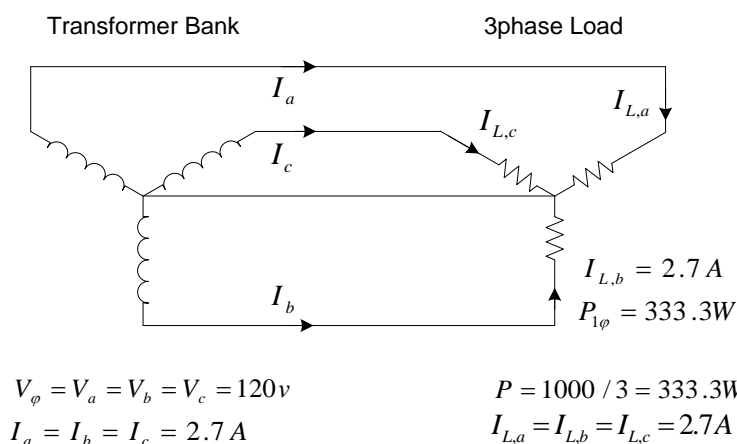


Figure 4.3. “Y” Transformer connected to balanced three phase star load

First the loss factor is calculated by method (a):

$$\text{Transformer bank loss factor} = \frac{\text{Bank } I^2}{\text{Balanced } I^2} = \frac{3 \times 2.7^2}{3 \times 2.7^2} = 1$$

In Table 4.1 apparent power, power factor and loss factor which are calculated by these three approaches are shown. Note that in this table, loss factors are calculated by method (b), in order to show the difference with the real loss factor which is calculated by method (a).

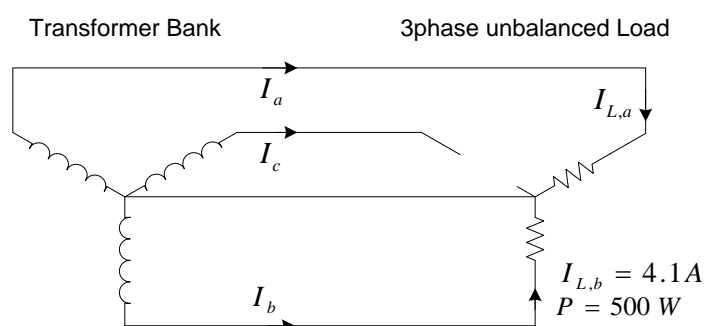
**Table 4.1.**

	System volt-amperes	PF	Loss factor = $\frac{1}{PF^2}$
Vectorial	1000	1	1
Arithmetic	1000	1	1
Effective	$S_e = 3V_e I_e = 1000$	1	1

Where  $V_e$  and  $I_e$  are effective voltage and effective current which are calculated by (4.7) and (4.8).

**Case 2.** “Y” Transformer connected to “Y” unbalanced load with two resistances (Fig. 4.4). Total power load that applied are 1000 watts, it means there is  $1000/2 = 500$ w in each load. So load current in each phase is equal to:

$$I_{L,a} = I_{L,b} = I_{L,c} = \frac{P_{1\phi}}{V_\phi} = \frac{500}{120} = 4.1 \text{ A}$$



$$\begin{aligned} V_\phi = V_a = V_b = V_c &= 120 \text{ v} & P &= 1000 / 2 = 500 \text{ W} \\ I_a = I_b &= 4.1 \text{ A} \quad I_c = 0 & I_{L,a} = I_{L,b} &= 4.1 \text{ A} \quad I_{L,c} = 0 \end{aligned}$$

Figure 4.4. “Y” Transformer connected to unbalanced load with two resistances

$$\text{Transformer bank loss factor} = \frac{\text{Bank } I^2}{\text{Balanced } I^2} = \frac{2 \times 4.1^2}{3 \times 2.7^2} = 1.5$$

In Table 4.2 apparent power, power factor and loss factor which are calculated by these three approaches are shown.

**Table 4.2.**

	System volt-amperes	PF	Loss factor = $\frac{1}{PF^2}$
Vectorial	1000	1	1
Arithmetic	1000	1	1
Effective	$S_e = 3V_e I_e = 1224.8$	0.81	1.5

It means, two equal resistor loads connected line to neutral on a “Y” system will give 81% power factor and result in 150% of the loss caused by a balanced load.

**Case 3.** “Y” Transformer connected to “Δ” unbalanced load with one resistance (Fig. 4.5). More details are explained in this case.

Total power load that applied are 1000 watts, it means there is 1000w single resistance load. So load current is equal to:



$$I_{L,a} = I_{L,b} = I_{L,c} = \frac{P_{1\phi}}{V_L} = \frac{1000}{208} = 4.8 \text{ A}$$

$$\text{Transformer bank loss factor} = \frac{\text{Bank } I^2}{\text{Balanced } I^2} = \frac{2 \times 4.8^2}{3 \times 2.7^2} = 2$$

It means, a single resistor connected line to line, to a “Y” transformer bank can be shown to cause twice the transformer load loss as the same watt load in a balanced connection.

By considering Fig 4.5(c), active and reactive powers for each phase can be calculated as follow:

$$P_a = V_a I_a \cos \varphi_a = 499.9 \text{ W}$$

$$P_b = V_b I_b \cos \varphi_b = 499.9 \text{ W}$$

$$P_c = V_c I_c \cos \varphi_c = 0$$

$$Q_a = V_a I_a \sin \varphi_a = -288.6 \text{ Var}$$

$$Q_b = V_b I_b \sin \varphi_b = +288.6 \text{ Var}$$

$$Q_c = V_c I_c \sin \varphi_c = 0$$

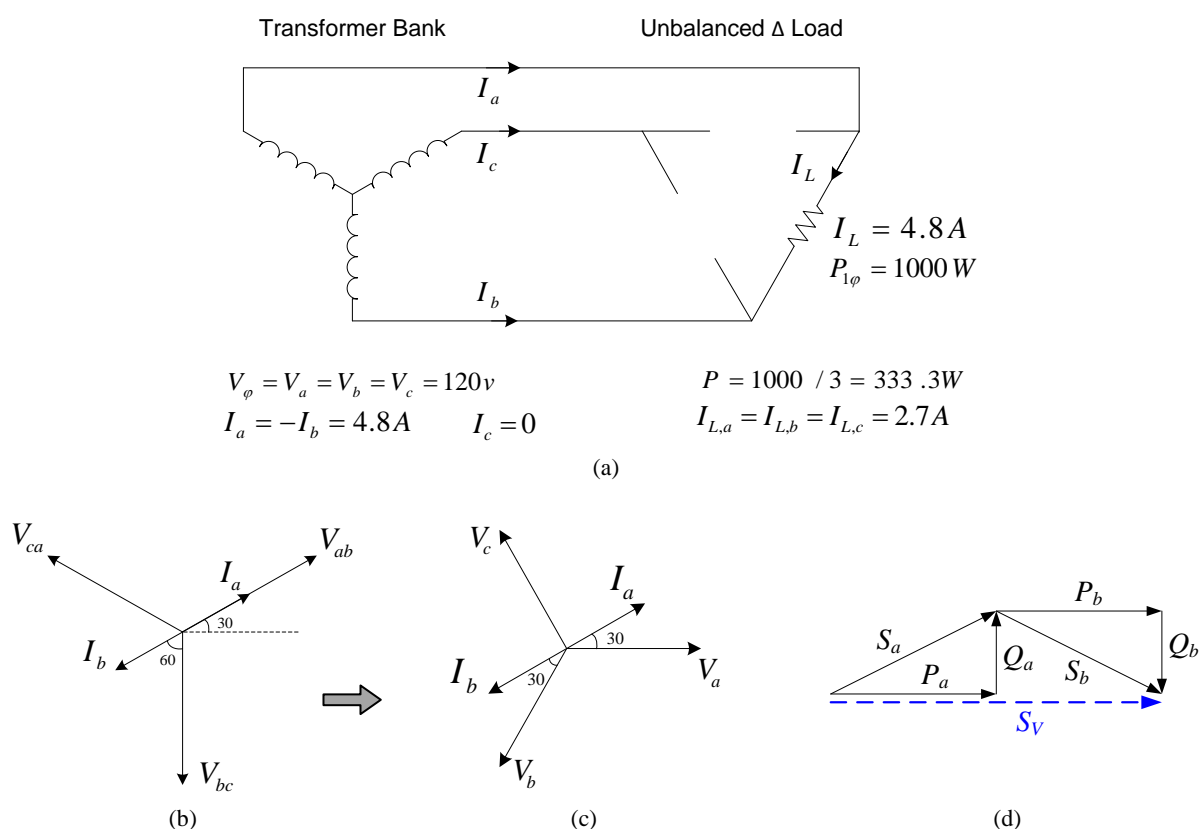


Figure 4.5. “Y” Transformer connected to “Δ” unbalanced load with one resistance; a) circuit diagram, b) line currents and voltages phasor diagram, c) line currents and phase voltages phasor diagram, d) power triangles (vectorial power)

where as it is shown in Fig. 4.5(c),  $\varphi_a = \varphi_b = 30^\circ$ .

The arithmetic and vectorial apparent powers are:

$$S_A = S_a + S_b + S_c = V_a I_a + V_b I_b + V_c I_c = 1154.6$$

$$S_V = \sqrt{P_{3\phi}^2 + Q_{3\phi}^2} = 1000$$

In Table 4.3 apparent power, power factor and loss factor which are calculated by these three approaches are shown. For instance power factors are calculated as follow:

$$PF_V = \frac{P}{S_V} = \frac{1000}{1000} = 1$$

$$PF_A = \frac{P}{S_A} = \frac{1000}{1154.6} = 0.86$$

$$PF_e = \frac{P}{S_e} = \frac{1000}{1414} = 0.7$$

Table 4.3.

	System volt-amperes	PF	Loss factor = $\frac{1}{PF^2}$
Vectorial	1000	1	1
Arithmetic	1154.6	0.86	1.33
Effective	$S_e = 3V_e I_e = 1414$	0.7	2

Twice the load loss would be anticipated from a load having a 70% power factor. Indeed the single resistor connected line to line would be calculated at 70% power factor using this method.

Considering equations from (5.34) to (5.38) of next chapter, one can apply instantaneous power theory in this case as follow (this part of example is discussed in details in the next chapter):

Voltages and currents can be written as

$$v_a = 120\sqrt{2} \cos(\omega t)$$

$$v_b = 120\sqrt{2} \cos(\omega t - 2\pi/3)$$

$$v_c = 120\sqrt{2} \cos(\omega t + 2\pi/3)$$

$$i_a = 4.81\sqrt{2} \cos(\omega t + \pi/6)$$

$$i_b = -4.81\sqrt{2} \cos(\omega t + \pi/6)$$

$$i_c = 0$$

At first, the three phase unbalanced currents phasor ( $I_a, I_b, I_c$ ) are transformed into three symmetrical components; the positive-sequence  $I_+$ , the negative-sequence  $I_-$ , and the zero-sequence  $I_0$ . They are calculated as

$$\begin{bmatrix} I_+ \\ I_- \\ I_0 \end{bmatrix} = \frac{1}{3} \begin{bmatrix} 1 & \alpha & \alpha^2 \\ 1 & \alpha^2 & \alpha \\ 1 & 1 & 1 \end{bmatrix} \begin{bmatrix} I_a \\ I_b \\ I_c \end{bmatrix}$$

where the constant  $\alpha$  is a complex number that acts as a  $120^\circ$  phase shift operator, that is,

$$\alpha = 1 \angle 120^\circ = e^{j(2\pi/3)} = -\frac{1}{2} + j\frac{\sqrt{3}}{2}$$

So the current of each phase by using symmetrical components can be written as follow

$$i_a = 4.81\sqrt{2/3} \cos(\omega t) + 4.81\sqrt{2/3} \cos(\omega t + \pi/3)$$

$$i_b = 4.81\sqrt{2/3} \cos(\omega t - 2\pi/3) + 4.81\sqrt{2/3} \cos(\omega t + \pi)$$

$$i_c = 4.81\sqrt{2/3} \cos(\omega t + 2\pi/3) + 4.81\sqrt{2/3} \cos(\omega t - \pi/3)$$

The first parts of above equations are positive components and the second parts are negative components (Fig. 4.6).

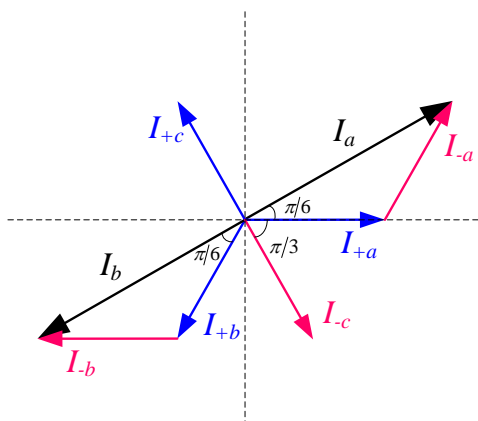


Figure 4.6. Unsymmetrical currents and its symmetrical components.

Applying the Clarke transformation yields the following voltages and currents:

$$\begin{aligned}v_{\alpha} &= 120\sqrt{3} \cos(\omega t) \\v_{\beta} &= 120\sqrt{3} \sin(\omega t) \\i_{\alpha} &= 4.81 \cos(\omega t) + 4.81 \cos(\omega t + \pi/3) \\i_{\beta} &= 4.81 \sin(\omega t) - 4.81 \sin(\omega t + \pi/3)\end{aligned}$$

The real and imaginary powers are calculated and separated in their average and oscillating components:

$$\begin{aligned}\bar{p} &= 3V_+I_+ \cos(\varphi_{v_+} - \varphi_{i_+}) = 1000 \\ \tilde{p} &= 3V_+I_- \cos(2\omega t + \varphi_{v_+} + \varphi_{i_-}) = 1000 \cos(2\omega t + \pi/3) \\ \bar{q} &= 3V_+I_+ \sin(\varphi_{v_+} - \varphi_{i_+}) = 0 \\ \tilde{q} &= 3V_+I_- \sin(2\omega t + \varphi_{v_+} + \varphi_{i_-}) = 1000 \sin(2\omega t + \pi/3)\end{aligned}$$

## References

- [1] Y. Akagi, A. Nabae., “Instantaneous reactive power compensator comprising switching devices without energy storage components”, *IEEE Transactions on Industrial Applications*, vol. IA-20, pp. 625–630, 1984.
- [2] L. S. Czarnecki, “What is wrong with the Budeanu Concept of Reactive Power and Distortion Power and why it should be abandoned”, *IEEE Transactions on Instrumentation and Measurement*, vol. IM-36, no. 3, pp. 834–837, 1987.
- [3] L. S. Czarnecki, “Powers in non-sinusoidal networks: their interpretation, analysis, and measurement”, *IEEE Transactions on Instrumentation and Measurement*, vol. 39, no. 2, pp. 340–345, 1990.
- [4] L. S. Czarnecki, “Misinterpretations of some power properties of electric circuits”, *IEEE Transactions on Power Delivery*, vol. 9, no. 4, pp. 1760–1769, 1994.
- [5] IEEE Standard 1459-2000, “Standard Definitions for the Measurement of Electric Power Quantities under Sinusoidal, Non-sinusoidal, Balanced or Unbalanced Conditions”, 2000.
- [6] IEEE Working Group on Non-sinusoidal Situations, “Effects on meter performance and definitions of power; practical definitions for power in systems with non-sinusoidal waveforms and unbalanced loads: a discussion”, *IEEE Transactions on Power Delivery*, vol. 11, no. 1, pp. 79–101, 1996.

## V. INSTANTANEOUS POWER THEORY

Electric systems with high nonlinear loads are common since the introduction of power electronics devices for controlling AC voltage or current or for converting them into different frequency, including DC. These devices brought more efficiency for the system and especially brought more flexibility, allowing very lightweight power supply for wide range speed control in AC and DC drives and so on. However, harmonic pollution came together with these applications and its associated problems became more appreciable with the increase of the percentage of power drawn by the nonlinear load. All the problems related to the harmonic components in the electric system forced the researches to study, understand, and propose new ways to eliminate these harmonics. In this sense, one of the theories is the instantaneous power theory or  $p$ - $q$  theory. This theory was first introduced by Akagi, Kanazawa and Nabae in 1983 [1] in Japanese. Since then, it has been extended and is presented in a book [2].

Generally, we use the term "power conditioning" with a much broader meanings term "harmonic filtering". In other words, the power conditioning is not confined to harmonic filtering, but it can do reactive power control for power factor correction, power flow control, voltage regulation, load balancing, voltage flicker reduction, and/or their combinations.

Since the emergence of sinusoidal voltage sources, the electric power network is more efficient if the load current is in phase with the source voltage. Therefore, the concept of reactive power was defined to represent the quantity of electric power due to the load current component that is not in phase with the source voltage. In a single-phase circuit, the average of this reactive power during one period of the line frequency is zero. In other words, this power does not contribute to energy transfer from the source to the load. In a three-phase circuit, the load current components not in phase with source voltages do not carry out active power.

### Example (5.1)

Consider the following sinusoidal, balanced, phase system of voltages and line currents of a three-phase linear circuit.

$$\begin{cases} v_a(t) = \sqrt{2} V \cos(\omega t) \\ v_b(t) = \sqrt{2} V \cos\left(\omega t - \frac{2\pi}{3}\right) \\ v_c(t) = \sqrt{2} V \cos\left(\omega t + \frac{2\pi}{3}\right) \end{cases} \quad \begin{cases} i_a(t) = \sqrt{2} I \cos(\omega t - \varphi) \\ i_b(t) = \sqrt{2} I \cos\left(\omega t - \varphi - \frac{2\pi}{3}\right) \\ i_c(t) = \sqrt{2} I \cos\left(\omega t - \varphi + \frac{2\pi}{3}\right) \end{cases} \quad (5.1)$$

where the angle  $\varphi$  is the phase displacement between currents and the respective voltages.

Each phase current can be divided into two components:  $i_{af}$ ,  $i_{bf}$  and  $i_{cf}$  that are in phase with voltage  $v_a$ ,  $v_b$  and  $v_c$ , respectively, and  $i_{aq}$ ,  $i_{bq}$  and  $i_{cq}$  that are in quadrature with the corresponding voltages.

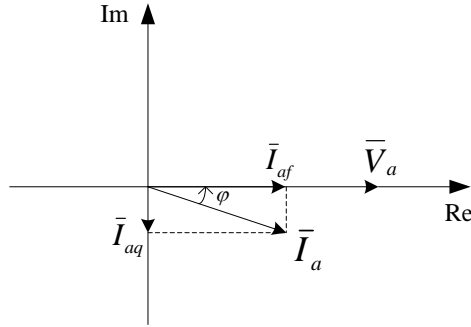


Figure 5.1. Current components;  $i_{af}$  in phase with voltage and  $i_{aq}$  in quadrature with voltage

$$i_a = i_{af} + i_{aq} \quad (5.2)$$

with

$$\begin{cases} i_{af} = \sqrt{2}I \cos \varphi \cos \theta \\ i_{aq} = \sqrt{2}I \sin \varphi \sin \theta \end{cases} \quad (5.3)$$

where  $\theta = \omega t$

The instantaneous active power is

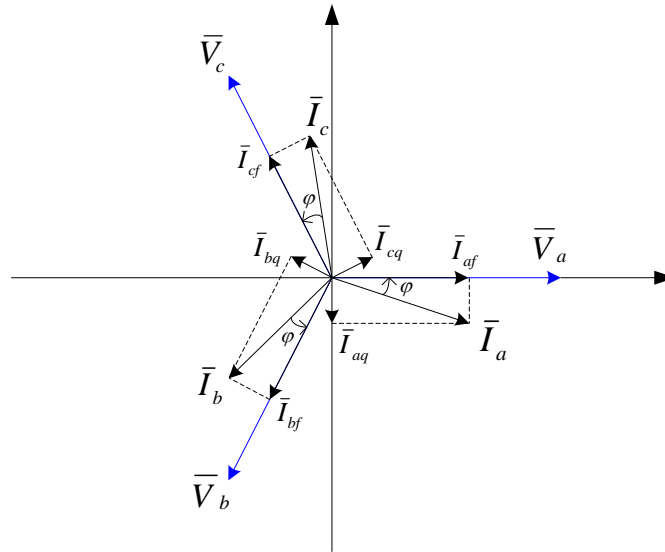


Figure 5.2. Three phase voltages, currents and currents components

$$\begin{aligned} p &= v_a i_a + v_b i_b + v_c i_c \\ p_1 &= v_a i_{af} + v_b i_{bf} + v_c i_{cf} \\ p_2 &= v_a i_{aq} + v_b i_{bq} + v_c i_{cq} \\ p_1 &= 3VI \cos \varphi \\ p_2 &= 0 \end{aligned} \quad (5.4)$$

Eq. (5.4) shows that the instantaneous active power is produced only by the in-phase component of the currents.

In parallel with the definition of reactive power, the concept of apparent power as well as power factor was created. Apparent power gives the idea of how much power can be delivered or consumed by generator or load if voltage and current are in phase. Displacement factor gives the relation

between the average power actually delivered or consumed in a circuit and the apparent power in the same point. Naturally, the higher the power factor, the better is the circuit utilization. Consequently, the power factor gives a figure of circuit efficiency not only electrically but also economically. Therefore, electric power utilities have specified lower limits for the power factor.

One of the main concerns related to electric equipment was displacement factor correction, which could be done by using capacitor banks or, in some cases, reactors. For all situations, the load acted as a linear circuit drawing a sinusoidal current from a sinusoidal voltage source. Hence, the conventional power theory, based on active-, reactive- and apparent-power definitions, was sufficient for analysis and design of power systems. Nevertheless, some papers were published, in 1920, showing that the conventional concept of reactive and apparent power loses its usefulness in non-sinusoidal cases [3]. Three important approaches to power definitions under non-sinusoidal conditions were introduced by Budeanu [4][5] in 1927, Fryze [6] in 1932, and Czarnecki [7] in 1987. Fryze and Czarnecki defined power in time domain, whereas Budeanu did it in frequency domain.

## 5.1. The $p$ - $q$ Theory

### 5.1.1. Basis of the $p$ - $q$ theory

The  $p$ - $q$  theory is based on a set of instantaneous powers defined in time domain. No restrictions are imposed on the voltage or current waveforms, and it can be applied in three-phase systems, with or without neutral wire. Traditional concepts of powers are characterized by treating a three-phase system as three single-phase circuits. The  $p$ - $q$  theory firstly transforms voltages and currents from  $abc$  to  $\alpha\beta 0$  coordinates, and then defines instantaneous powers on these coordinates. Hence, this theory always considers the three-phase system as a whole and not as a superposition or sum of three single-phase circuits.

### 5.1.2. The Clarke transformation

The Clarke transformation [8] and its inverse transformation of a three-phase system of generic voltages are given by

$$\begin{bmatrix} v_\alpha \\ v_\beta \\ v_0 \end{bmatrix} = \sqrt{\frac{2}{3}} \begin{bmatrix} 1 & -1/2 & -1/2 \\ 0 & \sqrt{3}/2 & -\sqrt{3}/2 \\ 1/\sqrt{2} & 1/\sqrt{2} & 1/\sqrt{2} \end{bmatrix} \begin{bmatrix} v_a \\ v_b \\ v_c \end{bmatrix} \quad (5.5)$$

$$\begin{bmatrix} v_a \\ v_b \\ v_c \end{bmatrix} = \sqrt{\frac{2}{3}} \begin{bmatrix} 1 & 0 & 1/\sqrt{2} \\ -1/2 & \sqrt{3}/2 & 1/\sqrt{2} \\ -1/2 & -\sqrt{3}/2 & 1/\sqrt{2} \end{bmatrix} \begin{bmatrix} v_\alpha \\ v_\beta \\ v_0 \end{bmatrix} \quad (5.6)$$

Similarly, a three-phase generic instantaneous line currents  $i_a$ ,  $i_b$  and  $i_c$  can be transformed to the  $\alpha\beta 0$ -axes.

One advantage of applying the  $\alpha\beta 0$  transformation is to separate zero-sequence components from the other components. The  $\alpha$ - and  $\beta$ -axes do not contribute to zero-sequence components. No zero-sequence current exists in a three-phase three-wire system, so that  $i_0$  can be eliminated from the above equations, thus resulting in simplification. If a three-phase system of voltages is symmetric or is formed by a direct (positive) and inverse (negative) sequence, no zero-sequence voltage is also present, so that  $v_0$  can be eliminated. However, when zero-sequence voltage and current components are present, the complete transformation has to be considered.

### Example (5.2)

The voltages and currents in (5.1) consist of the fundamental positive sequence. These voltages and currents can be transformed to the  $\alpha\beta$  -reference frame as given by

$$\begin{cases} v_\alpha = \sqrt{3} V \cos(\omega t) \\ v_\beta = \sqrt{3} V \sin(\omega t) \end{cases} \quad \begin{cases} i_\alpha = \sqrt{3} I \cos(\omega t - \varphi) \\ i_\beta = \sqrt{3} I \sin(\omega t - \varphi) \end{cases} \quad (5.7)$$

Note that their amplitudes in the  $\alpha\beta$  frame differ from the ones in the  $a, b, c$  frame.

### 5.1.3. Three-phase instantaneous active power in terms of $\alpha\beta$ voltage and current components

The Clarke transformation and its inverse transformation as defined above have the property of being invariant to the power. This feature is very suitable when the focus is the analysis of power in three-phase systems. Refer to appendix (b).

All traditional power definitions require as a precondition that the system be in steady-state. The three-phase instantaneous active power has a clear and universally accepted physical meaning, and is also valid during transient states.

The instantaneous active power of a three-phase system,  $p_{3\varphi}(t)$ , is calculated from the instantaneous phase voltages and line currents in terms of  $\alpha\beta 0$  components is

$$p_{3\varphi} = v_a i_a + v_b i_b + v_c i_c = v_\alpha i_\alpha + v_\beta i_\beta + v_0 i_0 \quad (5.8)$$

In a system without neutral wire,  $v_a$ ,  $v_b$  and  $v_c$  are measured from a common point of reference. Some time it is called "ground" or "fictitious star point". However, this reference point can be set arbitrarily and  $p_{3\varphi}$ , calculated from (5.8) results always in the same value, for all arbitrarily chosen reference points for voltage measurement.

### 5.1.4. Instantaneous $p$ - $q$ powers

The  $p$ - $q$  power theory is defined for three-phase systems, with or without neutral conductor. Three instantaneous powers are defined: the instantaneous real power  $p$ , the instantaneous imaginary power  $q$  and the instantaneous zero-sequence power  $p_0$ . They are

$$\begin{bmatrix} p \\ q \\ p_0 \end{bmatrix} = \begin{bmatrix} v_\alpha & v_\beta & 0 \\ v_\beta & -v_\alpha & 0 \\ 0 & 0 & v_0 \end{bmatrix} \begin{bmatrix} i_\alpha \\ i_\beta \\ i_0 \end{bmatrix} \quad (5.9)$$

By (5.9),  $p_{3\varphi}$  in (5.8) is equal to

$$p_{3\varphi} = p + p_0 \quad (5.10)$$

In three-wire systems only the instantaneous powers defined on the  $\alpha\beta$ -axes exist because  $i_0 = 0$ . Hence, the instantaneous real power represents the total energy flow per time unity; i.e. it is  $p_{3\varphi} = p$ . Hereafter only three-wire systems will be considered.

The instantaneous complex power  $\mathbf{s}$  is defined as the product of the voltage vector  $\mathbf{v}$  and the conjugate of the current vector  $\mathbf{i}^*$ , given in the form of complex number:

$$\mathbf{s} = \mathbf{v} \cdot \mathbf{i}^* = (v_\alpha + jv_\beta)(i_\alpha - ji_\beta) = (v_\alpha i_\alpha + v_\beta i_\beta) + j(v_\beta i_\alpha - v_\alpha i_\beta) \quad (5.11)$$

The instantaneous real and imaginary powers defined in (5.9) are part of the instantaneous complex power,  $\mathbf{s}$ , defined in (5.11). The original definition of  $p$  and  $q$  in [1] was based on the following equation:

$$\begin{bmatrix} p \\ q \end{bmatrix} = \begin{bmatrix} v_\alpha & v_\beta \\ -v_\beta & v_\alpha \end{bmatrix} \begin{bmatrix} i_\alpha \\ i_\beta \end{bmatrix} \quad (5.12)$$

Equations (5.9) and (5.12) are applicable to the analysis and design in the same manner. However, this thesis adopts (5.9), because a positive value of the instantaneous imaginary power  $q$  in (5.9) correspond to the product of a positive sequence voltage and a lagging (inductive) positive sequence current, in agreement with the conventional concept of reactive power. The instantaneous imaginary power  $q$  has a non-traditional physical meaning that will be explained in the next section.

## 5.2. The $p$ - $q$ Theory for Three-Wire Systems

The  $\alpha\beta$  currents can be put as functions of voltages and the real and imaginary powers  $p$  and  $q$ . This is very suitable expression for better explaining the physical meaning of the powers defined in (5.6). From this equation it is possible to write:

$$\begin{bmatrix} i_\alpha \\ i_\beta \end{bmatrix} = \frac{1}{v_\alpha^2 + v_\beta^2} \begin{bmatrix} v_\alpha & v_\beta \\ v_\beta & -v_\alpha \end{bmatrix} \begin{bmatrix} p \\ q \end{bmatrix} \quad (5.13)$$

This equation can have its terms expanded as

$$\begin{bmatrix} i_\alpha \\ i_\beta \end{bmatrix} = \frac{1}{v_\alpha^2 + v_\beta^2} \begin{bmatrix} v_\alpha & v_\beta \\ v_\beta & -v_\alpha \end{bmatrix} \begin{bmatrix} p \\ 0 \end{bmatrix} + \frac{1}{v_\alpha^2 + v_\beta^2} \begin{bmatrix} v_\alpha & v_\beta \\ v_\beta & -v_\alpha \end{bmatrix} \begin{bmatrix} 0 \\ q \end{bmatrix} = \begin{bmatrix} i_{\alpha p} \\ i_{\beta p} \end{bmatrix} + \begin{bmatrix} i_{\alpha q} \\ i_{\beta q} \end{bmatrix} \quad (5.14)$$

The above currents components can be defined as:

- instantaneous active current on the  $\alpha$ -axis  $i_{\alpha p}$

$$i_{\alpha p} = \frac{v_\alpha}{v_\alpha^2 + v_\beta^2} p \quad (5.15)$$

- instantaneous reactive current on the  $\alpha$ -axis  $i_{\alpha q}$

$$i_{\alpha q} = \frac{v_\beta}{v_\alpha^2 + v_\beta^2} q \quad (5.16)$$

- instantaneous active current on the  $\beta$ -axis  $i_{\beta p}$

$$i_{\beta p} = \frac{v_\beta}{v_\alpha^2 + v_\beta^2} p \quad (5.17)$$

- instantaneous reactive current on the  $\beta$ -axis  $i_{\beta q}$

$$i_{\beta q} = \frac{-v_\alpha}{v_\alpha^2 + v_\beta^2} q \quad (5.18)$$

The  $\alpha, \beta$  components of the instantaneous real power are defined as  $p_\alpha$  and  $p_\beta$ , respectively, and are calculated from the instantaneous voltages and currents on the  $\alpha\beta$ -axes as follows:

$$\begin{bmatrix} p_\alpha \\ p_\beta \end{bmatrix} = \begin{bmatrix} v_\alpha i_\alpha \\ v_\beta i_\beta \end{bmatrix} = \begin{bmatrix} v_\alpha i_{\alpha p} \\ v_\beta i_{\beta p} \end{bmatrix} + \begin{bmatrix} v_\alpha i_{\alpha q} \\ v_\beta i_{\beta q} \end{bmatrix} \quad (5.19)$$

By (5.15) and (5.6) the instantaneous real power can be given by the sum of  $p_\alpha$  and  $p_\beta$ . Therefore, rewriting this sum:

$$\begin{aligned} p &= v_\alpha i_{\alpha p} + v_\beta i_{\beta p} + v_\alpha i_{\alpha q} + v_\beta i_{\beta q} \\ &= \frac{v_\alpha^2}{v_\alpha^2 + v_\beta^2} p + \frac{v_\beta^2}{v_\alpha^2 + v_\beta^2} p + \frac{v_\alpha v_\beta}{v_\alpha^2 + v_\beta^2} q + \frac{-v_\alpha v_\beta}{v_\alpha^2 + v_\beta^2} q \end{aligned} \quad (5.20)$$

In the above equation, there are two important points. One is that the instantaneous real power is given only by

$$v_\alpha i_{\alpha p} + v_\beta i_{\beta p} = p_{\alpha p} + p_{\beta p} = p \quad (5.21)$$



The other point is that the following relation exists for the terms dependent on  $q$

$$v_\alpha i_{\alpha q} + v_\beta i_{\beta q} = p_{\alpha q} + p_{\beta q} = 0 \quad (5.22)$$

The meaning of (5.22) in the sinusoidal case can be easily understood by comparing it with (5.4). The above equations suggest the separation of the powers in the following types:

- instantaneous active power contribution on the  $\alpha$ -axis  $p_{\alpha p}$

$$p_{\alpha p} = v_\alpha i_{\alpha p} = \frac{v_\alpha^2}{v_\alpha^2 + v_\beta^2} p \quad (5.23)$$

- instantaneous reactive power contribution on the  $\alpha$ -axis  $p_{\alpha q}$

$$p_{\alpha q} = v_\alpha i_{\alpha q} = \frac{v_\alpha v_\beta}{v_\alpha^2 + v_\beta^2} q \quad (5.24)$$

- instantaneous active power contribution on the  $\beta$ -axis  $p_{\beta p}$

$$p_{\beta p} = v_\beta i_{\beta p} = \frac{v_\beta^2}{v_\alpha^2 + v_\beta^2} p \quad (5.25)$$

- instantaneous active power contribution on the  $\beta$ -axis  $p_{\beta q}$

$$p_{\beta q} = v_\beta i_{\beta q} = \frac{-v_\alpha v_\beta}{v_\alpha^2 + v_\beta^2} q \quad (5.26)$$

It should be noted that Watt [W] is the measure unit of all the powers,  $p_{\alpha p}$ ,  $p_{\alpha q}$ ,  $p_{\beta p}$  and  $p_{\beta q}$ , because each power is defined by the product of voltages and currents on the same axis.

The above equations lead to the following important conclusions:

- The instantaneous current  $i_\alpha$  is divided in the instantaneous active component  $i_{\alpha p}$  and in the instantaneous reactive component  $i_{\alpha q}$  as shown in (5.14). This same division is made for the currents on the  $\beta$ -axis.
- The sum of the  $\alpha$ -axis instantaneous active power  $p_{\alpha p}$ , given in (5.23), and the  $\beta$ -axis instantaneous active power  $p_{\beta p}$ , given in (5.25), corresponds to the instantaneous real power  $p$ .
- The sum of  $p_{\alpha q}$  and  $p_{\beta q}$  is always zero. Therefore, they do not contribute to the instantaneous (or average) energy flow between the source and the load in a three-phase circuit. This is the reason that they were named instantaneous reactive power on the  $\alpha$ - and  $\beta$ -axes. The instantaneous imaginary power  $q$  is a quantity that gives the magnitude of the powers  $p_{\alpha q}$  and  $p_{\beta q}$ .
- Because the sum of  $p_{\alpha q}$  and  $p_{\beta q}$  is always zero, their compensation do not need any energy storage element, as it will be shown later.

If the  $\alpha\beta$  variables of the instantaneous imaginary power  $q$  as defined in (5.9) are replaced by their equivalent expressions referred to the  $abc$  axes using (5.5) and similarly for the currents, the following relation can be found:

$$\begin{aligned} q &= v_\beta i_\alpha - v_\alpha i_\beta = \frac{1}{\sqrt{3}} [(v_a - v_b)i_c + (v_b - v_c)i_a + (v_c - v_a)i_b] \\ &= \frac{1}{\sqrt{3}} (v_{ab}i_c + v_{bc}i_a + v_{ca}i_b) \end{aligned} \quad (5.27)$$

Note that  $q$ , on the  $\alpha\beta$  reference frames, is defined as the sum of products of voltages and currents on different axes. Likewise, the imaginary power  $q$ , when calculated directly from the  $abc$  phase voltages and line currents, results from the sum of products of line voltages and line currents in different phases. This expression is similar to that implemented in some instruments for measuring the three-phase reactive power. The difference is that voltage and current phasors are used in those instruments. Here, instantaneous values of voltage and current are used instead.

At this point, the following important remark can be made. The imaginary power  $q$  is proportional to the quantity of energy that is being exchanged between the phases of the system. As was shown, the imaginary power  $q$  does not contribute to the total energy flow between the source and the load, and vice-versa.

Figure 5.3 shows the above explanation about the real and imaginary power. It is important to note that in the conventional power theory, reactive power was derived as a component of the instantaneous (active) power that has an average value equal to zero. Here, it is not so. The imaginary power means a sum of products of instantaneous three-phase voltage and current portions that do not contribute to the energy transfer between two sub-systems at any time. The term "instantaneous reactive power" is used as a synonym of the instantaneous imaginary power and therefore having the same physical meaning.

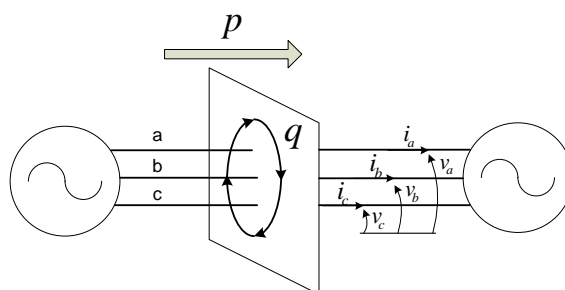


Figure 5.3. Physical meaning of the instantaneous real and imaginary powers.

For better understand the meaning of  $p$  and  $q$ , two examples will be presented for sinusoidal voltages supplying linear and nonlinear load.

### Example (5.3)

It is assumed that the voltage source is balanced and purely sinusoidal, as in (5.1), and supplying power to a three-phase balanced impedance. The line currents are as in (5.1) and transformation of these voltages and currents were calculated in example (2). By use of (5.9), real and imaginary powers are calculated:

$$\begin{aligned} p &= 3VI \cos \varphi \\ q &= 3VI \sin \varphi \end{aligned} \quad (5.28)$$

Both instantaneous powers are constant in this example. The real power  $p$  is equal to the conventional definition of the three-phase active power  $P_{3\phi}$  whereas the imaginary power  $q$  is equal to the conventional three-phase reactive power  $Q_{3\phi}$ . This example shows the correspondences between the  $p$ - $q$  theory and the conventional theory in the case of having sinusoidal balanced voltages and linear loads.

### Example (5.4)

It is assumed that the voltage source is balanced and purely sinusoidal, as in (5.1), and the load is a thyristor rectifier operating with a firing angle equal to  $30^\circ$  (Fig. 5.4). It is well known that the three phase current waveform of this system contain, besides the fundamental, harmonics on the order  $(6n \pm 1; n = 1, 2, 3, \dots)$ . The  $(6n - 1)$ th harmonics are of the negative-sequence type, whereas the  $(6n + 1)$ th harmonics are of the positive sequence type. The line currents of a six-pulse thyristor rectifier operating with a firing angle equal to  $30^\circ$  can be represented as:

$$\begin{aligned}
 i_a(t) &= \sqrt{2} I_1 \cos(\omega t - \varphi) - \sqrt{2} I_5 \cos(5\omega t - \varphi) + \sqrt{2} I_7 \cos(7\omega t - \varphi) \\
 i_b(t) &= \sqrt{2} I_1 \cos\left(\omega t - \frac{2\pi}{3} - \varphi\right) - \sqrt{2} I_5 \cos\left(5\omega t + \frac{2\pi}{3} - \varphi\right) + \sqrt{2} I_7 \cos\left(7\omega t - \frac{2\pi}{3} - \varphi\right) \\
 i_c(t) &= \sqrt{2} I_1 \cos\left(\omega t + \frac{2\pi}{3} - \varphi\right) - \sqrt{2} I_5 \cos\left(5\omega t - \frac{2\pi}{3} - \varphi\right) + \sqrt{2} I_7 \cos\left(7\omega t + \frac{2\pi}{3} - \varphi\right)
 \end{aligned} \tag{5.29}$$

These currents can be transformed to the  $\alpha\beta$ -reference frame as given by:

$$\begin{aligned}
 i_\alpha(t) &= \sqrt{3} I_1 \cos(\omega t - \varphi) - \sqrt{3} I_5 \cos(5\omega t - \varphi) + \sqrt{3} I_7 \cos(7\omega t - \varphi) \\
 i_\beta(t) &= \sqrt{3} I_1 \sin(\omega t - \varphi) + \sqrt{3} I_5 \sin(5\omega t - \varphi) + \sqrt{3} I_7 \sin(7\omega t - \varphi)
 \end{aligned} \tag{5.30}$$

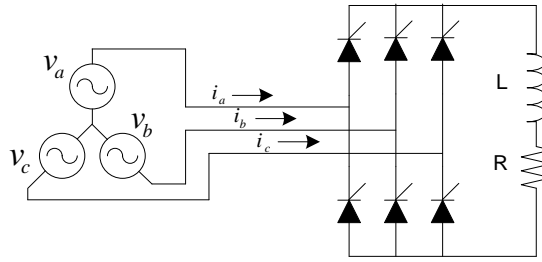


Figure 5.4. Three-phase voltage source supplying a thyristor rectifier.

by use of (5.9),  $p$  and  $q$  are calculated as follow:

$$\begin{aligned}
 p &= 3VI_1 \cos(-\varphi) - 3VI_5 \cos(6\omega t - \varphi) + 3V I_7 \cos(6\omega t - \varphi) \\
 q &= -3VI_1 \sin(-\varphi) - 3V I_5 \sin(6\omega t - \varphi) - 3V I_7 \sin(6\omega t - \varphi)
 \end{aligned} \tag{5.31}$$

The instantaneous input power at the ac side of the rectifier is equal to the output power at the DC side if there are no losses in the rectifier. The imaginary power is only defined for AC multi-phase circuits, so it can be only calculated at the AC side. These two powers have constant values superposed by oscillating components. Therefore, it is interesting to separate  $p$  and  $q$  in two parts:

$$\begin{aligned}
 \text{real power:} & \quad p = \bar{p} + \tilde{p} \\
 \text{imaginary power:} & \quad q = \bar{q} + \tilde{q}
 \end{aligned} \tag{5.32}$$

Where  $\bar{p}$  and  $\tilde{p}$  represent the average and oscillating parts of  $p$ ;  $\bar{q}$  and  $\tilde{q}$  represent the average and oscillating parts of  $q$ .

The real power  $p$  represents the total (three-phase) energy flow per time unity in the circuit. The average value  $\bar{p}$  represents the energy flowing per time unity in one direction only. If  $\bar{p}$  and  $\bar{q}$  are calculated in terms of  $abc$ -components, from (5.1), and (5.28), they result in

$$\begin{aligned}
 \bar{p} &= 3VI_1 \cos \varphi \\
 \bar{q} &= 3VI_1 \sin \varphi
 \end{aligned} \tag{5.33}$$

As one can see, these are the same results of calculating in  $\alpha\beta$ -reference frame. The oscillating part  $\tilde{p}$  represents the oscillating energy flow per time unity, which naturally produces zero average value, representing an amount of additional energy flowing in the system without effective contribution to the energy transfer from the source to the load or from the load to the source. The oscillating parts were calculated in the last example in  $\alpha\beta$ -reference frame are:

$$\begin{aligned}\tilde{p} &= 3V(-I_5 + I_7) \cos(6\omega t - \varphi) \\ \tilde{q} &= -3V(I_5 + I_7) \sin(6\omega t - \varphi)\end{aligned}\quad (5.34)$$

Note that in this example the real and imaginary powers have only an oscillating component at six times the line frequency.

### 5.3. The $p$ - $q$ Powers for Non-Sinusoidal Cases

#### 5.3.1. The zero-sequence power in a three-phase system

To understand the nature of the zero-sequence power, it is considered a three-phase sinusoidal voltage source with positive- and zero-sequence voltages at the angular frequency. The symmetrical components of this voltage source are calculated based on their phasors. Although this analysis is valid only for the steady-state condition, it is very elucidating. These symmetrical components are then transformed back to the time domain and rewritten as time functions as:

$$\begin{aligned}v_a &= \sqrt{2}V_+ \cos(\omega t + \varphi_{v+}) + \sqrt{2}V_0 \cos(\omega t + \varphi_{v0}) \\ v_b &= \sqrt{2}V_+ \cos(\omega t - 2\pi/3 + \varphi_{v+}) + \sqrt{2}V_0 \cos(\omega t + \varphi_{v0}) \\ v_c &= \sqrt{2}V_+ \cos(\omega t + 2\pi/3 + \varphi_{v+}) + \sqrt{2}V_0 \cos(\omega t + \varphi_{v0})\end{aligned}\quad (5.35)$$

It is assumed that the current also has positive- and zero-sequence components, that is,

$$\begin{aligned}i_a &= \sqrt{2}I_+ \cos(\omega t + \varphi_{i+}) + \sqrt{2}I_0 \cos(\omega t + \varphi_{i0}) \\ i_b &= \sqrt{2}I_+ \cos(\omega t - 2\pi/3 + \varphi_{i+}) + \sqrt{2}I_0 \cos(\omega t + \varphi_{i0}) \\ i_c &= \sqrt{2}I_+ \cos(\omega t + 2\pi/3 + \varphi_{i+}) + \sqrt{2}I_0 \cos(\omega t + \varphi_{i0})\end{aligned}\quad (5.36)$$

Applying the Clarke transformation, the following voltages and currents on the  $\alpha\beta 0$  reference frames are obtained:

$$\begin{aligned}v_\alpha &= \sqrt{3}V_+ \cos(\omega t + \varphi_{v+}) \\ v_\beta &= \sqrt{3}V_+ \sin(\omega t + \varphi_{v+}) \\ v_0 &= \sqrt{6}V_0 \cos(\omega t + \varphi_{v0})\end{aligned}\quad (5.37)$$

and

$$\begin{aligned}i_\alpha &= \sqrt{3}I_+ \cos(\omega t + \varphi_{i+}) \\ i_\beta &= \sqrt{3}I_+ \sin(\omega t + \varphi_{i+}) \\ i_0 &= \sqrt{6}I_0 \cos(\omega t + \varphi_{i0})\end{aligned}\quad (5.38)$$

Since the real and imaginary powers defined by (5.31) depend only on the positive-sequence voltage and current, these powers are similar in content and in meaning to those analyzed in the previous section. Therefore, the analysis here will be focused on the zero-sequence power  $p_0$  that is given by

$$p_0 = 3V_0 I_0 \cos(\varphi_{v0} - \varphi_{i0}) + 3V_0 I_0 \cos(2\omega t + \varphi_{v0} + \varphi_{i0}) = \bar{p}_0 + \tilde{p}_0 \quad (5.39)$$

This power has the same characteristics as the instantaneous power in a single phase circuit. It has an average value and an oscillating component at twice the line frequency. The average value  $\bar{p}_0$  represents a unidirectional energy flow. It has the same characteristics as the conventional (average) active power. The oscillating component  $\tilde{p}_0$  also transfers energy instantaneously. However, it has an average value equal to zero, because it is oscillating. The analysis shows that, in principle, the average value of the zero-sequence power helps to increase the total energy transfer, and in this sense, it can be considered as appositive point. However, even for the simplest case of a zero-sequence component in the voltage and current, the zero-sequence power  $p_0$  cannot produce constant power  $\bar{p}_0$  alone. In other words,  $p_0$  always consists of  $\tilde{p}_0$  plus  $\bar{p}_0$ , if  $\cos(\varphi_{v0} - \varphi_{i0}) \neq 0$ . The elimination of  $\tilde{p}_0$  is

accompanied by the elimination of  $\bar{p}_0$  together. This is one interesting characteristic of this power, and this is one of the reasons why it is not welcome in most circuits. In summary, the zero-sequence power  $p_0$  exists only if there are zero-sequence voltage and current. It is an instantaneous active power contributing to energy flow, just like in a single-phase circuit. The average zero-sequence power  $\bar{p}_0$  is always associated to the oscillating component  $\tilde{p}_0$ . Therefore, there is no way to eliminate the oscillating component and keep the average part alone.

### 5.3.2. Presence of Negative-Sequence Components

For a three-phase, balanced, positive-sequence voltage, the presence of the negative-sequence components may be a serious problem. This section will analyze the case in which the voltages are sinusoidal waveforms with a frequency of  $\omega$ , consisting of positive-, negative-, and zero-sequence components as given below:

$$\begin{aligned} v_a &= \sqrt{2}V_+ \cos(\omega t + \varphi_{v+}) + \sqrt{2}V_- \cos(\omega t + \varphi_{v-}) + \sqrt{2}V_0 \cos(\omega t + \varphi_{v0}) \\ v_b &= \sqrt{2}V_+ \cos(\omega t - 2\pi/3 + \varphi_{v+}) + \sqrt{2}V_- \cos(\omega t + 2\pi/3 + \varphi_{v-}) + \\ &\quad \sqrt{2}V_0 \cos(\omega t + \varphi_{v0}) \\ v_c &= \sqrt{2}V_+ \cos(\omega t + 2\pi/3 + \varphi_{v+}) + \sqrt{2}V_- \cos(\omega t - 2\pi/3 + \varphi_{v-}) + \\ &\quad \sqrt{2}V_0 \cos(\omega t + \varphi_{v0}) \end{aligned} \quad (5.40)$$

and the current consist of

$$\begin{aligned} i_a &= \sqrt{2}I_+ \cos(\omega t + \varphi_{i+}) + \sqrt{2}I_- \cos(\omega t + \varphi_{i-}) + \sqrt{2}I_0 \cos(\omega t + \varphi_{i0}) \\ i_b &= \sqrt{2}I_+ \cos(\omega t - 2\pi/3 + \varphi_{i+}) + \sqrt{2}I_- \cos(\omega t + 2\pi/3 + \varphi_{i-}) + \\ &\quad \sqrt{2}I_0 \cos(\omega t + \varphi_{i0}) \\ i_c &= \sqrt{2}I_+ \cos(\omega t + 2\pi/3 + \varphi_{i+}) + \sqrt{2}I_- \cos(\omega t - 2\pi/3 + \varphi_{i-}) + \\ &\quad \sqrt{2}I_0 \cos(\omega t + \varphi_{i0}) \end{aligned} \quad (5.41)$$

Applying the Clarke transformation yields the following voltages and currents:

$$\begin{aligned} v_\alpha &= \sqrt{3}V_+ \cos(\omega t + \varphi_{v+}) + \sqrt{3}V_- \cos(\omega t + \varphi_{v-}) \\ v_\beta &= \sqrt{3}V_+ \sin(\omega t + \varphi_{v+}) - \sqrt{3}V_- \sin(\omega t + \varphi_{v-}) \\ v_0 &= \sqrt{6}V_0 \cos(\omega t + \varphi_{v0}) \end{aligned} \quad (5.42)$$

and

$$\begin{aligned} i_\alpha &= \sqrt{3}I_+ \cos(\omega t + \varphi_{i+}) + \sqrt{3}I_- \cos(\omega t + \varphi_{i-}) \\ i_\beta &= \sqrt{3}I_+ \sin(\omega t + \varphi_{i+}) - \sqrt{3}I_- \sin(\omega t + \varphi_{i-}) \\ i_0 &= \sqrt{6}I_0 \cos(\omega t + \varphi_{i0}) \end{aligned} \quad (5.43)$$

The zero-sequence voltage and current are the same as those in the previous case; the zero-sequence power is equal to that in the previous case. Nothing changed in it due to the presence of negative-sequence components, as expected. On the other hand, the real and imaginary powers changed considerably. The powers given below are separated in their average and oscillating components:

$$\begin{aligned} \bar{p} &= 3V_+I_+ \cos(\varphi_{v+} - \varphi_{i+}) + 3V_-I_- \cos(\varphi_{v-} - \varphi_{i-}) \\ \bar{q} &= 3V_+I_+ \sin(\varphi_{v+} - \varphi_{i+}) - 3V_-I_- \sin(\varphi_{v-} - \varphi_{i-}) \\ \tilde{p} &= 3V_+I_- \cos(2\omega t + \varphi_{v+} + \varphi_{i-}) + 3V_-I_+ \cos(2\omega t + \varphi_{v-} + \varphi_{i+}) \\ \tilde{q} &= 3V_+I_- \sin(2\omega t + \varphi_{v+} + \varphi_{i-}) - 3V_-I_+ \sin(2\omega t + \varphi_{v-} + \varphi_{i+}) \end{aligned} \quad (5.44)$$

The following conclusions can be written from the above equations for the real and imaginary powers:

- The positive- and negative-sequence components in voltages and currents may contribute to the average real and imaginary powers.
- The instantaneous real and imaginary powers contain oscillating components due to the cross product of the positive-sequence voltage and the negative-sequence current, and the negative-sequence voltage and the positive-sequence current. Hence, even circuits without harmonic components may have oscillating real or imaginary powers.

### 5.3.3. General Case Including Distortions and Imbalances in the Voltages and in the Currents

This section will discuss the generalized three-phase, four-wire system including not only those components at the fundamental frequency, but also harmonics components.

General equations relating the instantaneous powers in the  $p$ - $q$  theory and the theory of symmetrical components (also called the *Fortescue components*) are valid in the steady state. The theory of symmetrical components based on phasors is valid only in the steady state. However, these general equations are fundamental in elucidating some important characteristics of the  $p$ - $q$  theory that are valid even during transients.

For the present analysis, a three-phase, four-wire system considered in the steady state has generic, but periodic, voltages and currents. They may include the fundamental component as well as harmonic components. Further, each three-phase group of phasors in a given frequency may be unbalanced, which means that it may consist of positive-, negative-, and zero-sequence components, according to the symmetrical component theory. Generic periodic voltages and currents can be decomposed into *Fourier series* as:

$$v_k(t) = \sum_{n=1}^{\infty} \sqrt{2} V_{kn} \cos(\omega_n t + \varphi_{kn}) \quad k = (a, b, c) \quad (5.45)$$

$$i_k(t) = \sum_{n=1}^{\infty} \sqrt{2} I_{kn} \cos(\omega_n t + \delta_{kn}) \quad k = (a, b, c) \quad (5.46)$$

where  $n$  indicates the harmonic order. Equations (5.45) and (5.46) can be written in terms of phasors, including the fundamental ( $n = 1$ ) and harmonic phasors, as follows:

$$\bar{V}_k = \sum_{n=1}^{\infty} V_{kn} \angle \varphi_{kn} = \sum_{n=1}^{\infty} \bar{V}_{kn} \quad k = (a, b, c) \quad (5.47)$$

$$\bar{I}_k = \sum_{n=1}^{\infty} I_{kn} \angle \delta_{kn} = \sum_{n=1}^{\infty} \bar{I}_{kn} \quad k = (a, b, c) \quad (5.48)$$

Then, the symmetrical-components transformation is applied to each  $a$ - $b$ - $c$  harmonic group of phasors of voltages or currents to determine their positive-, negative-, and zero-sequence components, that is,

$$\begin{bmatrix} \bar{V}_{+n} \\ \bar{V}_{-n} \\ \bar{V}_{0n} \end{bmatrix} = \frac{1}{3} \begin{bmatrix} 1 & \alpha & \alpha^2 \\ 1 & \alpha^2 & \alpha \\ 1 & 1 & 1 \end{bmatrix} \begin{bmatrix} \bar{V}_{an} \\ \bar{V}_{bn} \\ \bar{V}_{cn} \end{bmatrix} \quad (5.49)$$

The subscripts “0”, “+”, and “-” correspond to the zero-, positive-, and negative- sequence components, respectively. The complex number  $\alpha$  in the transformation matrix is the  $120^\circ$  phase-shift operator:

$$\alpha = 1 \angle 120^\circ = e^{j(2\pi/3)} \quad (5.50)$$

The inverse transformation of (5.49) is given by

$$\begin{bmatrix} \bar{V}_{an} \\ \bar{V}_{bn} \\ \bar{V}_{cn} \end{bmatrix} = \begin{bmatrix} 1 & 1 & 1 \\ \alpha^2 & \alpha & 1 \\ \alpha & \alpha^2 & 1 \end{bmatrix} \begin{bmatrix} \bar{V}_{+n} \\ \bar{V}_{-n} \\ \bar{V}_{0n} \end{bmatrix} \quad (5.51)$$

Equivalent functions of time can be derived from the phasors given by (5.51). Hence, rewriting the harmonic voltages in terms of symmetrical components in the time domain, yield the following expressions for the  $n$ th  $a$ - $b$ - $c$  group of harmonic voltages:

$$\begin{aligned} v_{an}(t) &= \sqrt{2}V_{+n} \cos(\omega_n t + \varphi_{+n}) + \sqrt{2}V_{-n} \cos(\omega_n t + \varphi_{-n}) + \sqrt{2}V_{0n} \cos(\omega_n t + \varphi_{0n}) \\ v_{bn}(t) &= \sqrt{2}V_{+n} \cos(\omega_n t + \varphi_{+n} - 2\pi/3) + \sqrt{2}V_{-n} \cos(\omega_n t + \varphi_{-n} + 2\pi/3) + \sqrt{2}V_{0n} \cos(\omega_n t + \varphi_{0n}) \\ v_{cn}(t) &= \sqrt{2}V_{+n} \cos(\omega_n t + \varphi_{+n} + 2\pi/3) + \sqrt{2}V_{-n} \cos(\omega_n t + \varphi_{-n} - 2\pi/3) + \sqrt{2}V_{0n} \cos(\omega_n t + \varphi_{0n}) \end{aligned} \quad (5.52)$$

Similarly, the instantaneous line currents are found to be

$$\begin{aligned} i_{an}(t) &= \sqrt{2}I_{+n} \cos(\omega_n t + \delta_{+n}) + \sqrt{2}I_{-n} \cos(\omega_n t + \delta_{-n}) + \sqrt{2}I_{0n} \cos(\omega_n t + \delta_{0n}) \\ i_{bn}(t) &= \sqrt{2}I_{+n} \cos(\omega_n t + \delta_{+n} - 2\pi/3) + \sqrt{2}I_{-n} \cos(\omega_n t + \delta_{-n} + 2\pi/3) + \sqrt{2}I_{0n} \cos(\omega_n t + \delta_{0n}) \\ i_{cn}(t) &= \sqrt{2}I_{+n} \cos(\omega_n t + \delta_{+n} + 2\pi/3) + \sqrt{2}I_{-n} \cos(\omega_n t + \delta_{-n} - 2\pi/3) + \sqrt{2}I_{0n} \cos(\omega_n t + \delta_{0n}) \end{aligned} \quad (5.53)$$

The above decomposition into symmetrical components allows the analysis of an unbalanced three-phase system as a sum of two balanced three-phase systems plus the zero-sequence component. The harmonic voltages and currents in terms of symmetrical components, as given in (5.52) and (5.53), can replace the terms in the series given in (5.45) and (5.46), respectively. If the  $\alpha\beta 0$  transformation is applied, the following expressions for the generic voltage and current transformed in the  $\alpha\beta 0$  reference frames can be obtained:

$$\begin{aligned} v_\alpha(t) &= \sum_{n=1}^{\infty} \sqrt{3}V_{+n} \cos(\omega_n t + \varphi_{+n}) + \sum_{n=1}^{\infty} \sqrt{3}V_{-n} \cos(\omega_n t + \varphi_{-n}) \\ v_\beta(t) &= \sum_{n=1}^{\infty} \sqrt{3}V_{+n} \sin(\omega_n t + \varphi_{+n}) - \sum_{n=1}^{\infty} \sqrt{3}V_{-n} \sin(\omega_n t + \varphi_{-n}) \\ v_0(t) &= \sum_{n=1}^{\infty} \sqrt{6}V_{0n} \cos(\omega_n t + \varphi_{0n}) \end{aligned} \quad (5.54)$$

and

$$\begin{aligned} i_\alpha(t) &= \sum_{n=1}^{\infty} \sqrt{3}I_{+n} \cos(\omega_n t + \delta_{+n}) + \sum_{n=1}^{\infty} \sqrt{3}I_{-n} \cos(\omega_n t + \delta_{-n}) \\ i_\beta(t) &= \sum_{n=1}^{\infty} \sqrt{3}I_{+n} \sin(\omega_n t + \delta_{+n}) - \sum_{n=1}^{\infty} \sqrt{3}I_{-n} \sin(\omega_n t + \delta_{-n}) \\ i_0(t) &= \sum_{n=1}^{\infty} \sqrt{6}I_{0n} \cos(\omega_n t + \delta_{0n}) \end{aligned} \quad (5.55)$$

It is possible to see that the positive- and negative-sequence components contribute to the  $\alpha$ - and  $\beta$ -axis voltages and currents, whereas the 0-axis and current comprise only zero-sequence components. Further, the real power  $p$ , the imaginary power  $q$ , and the zero-sequence power  $p_0$ , as defined in (5.31), can be calculated by using the generic voltages and currents in terms of symmetrical components given by (5.54) and (5.55).

The relation between the conventional concepts of powers and the new powers defined in the  $p$ - $q$  theory is better visualized if the powers  $p$ ,  $q$ , and  $p_0$  are separated in their average values  $\bar{p}, \bar{q}, \bar{p}_0$  and their oscillating parts  $\tilde{p}, \tilde{q}, \tilde{p}_0$ .

$$\begin{aligned} \text{Real power:} \quad p &= \bar{p} + \tilde{p} \\ \text{Imaginary power:} \quad q &= \bar{q} + \tilde{q} \\ \text{Zero-sequence power:} \quad p_0 &= \bar{p}_0 + \tilde{p}_0 \end{aligned} \tag{5.56}$$

The resulting power expressions are as follows:

$$\bar{p}_0 = \sum_{n=1}^{\infty} 3V_{0n} I_{0n} \cos(\varphi_{0n} - \delta_{0n}) \tag{5.57}$$

$$\bar{p} = \sum_{n=1}^{\infty} 3V_{+n} I_{+n} \cos(\varphi_{+n} - \delta_{+n}) + \sum_{n=1}^{\infty} 3V_{-n} I_{-n} \cos(\varphi_{-n} - \delta_{-n}) \tag{5.58}$$

$$\bar{q} = \sum_{n=1}^{\infty} 3V_{+n} I_{+n} \sin(\varphi_{+n} - \delta_{+n}) + \sum_{n=1}^{\infty} -3V_{-n} I_{-n} \sin(\varphi_{-n} - \delta_{-n}) \tag{5.59}$$

$$\begin{aligned} \tilde{p}_0 &= \left\{ \sum_{\substack{m=1 \\ m \neq n}}^{\infty} \left[ \sum_{n=1}^{\infty} 3V_{0m} I_{0n} \cos((\omega_m - \omega_n)t + \varphi_{0m} - \delta_{0n}) \right] \right. \\ &\quad \left. + \sum_{m=1}^{\infty} \left[ \sum_{n=1}^{\infty} -3V_{0m} I_{0n} \cos((\omega_m + \omega_n)t + \varphi_{0m} + \delta_{0n}) \right] \right\} \end{aligned} \tag{5.60}$$

$$\begin{aligned} \tilde{p} &= \left\{ \sum_{\substack{m=1 \\ m \neq n}}^{\infty} \left[ \sum_{n=1}^{\infty} 3V_{+m} I_{+n} \cos((\omega_m - \omega_n)t + \varphi_{+m} - \delta_{+n}) \right] \right. \\ &\quad + \sum_{\substack{m=1 \\ m \neq n}}^{\infty} \left[ \sum_{n=1}^{\infty} 3V_{-m} I_{-n} \cos((\omega_m - \omega_n)t + \varphi_{-m} - \delta_{-n}) \right] \\ &\quad + \sum_{m=1}^{\infty} \left[ \sum_{n=1}^{\infty} -3V_{+m} I_{-n} \cos((\omega_m + \omega_n)t + \varphi_{+m} + \delta_{-n}) \right] \\ &\quad \left. + \sum_{m=1}^{\infty} \left[ \sum_{n=1}^{\infty} -3V_{-m} I_{+n} \cos((\omega_m + \omega_n)t + \varphi_{-m} + \delta_{+n}) \right] \right\} \end{aligned} \tag{5.61}$$

$$\begin{aligned} \tilde{p} &= \left\{ \sum_{\substack{m=1 \\ m \neq n}}^{\infty} \left[ \sum_{n=1}^{\infty} 3V_{+m} I_{+n} \sin((\omega_m - \omega_n)t + \varphi_{+m} - \delta_{+n}) \right] \right. \\ &\quad + \sum_{\substack{m=1 \\ m \neq n}}^{\infty} \left[ \sum_{n=1}^{\infty} -3V_{-m} I_{-n} \sin((\omega_m - \omega_n)t + \varphi_{-m} - \delta_{-n}) \right] \\ &\quad + \sum_{m=1}^{\infty} \left[ \sum_{n=1}^{\infty} -3V_{+m} I_{-n} \sin((\omega_m + \omega_n)t + \varphi_{+m} + \delta_{-n}) \right] \\ &\quad \left. + \sum_{m=1}^{\infty} \left[ \sum_{n=1}^{\infty} 3V_{-m} I_{+n} \sin((\omega_m + \omega_n)t + \varphi_{-m} + \delta_{+n}) \right] \right\} \end{aligned} \tag{5.62}$$

These generic power expressions elucidate the relations between the conventional and the instantaneous concepts of active and reactive power. For instance, it is possible to see that the well-



known three-phase fundamental active power ( $P = 3VI \cos \varphi$ ) is one term of the average real power  $\bar{p}$ , whereas the three-phase reactive power ( $Q = 3VI \sin \varphi$ ) is included in the average imaginary power  $\bar{q}$ . All harmonics in voltage and current can contribute to the average powers  $\bar{p}$  and  $\bar{q}$  if they have the same frequency and have the same sequence component (positive or negative), as shown in (5.58) and (5.59). The presence of more than one harmonic frequency and/or sequence components also produce  $\tilde{p}$  and  $\tilde{q}$ , according to (5.61) and (5.62). On the other hand, the zero-sequence power  $p_0 = \bar{p}_0 + \tilde{p}_0$ , that is, the sum of (5.57) and (5.60), always has the average part associated with an oscillating part  $\tilde{p}_0$ . Therefore, if the oscillating part is eliminated by a compensator, this compensator should be able to also deal with the average part  $\bar{p}_0$  that may be present.

### References:

- [1] H. Akagi, Y. Kanazawa, and A. Nabae, "Generalized Theory of Instantaneous Reactive Power and Its Applications", *Transactions of the IEE-Japan*, Part B, vol. 103, no.7, pp. 483-490, 1983 (in Japanese).
- [2] H. Akagi, E. H. Watanabe and M. Aredes, "Instantaneous Power Theory and Applications to Power Conditioning", IEEE Press / Wiley Interscience, 2007.
- [3] W.V. Lyon, "Reactive Power and Unbalanced Circuits", *Electrical World*, vol. 75, no. 25, pp. 1417-1420, 1920.
- [4] C.I. Budeanu, "Puissances reactives et fictives", Instytut Romain de l'Energie, pub. no. 2, Bucharest, 1927.
- [5] C.I. Budeanu, "The Different Options and Conceptions Regarding Active Power in Non-sinusoidal Systems", Instytut Romain de l'Energie, pub. no. 4, Bucharest, 1927.
- [6] S. Fryze, "Wirk-, Blind- und Scheinleistung in elektrischen Stromkreisen mit nicht-sinusformigem Verlauf von Strom und Spannung," *ETZ-Arch. Elektrotech.*, vol. 53, pp. 596-599, 625-627, 700-702, 1932.
- [7] L.s. Czarnecki, "What is wrong with the Budeanu concept of reactive and distortion power and why it should be abandoned", *IEEE Trans. Instr. Meas.*, vol. IM-36, No.3, pp. 834-837, Sep. 1987.
- [8] E. Clarke, *Circuit Analysis of A-C Power Systems*, vol. 1, Symmetrical and Related Components, New York: John Wiley and Sons, 1943.
- [9] Y. Xu, L. M. Tolbert, F. Z. Peng, J. N. Chiasson, J. Chen, "Compensation-based non-active power definition", *IEEE Power Electronics Letters*, vol. 1, no. 2, pp. 45-50, June 2003.
- [10] X. Yan, L.M. Tolbert, and J.D. Kueck, "Voltage and Current Unbalance Compensation Using a Parallel Active Filter", *Proc. of Power Electronics Specialists Conf. (PESC)*, 2007, pp. 2919 – 2925.
- [11] H. Akagi, Y. Kanazawa, and A. Nabae, "Instantaneous reactive power compensators comprising switching devices without energy storage components," *IEEE Trans. Ind. Appl.*, vol. IA-20, pp. 625-631, 1984.

## VI. COMPENSATION

### 6.1. Harmonic and Reactive Power Compensation

The reactive and harmonic compensation is carried by absorb or inject appropriate currents into the circuit through a compensator i.e., shunt active filter as shown in Fig. 6.1. This figure shows a basic compensation scheme of the instantaneous reactive power. Where  $p_s$  and  $q_s$  are the instantaneous real and imaginary powers on the source side,  $p_c$  and  $q_c$  are those on the compensator side,  $p$  and  $q$  are those on the load side. The reactive power compensator eliminates the instantaneous reactive powers on the source side, which are caused by the instantaneous imaginary power on the load side. The compensator consists of only switching devices without energy storage components, because  $p_c$  is always zero [1].

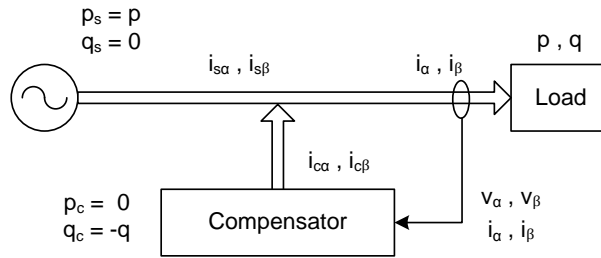


Figure 6.1. Compensation general schematic shown by  $p$ - $q$  theory in  $\alpha\beta$  reference frame

When voltage and current are represented by  $v$  and  $i$  for compensation of the objective load, the real part  $p$  and imaginary part  $q$  of the multi phase circuit instantaneous power are expressed by the following equations:

$$\begin{aligned} p &= v_{\alpha}i_{\alpha} + v_{\beta}i_{\beta} \\ q &= v_{\beta}i_{\alpha} - v_{\alpha}i_{\beta} \end{aligned} \quad (6.1)$$

From the above equations, the fundamental component of load current for both the real part and imaginary part of the instantaneous power gets equal to  $\bar{p}$  and  $\bar{q}$ , the DC components whose magnitudes are constant and harmonics component equals the ripple components  $\tilde{p}$  and  $\tilde{q}$ . Thus, if two-phase coordinate load current  $i_{\alpha}$  and  $i_{\beta}$  are expressed with the instantaneous power divided into respective component, the following equations will result:

$$\begin{aligned} i_{\alpha} &= \frac{v_{\alpha}}{v_{\alpha}^2 + v_{\beta}^2} \bar{p} + \frac{v_{\beta}}{v_{\alpha}^2 + v_{\beta}^2} \bar{q} + \frac{v_{\alpha}}{v_{\alpha}^2 + v_{\beta}^2} \tilde{p} + \frac{v_{\beta}}{v_{\alpha}^2 + v_{\beta}^2} \tilde{q} \\ i_{\beta} &= \frac{v_{\beta}}{v_{\alpha}^2 + v_{\beta}^2} \bar{p} + \frac{-v_{\alpha}}{v_{\alpha}^2 + v_{\beta}^2} \bar{q} + \frac{v_{\beta}}{v_{\alpha}^2 + v_{\beta}^2} \tilde{p} + \frac{-v_{\alpha}}{v_{\alpha}^2 + v_{\beta}^2} \tilde{q} \end{aligned} \quad (6.2)$$

where  $\bar{p}$  and  $\tilde{p}$  are the DC and AC components of the instantaneous real power and  $\bar{q}$  and  $\tilde{q}$  are the DC and AC components of the instantaneous imaginary power. The first term of the right hand side of (6.2) is the instantaneous value of the conventional fundamental active current. The second term is the instantaneous value of the conventional fundamental reactive current. The third term is the instantaneous value of the harmonic currents which represents the AC component of the instantaneous real power. The fourth term is the instantaneous value of the harmonic currents which represents the AC component of the instantaneous imaginary power. Accordingly, the sum of the third and fourth terms is the instantaneous value of the conventional harmonic currents. The instantaneous reactive power compensator eliminates both the second and fourth terms. For this reason, the displacement factor is unity not only in steady states but also in transient states [2].

From (5.11), the instantaneous compensating currents on the  $\alpha\beta$  coordinates,  $i_{c\alpha}$  and  $i_{c\beta}$  are given by,

$$\begin{bmatrix} i_{c\alpha} \\ i_{c\beta} \end{bmatrix} = \frac{1}{v_\alpha^2 + v_\beta^2} \begin{bmatrix} v_\alpha & v_\beta \\ v_\beta & -v_\alpha \end{bmatrix} \begin{bmatrix} 0 \\ -q \end{bmatrix} \quad (6.3)$$

In this stage, if the current which is expressed by the following equations can be supplied to the power system from the compensator:

$$\begin{aligned} i_{c\alpha} &= \frac{-v_\beta}{v_\alpha^2 + v_\beta^2} q \\ i_{c\beta} &= \frac{v_\alpha}{v_\alpha^2 + v_\beta^2} q \end{aligned} \quad (6.4)$$

the result will be:

$$\begin{aligned} i_{s\alpha} &= i_\alpha + i_{c\alpha} = \frac{v_\alpha}{v_\alpha^2 + v_\beta^2} \bar{p} + \frac{v_\alpha}{v_\alpha^2 + v_\beta^2} \tilde{p} \\ i_{s\beta} &= i_\beta + i_{c\beta} = \frac{v_\beta}{v_\alpha^2 + v_\beta^2} \bar{p} + \frac{v_\beta}{v_\alpha^2 + v_\beta^2} \tilde{p} \end{aligned} \quad (6.5)$$

As this is clear in above equation, the reactive components are compensated but the harmonic components still exist.

Likewise, if  $\tilde{p}$  and  $\tilde{q}$  components of the compensator current are controlled and supplied to the power system, as the third term and fourth term of (6.2) are deleted, source currents  $i_{s\alpha}$  and  $i_{s\beta}$  will become fundamental components which do not contain harmonics component, thus allowing the equipment to act as an active filter:

$$\begin{aligned} i_{c\alpha} &= \frac{-v_\alpha}{v_\alpha^2 + v_\beta^2} \tilde{p} + \frac{-v_\beta}{v_\alpha^2 + v_\beta^2} \tilde{q} \\ i_{c\beta} &= \frac{-v_\beta}{v_\alpha^2 + v_\beta^2} \tilde{p} + \frac{v_\alpha}{v_\alpha^2 + v_\beta^2} \tilde{q} \end{aligned} \quad (6.6)$$

the following will be resulted:

$$\begin{aligned} i_{s\alpha} &= i_\alpha + i_{c\alpha} = \frac{v_\alpha}{v_\alpha^2 + v_\beta^2} \bar{p} + \frac{v_\beta}{v_\alpha^2 + v_\beta^2} \bar{q} \\ i_{s\beta} &= i_\beta + i_{c\beta} = \frac{v_\beta}{v_\alpha^2 + v_\beta^2} \bar{p} + \frac{-v_\alpha}{v_\alpha^2 + v_\beta^2} \bar{q} \end{aligned} \quad (6.7)$$

Finally if the current expressed by the following equations can be supplied to the power system from the compensator:

$$\begin{aligned} i_{c\alpha} &= \frac{-v_\alpha}{v_\alpha^2 + v_\beta^2} \tilde{p} + \frac{-v_\beta}{v_\alpha^2 + v_\beta^2} (\bar{q} + \tilde{q}) \\ i_{c\beta} &= \frac{-v_\beta}{v_\alpha^2 + v_\beta^2} \tilde{p} + \frac{v_\alpha}{v_\alpha^2 + v_\beta^2} (\bar{q} + \tilde{q}) \end{aligned} \quad (6.8)$$

the result will be:

$$\begin{aligned} i_{s\alpha} &= i_{\alpha} + i_{c\alpha} = \frac{v_{\alpha}}{v_{\alpha}^2 + v_{\beta}^2} \bar{p} \\ i_{s\beta} &= i_{\beta} + i_{c\beta} = \frac{v_{\beta}}{v_{\alpha}^2 + v_{\beta}^2} \bar{p} \end{aligned} \quad (6.9)$$

This means that the effective fundamental component current only flows and the latter can be improved into a sinusoidal waveform current by power factor 1, that is, an equipment compensating for harmonics and reactive power is feasible.

## 6.2. Shunt Active Filter For Harmonic And Reactive Compensation

The shunt active filter for load current compensation, as shown in Fig. 6.2, is one of the most common active filters. The controller of this system consists of four functional control blocks:

- 1- Instantaneous power calculation; this block calculates the instantaneous powers of the nonlinear load. According to the  $p-q$  theory, in this system only the real and imaginary powers exist, because the zero-sequence power is zero.
- 2- Power compensating selection; this block determines the behavior of the shunt active filter. It means, the block selects the parts of the real and imaginary powers of the nonlinear load that should be compensated by the shunt active filter.
- 3- DC-voltage regulator; this block determines an extra amount of real power, represented by  $\bar{p}_{loss}$  in Fig. 6.2, that causes an additional flow of energy to the DC capacitor in order to keep its voltage around a fixed reference value. This real power  $\bar{p}_{loss}$  is added to the compensating real power  $p_c$ , which together with the compensating imaginary power  $q_c$ , are passed to the current reference calculation block.
- 4- Current reference calculation; this block determines the instantaneous compensating current references from the compensating powers and voltages.

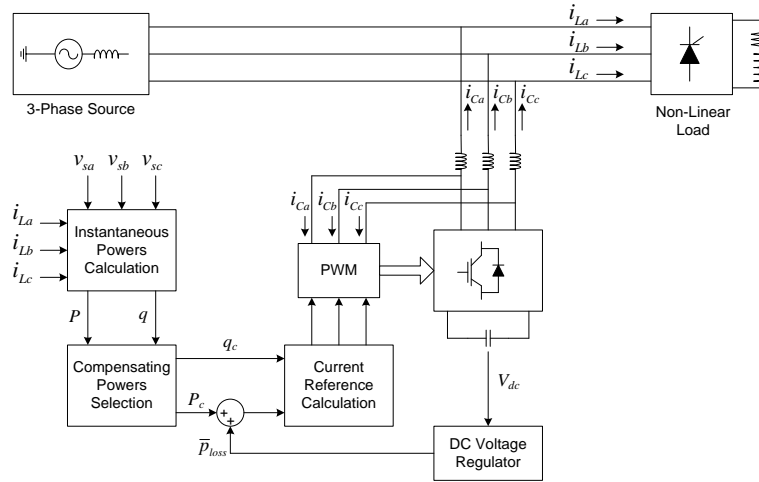


Figure 6.2. Basic configuration of shunt active filter and control blocks.

In order to compensate reactive power, shunt active filter should filter the portion of load current that produce imaginary power. In this case, it should compensate the instantaneous reactive currents that are mentioned in (6.4). On the other case, the shunt active filter should supply the oscillating portion of the instantaneous active current of the load in order to draw a constant instantaneous power from source, that is,

$$\begin{aligned} i_{\alpha\bar{p}} &= \frac{v_{\alpha}}{v_{\alpha}^2 + v_{\beta}^2} (-\bar{p}) \\ i_{\beta\bar{p}} &= \frac{v_{\beta}}{v_{\alpha}^2 + v_{\beta}^2} (-\bar{p}) \end{aligned} \quad (6.10)$$

The reason for adding a minus sign to the real power in the above equation is to match them with the current directions adopted in Fig. 6.2 in order to compensate  $(-\tilde{p})$ , which implies an oscillating flow of energy, the DC capacitor of the PWM converter must be made large enough to behave as an energy storage element. If the shunt active filter compensates the oscillating real and imaginary power of the load, it guarantees that only a constant real power  $\bar{p}$  (average real power of the load) is drawn from the power system. Therefore as mentioned before, harmonic currents will be compensated.

A DC-voltage regulator should be added to the control strategy, as shown in Fig. 6.2. In fact, a small amount of average real power ( $\bar{p}_{loss}$ ), must be drawn continuously from the power system to supply switching and ohmic losses in the converter. Otherwise, this energy would be supplied by the DC capacitor, which would discharge continuously.

As shown in Fig. 6.3, the real power of the nonlinear load should be continuously measured, and somehow “instantaneously” separated into its average ( $\bar{p}$ ) and oscillating ( $\tilde{p}$ ) parts. This would be the function of the block named “powers-compensating selection” in Fig. 6.2. In a real implementation, the separation of  $\bar{p}$  and  $\tilde{p}$  from  $p$  is realized through a Low-Pass Filter (LPF). The oscillating real power is determined by the difference, that is,  $\tilde{p} = p - \bar{p}$ .

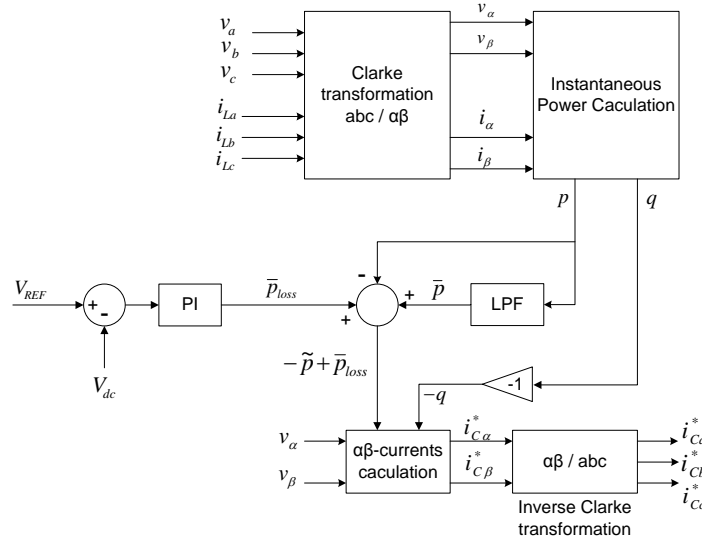


Figure 6.3. Control block for the constant instantaneous power control strategy.

Figure 6.3 summarizes the complete algorithm of a controller that compensates the oscillating real power and the imaginary power of the load. In this case, only the fundamental positive-sequence component of the load current ( $I_{+1}$ ) can produce the constant real power. If the supply voltage were unbalanced and/or distorted, the compensated current would not be sinusoidal, and would not draw constant real power.

### 6.3. Unbalancing

The sinusoidal source current control strategy is a compensation method that makes the active filter compensate the current of a nonlinear load to force the compensated source current to become sinusoidal and balanced. In order to make the compensated current sinusoidal and balanced, the shunt active filter should compensate all harmonic components as well as the fundamental components that differ from the fundamental positive-sequence current  $I_{+1}$ . Only this component is left to be supplied by the source. In order to determine the fundamental positive-sequence component of the load current, a positive-sequence detector is needed in the active filter controller. The control block diagram for the sinusoidal current control strategy is shown in Fig. 6.4 if compared with the control block diagram of the harmonic and reactive power compensation (Fig. 6.3), the unique difference is the insertion of a positive-sequence detector block, which extracts “instantaneously” the fundamental positive-sequence voltages  $v'_a$ ,  $v'_b$  and  $v'_c$  that correspond to the phasor  $V_{+1}$  of the system voltage  $v_a$ ,  $v_b$  and  $v_c$ . Therefore, the rest of active filter controller shown in Fig. 6.4 determines the compensating current references if the system voltage contains only a fundamental positive-sequence component.

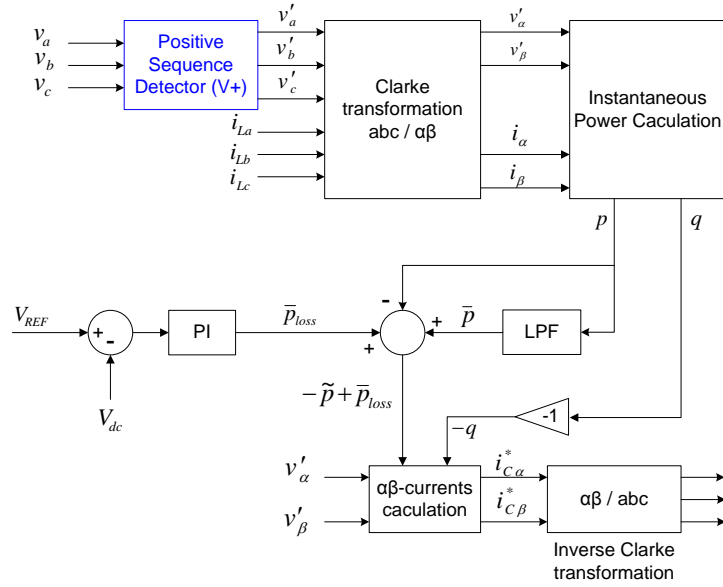


Figure 6.4. The control block diagram for the sinusoidal current control strategy.

The real and imaginary powers calculated in Fig. 6.4 do not match the actual powers of the load, because the unbalance at the fundamental frequency (fundamental negative-sequence) and harmonics, which eventually may be present in the system voltage, are not being considered. However, the calculated real and imaginary powers are still useful for determining all unbalances and harmonics present in the load current. The general equations of powers in terms of symmetrical components given in chapter 5, equations (5.55) to (5.60), are helpful for understanding this point. First, note that the instantaneous phase voltages  $v'_a$ ,  $v'_b$  and  $v'_c$  that correspond to the phasor  $V_{+1}$  of the fundamental positive-sequence voltage are transformed into the  $\alpha\beta$  coordinates by means of the Clark transformation block. Then, they are used in both the instantaneous powers calculation block and in the  $\alpha\beta$  currents calculation block. Together with the power being compensated, that is,  $-\tilde{p}$  and  $-q$ , the  $\alpha\beta$  currents calculation block determines exactly all current components in the load current that produce  $-\tilde{p}$  and  $q = \bar{q} + \tilde{q}$  with  $V_{+1}$ . In terms of symmetrical components, since only  $V_{+1}$  is being considered, only  $I_{+1}$  produces  $\bar{p}$  and  $\bar{q}$  [equations (5.55) to (5.60)]. Therefore, if the shunt active filter compensates the power portions  $\tilde{p}$  and  $\tilde{q}$  of the calculated powers  $p$  and  $q$ , certainly it is compensating all components in the load current that are different from  $I_{+1}$  of the load. Note that this includes also the fundamental negative-sequence component  $I_{-1}$ .

The positive-sequence detector that will be describe, can determine instantaneously and accurately the amplitude, the frequency, as well as the phase angle of voltage component  $V_{+1}$ . The amplitude and phase angle of  $V_{+1}$  may be necessary in other controllers, although they are not important in the control algorithm implemented in Fig. 6.4. In order to extract the fundamental negative-sequence current and all current harmonics from the load current, it is necessary only that  $v'_a$ ,  $v'_b$  and  $v'_c$  have the same frequency as the actual system voltage. The amplitude could be arbitrarily chosen but must be equal in all three phases. The phase angle could also be arbitrarily chosen, but the displacement angles between phases must be maintained equal to  $2\pi/3$ . However, in order to properly compensate the portion of the fundamental positive-sequence current that is orthogonal to the fundamental positive-sequence voltage, the phase angle and the frequency of the fundamental positive-sequence voltage  $V_{+1}$  must be accurately determined. Otherwise, the active filter controller cannot exactly determine the fundamental reactive power of the load ( $\bar{q}$ ) that, in turn, cannot produce ac currents ( $I_{+1}$ ) orthogonal to the ac voltages ( $V_{+1}$ ) to produce only  $\bar{q}$ . Fortunately, the positive-sequence voltage detector used in Fig. 6.4, as will be explained later in this section, can determine accurately the voltage component  $V_{+1}$ .

The compensating powers  $\tilde{p}$  and  $\tilde{q}$  in the active filter controller includes all fundamental negative-sequence power, the fundamental reactive power, as well as the harmonic power. In other words, the active filter controller handles the load as “connected to a sinusoidal balanced voltage source”. Thus,

if  $\tilde{p}$ ,  $\tilde{q}$ , and  $\tilde{q}$  are compensated by the shunt active filter, the source currents must be sinusoidal and contain only the active portion of the fundamental positive-sequence current that is in phase with  $V_{+1}$ .

### 6.3.1. Using phase-locked-loop in positive-sequence voltage detector

An important part of the positive-sequence detector is the phase-locked-loop (PLL) circuit. Fig. 6.5 shows the complete functional block diagram of the fundamental positive-sequence voltage detector.

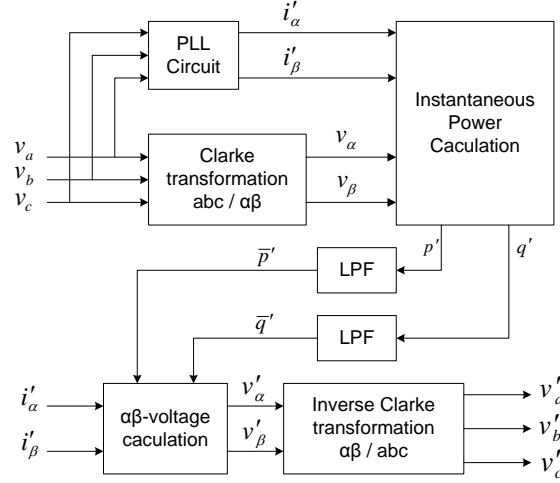


Figure 6.5. Fundamental positive-sequence voltage detector

The fundamental positive-sequence voltage detector is based on the dual  $p$ - $q$  theory and concept of voltage compensation. The voltages  $v_a$ ,  $v_b$ , and  $v_c$  are transformed into  $\alpha\beta$  axes to determine  $v_\alpha$  and  $v_\beta$ . They are used together with auxiliary currents  $i'_\alpha$  and  $i'_\beta$ , produced in PLL circuit, to calculate the auxiliary powers  $p'$  and  $q'$ , as shown in Fig. 6.5. It is assumed that the auxiliary currents  $i'_\alpha$  and  $i'_\beta$  with any magnitude are derived only from an auxiliary positive-sequence current  $I'_{+1}$  at the fundamental frequency, detected by the PLL circuit. In terms of symmetrical components, using the general equation (5.55) from chapter 5, the fundamental positive-sequence component ( $n = 1$ ) is

$$\begin{cases} i'_\alpha = \sqrt{3} I'_{+1} \cos(\omega t + \delta_{+1}) \\ i'_\beta = \sqrt{3} I'_{+1} \sin(\omega t + \delta_{+1}) \end{cases} \quad (6.11)$$

For extracting the fundamental positive-sequence voltage, the amplitude of the auxiliary currents  $i'_\alpha$  and  $i'_\beta$  are not important, and can be chosen arbitrarily. For simplicity, they are set to unity. In other words, the absolute values of the auxiliary powers  $p'$  and  $q'$ , as the auxiliary currents  $i'_\alpha$  and  $i'_\beta$ , have no physical meaning. Note that they are used together in the voltage calculation, represented by the  $\alpha\beta$  voltage calculation block in Fig. 6.5.

The phase angle  $\delta_{+1}$  of  $i'_\alpha$  and  $i'_\beta$  can also be chosen arbitrarily, because different values of  $\delta_{+1}$  vary simultaneously the auxiliary powers  $p'$  and  $q'$ , so that the results from the  $\alpha\beta$  voltage calculation block will be always the same. Again, for simplicity, they are set to zero. Only the fundamental frequency ( $\omega_1$ ) must be determined accurately by the PLL. Thus, (6.11) is simplified to form the needed auxiliary currents:

$$\begin{cases} i'_\alpha = \cos(\omega t) \\ i'_\beta = \sin(\omega t) \end{cases} \quad (6.12)$$

An important conclusion that can be drawn from the general equation (5.55) to (5.60) is useful for determining the fundamental positive-sequence component  $V_{+1}$  of the system voltages. From those equations, it is possible to see that only the fundamental positive-sequence voltage component  $V_{+1}$  contributes to the average values of the auxiliary powers  $p'$  and  $q'$ , represented by  $\bar{p}'$  and  $\bar{q}'$  in Fig. 6.5.

This is assured because (6.12) represents auxiliary currents in the  $\alpha\beta$  axes composed only from  $I_{+1}$ . The influence of the fundamental negative-sequence  $V_{-1}$  and other voltage harmonics will appear only in the oscillating components  $\tilde{p}'$  and  $\tilde{q}'$  of the auxiliary powers, which are being excluded from the inverse voltage calculation. Two fifth order butterworth low-pass filters with cutoff frequency at 50 Hz are typically used for obtaining the average powers  $\bar{p}'$  and  $\bar{q}'$ .

The  $\alpha\beta$  voltage calculation block of Fig. 6.5 calculates the instantaneous voltages  $v'_\alpha$  and  $v'_\beta$ , which correspond to time functions of the fundamental positive-sequence phasor  $V_{+1}$  of the system voltage:

$$\begin{bmatrix} v'_\alpha \\ v'_\beta \end{bmatrix} = \frac{1}{i'^2_\alpha + i'^2_\beta} \begin{bmatrix} i'_\alpha & -i'_\beta \\ i'_\beta & i'_\alpha \end{bmatrix} \begin{bmatrix} \bar{p}' \\ \bar{q}' \end{bmatrix} \quad (6.13)$$

For several applications, the transformed voltages from (6.13) are useful, and may be directly used in an active filter controller. Especially in the case of using (6.13) in a real implementation of a controller, it should be considered that, in steady state,

$$i'^2_\alpha + i'^2_\beta = \sin^2(\omega_1 t) + \cos^2(\omega_1 t) = 1 \quad (6.14)$$

and the division in (6.13) may be avoided.

If necessary, the instantaneous  $abc$  phase voltages  $v'_a$ ,  $v'_b$ , and  $v'_c$  can be calculated by applying the inverse Clarke transformation, disregarding the zero-sequence component  $v_0$ :

$$\begin{bmatrix} v'_a \\ v'_b \\ v'_c \end{bmatrix} = \sqrt{\frac{2}{3}} \begin{bmatrix} 1 & 0 \\ -1/2 & \sqrt{3}/2 \\ -1/2 & -\sqrt{3}/2 \end{bmatrix} \begin{bmatrix} v'_\alpha \\ v'_\beta \end{bmatrix} \quad (6.15)$$

Simulation results have shown that the fundamental positive-sequence voltage detector presented above has a good dynamic and a satisfactory accuracy even under nonsinusoidal conditions. The PLL circuit must provide accurately the auxiliary currents  $i'_\alpha$  and  $i'_\beta$ , corresponding to sinusoidal functions at the fundamental frequency.

#### 6.4. MATLAB Simulation Results

As will be shown below, there are some simulation results that are related to  $p$ - $q$  theory on previous sections.

##### **Example (6.1)**

Harmonic compensation of nonlinear load connected to sinusoidal balanced voltage; compensating the oscillating real and imaginary power ( $\tilde{p}$ ,  $\tilde{q}$ ). (Start to compensate at  $t=0.4$ )

This case is referred to the example (5.4). Here we assumed that three-phase voltage source is balanced and purely sinusoidal

$$\begin{cases} v_a(t) = \sqrt{2} V \cos(\omega t) \\ v_b(t) = \sqrt{2} V \cos\left(\omega t - \frac{2\pi}{3}\right) \\ v_c(t) = \sqrt{2} V \cos\left(\omega t + \frac{2\pi}{3}\right) \end{cases} \quad (6.16)$$

where  $V = 380_V$  and  $f = 50_{HZ}$

The load is a thyristor rectifier operating with firing angle equal to  $30^\circ$ . On the DC side of the rectifier there is a resistor  $R = 25_\Omega$  and inductor  $= 100_{mH}$ . Figure 6.6 shows the idealized circuit includes three-phase source, shunt active filter and thyristor rectifier as a load.



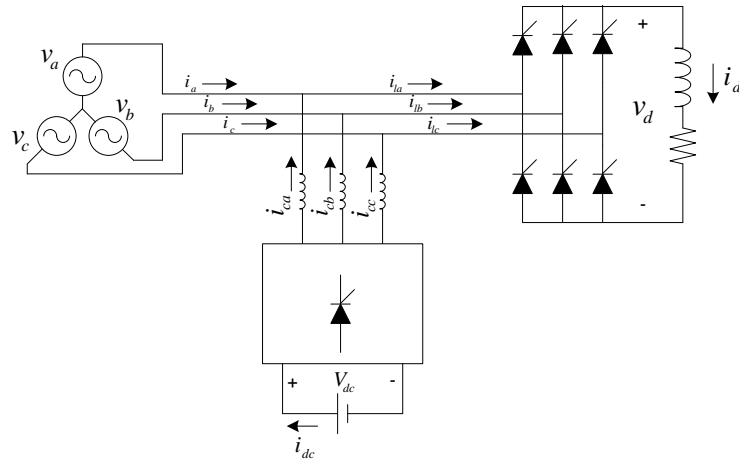


Figure 6.6. Compensating circuit configuration with nonlinear load

Figure 6.7 shows the rectifier DC output voltage waveform  $v_d$  and current waveform  $i_d$ . Figure 6.8 shows the source voltages and currents before and after harmonic compensation that is started at  $t=0.4$ sec. Figure 6.9(a) shows the  $a$ -phase voltage and current waveforms before compensation. It is clear that this current waveform contains, besides the fundamental, harmonics. Also in Fig. 6.9, three-phase voltage and current are shown together before and after compensation. One can deduce that power factor is not unit; it means that there is imaginary power  $q$  before and  $\bar{q}$  after the compensation in the system.

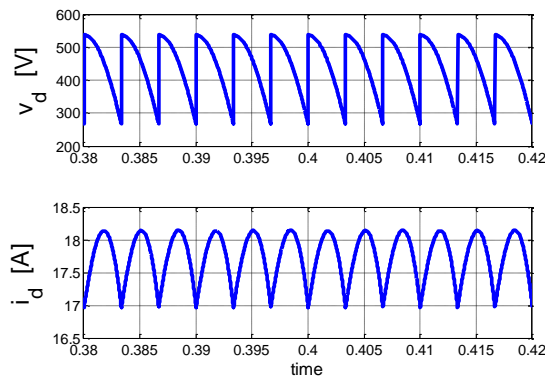


Figure 6.7. load DC link voltage and current; Thyristor with  $30^\circ$  conducting as a load

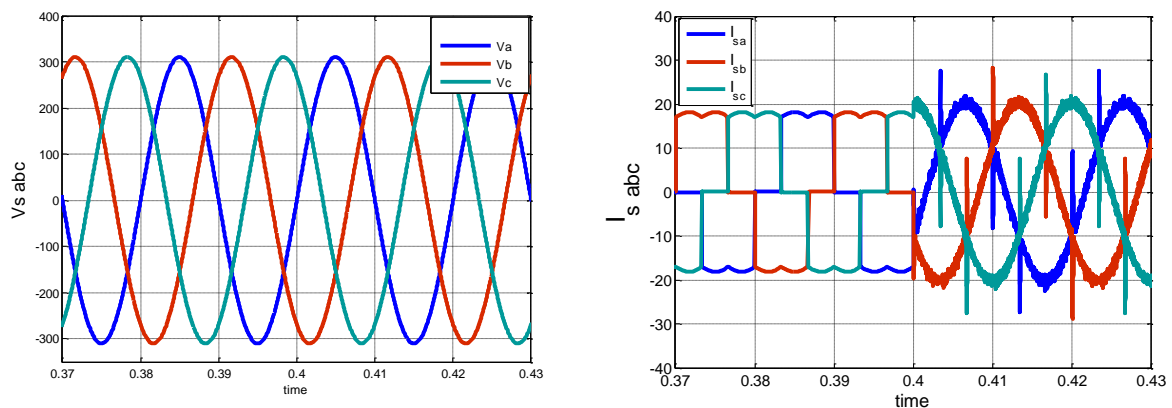


Figure 6.8. Three phase voltages and currents of source.

In order to better observation in this case, in the next figures, voltages and currents are shown in per-unit. Voltage and current base are defined as follow:

In this case we have a variac with 12kVA output as a source and the output RMS phase-to-phase voltage is  $V_s = 380$  that we consider as a base voltage. Therefore the base current can be obtained as follow:

$$I_B = \frac{S_B}{\sqrt{3}V_B} = \frac{12000}{\sqrt{3} \times 380} \approx 18 \text{ A} \quad (6.17)$$

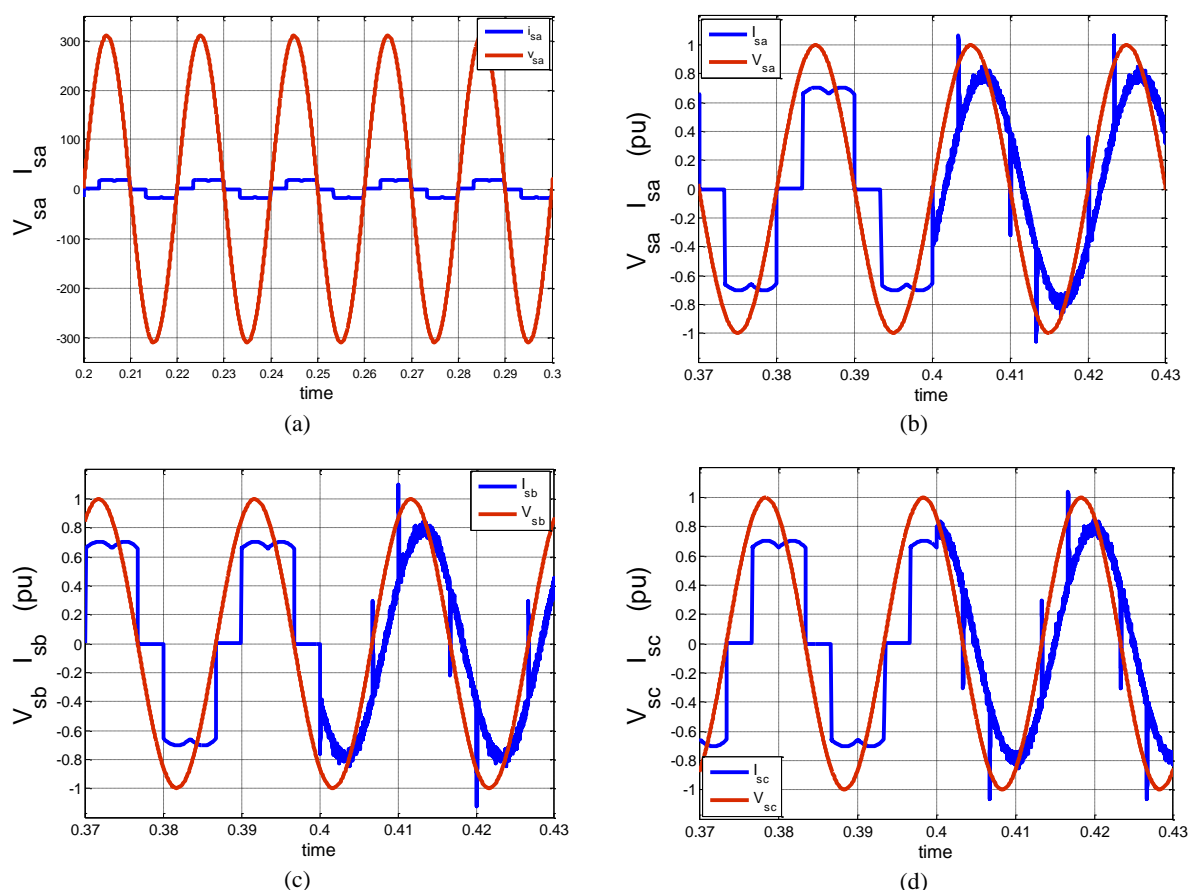


Figure 6.9. Three-phase source voltages and currents. a) phase *a* before compensation is shown by real value. b,c,d) three-phase *a,b,c* voltage and current before and after compensation, in per-unit, respectively.

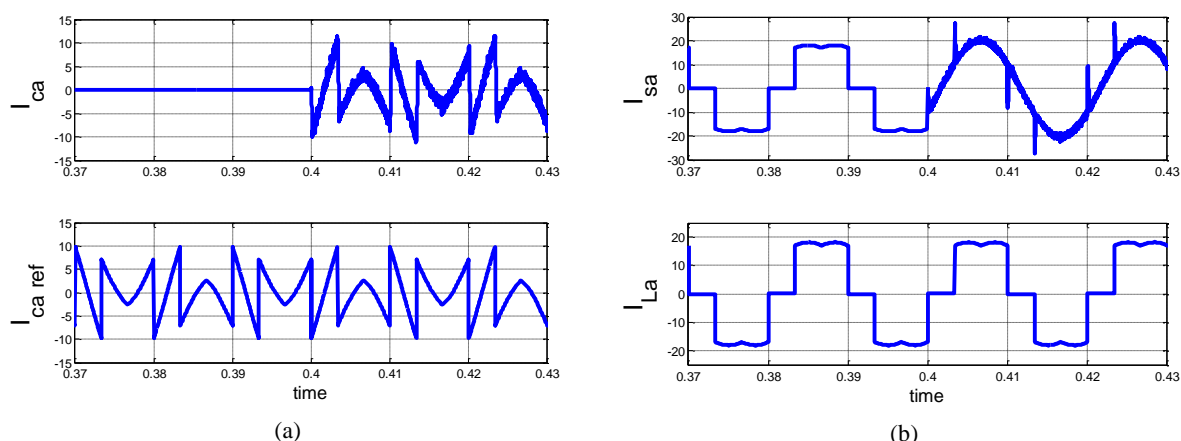


Figure 6.10. Waveforms of phase “a”; a) compensating current of shunt active filter and reference current, b) source and load currents

Figures 6.9(b), (c), (d) show the three-phase voltages and currents together in per-unit value.  $i_{a\tilde{p}}$  is the current that is responsible for producing the oscillating real power  $\tilde{p}$  and  $i_{a\tilde{q}}$  is the current that

produces the oscillating imaginary power  $\tilde{q}$ . Figure 6.10(a) shows the  $a$ -phase current that is injected from active filter to grid in order to compensate the sum of  $i_{a\tilde{p}}$  and  $i_{a\tilde{q}}$ .

### Example (6.2)

Reactive and harmonic compensation of previous example; compensating the oscillating real power ( $\tilde{p}$ ) and instantaneous imaginary power ( $q = \tilde{q} + \bar{q}$ ). In this case, compensation is done with the same circuit of the previous example. The results are shown in the following figures. Figure 6.11 shows the source currents before and after compensation that is started at  $t=0.4$ sec.

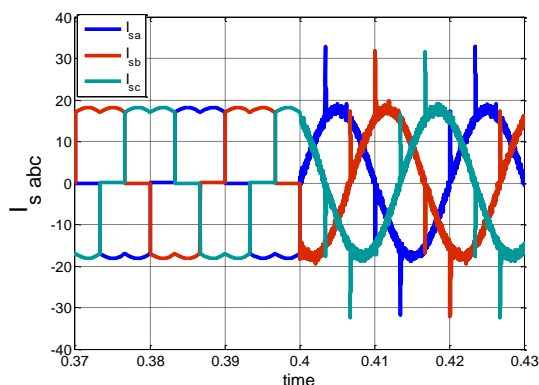


Figure 6.11. Three-phase source currents. Compensation is started at  $t=0.4$ .

Figure 6.12(a) shows the  $a$ -phase voltage and current waveforms before compensation on per-unit scale. It is clear that this current waveform contains, besides the fundamental, harmonics and reactive power. Also in Fig. 6.12, voltage and current of each phase are shown together before and after compensation. One can see that power factor becomes unit after compensation; it means that imaginary power ( $q$ ) is compensated in the system.

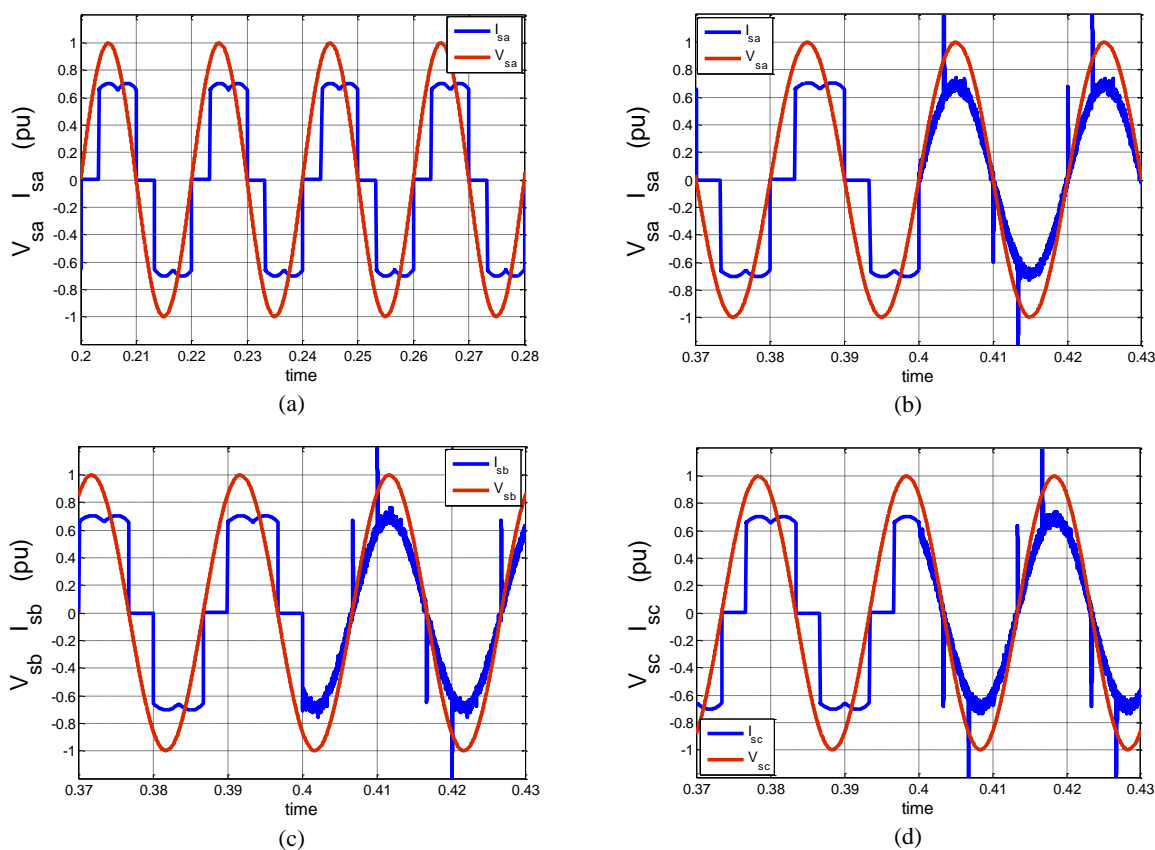


Figure 6.12. Three-phase source voltages and currents. a) phase a before compensation. b,c,d) three-phase  $a, b, c$  voltage and current before and after compensation in per-unit, respectively.

$i_{aq}$  is the current that is responsible for producing the imaginary power  $q$ . Fig. 6.13(a) shows the  $a$ -phase compensating current that is injected from active filter to the grid, in order to compensate the sum of  $i_{a\tilde{p}}$  and  $i_{aq}$ .

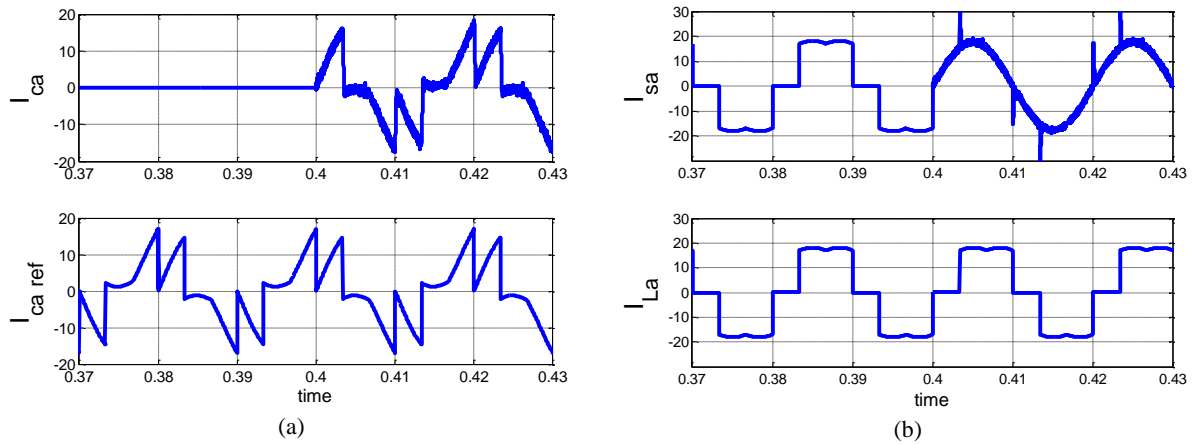


Figure 6.13. phase  $a$  waveforms; a) compensating current of shunt active filter, reference current, b) source and load currents

### Example (6.3)

Compensating unbalanced load that is connected to sinusoidal balanced voltage source (compensation is started at  $t=0.4$ ).

In this case we consider unbalanced currents load due to unbalanced load. In simulation if source and transmission lines are considered ideal and without impedance and losses (case 1), one can see the voltage on PCC point is balanced before and after compensation. If source and transmission lines are considered with impedance or losses (case 2), then voltages are unbalanced at PCC point. After compensation with shunt active filter both the unbalancing problems for voltages and currents will be solved. It means, installing compensator near to the nonlinear and unbalanced load leads to prevent load distortions and therefore protects the grid. In this example star unbalanced load is:

$$R_{la} = 20 + .05j, \quad R_{lb} = 10 + 0j, \quad R_{lc} = 10 + .05j$$

**Case 1.** In this case source and transmission lines are considered ideal. Figure 6.14 (a) shows voltage at PCC point before and after compensation. In this case PCC voltages are completely equal to source voltages. Figure 6.14 (b) shows load currents that are unbalanced and are unchanged before and after the compensation.

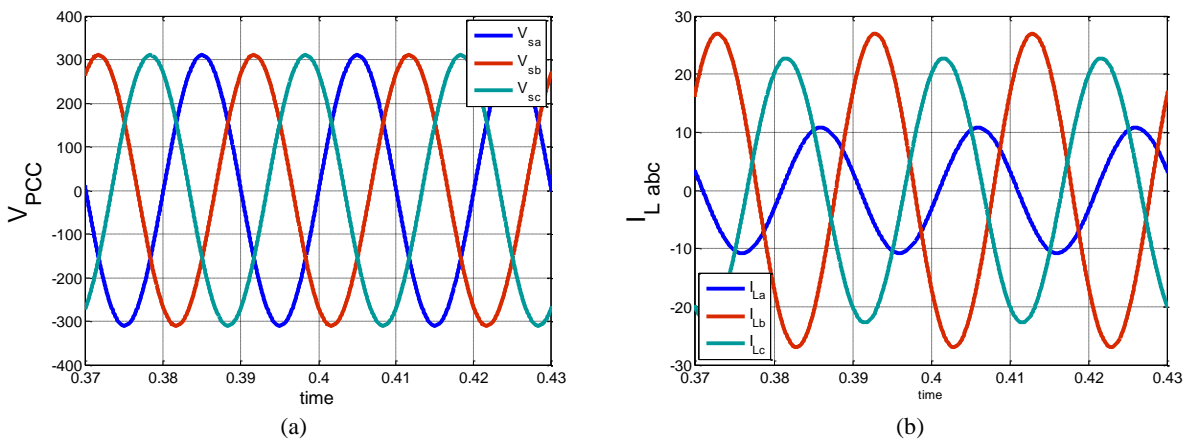


Figure 6.14. Simulation result of an ideal system (without considering the transmission losses or source impedance). a) Voltage at PCC point. b) unbalanced load currents

**Case 2.** In this case source and transmission lines are considered real (non-ideal). Figure 6.15(a) shows voltage at PCC point before and after compensation. In this case PCC voltages were unbalanced before compensation ( $t=0.4$ ) due to unbalanced load currents and their effects on

resistance on the source side. Due to compensating the unbalanced load currents, one can see PCC voltages are balanced. Figure 6.15(b) shows the load currents that are unbalanced all the time but there are some different before and after the compensation due to change on PCC voltages.

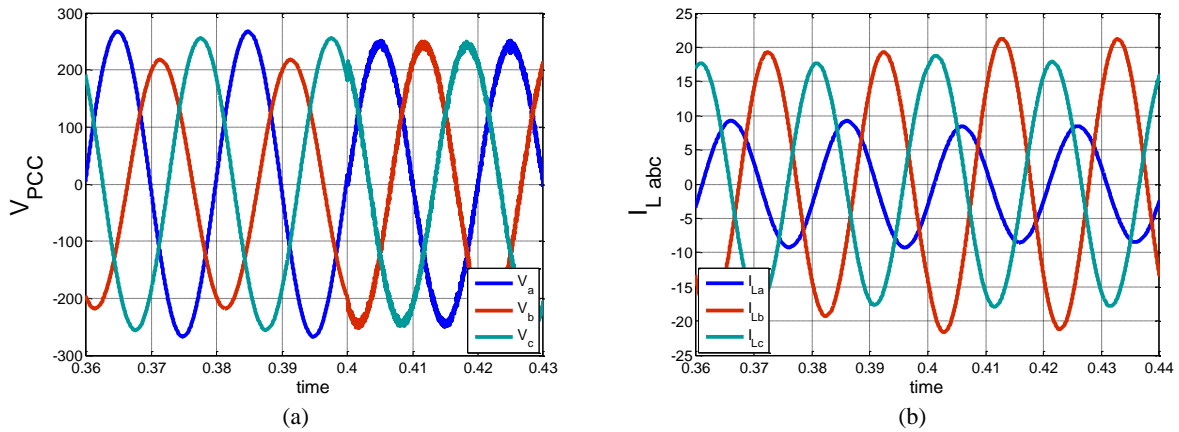


Figure 6.15. Simulation result of non-ideal system; a) Voltage at PCC point. b) unbalanced load currents.

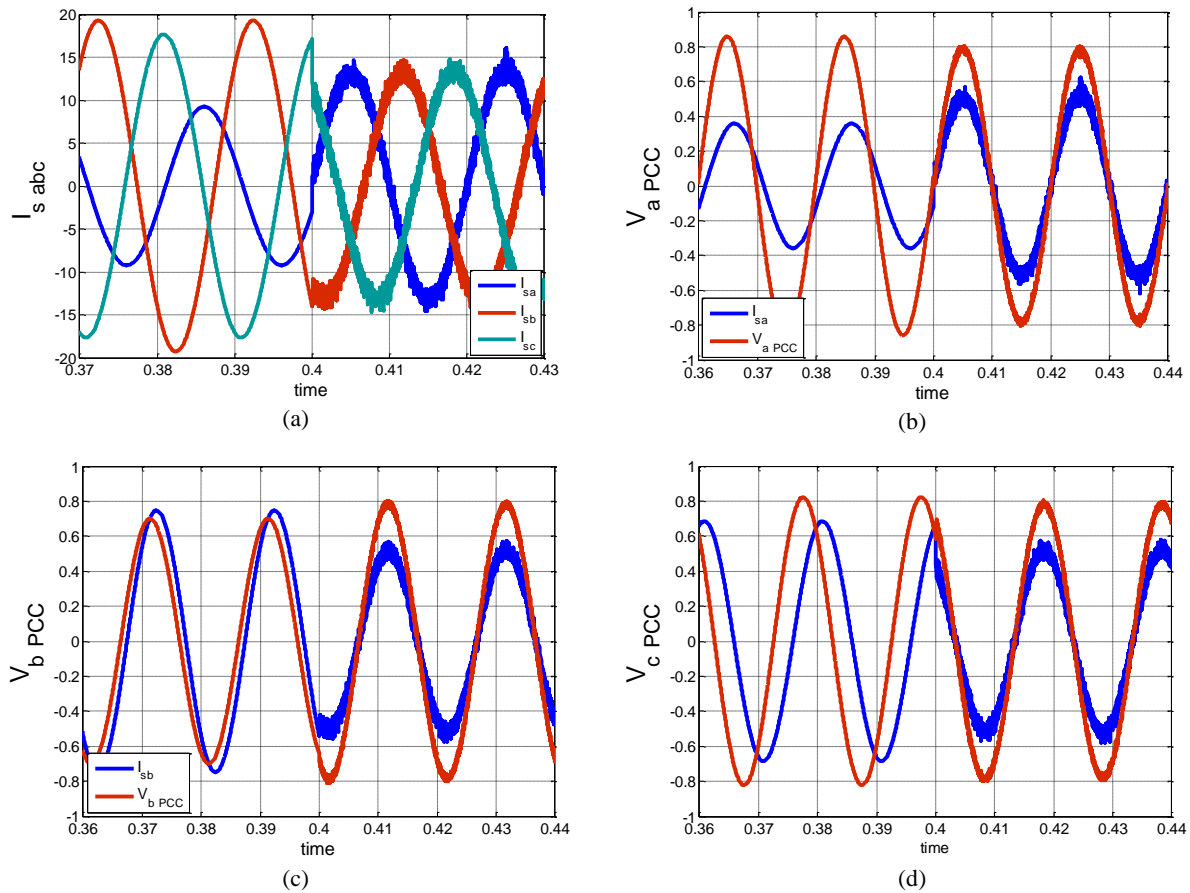


Figure 6.16. a) Three-phase source currents. Compensation is started at  $t=0.4$ . b,c,d) three-phase  $a, b, c$  voltage and current before and after compensation on per-unit, respectively.

Before compensation, source currents and load currents are the same as shown in Fig. 6.15(b) and Fig. 6.16(a), but after injecting the compensating currents from active filter source currents are balanced. Fig. 6.16(a) shows the source or lines currents. Fig. 6.16(a,b,c) shows each phase voltage and current together in per-unit. Considering this figures, one can see in this example the worst load (unbalanced and inductive) are exemplified. It is clear that imaginary power and unbalancing distortions are compensated together. Figure 6.17 shows the reference currents and output currents of shunt active filter.

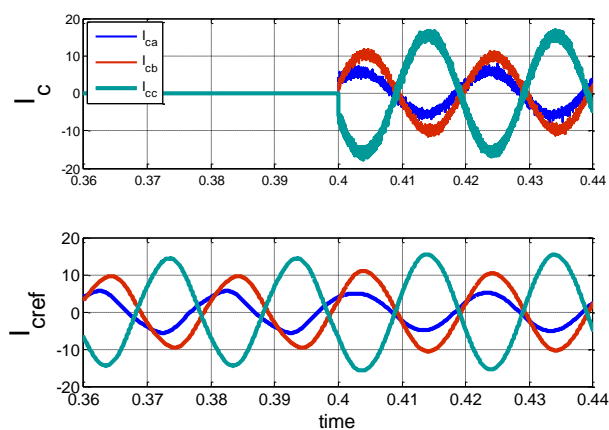


Figure 6.17. Three-phase compensating currents of shunt active filter and reference currents

### References:

- [1] H. Akagi, E. H. Watanabe and M. Aredes, "Instantaneous Power Theory and Applications to Power Conditioning", IEEE Press / Wiley Interscience, 2007.
- [2] H. Akagi, Y. Kanazawa, and A. Nabae, "Instantaneous reactive power compensators comprising switching devices without energy storage components," *IEEE Trans. Ind. Appl.*, vol. IA-20, pp. 625-631, 1984.

## VII. DESIGN OF A BIDIRECTIONAL BATTERY CHARGER

The selected battery charger topology able to carry out the mentioned capabilities is shown in Fig. 7.1, where the point of common coupling (PCC) towards the power grid and an EV battery attached to the charger are also shown. The battery charger consists of a DC-link capacitor  $C_{dc}$ , a three phase bidirectional VSC connected to a DC/DC converter, and passive filters.

The passive filters are, due to the switched operation of the VSCs, essential components of the battery charger topology. The output voltage pulses of the VSCs are filtered by passive filters, reducing the high frequency current components. Hence, sinusoidal line currents as well as a low ripple battery current are obtained. The passive filters shown in Fig. 7.1 are inductors (L-filters) but LCL-filters can be also used.

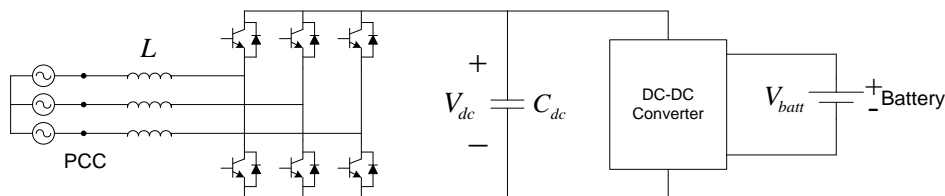


Figure 7.1. Typical battery charger topology

The line side of the battery charger topology forms an equivalent shunt active filter (AF). The decoupling of the converters provided by the DC-link capacitor ensures that the functionality of the shunt AF is separated from the battery side operation. Therefore, harmonic filtering as well as reactive power compensation and load balancing may be accomplished by the topology selected. However, the lack of a neutral conductor makes balancing of zero-sequence current components impossible. Thus, only negative sequence current balancing is achievable.

Finally, the DC/DC converter enables charging of EV batteries of different voltage levels. Furthermore, it allows bi-directional battery current and thus the battery charger is able to function as a small generator. The design of the DC/DC converter is outside the scope of this thesis.

In the converter circuit, the parameters of the energy storage elements such as inductors (L) and capacitors (C) are pretty important factors, which affect directly the work of the converter. So, the topology of the Bidirectional Battery Charger (BBC) studied in this chapter is the same as in Fig. 7.1 and the design of power circuit includes three main parameters:

- 1) Selection of reference value of dc side voltage,  $V_{dc}$
- 2) Selection of dc side capacitor,  $C_{dc}$
- 3) Selection of filter inductor,  $L_f$  (that will be explained in the next chapters)

On the other hand, the design of three-phase inverters requires values for the average, RMS, and peak currents in the inverter in order to select the right components.

## 7.1. DC-link

Several methods are presented for the design parameters in literatures:

- For proper operation of the system as a PWM rectifier a minimum DC-link voltage is required. Generally it can be determined by the peak value of line-to-line grid voltage. Defining the natural DC-link voltage value, as possible to obtain in case of not operating transistors, their freewheeling diodes becomes a standard three-phase diode bridge. Therefore, the boost nature of the active rectifier leads to:

$$V_{dc} > \sqrt{3} \times \sqrt{2} V_f = 2.45 V_f \quad (7.1)$$

where  $V_f$  is the converter output voltage.

- For a typical active filter, the DC bus nominal voltage  $V_{dc}$  must be greater than or equal to line-line peak voltage (plus the drop on L-filter) in order to actively control  $i_f$  [1]. Considering a Space Vector Modulation (SVM) it is calculated by the condition:

$$M_{a,max} \frac{V_{dc}}{\sqrt{3}} > \hat{V}_f \quad (7.2)$$

where,  $M_{a,max}$  is the maximum value of the amplitude modulation index (Generally for SVM technique,  $Modulation\ Index = \frac{\hat{V}_f}{V_{dc}/\sqrt{3}}$ ).

- In [2], if it is assumed that the PWM converter operates in the linear modulation mode (i.e.  $0 \leq M_a \leq 1$ ) then,

$$M_a = \frac{\hat{V}_{f1}}{V_{dc}/2} \quad \text{for} \quad M_a = 1, \quad V_{dc} = 2\hat{V}_{f1} \quad (7.3)$$

where,  $\hat{V}_{f1}$  is the peak of the fundamental component of converter AC-side voltage.

If the inductance output filter is small due to the choice of a high switching frequency, the voltage  $V_{f1}$  is approximately equal to the source voltage [3], then (7.3) will be:

$$V_{dc} = 2\hat{V}_s \quad (7.4)$$

A value of  $1.1V_{dc}$  is used, based on the assumption that the DC voltage is regulated to be 10% above the peak input voltage [3]. However, the required  $V_{dc}$  can be reduced if the sine reference for PWM is modulated with third and ninth harmonics or SVM is applied. The minimum required voltage can then be expressed in terms of the source voltage as:

$$V_{dc} = 1.1 \times 2\hat{V}_s \quad (7.5)$$

The increasing of DC-link capacitor reference voltage does not have much impact on the current  $THD_i$ . However, it degrades the quality of source voltage thus its  $THD_v$ . This is due to the significant difference in potential under which IGBT's are switching.

The DC-link capacitor  $C_{dc}$  provides an intermediate energy storage, which decouples the three phase VSC from the half bridge DC/DC converter. Hence, the VSCs can be operated independently of each other as long as the average power flow is balanced between the VSCs. The instantaneous difference in active power is stored in  $C_{dc}$ , which causes the DC-link voltage  $V_{dc}$  to vary. Hence, the value of  $C_{dc}$  is determined by the constraint on the maximum allowed DC-link voltage ripple  $\Delta V_{dc}$  [4].

The DC-link capacitor should be large enough to handle transients, i.e. load changes, without any severe effect on the DC-link voltage. However in shunt AF applications, the limiting factor of the DC-link capacitor size is determined by the instantaneous active power redirected by the shunt AF. This means that the instantaneous active power contained in the conditioning current is temporarily stored



in the DC-link capacitor. The worst case corresponds to long periods of charging/discharging of the DC-link capacitor. This implies that load balancing at rated power of the negative-sequence current component gives the limiting design constraint on the DC-link capacitor size.

A design expression for the DC-link capacitor value is derived based on simplified analysis of the instantaneous active power flow in the battery charger when performing load balancing at rated power. The instantaneous active power flow through the PCC can be expressed, in the synchronously rotating reference  $dq$ -frame with  $q$ -axis oriented along the grid voltage vector for the sake of simplicity, (even if  $d$ -axis is considered oriented along the grid voltage vector, the final result will be the same) as

$$p_{PCC} = v_d i_d + v_q i_q = \{v_d = 0\} = v_q i_q \quad (7.6)$$

where  $v_q$  and  $i_q$  are the  $q$ -axis components of the grid voltage vector and the negative-sequence current vector, respectively. Hence, they are given by

$$\begin{cases} v_q = V_{s1} \\ i_q = \text{Im}(\sqrt{3}I_n e^{-j2\omega_1 t}) = \sqrt{3}I_n \sin(-2\omega_1 t) \end{cases} \quad (7.7)$$

where subscript 1 denotes fundamental component. If the line filter and the three phase VSC are considered loss less, the instantaneous active power flow through the PCC should correspond to the power flow in the DC-link capacitor, i.e.

$$p_C = i_C V_{dc} = p_{PCC} \quad (7.8)$$

Substituting (7.6) into (7.8) and rearranging gives an expression for the average DC-link capacitor current

$$i_C = \frac{v_q}{V_{dc}} i_q \quad (7.9)$$

The differential equation for the DC-link voltage can then be written

$$\frac{d}{dt} V_{dc} = \frac{1}{C_{dc}} \frac{v_q}{V_{dc}} i_q \quad (7.10)$$

Linearization of (7.10) around the average DC-link voltage  $V_{dc}$  gives

$$\frac{d}{dt} \Delta V_{dc} = \frac{1}{C_{dc}} \frac{v_q}{\bar{V}_{dc}} i_q \quad (7.11)$$

where  $\Delta V_{dc}$  corresponds to the DC-link voltage ripple. Substituting (7.7) into (7.11) and solving the differential equation, a design expression for the DC-link capacitor is found by rearrangement of the solution as

$$C_{dc} = \frac{S_n}{\bar{V}_{dc} \Delta V_{dc}} \frac{1}{2\omega_1} \quad (7.12)$$

where  $S_n$  is the rated power of the battery charger.

## 7.2. Switch design

The switches in an inverter are implemented as shown in Fig. 7.2. The symbol for the transistor is used to represent any one of several high-speed power semiconductor devices, including the bipolar junction transistor, the power MOSFET, the insulated gate bipolar transistor (IGBT), and etc. The free-wheeling diode in parallel with the transistor is required for inductive loads.

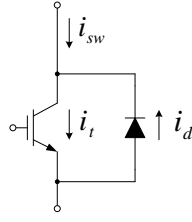


Figure 7.2. Practical switch for an inverter.

Proper design of a PWM inverter requires knowledge of the power dissipated in the semiconductor devices for worst case conditions. The power losses in a device can be classified as on-state or conduction losses, switching losses, and off-state losses [5]. For a device modeled in the on-state as a voltage source  $V_{on}$  in series with a resistor  $R_{on}$ , the conduction losses are given by

$$P_{cond} = V_{on} \cdot I_{avg} + R_{on} \cdot I^2 \quad (7.13)$$

where the average value of the instantaneous device current  $i(t)$  is

$$I_{avg} = \frac{1}{T} \int_0^T i(t) dt \quad (7.14)$$

and the root-mean-square (RMS) value is

$$I = \sqrt{\frac{1}{T} \int_0^T i^2(t) dt} \quad (7.15)$$

Here, the device current is assumed to be periodic with period  $T$ . The relationship expressed by (7.13) is important in that it provides the motivation to investigate the average and RMS currents in the transistors and diodes of a PWM inverter.

### 7.2.1. General relationships concerning transistor and diode currents in a switch

Figure 7.3 shows a single leg of a three-phase inverter. The upper branch of the leg consists of the components connected to the plus terminal of the DC voltage source, while the components connected to the minus terminal form the lower branch.

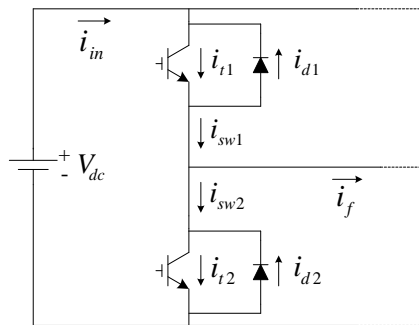


Figure 7.3. Single leg of a PWM inverter.

The currents in a PWM inverter are generally complex. Some important relationships concerning the average and RMS inverter currents can be derived by first applying Kirchhoff's current law to either branch in Fig. 7.3 to get:

$$i_{sw} = i_t - i_d \quad (7.16)$$

Using this expression and the definition of average current (7.14), it is easy to show that the average branch, transistor, and diode currents are related as follows:

$$I_{sw,avg} = I_{t,avg} - I_{d,avg} \quad (7.17)$$

Since the supply current  $i_{in}$  is the sum of the three branch currents, the average supply is given by

$$I_{in,avg} = 3I_{sw,avg} \quad (7.18)$$

This assumes, of course, that the average values of the three branch currents are equal. A relationship involving the RMS currents can be obtained by combining (7.16) with the definition of RMS current (7.15) to get

$$I_{sw}^2 = I_t^2 + I_d^2 - \frac{2}{T} \int_0^T i_t i_d dt \quad (7.19)$$

The currents in a leg of an inverter are such that, at any point in time, the current path includes only one device. This means, for example, that if a transistor is conducting current, then the current in the associated diode is zero and vice versa. Thus, the product of  $i_t$  and  $i_d$  in (7.19) is zero for all values of  $t$ . Consequently,

$$I_{sw}^2 = I_t^2 + I_d^2 \quad (7.20)$$

Another important relationship concerning RMS values can be obtained by applying Kirchhoff current law to the node associated with the line current to get

$$i_f = i_{sw1} - i_{sw2} \quad (7.21)$$

Using the same procedure as before, it is easy to show that

$$I_f^2 = I_{sw1}^2 + I_{sw2}^2 \quad (7.22)$$

Under the assumption that  $I_{sw1} = I_{sw2} = I_{sw}$ , then

$$I_f^2 = 2I_{sw}^2 \quad (7.23)$$

or

$$I_{sw} = \frac{1}{\sqrt{2}} I_f \quad (7.24)$$

Unfortunately, there is no simple relationship between the RMS branch currents and the RMS supply current. The frequency ratio  $K_f$  is an important quantity that characterizes the PWM waveforms. It can be defined as the ratio of the frequency at which the switches operate (switching frequency) to the fundamental,  $f_1$  of the periodic waveforms.

It is important to mention that no assumptions were made about the PWM method in deriving the previous relationships. For an inductive load, as the frequency ratio increases, for a given set of conditions, the ripple in the line current decreases. The above mentioned relationships can be used to place some bounds on the average and RMS inverter currents for a given set of conditions. For example, the RMS line current is usually known, so the RMS branch current can be calculated using (7.24). As a consequence of (7.20), the maximum value that the RMS transistor current can take on is a value equal to the RMS branch current. The same applies for the RMS diode current.

On the other hand, the RMS value of the transistor current can be calculated by

$$I_t = \sqrt{\frac{1}{T_1} \int_0^{T_1} i_t^2(t) dt} \quad (7.25)$$

where  $T_1$  is the period of the AC line waveform. The integral can be expressed as a sum of integrals over all of the switching periods contained in one AC line period (Fig. 7.4):

$$I_t = \sqrt{\frac{1}{T_1} T_s \sum_{n=1}^{T_1/T_s} \left( \frac{1}{T_s} \int_{(n-1)T_s}^{nT_s} i_t^2(t) dt \right)} \quad (7.26)$$

where  $T_s$  is the switching period. The quantity inside the parentheses is the value of  $i_t^2$  averaged over the  $n^{\text{th}}$  switching period. The summation can be approximated by an integral in the case when  $T_s$  is much less than  $T_1$ . This approximation corresponds to taking the limit as  $T_s$  tends to zero, as follows:

$$\begin{aligned} I_t &\approx \sqrt{\frac{1}{T_1} \lim_{T_s \rightarrow 0} \left[ T_s \sum_{n=1}^{T_1/T_s} \left( \frac{1}{T_s} \int_{(n-1)T_s}^{nT_s} i_t^2(\tau) d\tau \right) \right]} = I_t = \sqrt{\frac{1}{T_1} \int_0^{T_1} \frac{1}{T_s} \int_t^{t+T_s} i_t^2(\tau) d\tau} \\ &= \sqrt{\langle i_t^2(t) \rangle_{T_s} \rangle_{T_1}} \end{aligned} \quad (7.27)$$

so  $i_t^2$  is first averaged over one switching period. The result is then averaged over the AC line period, and the square root is taken of the result.

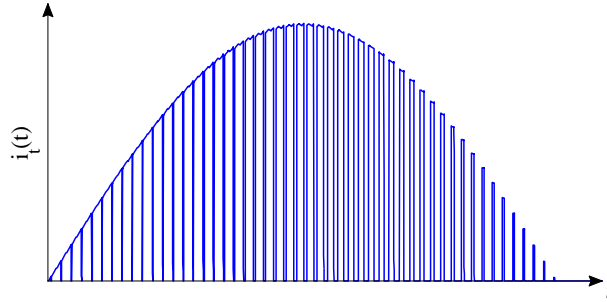


Figure 7.4. Modulated transistor current waveform

### 7.2.2. Single phase inverter example

For the single phase inverter, the transistor current  $i_t(t)$  is equal to the output current  $i_f(t)$  when the transistor conducts, and is zero when the transistor is off. Therefore, the average of  $i_t^2(t)$  over one switching period is

$$\langle i_t^2(t) \rangle_{T_s} = \frac{1}{T_s} \int_t^{t+T_s} i_t^2(t) dt = d(t) i_f^2(t) \quad (7.28)$$

Let the output voltage and current be given by

$$v_f(t) = \hat{V}_f \sin(\omega t) \quad (7.29)$$

$$i_f(t) = \hat{I}_f \sin(\omega t) \quad (7.30)$$

With a constant input voltage  $V_{dc}$ , the transistor modulation function must obey the relationship

$$\frac{v_f(t)}{V_{dc}} = [2d(t) - 1] \quad (7.31)$$

Substitution of (7.29) into (7.31) and solution for  $d(t)$  yields

$$d(t) = \frac{1}{2} \left( 1 + \frac{\hat{V}_f \sin(\omega t)}{V_{dc}} \right) \quad (7.32)$$

Hence, knowing the modulation function for one phase leg of the full bridge arrangement in Fig. 7.5, the RMS current and the average current can be calculated as a function of the output current  $i_f$  and the modulation index  $M_a$ . The modulation function  $d(t)$  is given by [6]:

$$d(t) = \frac{1}{2} (1 + M_a \sin(\omega t)) \quad (7.33)$$

where modulation index for single phase converter is  $M_a = \frac{\hat{V}_f}{V_{dc}}$ ,

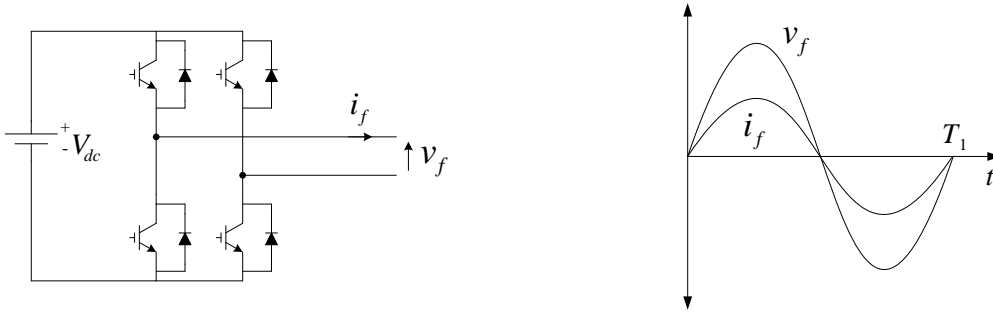


Figure 7.5. Test topology for deriving the switch parameters.

Substitution of (7.33) into (7.28) yields the following expression

$$\langle i_t^2(t) \rangle_{T_s} = \hat{i}_f^2 \left( \frac{1}{2} + \frac{M_a}{2} \sin(\omega t) \right) \sin^2(\omega t) \quad (7.34)$$

One can now put this expression into (7.27) which can be further simplified to

$$\langle I_t \rangle_{T_1} = \sqrt{\frac{1}{T_1} \hat{i}_f^2 \int_0^{T_1/2} \left( \frac{\sin^2(\omega t)}{2} + \frac{M_a}{2} \sin^3(\omega t) \right) dt} \quad (7.35)$$

Due to conduction of transistor for half period (that is shown in Fig. 7.8), integral is computed for half period. This type of integral arises in following calculations. The values of the integral for several choices of  $n$  are listed in table 7.2. The integral can be evaluated with the help of the following formula:

$$\frac{1}{\pi} \int_0^{\pi} \sin^n(\theta) d\theta = \begin{cases} \frac{2}{\pi} \cdot \frac{2 \cdot 4 \dots (n-1)}{1 \cdot 3 \cdot 5 \dots (n)} & \text{if } n \text{ is odd and } n > 1 \\ \frac{1 \cdot 3 \cdot 5 \dots (n-1)}{2 \cdot 4 \cdot 6 \dots (n)} & \text{if } n \text{ is even} \end{cases} \quad (7.36)$$

**Table 7.2. Solution of the integral of Eq. (7.36), for several values of  $n$** 

$n$	$\frac{1}{\pi} \int_0^\pi \sin^n(\theta) d\theta$
1	$\frac{2}{\pi}$
2	$\frac{1}{2}$
3	$\frac{4}{3\pi}$
4	$\frac{3}{8}$
5	$\frac{16}{15\pi}$

Evaluation of the integral in (7.35) using (7.36) leads to the following result:

$$\langle I_t \rangle_{T_1} = \hat{I}_f \cdot \sqrt{\left(\frac{1}{8} + \frac{M_a}{3\pi}\right)} = I_f \cdot \sqrt{\left(\frac{1}{4} + \frac{2M_a}{3\pi}\right)} \quad (7.37)$$

It can be seen that the RMS transistor current is maximized by choosing the input DC voltage  $V_{dc}$  to be as small as possible ( $M_a = \frac{\hat{V}_f}{V_{dc}}$ ). The worst that can be done is to choose  $V_{dc} = \hat{V}_f$  which leads to

$$I_t = 0.68I_f \quad (7.38)$$

A similar analysis for the RMS diode current leads to the following expression

$$\langle I_d \rangle_{T_1} = \sqrt{\frac{1}{T_1} \int_{\frac{T_1}{2}}^{T_1} ((1-d(t)) \cdot i_f^2) dt} = \hat{I}_f \cdot \sqrt{\left(\frac{1}{8} - \frac{M_a}{3\pi}\right)} \quad (7.39)$$

The maximum value for average current and RMS current of transistor is when the displacement factor of output voltage and current is unit. So, the average current through the transistor  $I_{t,avg}$  is:

$$\langle I_{t,avg} \rangle_{T_1} = \frac{1}{T_1} \int_0^{\frac{T_1}{2}} (d(t) \cdot \hat{I}_f \cdot \sin(\omega t)) dt = \left(\frac{1}{2\pi} + \frac{M_a}{8}\right) \cdot \hat{I}_f \quad (7.40)$$

The maximum value for average current and RMS current of diode is when the displacement factor of output voltage and current is zero. Similarly, the average current for the diode is derived:

$$\langle I_{d,avg} \rangle_{T_1} = \frac{1}{T_1} \int_{\frac{T_1}{2}}^{T_1} ((1-d(t)) \cdot \hat{I}_f \cdot \sin(\omega t)) dt = \left(\frac{1}{2\pi} - \frac{M_a}{8}\right) \cdot \hat{I}_f \quad (7.41)$$

Using (7.37)-(7.41) the transistor and diode currents can be calculated for any given output current  $I_f$  and output voltage  $V_f$ .

As an example if we consider phase displacement ( $\varphi$ ) of the output voltage and current is not zero, so the average current through the transistor  $I_{t,avg}$  is:

$$\begin{aligned}
 \langle I_{t,avg} \rangle_{T_1} &= \frac{1}{T_1} \int_{\varphi}^{\frac{T_1}{2}} (d(t) \cdot \hat{I}_f \sin(\omega t - \varphi)) dt \\
 &= \frac{1}{2\pi} \int_{\varphi}^{\pi} \left( \frac{1}{2} (1 + M_a \sin(\omega t)) \cdot \hat{I}_f \sin(\omega t - \varphi) \right) dt
 \end{aligned} \tag{7.42}$$

By calculating the above integral, the average current that is a function of modulation index  $M_a$  and phase displacement  $\varphi$  and peak of output current  $\hat{I}_f$  is determined by:

$$\langle I_{t,avg} \rangle_{T_1} = \frac{\hat{I}_f}{4\pi} \left[ (\cos \varphi + 1) + \frac{M_a}{2} \left( (\pi - \varphi) \cos \varphi + \frac{\sin(\varphi)}{2} \right) \right] \tag{7.43}$$

In order to verifying average current of transistor as a function of modulation index and phase angle,  $\hat{I}_f$  is considered constant. This function is shown in Fig. 7.6 with the range of  $(0 < M_a < 1)$  and  $(0 < \varphi < \frac{\pi}{2})$ . From the figure it is clear that the maximum value for transistor average current is when the power factor is unit ( $\varphi = 0$ ).

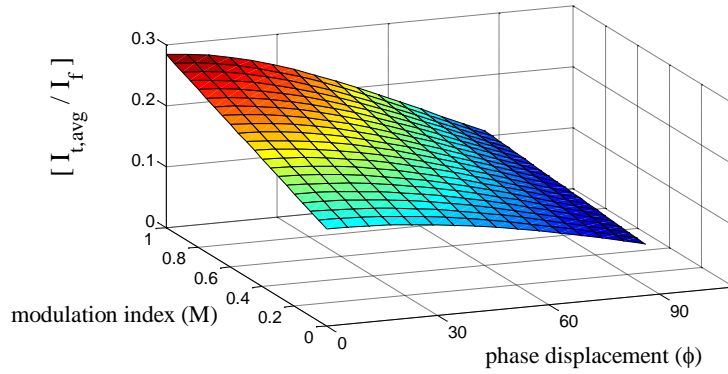


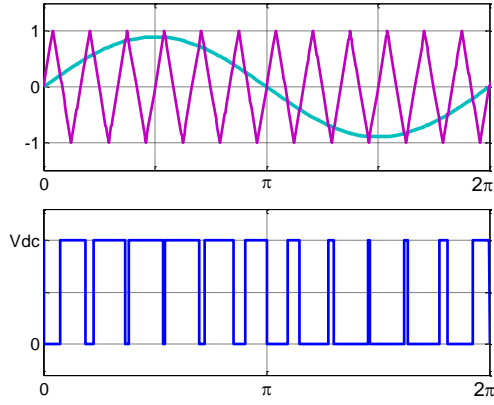
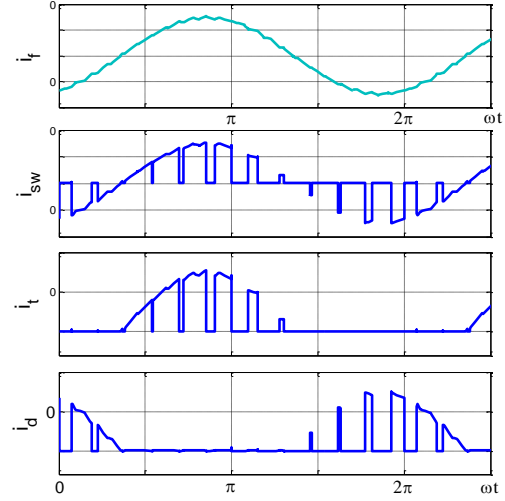
Figure 7.6. Transistor average current as a function of modulation index and phase displacement.

Computer-aided analysis can be used to get more accurate values for the average and RMS currents in a three-phase inverter. A computer-aided method based on Fourier series techniques has been presented in [7]. These types of analyses work reasonably well for small values of frequency ratio. They can be time consuming, and not very practical for large values of frequency ratio. It is reasonable to assume that, for large values of  $K_f$ , the line current is indeed almost a pure sinusoid. Once this assumption has been made, the inverter current waveforms can easily be generated and analyzed to determine the average and RMS values.

In order to generate the approximate inverter current waveforms, it is necessary to choose a PWM method. A simple sinusoidal PWM technique was chosen for the analysis presented in this section. As shown in Fig. 7.7, the method compares a triangle wave carrier with a sine wave modulating function. The technique is characterized by the modulation index  $M_a$ , which is the ratio of the peak sine wave to triangle wave amplitudes, and the frequency ratio  $K_f$ , which is the ratio of the triangle wave to sine wave frequencies. Fig. 7.8 shows a pure sine wave line current and the currents that result in the plus branch of an inverter leg. The phase angle between the line current in Fig. 7.7 and the sine wave modulating function in Fig. 7.8 is represented by  $\varphi$ . The displacement factor PF is given by

$$PF = \cos \varphi \tag{7.44}$$

In general, the results calculated for the currents in the plus branch of an inverter leg are very nearly the same as those for the currents in the minus branch, and the results for all quantities are only slightly dependent on the frequency ratio.


 Figure 7.7. Sinusoidal PWM ( $K_f = 12$ ,  $M_a = 0.8$ ).

 Figure 7.8. Approximate inverter current waveforms; Line current, switch current, transistor current, diode current. ( $K_f = 12$ ,  $PF = 0.9$ ,  $M_a = 0.9$ ).

Careful study of the data resulted in [8] shows that the average and RMS values calculated for a particular inverter current remain relatively constant when the product of the power factor and the modulation index was held constant for different combinations of PF and  $M_a$ . Unfortunately there is no simple analytical relationship between the output current  $I_f$  and the current in the diode  $I_d$  and transistor (or IGBT)  $I_t$ . In fact, the current distribution between diode and transistor is a function of both power factor ( $\cos \varphi$ ) and modulation index  $M_a$  as it was shown in the previous example by a single phase converter. In [8] the average current through the diode and transistor is approximated by:

$$I_{sw,avg} \approx 0.3536K \cdot I_f \quad (7.45)$$

$$I_{t,avg} \approx (0.2251 + 0.1768K) \cdot I_f \quad (7.46)$$

$$I_{d,avg} \approx (0.2251 - 0.1768K) \cdot I_f \quad (7.47)$$

where the factor K is defined by:

$$K \triangleq M_a \cdot |\cos(\varphi)| \quad (7.48)$$

The average DC-link current can also be expressed in terms of K and is given by

$$I_{in,avg} = 3I_{sw,avg} \approx 1.0608K \cdot I_f \quad (7.49)$$

The RMS branch current is constant, and is simply

$$I_{sw} = \frac{1}{\sqrt{2}} I_f \approx 0.7071 \cdot I_f \quad (7.50)$$

and the RMS diode and transistor currents are given by:

$$I_t \approx (0.5 + 0.1824K) \cdot I_f \quad (7.51)$$

$$I_d \approx \sqrt{(0.25 - 0.1824 \cdot K - 0.0333K^2)} \cdot I_f \quad (7.52)$$

Unfortunately, the RMS supply current is not a simple function of K.

The expressions in above equations are valid when the power flow is out of the considered inverter. In case the power flows into the considered inverter the equations for the diode current quantities and IGBT current quantities are to be interchanged.



**Example 1.** Consider operation at 50 Hz and assume the following conditions:

$$I_{f,rms} = 100 \text{ A} , PF = 0.9 , M_a = 1$$

The combined factor K is calculated using (7.48)

$$K = PF \cdot M_a = 0.9$$

The average and RMS inverter currents are calculated using (7.45)-(7.52):

$$I_{sw,avg} \approx 0.3536(0.9)100 = 31.82 \text{ A}$$

$$I_{t,avg} \approx (0.2251 + 0.1768(0.9)) \cdot 100 = 38.42 \text{ A}$$

$$I_{d,avg} \approx (0.2251 - 0.1768(0.9)) \cdot 100 = 6.598 \text{ A}$$

$$I_{in,avg} \approx (1.0608(0.9)) \cdot 100 = 95.47 \text{ A}$$

$$I_{sw,rms} \approx \frac{100}{\sqrt{2}} = 70.71 \text{ A}$$

$$I_t \approx (0.5 + 0.1824(0.9)) \cdot 100 = 66.42 \text{ A}$$

$$I_d \approx \sqrt{(0.25 - 0.1824 \cdot (0.9) - 0.0333(0.9)^2)} \cdot 100 = 24.26 \text{ A}$$

### 7.3. Calculation of average and RMS value of the inverter input current

For preparing the analytical calculation of the capacitor-current stress, a brief review of the fundamentals of the inverter control and of the formation of the inverter input current  $i_{in}$  is presented. Owing to the symmetries of an ideal three-phase voltage system and the phase-symmetric structure of the converter power circuit, the analysis can be limited to a  $\frac{\pi}{3}$  wide interval of the inverter-output-voltage fundamental period.

#### 7.3.1. Switching mode on space vector modulation

For stationary operation, the reference value of the inverter output voltage can be represented by a space vector

$$\vec{v}_{f1} = \hat{V}_f e^{j\theta_f} , \quad \theta_f = \omega_1 t \quad (7.53)$$

with constant magnitude  $\hat{V}_f$ .  $v_{f1}$  is associated with the fundamental of the pulse-width-modulated inverter-output phase voltages which is approximated within each pulse half period  $t_\mu \in [0, T_p)$  by switching between the immediately neighboring inverter output-voltage space vectors. For instance for the angle interval (Fig. 7.9) which is considered in the following, the switching state sequence in sector II is

$$\dots |_{t_\mu=0} (000) - (010) - (110) - (111) |_{t_\mu=\frac{1}{2}T_p} (111) - (110) - (010) - (000) |_{t_\mu=T_p} \dots \quad (7.54)$$

where each inverter switching state is characterized by the triple  $(s_a, s_b, s_c)$  of the associated phase switching functions  $s_i$ , where  $i = a, b, c$ . Here is defined  $s_i = 1$  if the output voltage of phase  $i$  referred to the fictitious centre point of the DC-link is positive,  $v_{f,i} = +V_{dc}/2$ , and  $s_i = 0$  if the output voltage of phase  $i$  is negative,  $v_{f,i} = -V_{dc}/2$ .

The relative on-times (duty cycle) of the switching states  $V_3(010)$  and  $V_2(110)$  are as follow,

$$\begin{aligned} d_{(010)} &= d_3 = \frac{\sqrt{3}M_a}{2} \sin\left(\theta_f - \frac{\pi}{3}\right) \\ d_{(110)} &= d_2 = \frac{\sqrt{3}M_a}{2} \sin\left(\theta_f + \frac{\pi}{3}\right) \end{aligned} \quad (7.55)$$

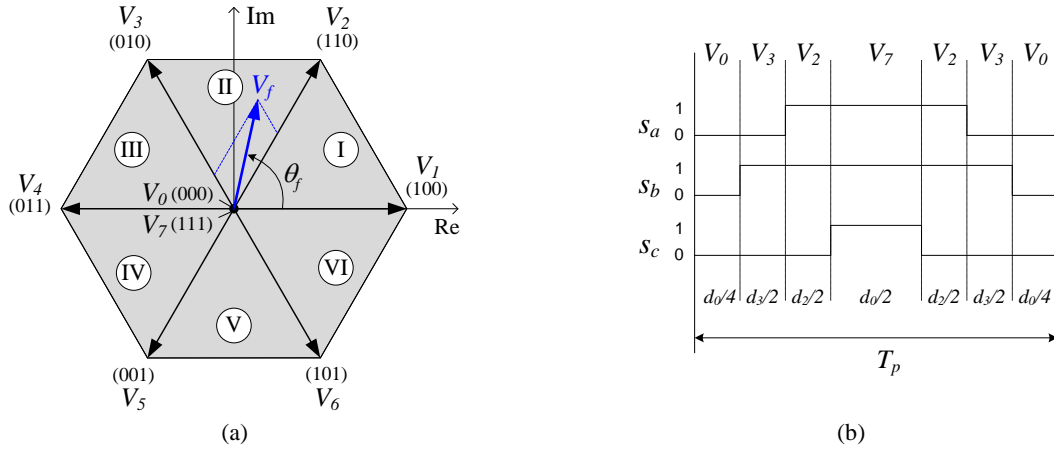


Figure 7.9. Space vectors of the inverter output voltage assigned to the active switching states and to the zero switching states  $V_0(000)$  and  $V_7(111)$ ; a) Space vector diagram, b) Seven-segment switching sequence in sector II

which can be determined by simple geometrical considerations (Fig. 7.9) and are defined by the location  $\theta_f$  of the respective pulse half period within the fundamental period of the inverter output voltage and by the relative amplitude of the inverter-output-voltage fundamental and/or the modulation index

$$M_a = \frac{\hat{V}_f}{\frac{1}{2}V_{dc}}, \quad M_a \in \left[0, \frac{2}{\sqrt{3}}\right] \quad (7.56)$$

where the DC-link voltage is assumed to be constant. In contrast, the distribution of the total on-time of the zero switching states  $V_0(000)$  and  $V_7(111)$  are

$$d_{(000)} + d_{(111)} = d_0 = 1 - (d_3 + d_2) \quad (7.57)$$

### 7.3.2. Inverter input current

As becomes immediately clear by considering the inverter bridge legs as two-pole switches between the positive and negative DC-link ( $s_i = 1$  and/or 0) as shown in Fig. (7.10), the input current  $i_{in}$  of the inverter is determined by

$$i_{in} = s_a i_{fa} + s_b i_{fb} + s_c i_{fc} \quad (7.58)$$

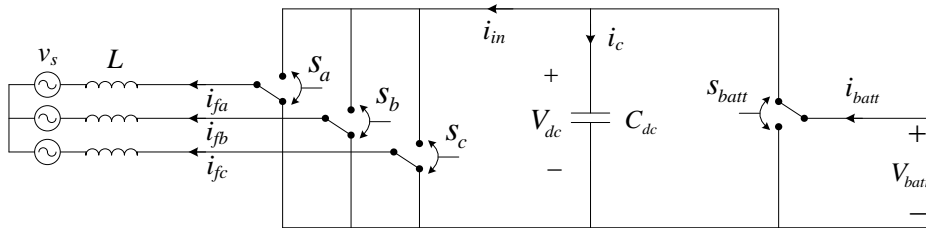


Figure 7.10. Simplified ideal model of the VSCs.

Here the dead-time interval, which has to be considered for the gating of the transistors of a bridge leg in practice, and the reverse recovery current of the freewheeling diodes, which have a minor influence on the shape of  $i_{in}$ , are neglected. The input inverter current  $i_{in}$  is formed by segments of the inverter output phase currents  $i_{fi}$  and is dependent on the inverter switching state. For the switching state  $V_3(010)$ , the output terminal of phase  $b$  is connected to the positive DC bus and phases  $a$  and  $c$  are switched to the negative polarity of the DC-link; therefore,  $i_{in}$  and  $i_{fb}$  show identical time behavior. For switching state  $V_2(110)$  the current is  $i_{in} = -i_{fc}$ , since

$$i_{fa} + i_{fb} + i_{fc} = 0 \quad (7.59)$$

has to be considered. Only during the zero states (000) and (111) no current will appear at the converter input. The distribution  $d_0$  of the zero states between the beginning and the end of a pulse half period therefore, to a first approximation, only has an influence on the position of the current-conduction intervals  $i_{in} = i_{fb}$  and  $i_{in} = -i_{fc}$  within a pulse half period, but does not influence the shape of  $i_{in}$  in principle.

A purely sinusoidal shape of the inverter output currents

$$\begin{cases} i_{fa}(t) = \hat{I}_f \cos(\theta_f - \varphi) \\ i_{fb}(t) = \hat{I}_f \cos\left(\theta_f - \frac{2\pi}{3} - \varphi\right) \\ i_{fc}(t) = \hat{I}_f \cos\left(\theta_f + \frac{2\pi}{3} - \varphi\right) \end{cases} \quad (7.60)$$

corresponding to a space vector

$$\vec{i}_{f1} = \hat{I}_f \cdot e^{j(\theta_f - \varphi)} \quad (7.61)$$

is assumed where  $\varphi$  denotes the phase displacement of the fundamentals of the inverter output voltage  $v_{f1}$  and the inverter output current  $i_{f1}$ . This is equivalent to only considering the fundamental of the phase currents, which to a first approximation show a constant value within a pulse half period.

### 7.3.2.1. Average value of the inverter input current

Based on the considerations in previous section, the ‘local’ mean value of the inverter input current (related to a pulse half period) is

$$i_{in,avg} = \frac{2}{T_p} \int_0^{\frac{1}{2}T_p} i_{in}(t) dt_\mu \quad (7.62)$$

Equation (7.62) can be expressed as

$$i_{in,avg} = d_3 i_{fb} - d_2 i_{fc} \quad (7.63)$$

with this, and (7.55) and (7.60), we obtain

$$i_{in,avg} = I_{in,avg} = \frac{3}{4} \hat{I}_f M_a \cos \varphi \quad (7.64)$$

Corresponding to the constant power supplied by a symmetrical and sinusoidal three-phase voltage/current system, the inverter input current shows a constant local average value  $i_{in,avg} = I_{in,avg}$ , i.e. the local and ‘global’ (related to the fundamental of the output voltage) mean values are identical. For  $\cos \varphi = 0$  the inverter generates only fundamental reactive power and/or no power is supplied from the DC-link (harmonic power components are neglected). Accordingly, we have  $I_{in,avg} = 0$ , and the inverter input current  $i_{in}$  is defined by segments out of the vicinity of the zero crossings of the output phase currents  $i_{fi}$  with alternating signs.

On the contrary, for  $\cos \varphi = 1$  we have purely active power operation and/or maximum current is supplied by the DC-link. There,  $i_{in}$  is formed by segments of identical signs near the vicinity of the maximum of the phase currents  $i_{fi}$ . For a given value of the fundamental displacement factor  $\cos \varphi$  of the output-current/voltage system,  $I_{in,avg}$  will rise linearly with increasing modulation index  $M_a$ . This can be explained by considering the linear increase of the width of the current pulses (Eq. 7.55) appearing at the inverter input for increasing modulation index  $M_a$  or by the increase of the inverter

output power owing to the proportional increase of the fundamental output voltage as a consequence of the higher modulation index  $M_a$  (Eq. 7.57). Note that, besides the (global) mean value,  $i_{in}$  ideally does not contain any low-frequency harmonics but only harmonics of the switching frequency.

### 7.3.2.2. RMS value of the inverter input current

For the local RMS value of the inverter input current

$$i_{in,rms} = \sqrt{\frac{2}{T_P} \int_0^{\frac{1}{2}T_P} i_{in}^2(t) dt_\mu} \quad (7.65)$$

we have in analogy to (7.64):

$$i_{in,rms}^2 = d_3 i_{fb}^2 + d_2 i_{fc}^2 \quad (7.66)$$

Therefore, with

$$I_{in}^2 = \frac{3}{\pi} \int_{\frac{\pi}{3}}^{\frac{2\pi}{3}} i_{in,rms}^2 d\theta_f \quad (7.67)$$

and (7.55) results in the global RMS value  $I_{in}$  of  $i_{in}$  being

$$I_{in} = I_{f,rms} \sqrt{\frac{2\sqrt{3}}{\pi} M_a \left( \frac{1}{4} + \cos^2 \varphi \right)} \quad (7.68)$$

In connection with (7.68) note that the RMS value of the inverter input current  $i_{in}$ , to a first approximation (as calculated by considering only the output phase current fundamentals), is independent of the inverter control scheme. As the fundamentals of the output phase currents  $i_{fb1}$  and  $i_{fc1}$  are assumed to be approximately constant within  $t_\mu \in [0, \frac{1}{2}T_P)$ , there is therefore no influence of the actual position of the switching state intervals  $d_3$  and  $d_2$  on the value of  $i_{rms}$ .

## References

- [1] A. M. Al-Zamil and D. A. Torrey, "A Passive Series, Active Shunt Filter for High Power Applications," *IEEE Trans. Power Electronics*, Vol. 16, No. 1, pp. 101-109, 2001.
- [2] G. K. Singh, A. K. Singh, R. Mitra, "A simple fuzzy logic based robust active power filter for harmonics minimization under random load variation," *Elsevier Electric Power Systems Research*, Vol. 77, Issue 8, Jun. 2007, pp. 1101-1111.
- [3] M. Rastogi, R. Naik, and N. Mohan, "A comparative evaluation of harmonic reduction techniques in three-phase utility interface of power electronic loads," *IEEE Trans. industry applications*, Vol. 30, No. 5, Sep./Oct. 1994.
- [4] M. Bojrup, "Advanced control of active filters in battery charger application," Ph.D. dissertation, Lund Univ. Technol., Lund, Sweden, 1999.
- [5] J. H. Rockot, "Losses in high-power bipolar transistors," *IEEE Trans. Power Electronics*, vol. PE-2, pp. 72-80, Jan. 1987.
- [6] A. Yazdani and R. Iravani, "Voltage-Sourced Converters in Power Systems: modeling, control and applications," John Wiley & Sons, Hoboken, New Jersey, USA, 2010.
- [7] P. D. Ziogas, E. P. Wiechmann, and V. R. Stefanovic, "A computer aided analysis and design approach for static voltage source inverters," *IEEE Trans. industry applications*, Vol. IA-21, pp. 1234-1241, Sep./Oct. 1985.
- [8] R. C. Thurston and S. F. Legowski, "A simple and accurate method of computing average and RMS currents in a three-phase PWM inverter," *IEEE Trans. Power Electronics*, Vol. 8, No. 2, pp. 192-199, April 1993.

## VIII. COMPENSATION CAPABILITY OF A BIDIRECTIONAL BATTERY CHARGER

In this chapter a Bidirectional Battery Charger (BBC) is considered, supplying its own load and in the same time compensating neighborhoods nonlinear loads (f.i. diode rectifier). Power capability of BBC is calculated when it has an active filtering function. This is done by computing the BBC current as a function of load power, load power factor and active power which can be delivered by the BBC. This capability should be calculated correctly otherwise a converter will not be able to deliver demanded power to the load or to proper compensate nonlinear load.

### 8.1. Bidirectional Charger Infrastructure

A fast charger should be capable of charging EVs with a grid-friendly current, i.e. sinusoidal line current with unity power factor. It should also be flexible enough to handle various battery types and sizes, with their individual voltage levels and current rating.

In order to increase the usage of a charger infrastructure, additional capabilities in terms of power grid conditioning can be included. This means that instead of having a negative impact on the power grid, a charger infrastructure may provide a tool for power grid operators to maintain, at least locally, a high power quality. The non-ideal, i.e. reactive, harmonic and unbalanced parts of the load current should be generated locally by the grid conditioning charger. The power grid supply would then only have to provide the active power of the load current. Fig. 8.1 describes schematically the operation principle of such a grid conditioning BBC. In this way, the load on distribution lines and transformers will be lowered and a more efficient supply of electrical energy obtained.

Another, more controversial capability that can be included in a charger infrastructure deals with peak power generation, i.e. active power support at high load. EV batteries attached to chargers may be considered as a potential energy reserve. During short periods of time, energy could be borrowed from the batteries and supplied to the power grid. This means that the charger operates as a small generator.

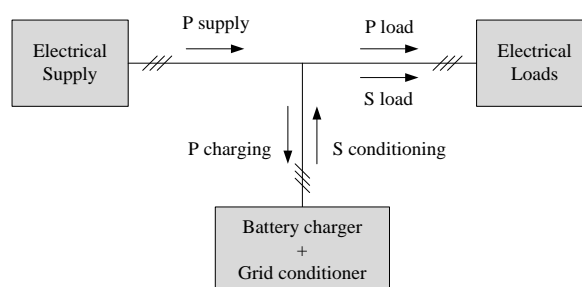


Figure 8.1. Schematic diagram of charger with grid conditioning capabilities.

This last capability has to be applied with great care, since the primary function of a charger has to be to charge EV batteries and not the opposite.

Summarizing, BBC leads to a number of capabilities desired for a charger infrastructure:

- Charging of EV's battery with sinusoidal line current and unity power factor.
- Grid conditioning capabilities such as reactive power compensation, harmonic filtering and load balancing.
- Possibility to act as a generator, i.e. provide active power support during short periods of time by borrowing energy from the EV batteries.

## 8.2. PWM Rectifier/inverter

Figure 8.2(b) shows a single-phase representation of the bidirectional inverter circuit presented in Fig 8.2(a). The  $L_f$  and  $R_f$  represent the line inductor. Magnitude of  $v_f$  depends on the modulation index of the inverter and DC voltage level.

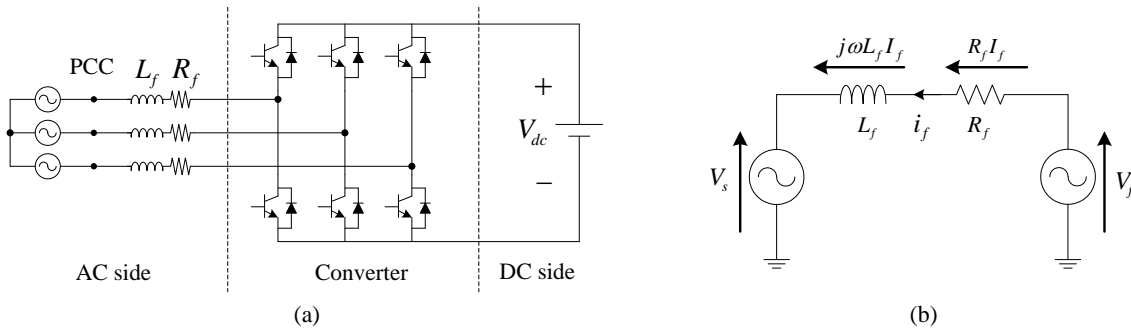


Figure 8.2. Simplified representation of three-phase battery charger for bi-directional power flow; a) Main circuit b) single-phase representation of the circuit

The line current  $i_f$  is controlled by the voltage drop across the inductance  $L$  interconnecting two voltage sources (grid and converter). It means that the inductance voltage  $v_L$  equals the difference between the line voltages  $v_s$  and the converter voltage  $v_f$ . When a phase angle  $\delta$  and amplitude of converter voltage  $v_f$  is controlled, indirectly phase and amplitude of line current is controlled. In this way average value and sign of DC current is controlled and is proportional to active power flowing through converter.

Fig. 8.3 presents general phasor diagram for both rectification and regeneration modes when power factor is unit. The figure shows that the voltage vector  $v_f$  is higher during regeneration than rectifier mode. Three phase grid voltage and the fundamental inverter line current are described as:

$$\begin{cases} v_a(t) = \sqrt{2} V_s \cos(\omega t) \\ v_b(t) = \sqrt{2} V_s \cos\left(\omega t - \frac{2\pi}{3}\right) \\ v_c(t) = \sqrt{2} V_s \cos\left(\omega t + \frac{2\pi}{3}\right) \end{cases} \quad \begin{cases} i_{fa}(t) = \sqrt{2} I_f \cos(\omega t) \\ i_{fb}(t) = \sqrt{2} I_f \cos\left(\omega t - \frac{2\pi}{3}\right) \\ i_{fc}(t) = \sqrt{2} I_f \cos\left(\omega t + \frac{2\pi}{3}\right) \end{cases} \quad (8.1)$$

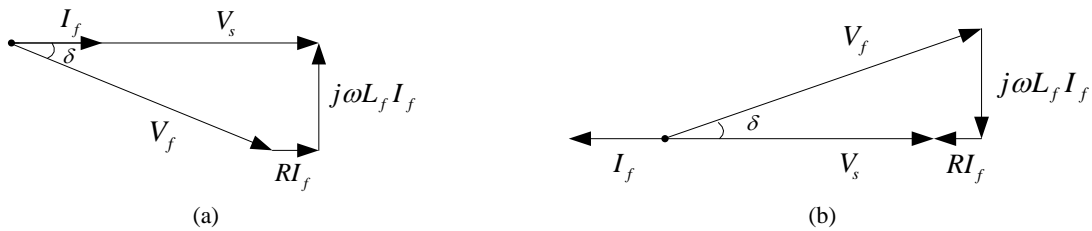


Figure 8.3. Phasor diagram for the bidirectional inverter a) rectification at unity power factor b) inversion at unity power factor

we can transform equations (8.1) to a stationary  $\alpha\beta$  –frame, so the voltage and current in  $\alpha\beta$  –frame are expressed by:

$$\begin{bmatrix} v_{s\alpha} \\ v_{s\beta} \end{bmatrix} = \begin{bmatrix} \sqrt{3} V_s \cos(\omega t) \\ \sqrt{3} V_s \sin(\omega t) \end{bmatrix}, \quad \begin{bmatrix} i_{f\alpha} \\ i_{f\beta} \end{bmatrix} = \begin{bmatrix} \sqrt{3} I_f \cos(\omega t) \\ \sqrt{3} I_f \sin(\omega t) \end{bmatrix} \quad (8.2)$$

The active and reactive power supplied from the grid in the stationary reference  $\alpha\beta$  –frame is given by

$$p = v_{s\alpha} i_{f\alpha} + v_{s\beta} i_{f\beta} = 3V_s I_f \quad (8.3)$$

$$q = v_{s\beta} i_{f\alpha} - v_{s\alpha} i_{f\beta} = 0 \quad (8.4)$$

Similarly, the input voltages in the synchronous  $dq$  –coordinates are expressed by:

$$\begin{bmatrix} v_{sd} \\ v_{sq} \end{bmatrix} = \begin{bmatrix} \sqrt{3} V_s \\ 0 \end{bmatrix}, \quad \begin{bmatrix} i_{sd} \\ i_{sq} \end{bmatrix} = \begin{bmatrix} \sqrt{3} I_s \\ 0 \end{bmatrix} \quad (8.5)$$

It gives in the synchronous  $dq$  –coordinates:

$$p = v_{sd} i_{fd} + v_{sq} i_{fq} = 3V_s I_f \quad (8.6)$$

$$q = v_{sq} i_{fd} - v_{sd} i_{fq} \quad (8.7)$$

For a unity power factor operation, following conditions can be obtained:

$$i_{fq} = 0, \quad v_{sq} = 0, \quad v_{sd} = \sqrt{3} V_s, \quad i_{fd} = \sqrt{3} I_f, \quad \text{therefore } q = 0 \quad (8.8)$$

It is required to calculate a proper power ratio of charger, especially when it will have an active filtering function. Therefore, if it will be calculated wrongly a converter will not be able to deliver demanded power to the load or to proper compensation of nonlinear load.

It will be considered an ideal PWM rectifier under ideal AC line conditions (Fig. 8.4). The apparent power of converter is given using an RMS value of AC-side voltage and current as:

$$S_f = 3V_f I_f \quad (8.9)$$

For this expression, only fundamental components of PWM rectifier input current and voltage are taken into account.

$$S_f = \sqrt{P_f^2 + Q_f^2} \quad (8.10)$$

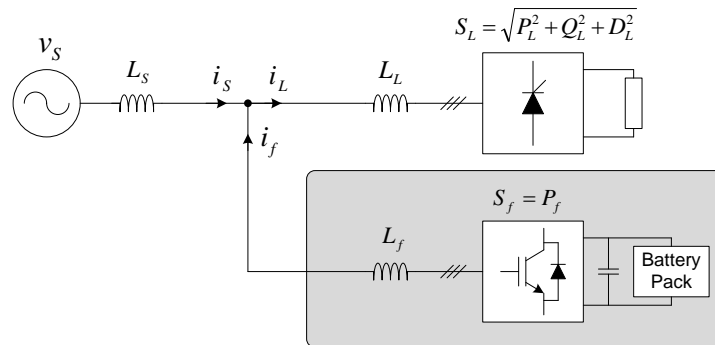


Figure 8.4. Bidirectional Battery Charger as a PWM rectifier/inverter.

where:

$$P_f = 3RI_f^2, \quad Q_f = 3X_L I_f^2, \quad S_f = 3Z_L I_f^2, \quad Z = \sqrt{R^2 + X_L^2} \quad (8.11)$$

For any ideal input inductance ( $R=0$ ), the apparent power can be expressed as follows:

$$S_f = \sqrt{P^2 + Q^2} = 3I_f \sqrt{V_s^2 + (X_L I_f)^2} \quad (8.12)$$

If we consider a unity power factor operation and omit converter losses, the input current  $I_f$  can be calculated as follows:

$$P_f = 3I_f V_s, \quad V_{LL} = \sqrt{3}V_s, \quad \text{then} \quad I_f = \frac{P_f}{\sqrt{3}V_{LL}} \quad (8.13)$$

Finally the expression for rating of PWM rectifier can be presented in the form:

$$S_f = P_f \sqrt{1 + \left( \frac{X_L P_f}{V_{LL}^2} \right)^2} \quad (8.14)$$

where  $P_f$  is BBC active power consumption or battery side active power,  $X_L$  reactance of the input filter,  $V_{LL}$  line to line voltage. It can be seen that the power ratio of PWM rectifier strongly depends and increase with increasing output power  $P_f$  and input inductor value  $L_f$ . Therefore, the input inductor value should be kept in reasonable value, otherwise for high power applications, high value of input inductor will increase demanded power ratio  $S_f$  of the converter.

### 8.3. Shunt Active Filter

As a shunt active filter, the converter compensates only neighborhoods nonlinear loads and does not supply active power  $P_f = 0$  (Fig. 8.5).

For considerations in this section following assumptions are made:

- Sinusoidal grid voltage,
- The thyristor rectifier operates in ideal conditions and commutation effect is neglected,
- The phase shift between a grid voltage and fundamental harmonic of thyristor rectifier input current changes in the range from  $0^\circ$  to  $30^\circ$  (displacement factor).

For calculations of the SAF kVA rating following points should consider:

- THD of a thyristor rectifier input current,
- Displacement power factor,
- Input inductor value.

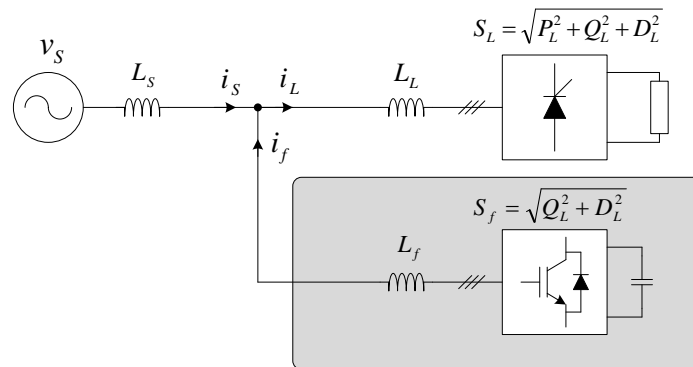


Figure 8.5. Bidirectional Battery Charger as an active filter.



Considering an ideal waveform of thyristor rectifier input current (rectangle waveform, as it is explained in Appendix A), we have:

$$i_L(t) = \frac{2\sqrt{3}}{\pi} I_0 \left[ \sin(\omega t - \varphi) - \frac{1}{5} \sin 5(\omega t - \varphi) + \frac{1}{7} \sin 7(\omega t - \varphi) \dots \right] \quad (8.15)$$

where  $I_0$  is calculated from active power that is delivered to the load as follow:

$$I_{L1} = \frac{\sqrt{6}}{\pi} I_0 = \frac{P_L}{3V_s \cos \varphi} \quad (8.16)$$

$$I_0 = \frac{\pi}{3\sqrt{6}V_s \cos \varphi} P_L \quad (8.17)$$

In the case of ideal compensation, all harmonics and the reactive power will be eliminated. So in this case the line current  $i_s$  can be presented as follows:

$$i_s(t) = \frac{2\sqrt{3}}{\pi} I_0 \sin(\omega t) \quad (8.18)$$

Then, from equations (8.15) and (8.18) the input current of BBC with active filtering function is expressed as:

$$i_f(t) = \frac{2\sqrt{3}}{\pi} I_0 \left[ -\sin(\omega t) + \sin(\omega t - \varphi) - \frac{1}{5} \sin 5(\omega t - \varphi) + \frac{1}{7} \sin 7(\omega t - \varphi) \dots \right] \quad (8.19)$$

In order to calculate RMS value of compensating current, three cases are considered. The first two cases are compensation of reactive power and compensation of harmonics separately. Then for the third case complete compensation is considered:

#### Case (a) Reactive compensation

As mentioned above phase shift between a grid voltage and fundamental harmonic of thyristor rectifier input current changes in the range from  $0^\circ$  to  $30^\circ$  (Fig. 8.6), therefore considering only reactive power compensation, RMS value of compensating current can be calculated as follow:

$$i_f(t) = \frac{2\sqrt{3}}{\pi} I_0 [-\sin(\omega t) + \sin(\omega t - \varphi)] \quad (8.20)$$

$$I_f = \sqrt{\frac{1}{2\pi} \int_0^{2\pi} (i_f(\omega t))^2 d(\omega t)} = \frac{2\sqrt{3}}{\pi} I_0 \sqrt{(1 - \cos \varphi)} \quad (8.21)$$

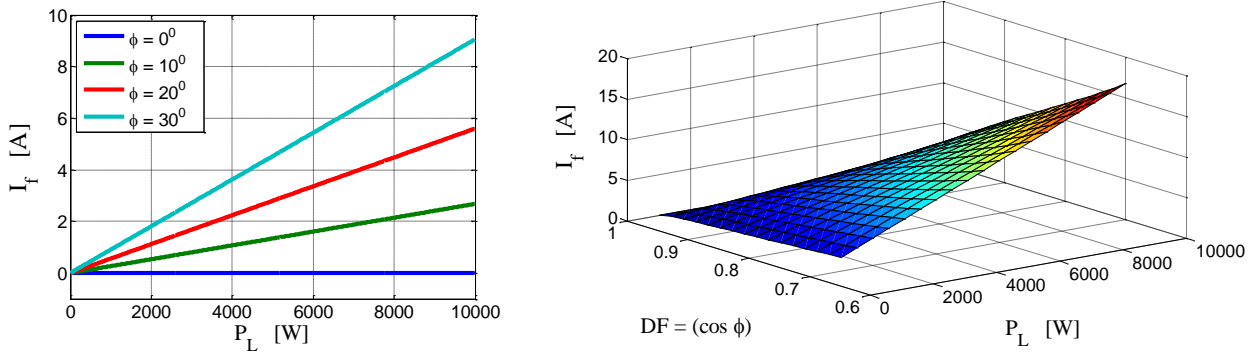


Figure 8.6. Compensating current versus thyristor rectifier output power  $P_L$ , with different Displacement Factor.

By substituting (8.17) in above equation RMS current can be expressed as a function of thyristor rectifier output power  $P_L$  (as a load) and load displacement factor ( $DF = \cos \varphi$ ) that is shown in Fig. 8.6:

$$I_f = \frac{P_L}{3V_s \cos \varphi} \sqrt{2(1 - \cos \varphi)} \quad (8.22)$$

### Case (b) Harmonic compensation

In this case the RMS value of compensating current, by considering only 5th, 7th, 11th, and 13th harmonics is calculated as follow:

$$i_f(t) = \frac{2\sqrt{3}}{\pi} I_0 \left[ -\frac{1}{5} \sin 5(\omega t - \varphi) + \frac{1}{7} \sin 7(\omega t - \varphi) \dots \right] \quad (8.23)$$

$$I_f = \sqrt{\sum_{h=5,7,11,13} I_h^2} = THD_L \cdot I_{L1} = 0.213 I_0 \quad (8.24)$$

where  $THD_L$  is the load current total harmonic distortion:

$$THD_L = \frac{I_{Distortion}}{I_{L1}} \times 100 = \frac{\sqrt{I_L^2 - I_{L1}^2}}{I_{L1}} \quad (8.25)$$

By substituting (8.17) in above equation RMS current can be expressed as follow (Fig. 8.7):

$$I_f = 0.273 \frac{P_L}{3V_s \cos \varphi} \quad (8.26)$$

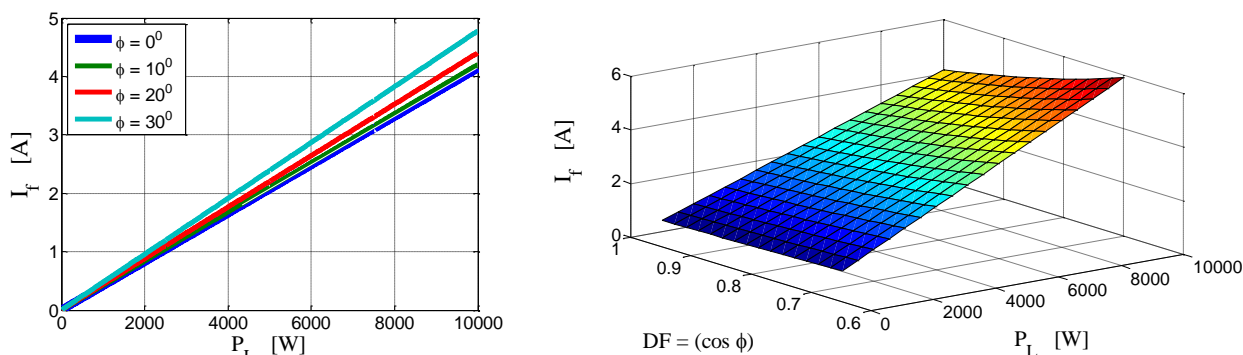


Figure 8.7. Compensating current versus thyristor rectifier output power  $P_L$  as a load, with different Displacement Factor. (harmonic compensation only for 5<sup>th</sup>, 7<sup>th</sup>, 11<sup>th</sup>, and 13<sup>th</sup> harmonics)

### Case (c) Reactive power and harmonic compensation

In this case the RMS value of compensating current, by considering both of the cases (a) and (b) is calculated as follow:

$$I_f = \sqrt{\sum_{h=1}^{13} I_h^2} = \frac{2\sqrt{3}}{\pi} I_0 \sqrt{(1.0373 - \cos \varphi)} \quad (8.27)$$

By substituting (8.17) in above equation RMS current can be expressed as a function of thyristor rectifier output power  $P_L$  (as a load) and load displacement factor ( $DF = \cos \varphi$ ) that is shown in Fig. 8.8:

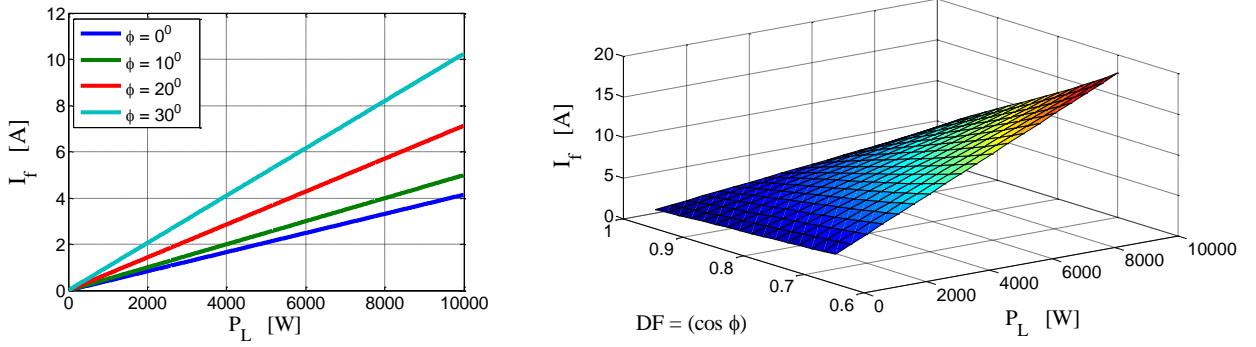


Figure 8.8. Compensating current function of the output power of thyristor rectifier (as a load) for different value of Displacement Factor. (Reactive power and harmonic compensation for 5<sup>th</sup>, 7<sup>th</sup>, 11<sup>th</sup>, and 13<sup>th</sup> harmonics)

$$I_f = \frac{P_L}{3V_s \cos \varphi} \sqrt{(2.0746 - 2\cos \varphi)} \quad (8.28)$$

The RMS value of input voltage on BBC having active filtering function can be calculated using following expression:

$$V_f = \sqrt{\frac{1}{2\pi} \int_0^{2\pi} \left( v_s(\omega t) - X_L \frac{di_f(\omega t)}{d(\omega t)} \right)^2 d(\omega t)} \quad (8.29)$$

Therefore, finally the kVA rating is calculated in this form:

$$S = 3V_f I_f \quad (8.30)$$

#### 8.4. BBC with Active Filtering Function

This section considers a power converter supplying its own load ( $P_f \neq 0$ ) and in the same time compensating neighborhoods nonlinear loads; diode rectifier/PWM Inverter (Fig. 8.9).

The kVA rating for converter having active filtering function is more complicated, because it should additionally include a compensation for a reactive  $Q_L$  and harmonic  $D_L$  powers.

In this section also, in order to calculate RMS value of compensating current, two cases are considered. Case (a) is V2G mode together with compensation of reactive power and Case (b) is V2G mode together with harmonic and reactive power compensation. For the sake of simplicity, only charging mode is calculated as an exchanging active power on V2G mode.

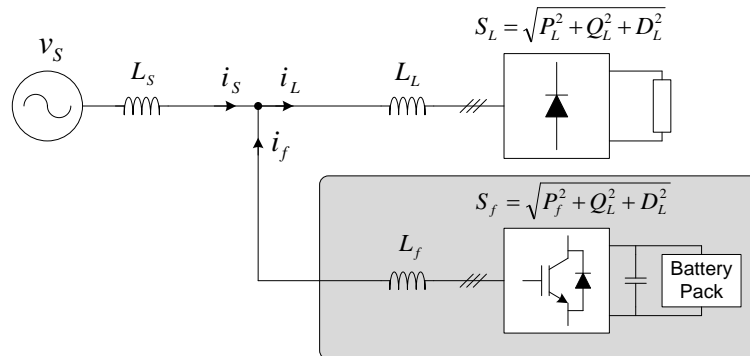


Figure 8.9. Bidirectional Battery Charger with Active Filtering operation.

**Case (a)**

Considering an ideal waveform of thyristor rectifier input current (rectangle waveform) with phase shift of the first harmonic and assuming ideal compensation for the line current by (8.18) Ideal input PWM Rectifier current and source current written as follows:

$$i_{f_{charge}}(t) = i_{f\alpha}(t) = -\frac{P_f}{3V_s} \sin(\omega t) \quad (8.31)$$

$$i_s(t) = \left( \frac{P_f}{3V_s} + \frac{2\sqrt{3}}{\pi} I_0 \right) \sin(\omega t) \quad (8.32)$$

The current  $i_{f_{charge}}$  flow from the PCC point to the BBC load, therefore the polarity is negative. This part of BBC current is considered as an active (or real) part that participates on exchanging active power, also this is the  $\alpha$ -component of BBC current (Fig. 8.10).

The input current of PWM Rectifier with active filtering function has following form:

$$i_f(t) = i_L(t) - i_s(t) = \frac{2\sqrt{3}}{\pi} I_0 \sin(\omega t - \varphi) - \left( \frac{P_f}{3V_s} + \frac{2\sqrt{3}}{\pi} I_0 \right) \sin(\omega t) \quad (8.33)$$

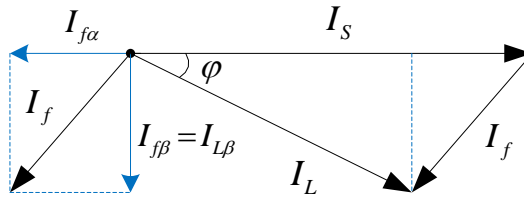


Figure 8.10. Diagram of the systems currents

where  $I_0$  is:

$$I_0 = \frac{\pi}{3\sqrt{6}V_s \cos \varphi} P_L \quad (8.34)$$

The RMS value of converter current is:

$$I_f = \sqrt{(I_s)^2 + (I_L)^2 - 2(I_s)(I_L) \cos \varphi} \quad (8.35)$$

$$I_f = \frac{1}{\sqrt{2}} \left[ \left( \frac{P_f}{3V_s} + \frac{2\sqrt{3}}{\pi} I_0 \right)^2 + \left( \frac{2\sqrt{3}}{\pi} I_0 \right)^2 - 2 \left( \frac{P_f}{3V_s} + \frac{2\sqrt{3}}{\pi} I_0 \right) \left( \frac{2\sqrt{3}}{\pi} I_0 \right) \cos \varphi \right]^{\frac{1}{2}} \quad (8.36)$$

**Case (b)**

In this case load current is considered like (8.15). The input current of PWM Rectifier with active filtering function has following form:

$$i_f(t) = \frac{2\sqrt{3}}{\pi} I_0 \left[ \sin(\omega t - \varphi) - \frac{1}{5} \sin 5(\omega t - \varphi) + \frac{1}{7} \sin 7(\omega t - \varphi) \dots \right] - \left( \frac{P_f}{3V_s} + \frac{2\sqrt{3}}{\pi} I_0 \right) \sin(\omega t) \quad (8.37)$$

The RMS value of converter current, if considering only 5th, 7th, 11th, 13th harmonics, is obtained as:

$$I_f = \sqrt{(I_s)^2 + (I_{L1})^2 - 2(I_s)(I_{L1}) \cos \varphi + (THD_L \cdot I_{L1})^2} \quad (8.38)$$

$$I_f = \frac{1}{\sqrt{2}} \left[ \left( \frac{P_f}{3V_s} + \frac{2\sqrt{3}}{\pi} I_0 \right)^2 + \left( \frac{2\sqrt{3}}{\pi} I_0 \right)^2 - 2 \left( \frac{P_f}{3V_s} + \frac{2\sqrt{3}}{\pi} I_0 \right) \left( \frac{2\sqrt{3}}{\pi} I_0 \right) \cos \varphi + 0.0746 \left( \frac{2\sqrt{3}}{\pi} I_0 \right)^2 \right]^{\frac{1}{2}} \quad (8.39)$$

Fig. 8.11 shows compensating current  $I_f$  (by Eq. 8.38) that is a function of the load power  $P_L$ , THD of load current, load displacement factor, and exchanged active power  $P_f$  by the BBC. In all above cases THD is considered as a function of fundamental component of the load current, as a consequence it is considered as a function of the load power. In Fig. 8.11(a,b) active power of BBC is considered constant and equal to 6 kW. Fig. 8.11(c) shows current of BBC for four different values of  $P_f$ , that are figured by four separated planes. Each plane shows the current of BBC with a range of load power ( $2 \text{ kW} \leq P_L \leq 10 \text{ kW}$ ) and a range of displacement factor ( $0.7 \leq DF \leq 1$ ).

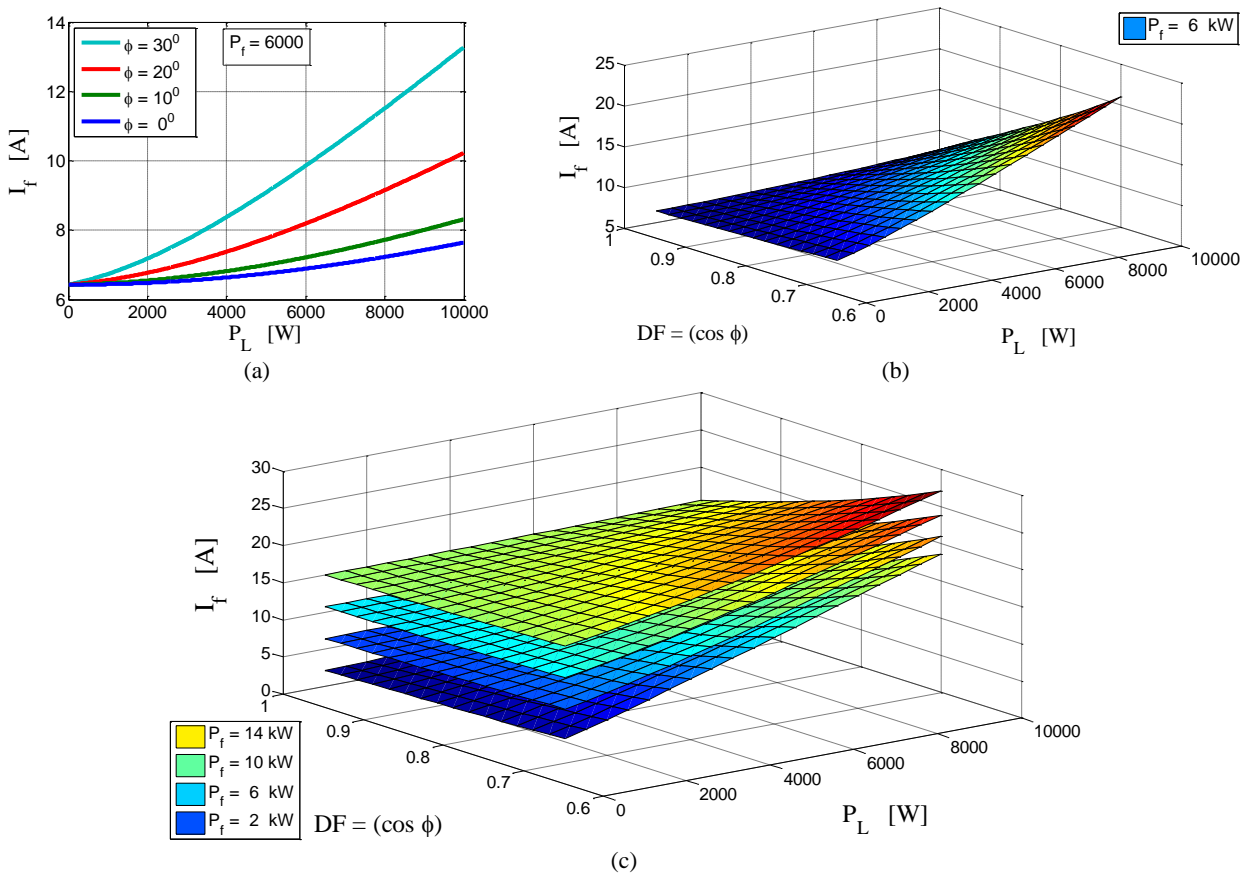


Figure 8.11. BBC current as a function of load power  $P_L$ , displacement factor  $DF$ , active power of BBC  $P_f$ , and THD of load current; (a,b) BBC current versus load power for different values of the displacement factor, (c) BBC current versus load power for different values of the displacement factor and BBC active power  $P_f$ .

## 8.5. Power capability calculating by instantaneous reactive power theory

### 8.5.1. Stationary reference $\alpha\beta$ –frame

The instantaneous reactive power theory (IRPT) proposed in previous chapters is a wide spread concept for load current identification in active filter applications. The idea is to verify capability of compensating power of BBC based on the decomposition of the instantaneous active and reactive power into their DC and AC components that are called average and oscillating parts of real and imaginary power, respectively. The fundamental active and reactive currents are given by the DC component of the instantaneous power. Consequently, the AC component corresponds to the

negative-sequence current component as well as the current harmonics. According to the IRPT, the corresponding vector representation of the instantaneous power  $\vec{s}$  in the stationary reference  $\alpha\beta$  –frame is defined as

$$\vec{s} = \vec{v}_{\alpha\beta}^* \cdot \vec{i}_{\alpha\beta} = p + jq \quad (8.40)$$

where  $p$  and  $q$  denotes the instantaneous real and imaginary power, respectively. Note, the difference from the normal definition of power as explained in previous chapters, where the conjugation is applied on the current vector and not the voltage vector as in (8.40). Furthermore voltage and current are represented as a vector in the stationary reference  $\alpha\beta$  –frame. In order to illustrate the IRPT, consider the case of a load current vector  $\vec{i}_{\alpha\beta,L}$  and an ideal grid voltage vector  $\vec{v}_{\alpha\beta,S}$  given by

$$\vec{v}_{\alpha\beta,S} = \sqrt{3}V_1 e^{j\omega_1 t} \quad (8.41)$$

$$\vec{i}_{\alpha\beta,L} = \sqrt{3}[I_1 e^{j(\omega_1 t - \varphi_1)} + I_{-1} e^{-j\omega_1 t} + I_{-5} e^{-j5\omega_1 t} + I_7 e^{j7\omega_1 t}] \quad (8.42)$$

where  $I_1$  is the RMS current of fundamental component. The factor  $\sqrt{3}$  is due to the power invariant  $abc/\alpha\beta$  transform as already has been explained in the previous chapter. Then the instantaneous power vector is obtained by inserting (8.41) and (8.42) into (8.40), which gives

$$\vec{s} = 3[V_1 I_1 e^{-j\varphi_1} + V_1 (I_{-1} e^{-j2\omega_1 t} + I_{-5} e^{-j6\omega_1 t} + I_7 e^{j6\omega_1 t})] \quad (8.43)$$

The average part (DC component) of the instantaneous power in (8.43) is divided into its corresponding average part of real and imaginary power according to

$$\vec{s}_{DC} = \bar{p} + j\bar{q} = 3V_1 I_1 e^{-j\varphi_1} = 3V_1 I_1 (\cos \varphi - j \sin \varphi) \quad (8.44)$$

The oscillating parts (AC component) of the instantaneous power is given by

$$\vec{s}_{AC} = \tilde{p} + j\tilde{q} = 3[V_1 (I_{-1} e^{-j2\omega_1 t} + I_{-5} e^{-j6\omega_1 t} + I_7 e^{j6\omega_1 t})] \quad (8.45)$$

Since the compensating current should correspond to the instantaneous power given by the average part of the imaginary and all oscillating parts, i.e.

$$\vec{s}_f = j\bar{q} + \vec{s}_{AC} \quad (8.46)$$

where  $\vec{s}_f$  is the compensating power and the compensating current is determined by the inverse relationship of (8.40), that is

$$\vec{i}_{\alpha\beta,f} = \frac{\vec{s}_f}{\vec{v}_{\alpha\beta,S}^*} \quad (8.47)$$

which in this case corresponds to

$$\vec{i}_{\alpha\beta,f} = \sqrt{3} \left[ I_1 \sin \varphi e^{j(\omega_1 t - \frac{\pi}{2})} + I_{-1} e^{-j\omega_1 t} + I_{-5} e^{-j5\omega_1 t} + I_7 e^{j7\omega_1 t} \right] \quad (8.48)$$

The compensating current in (8.48) contains all the undesired components of the load current in this case. Hence, these components are cancelled from the line current, which then only consists of the current component corresponding to the fundamental active power, i.e.

$$\vec{i}_{\alpha\beta,S} = \sqrt{3} I_1 \cos \varphi e^{j\omega_1 t} \quad (8.49)$$

### 8.5.2. Synchronous reference $dq$ –frame

Another approach for identifying the undesired components of the load current considers the instantaneous currents represented in the synchronously rotating reference  $dq$  –frame oriented to the grid voltage vector [4], [5]. This method resembles the IRPT method and under ideal conditions they are equivalent. The load current vector in the synchronous reference  $dq$  –frame is derived from the stationary reference  $\alpha\beta$  –frame by subtraction of the corresponding angle difference  $\theta = \omega_1 t$ . The representation of the load current vector of (8.42) in synchronous coordinates is then given by

$$\vec{i}_{dq,L} = \sqrt{3}[I_1 e^{-j\varphi_1} + I_{-1} e^{-j2\omega_1 t} + I_{-5} e^{-j6\omega_1 t} + I_7 e^{j6\omega_1 t}] \quad (8.50)$$

The DC component of the load current vector in synchronous coordinates is written

$$\vec{i}_{dq,L,DC} = \sqrt{3}I_1(\cos \varphi - j \sin \varphi) \quad (8.51)$$

where the average real and imaginary parts of instantaneous power correspond to the real and imaginary part of current components, respectively. The AC component of the load current vector corresponds to the negative-sequence current component and the current harmonics, that is

$$\vec{i}_{dq,L,AC} = \sqrt{3}[I_{-1} e^{-j2\omega_1 t} + I_{-5} e^{-j6\omega_1 t} + I_7 e^{j6\omega_1 t}] \quad (8.52)$$

As in the case of the IRPT, the instantaneous currents represented in synchronous coordinates provide complete information of the different load current components. The compensation current should correspond to the fundamental reactive current, i.e. the imaginary part of the DC component, and the AC components

$$\vec{i}_{dq,f} = \Im(\vec{i}_{dq,L,DC}) + \vec{i}_{dq,L,AC} \quad (8.53)$$

which is equivalent to the compensation current obtained from the IRPT.

Source current consists of the real part of current component corresponding to the fundamental active power, i.e.

$$\vec{i}_{dq,s} = \Re(\vec{i}_{dq,L,DC}) = \sqrt{3}I_1 \cos \varphi \quad (8.54)$$

The results of load current decomposition by the IRPT and by the representation of the instantaneous currents in synchronous coordinates are equivalent under ideal conditions. However, in the presence of grid voltage distortions, the obtained compensation currents differ. The distorted voltage implies that the corresponding current harmonics will contribute to the actual power flow, and hence to the DC component of the instantaneous power. Table 8.1 gives the correspondence between the conditioning components and their representation in the synchronous reference  $dq$  –frame.

**Table 8.1 Representation of the current components in the synchronously rotating reference  $dq$ -frame.**

Component	Sequence	Frequency	Vector
active	positive	$DC$	$i_d$
reactive	positive	$DC$	$j i_q$
unbalancing	negative	$2f_1$	$I_{-1} e^{-j2\omega_1 t}$
5 <sup>th</sup> harmonic	negative	$6f_1$	$I_{-5} e^{-j6\omega_1 t}$
7 <sup>th</sup> harmonic	positive	$6f_1$	$I_7 e^{j6\omega_1 t}$
11 <sup>th</sup> harmonic	negative	$12f_1$	$I_{-11} e^{-j12\omega_1 t}$
13 <sup>th</sup> harmonic	positive	$12f_1$	$I_{13} e^{j12\omega_1 t}$
...	...	...	...

**Example (8.1)**

In this example the ratings of the power components in the inverter system are determined. A detailed list of the inverter requirement for this inverter is,

- 50 kVA.
- Output voltage (or grid voltage): 380 three-phase / 220 single-phase.
- Output frequency : 50Hz.
- Output voltage THD : less than 5%

Consider two separate cases: (a) harmonics compensation, (b) reactive power compensation

The full load current of each phase is given by,

$$I_f = \frac{S_f}{3 V_s} = \frac{50.000}{3 \times 380} = 76 A$$

**Case (a)**

For the sake of simplicity, in order to compensate the harmonics, the output current  $i_f$  is assumed to consist of only 5th and 7th harmonics ( $i_{f5}$ ,  $i_{f7}$ ). Further, assuming  $I_{f5} = I_{L5} = \frac{1}{5}I_1$  and  $I_{f7} = I_{L7} = \frac{1}{7}I_1$  since this is a typical case of a rectifier type nonlinear load,  $I_1$  is the fundamental load current

$$I_f = \sqrt{\sum_{h=5,7} I_h^2} = THD_L \cdot I_{L1} = \sqrt{0.06} \cdot I_{L1} \quad (8.55)$$

Therefore, the fundamental RMS value of load current  $I_{L1}$  becomes,

$$I_{L1} = \frac{I_f}{THD_L} = 310 A \quad (8.56)$$

It means that the bidirectional converter is able to compensate the harmonics current of such a load with above fundamental current. So the load power can be calculated as follow:

$$S_L = 3V_s I_{L1} = 3 \times 220 \times 310 \approx 205 KVA \quad (8.57)$$

Here there is no need to compensate the reactive power so  $\bar{q} = 0$

$$\vec{s}_f = \vec{s}_{AC} = 3V_s(I_{-5}e^{-j6\omega_1 t} + I_7 e^{j6\omega_1 t}) \approx 41e^{-j6\omega_1 t} + 30e^{j6\omega_1 t} \quad (8.58)$$

As one can see, the power of BBC consists of AC component only, which means that the average (DC) component of power is zero. Because of this property the shunt active filters don't need any energy storage like battery hence by using capacitor it will be satisfied.

**Case (b)**

The full load current of each phase is 76A, so the RMS value of load current  $I_L$  is calculated by equation (8.59) that derived from (8.21). Fig. 8.12 shows load current versus different power factor that has limited from 0.87 to 0.96 ( $\varphi < \frac{\pi}{6}$ ).

$$I_L = \frac{I_f}{\sqrt{2(1 - \cos \varphi)}} \quad (8.59)$$



It means that the bidirectional converter is able to compensate the reactive power of such a load with current and power factor that are shown in Fig. 8.12(a). So the load power can be calculated as follow:

$$P_L = \frac{3I_f V_s \cos \varphi}{\sqrt{2(1 - \cos \varphi)}} \quad (8.60)$$

that means the bidirectional converter is able to compensate the reactive power of such a load with power  $P_L$  and power factor that are shown in Fig. 8.12(b).

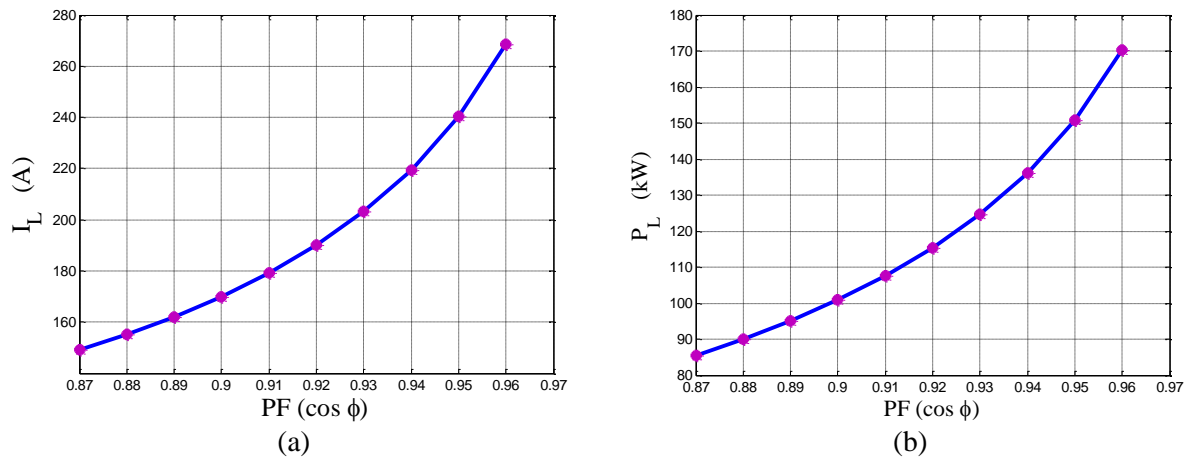


Figure 8.12. Capability of the BBC to compensate the reactive power; (a) Different Load Currents with specified power factor, and (b) Different load power with specified power factor, that can be supported by the BBC in this example.

## IX. L-FILTER DESIGN

Active Front End converters are used to improve power quality of drives and electronic loads at the point of common coupling to the grid. The conventional method to interface these converters to the grid is through a simple first order low-pass filter ie. L-filter. The equivalent line impedance can be regarded as large for the harmonics whereas it should ideally be zero for the fundamental frequency component. But such a filter is bulky, inefficient and cannot meet the regulatory requirements regarding interconnection of harmonic loads to grid [1]. Design of higher order LCL filters that are used in grid-connected inverter applications involves multiple constraints. The filter requirements are driven by tight filtering tolerances of standards such as IEEE 519-1992 and IEEE P1547.2- 2003 [2, 5]. The selection of the ripple current is a trade-off among inductor size, IGBT switching and conduction losses, and inductor coil and core losses. For a given filter the smaller the ripple current, the lower the IGBT switching and conduction losses. But the larger the inductor, resulting in larger coil and core losses. Typically, the ripple current can be chosen as 15%-20% of rated current [3].

### 9.1. Analysis of ripple current

#### 9.1.1. Single phase full-bridge inverter

Figure 9.1 describes a single-phase grid-connected inverter using full-bridge topology and its equivalent circuit. Grid voltage  $v_s$  is assumed ideal sinusoid. To simplify the analysis, the fundamental component of the inverter and grid voltage in Fig. 9.1(b) is assumed to be zero (by using superposition theory). Based on the superposition principle, the response of the filter to the composite input can be regarded as the summation of its responses to individual input components. In other words the fundamental component of the inverter and grid voltages are considered as a source of fundamental current, while voltage harmonics ( $v_{fH}$ ) are considered as a source of ripple current.

As can be seen in Fig. 9.2, single-phase full-bridge inverters normally use unipolar PWM, so that the inverter output voltage  $v_f$  has three step values; ( $V_{dc}$ , 0) in first half cycle, and ( $0$ ,  $-V_{dc}$ ) in second cycle.

When the switching frequency  $f_s$  is much higher than the utility frequency  $f$ , the time average value of the inverter output voltage  $v_{f,av}$  (that is equal to the fundamental component of inverter output voltage  $v_{f1}$ ) can be regarded to be constant during the switching period  $T_s$ .

Note that in the interface ( $0 < t < \frac{d_1}{2} T_s$ ) output voltage of inverter is equal to  $V_{dc}$  and so the voltage of inductor as shown in Fig. 9.1(c) is

$$\begin{aligned} v_L = v_{fH} &= (v_f - v_{f1}) = (V_{dc} - v_{f,av}) & \text{when } (0 < t < \frac{d_1}{2} T_s) \\ v_{f,av} &= d_1 V_{dc} \end{aligned} \quad (9.1)$$

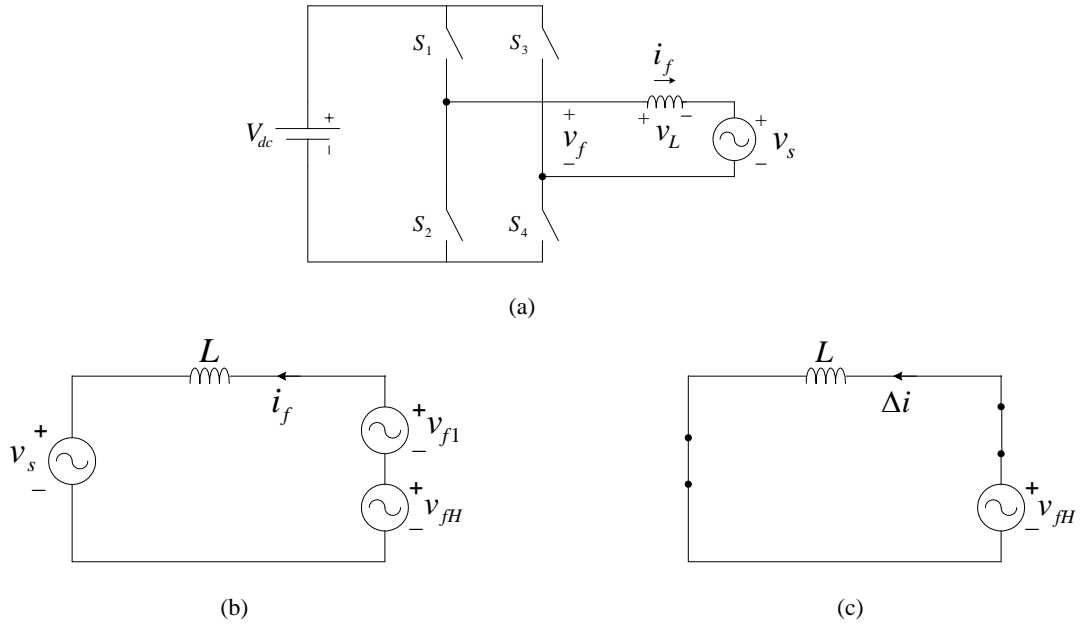


Figure 9.1. a) Topology of a single-phase full-bridge inverter, b) its equivalent circuit, c) and after imposing superposition theory.

Thus, the filter inductor current, by neglecting the fundamental current during any switching period, has typical waveform as shown by the lower axis in Fig. 9.2.

In this case, the peak-to-peak value of the filter inductor current  $\Delta i_{pp}$  that results from the unipolar<sup>1</sup> PWM switching can be calculated in a period of  $\frac{d_1}{2} T_s$  as:

$$\Delta i_{pp} = 2\Delta I_{max} = \frac{(V_{dc} - v_{f,av}) d_1}{L} \frac{T_s}{2} \quad (9.2)$$

Moreover, when the conditions described above are applied to full-bridge inverter, during the interval of  $0 < \omega t < \pi$  equations (9.3) and (9.4) can be deduced.

$$v_{f,av}(\omega t) = d_1(\omega t)V_{dc} \quad , \quad v_{f,av}(\omega t) = M_a V_{dc} \sin(\omega t) \quad (9.3)$$

$$d_1(\omega t) = M_a \sin(\omega t) \quad (9.4)$$

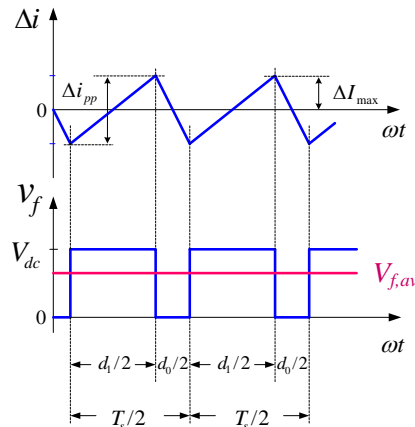


Figure 9.2. Output voltage and current waveforms of typical single-phase full-bridge inverters.

<sup>1</sup> In the case of unipolar PWM the relationship between the modulation index and duty ratio is  $d_1 = m$ , while for bipolar PWM is  $d_1 = \frac{1+m}{2}$  (where  $m = M_a \sin(\omega t)$ ).

From (9.3) and (9.4), the peak-to-peak value of the filter inductor current during  $0 < \omega t < \pi$  can be calculated by (9.5).

$$\Delta i_{pp}(\omega t) = \frac{V_{dc} T_s}{2L} (1 - M_a \sin(\omega t)) M_a \sin(\omega t) \quad (9.5)$$

Figure 9.3 shows magnitude distribution<sup>1</sup> of  $\Delta i_{pp}$  of grid connected full-bridge inverter according to the parameter of modulation index  $M_a$  during the period  $0 < \omega t < \pi$ .  $\Delta i_{pp}(\theta)$  has minimum or maximum value when the utility angle  $\theta$  is;  $\sin^{-1}(1/2M_a)$ ,  $\pi/2$ , and  $\pi - \sin^{-1}(1/2M_a)$ . These minimum or maximum values are obtained by  $d(\Delta i_{pp})/d\theta = 0$  (where  $\theta = \omega t$ ).

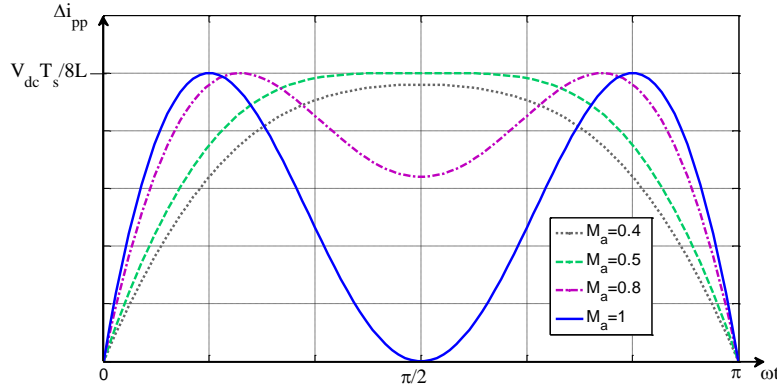


Figure 9.3. Magnitude distribution of  $\Delta i_{pp}$  of single-phase full-bridge inverters.

Since the voltage and current waveforms are half-cycle symmetry, the situation during  $\pi < \omega t < 2\pi$  repeats as that of during  $0 < \omega t < \pi$ .

As a consequence the maximum value of  $\Delta i_{pp}$  is

$$\Delta i_{pp,max} = \frac{V_{dc} T_s}{8L} \quad (9.6)$$

However the position of maximum point is changed with respect to the different modulation index. According to the harmonic standard [5], 15-20% of the rated current is allowable. The maximum ripple can now be calculated from (9.6). The ripple current depends on the DC link voltage, inductance, and the switching frequency. The DC link voltage and switching frequency are constant, thus the minimum constraint of inductance can be calculated from (9.7).

$$L_{min} = \frac{1}{8} \cdot \frac{V_{dc}}{\Delta i_{pp,max} \cdot f_s} \quad (9.7)$$

### 9.1.2. Three phase inverter

Figure 9.4 shows a three-phase grid-connected inverter using SVM switching technique in sector (I), while producing the inverter output by combination of two vectors  $V_1(100)$  and  $V_2(110)$ . As the same way, the peak-to-peak value of the filter inductor current  $\Delta i_{pp}$  that results from the SVM switching can be calculated but the duty cycle functions are different, as explained below.

Consider the load to be balanced, then the phase voltages  $v_{fa}$ ,  $v_{fb}$ ,  $v_{fc}$  with respect to a neutral point (n) chosen such that  $v_{fan} + v_{fbn} + v_{fcn} = 0$ . The phase voltage  $v_{fan}$ , as shown in Fig. 9.4, has three step values in sector (I);  $\frac{2V_{dc}}{3}$ ,  $\frac{V_{dc}}{3}$ , and 0.

<sup>1</sup> In fact  $\Delta i_{pp}$  is calculated in each switching period and in Fig. 9.3 it can be assumed that the solid curves are obtained by interpolating and calculating all these calculated points. The same assumption is considered for the other plots like as Fig. 9.8 to Fig. 9.10.

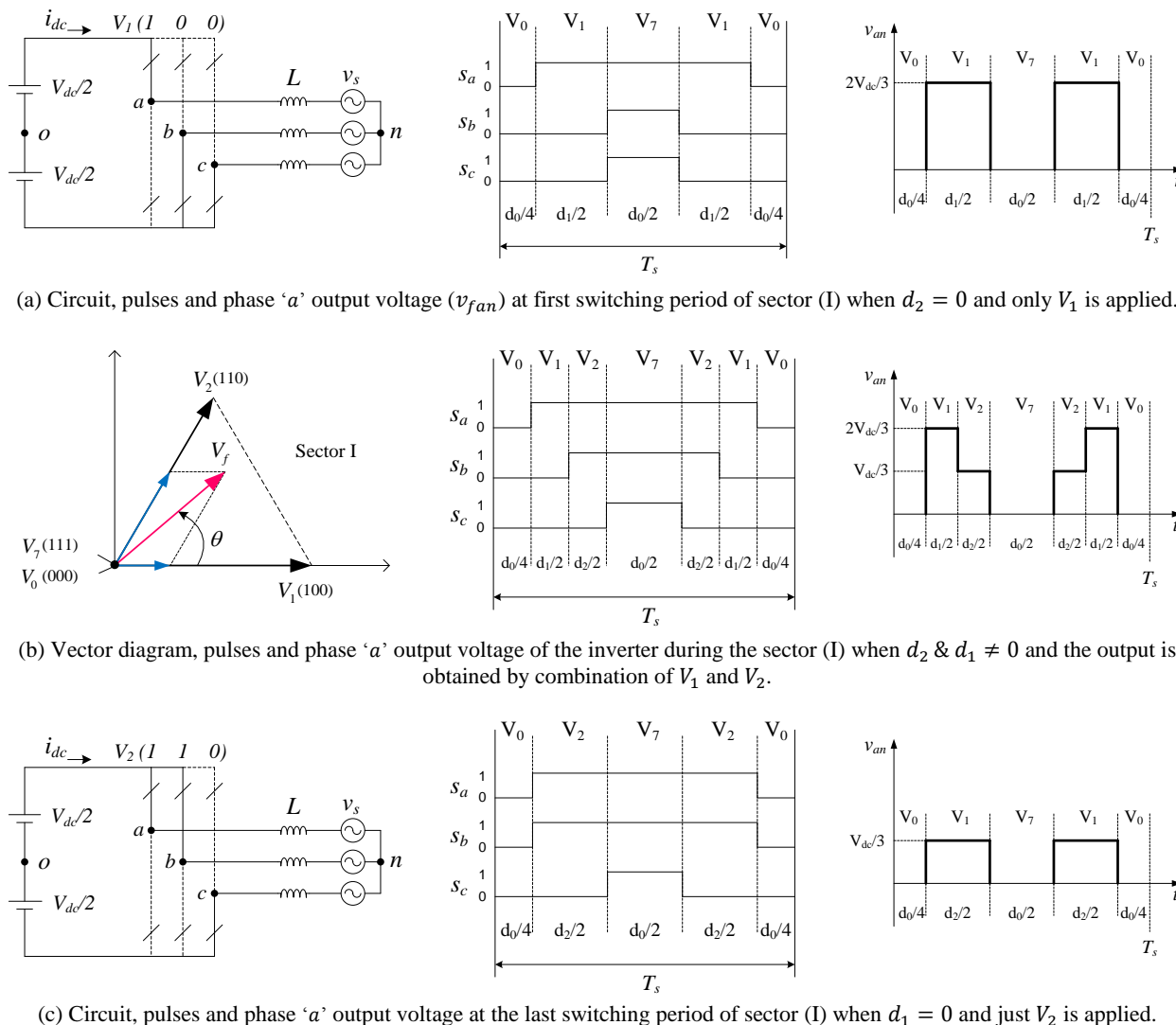


Figure 9.4. Three-phase grid-connected inverter using SVM switching technique in sector I ( $0 < \omega t < \frac{\pi}{3}$ ).

There are different types of SVM switching that one of them is symmetrical as shown in Fig. 9.5 and the other is asymmetrical. For the symmetrical case in each switching period, duty cycles  $d_1$  and  $d_2$  are divided into two equal halves ( $d_1/2, d_2/2$ ) as shown in Fig. 9.5(b).

In the case of asymmetrical SVM switching, decomposition of the phase voltage switching waveform for SVM to obtain a series of pulses as in Fig. 9.6 is a two step process. At first the waveform is decomposed to obtain stepped pulses as shown in Fig. 9.7(a), then this stepped pulse waveform is further decomposed to obtain pulses, similar to Fig. 9.2, as shown in Fig. 9.7(b) and Fig. 9.7(c).

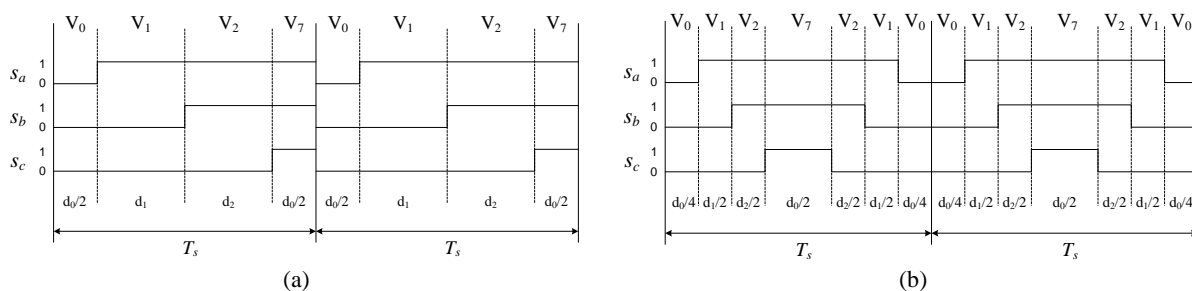
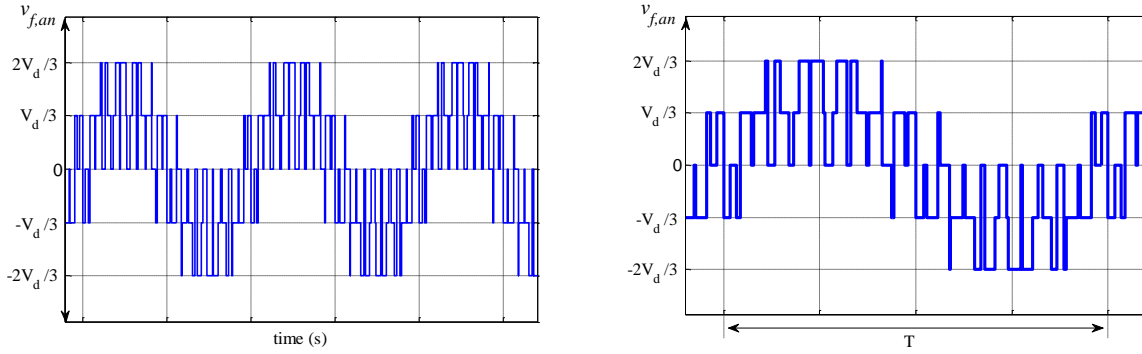


Figure 9.5. Typical phase gating signals of, a) typical asymmetrical switching, b) symmetrical switching


 Figure 9.6. Typical Phase voltage in one phase by SVM switching ( $v_{f,an}$ )

In the case of symmetrical SVM switching, first half cycle of a switching period should be considered, then the stepped pulse waveform is decomposed to obtain pulses, as shown in Fig. 9.7(d). The average value of the inverter output voltage  $v_{f,an_{av}}$  (considering phase 'a') can be considered to be constant during the switching period  $T_s$  if the switching frequency  $f_s$  is much higher than the grid frequency  $f$  [Fig. 9.6]. The average value of voltage in each switching period of sector (I) is:

$$v_{f,an_{av}} = d_1 \frac{2V_d}{3} + d_2 \frac{V_d}{3} = \frac{V_d}{3} (2d_1 + d_2) \quad (9.8)$$

where  $d_1$  and  $d_2$  are the duty cycle of vector  $V_1$  and  $V_2$  in sector (I), respectively. Furthermore  $d_1$  and  $d_2$  in sector (I) can be expressed as:

$$d_1(\omega t) = M_a \sin(\pi/3 - \omega t) \quad (9.9)$$

$$d_2(\omega t) = M_a \sin(\omega t) \quad (9.10)$$

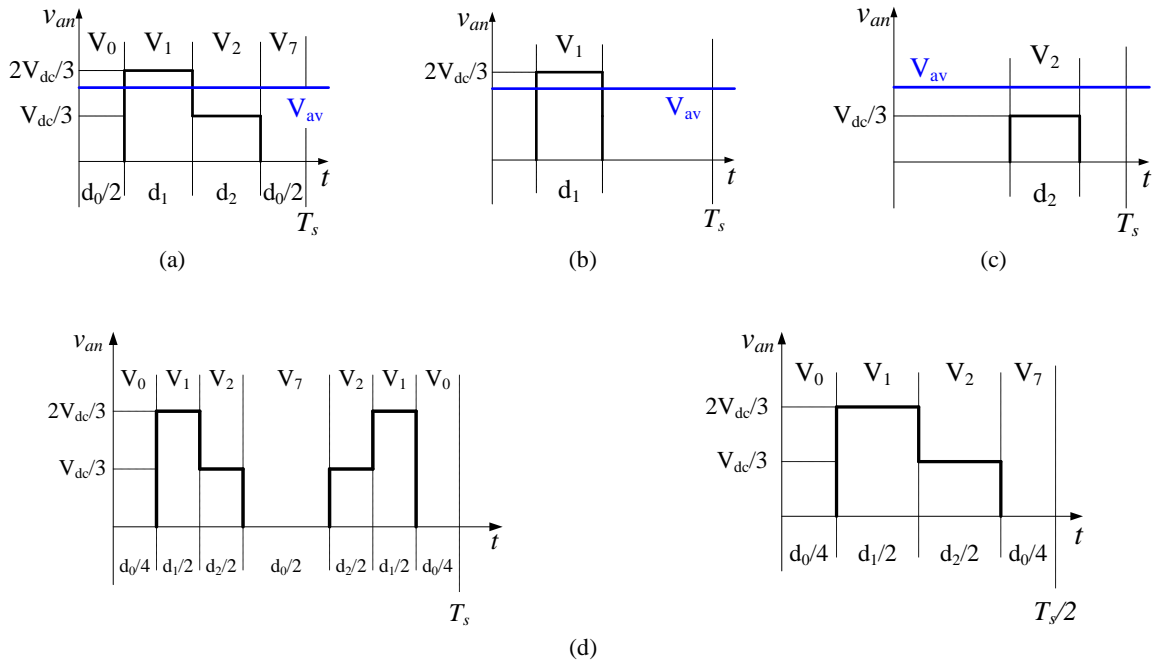


Figure 9.7. Phase voltage decomposition in one switching period; a,b,c) asymmetrical SVM switching, d) symmetrical SVM switching.

### 9.1.2.1. Ripple current due to vector $V_1$ in each switching period ( $\Delta i_{pp1}$ ):

In this case, the peak-to-peak value of the filter inductor current ( $\Delta i_{pp1}$ ) that results from the vector  $V_1$  of SVM switching, as shown in Fig. 9.7(b), can be calculated in a period of  $d_1 T_s$  as

$$\Delta i_{pp1} = \frac{d_1 T_s}{L} (v_{f,an} - v_{f,anav}) = \frac{d_1 T_s}{L} \left( \frac{2}{3} V_d - v_{f,anav} \right) = \frac{T_s V_d}{3L} d_1 (2 - 2d_1 - d_2) \quad (9.11)$$

Moreover, by substituting (9.9) and (9.10) in above equation during sector (I),  $\Delta i_{pp1}$  can be deduced as

$$\Delta i_{pp1} = \frac{V_d}{3L f_s} M_a \sin(\pi/3 - \omega t) \left( 2 - 2M_a \sin\left(\frac{\pi}{3} - \omega t\right) - M_a \sin(\omega t) \right), \quad (0 < \omega t < \frac{\pi}{3}) \quad (9.12)$$

Figure 9.8 shows magnitude distribution of  $\Delta i_{pp1}$  of phase 'a' according to different parameters of modulation index  $M_a$  during the period ( $0 < \omega t < \pi/3$ ). As one can see in Fig. 9.8 the ripple  $\Delta i_{pp1}(\omega t)$  has its maximum value when the utility angle is  $\omega t = 0$  and the modulation index is  $M_{a,r max} = 1/\sqrt{3}$ . It means the maximum ripple current in phase 'a' occurs when the reference vector in Fig. 9.4(b) is collinear with the vector  $V_1$ . At this instant the duty cycle  $d_2 = 0$ , and the resultant phase voltage will be as shown in Fig. 9.4(a). The  $M_{a,r max} = 1/\sqrt{3}$  is obtained by  $\frac{d(\Delta i_{pp1})}{dM_a} = 0$  and at  $\omega t = 0$  as

$$M_{a,r max} = \left. \frac{1}{2 \sin\left(\frac{\pi}{3} - \omega t\right) + \sin(\omega t)} \right|_{\omega t=0} = \frac{1}{\sqrt{3}} \approx 0.58 \quad (9.13)$$

As a consequence the maximum value of  $\Delta i_{pp1}$  is

$$\Delta i_{pp1,max} = \frac{V_{dc}}{6L f_s} \quad (9.14)$$

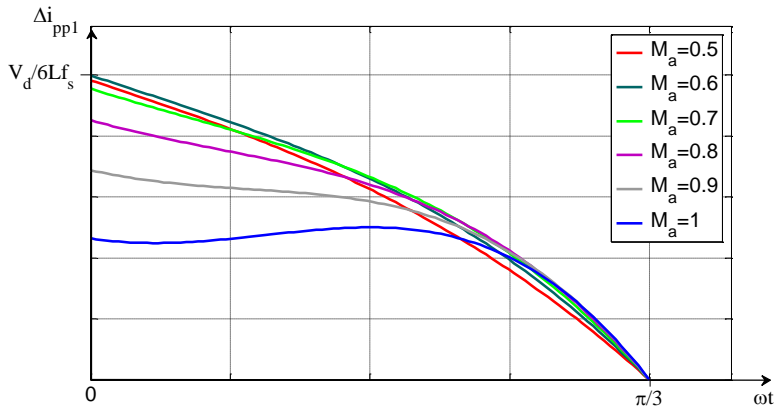


Figure 9.8. Magnitude distribution of  $\Delta i_{pp1}$  in sector I ( $0 < \omega t < \frac{\pi}{3}$ ).

### 9.1.2.2. Ripple current due to vector $V_2$ in each switching period ( $\Delta i_{pp2}$ ):

As the same way, the peak-to-peak value of the filter inductor current ( $\Delta i_{pp2}$ ) that results from the vector  $V_2$ , as shown in Fig. 9.7(c), can be calculated in a period of  $d_2 T_s$  as

$$\Delta i_{pp2} = \frac{d_2 T_s}{L} \left( \frac{V_d}{3} - v_{f,anav} \right) = \frac{T_s V_d}{3L} d_2 (1 - 2d_1 - d_2) \quad (9.15)$$

Moreover, by substituting (9.9) and (9.10) in above equation during sector (I),  $\Delta i_{pp2}$  can be deduced as

$$\Delta i_{pp2} = \frac{V_d}{3L f_s} M_a \sin(\omega t) \left( 1 - 2M_a \sin\left(\frac{\pi}{3} - \omega t\right) - M_a \sin(\omega t) \right), \quad 0 < \omega t < \frac{\pi}{3} \quad (9.16)$$

Figure 9.9 shows magnitude distribution of  $\Delta i_{pp2}$  of phase 'a' according to the different parameters of modulation index  $M_a$  during the period ( $0 < \omega t < \pi/3$ ).

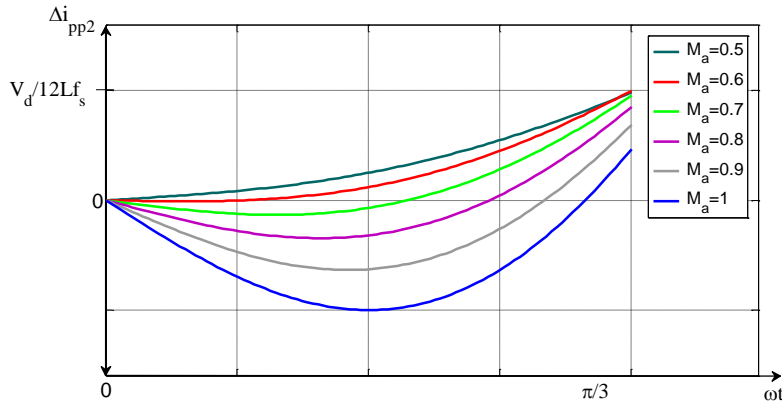


Figure 9.9. Magnitude distribution of  $\Delta i_{pp2}$  in sector I ( $0 < \omega t < \frac{\pi}{3}$ ).

Finally the peak-to-peak value of the filter inductor current  $\Delta i_{pp}$  that results from the both vectors  $V_1$  and  $V_2$ , as shown in Fig. 9.10, can be calculated as

$$\Delta i_{pp} = \Delta i_{pp1} + \Delta i_{pp2} \quad (9.17)$$

One can see the result for the maximum value of total ripple  $\Delta i_{pp,max}$  is the same as maximum ripple due to  $V_1$  that is

$$\Delta i_{pp,max} = \Delta i_{pp1,max} = \frac{V_{dc}}{6L f_s} \quad (9.18)$$

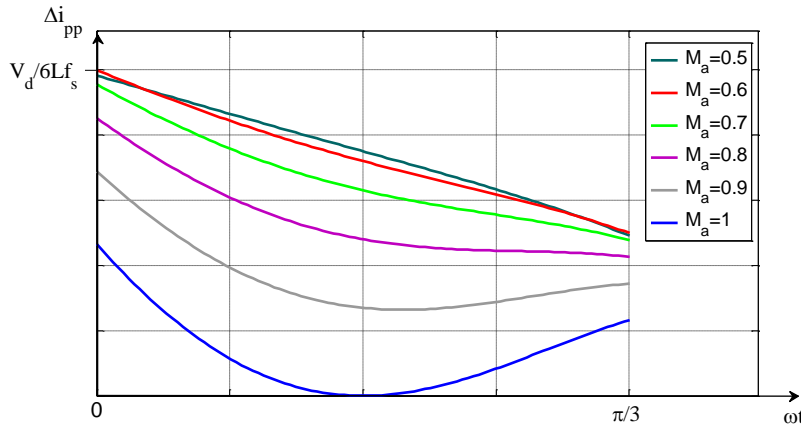


Figure 9.10. Magnitude distribution of  $\Delta i_{pp}$  in sector I ( $0 < \omega t < \frac{\pi}{3}$ ).



Equation (9.18) is true for asymmetrical SVM switchings. For symmetrical SVM switching the duty cycles  $d_1$  and  $d_2$  are split in two halves and hence:

$$\Delta i_{pp,max} = \Delta i_{pp1,max} = \frac{V_{dc}}{12 L f_s} \quad (9.19)$$

### Example

The step-by-step design procedure can be described by the following example, where rated power rating = 20 kW, and the rated RMS phase voltage is 230 V, DC bus voltage  $V_{dc} = 590$  V, switching frequency  $f_s = 10$  kHz, peak value of rated current  $\hat{I} = 42.42$  A (RMS current  $I = 30$  A).

Adopting maximum allowable value of current ripple  $\Delta i_{pp,max} = 10\% \hat{I}$ , total inductance for three phase system by SVM asymmetrical and symmetrical switching can be calculated according to (9.18) and (9.19)  $L = 2.3$  mH and  $L = 1.15$  mH, respectively.

## 9.2. L minimum value to interface active filter and grid for harmonic compensation

On the other hand the AC side inductor is aimed at impressing the required current at the output of the compensator and at filtering the voltage generated by the converter to maintain both the magnitude of the individual current harmonics and the total current harmonic distortion ( $THD_i$ ) within the limits fixed by the regulations and standards that are mentioned summary in the next section [5].

Under assumption that the mains impedance is negligible compared to both filter inductance and load inductance, the voltage harmonic  $V_{fh}$  at the converter output injects into the grid a current harmonic  $I_{fh}$  equal to

$$I_{fh} = \frac{V_{fh}}{h\omega L} \quad (9.20)$$

where  $\omega$  is the fundamental angular frequency and  $h$  is the harmonic order ( $h > 1$ ) and  $V_{fh}$  is determined from [6]. Both  $V_{fh}$ ,  $I_{fh}$  are RMS values. From (9.20),  $THD_i$  can be expressed as

$$THD_i = \frac{\sqrt{\sum_n I_{fh}^2}}{I_{f1,N}} = \frac{1}{\omega L I_{f1,N}} \sqrt{\sum_n \left(\frac{V_{fh}}{h}\right)^2} \quad (9.21)$$

where  $I_{f1,N}$  is the nominal magnitude of the fundamental component of the compensator output current. By imposing that the ratio of each current harmonic to  $I_{f1,N}$  and the  $THD_i$  value do not exceed the limits fixed by the standard, filter inductance is obtained as the prevailing quantity among the following ones:

$$L \geq \frac{V_{fh}}{h\omega I_{f1,N} \lambda_h^*}, \quad \text{for any } h \quad \lambda_h^* = \frac{I_{fh}}{I_{f1,N}} \quad (9.22)$$

$$L \geq \frac{1}{\omega I_{f1,N} THD_i^*} \sqrt{\sum_n \left(\frac{V_{fh}}{h}\right)^2} \quad (9.23)$$

where the standard limitation of  $THD_i$  and harmonics are denoted by  $THD_i^*$  and  $\lambda_h^*$  respectively. Equations (9.22) and (9.23) show that  $L$  depends on the voltage harmonic content at the converter output.

## 9.3. L maximum value to interface active filter and grid for harmonic compensation

From knowledge of current harmonics type, we can calculate the limit value of inductance that allows their filtering

$$i_{fH} = \sum_h \sqrt{2} I_h \cos(h\omega t + \varphi_h) \quad (9.24)$$

$i_{fH}$  represents the total current harmonics to be compensated. The voltage drop across the inductance is

$$v_L = \sqrt{2} L\omega \sum_h h I_h \cos(h\omega t + \varphi_h) \quad (9.25)$$

In the worst case, all harmonics are in phase and therefore the maximum value of the voltage to be generated by the converter will (by neglecting the term fundamental current)

$$\hat{V}_{fmax} = V_s \sqrt{2} + \sum_h h\omega L I_h \sqrt{2} \quad (9.26)$$

$V_s$  is the RMS voltage of the network and  $\hat{V}_f$  is the maximum amplitude of compensator voltage.

If we consider a scalar PWM modulation type (with modulation index  $M_a = \frac{\hat{V}_f}{V_{dc}/2}$ ) and a value of DC bus voltage of the converter,  $V_{dc}$ , the inductance value must be less than

$$L_{max} = \frac{V_{dc} - 2V_s \sqrt{2}}{2 \sum_h h\omega L I_h \sqrt{2}} \quad (9.27)$$

If maximum modulation for SVM switching is considered then the inductance maximum value is

$$L_{max} = \frac{V_{dc} - V_s \sqrt{6}}{\sqrt{6} \sum_h h\omega L I_h} \quad (9.28)$$

#### 9.4. Harmonics distortion standards

Since the power quality of the grid interface is influenced by the quality of the injection current, the current quality is generally regulated by utility companies. For example, the Total Demand Distortion (TDD) of 10-minute averaged value for the injection current on a distributed power generation systems should not goes over 5%, and the even harmonics should be limited under 25% to the neighbored odd harmonic limitation [4].

$$TDD = \left( \sqrt{\sum_{h=2}^{40} I_h^2} \right) / I_{rate} \quad (9.29)$$

Moreover, there exist higher order harmonics based on the switching frequency of the utility inverters which come from the circuit condition between the PWM switching pattern and the grid voltages. Thus to evaluate the influence of utility inverters to the power quality on a grid interface, not only the low order harmonics described by (9.29), but also the high order harmonics described by (9.30) should be considered [4].

$$I_{rms,sw} = \left( \sqrt{\sum_{h=41}^{\infty} I_h^2} \right) / I_{rate} \quad (9.30)$$

##### 9.4.1. IEEE 519 standards

Ideally, the harmonic distortion caused by a single consumer should be limited to an acceptable level at any point in the system; and the entire system should be operated without substantial harmonic

distortion anywhere in the system. The harmonic distortion limits recommended in IEEE 519 Standard establish the maximum allowable current distortion for a consumer.

Using information from [5], the harmonics limits are shown below in table 9.1. These limits should be used as system design values for the “worst case” for normal operation (conditions lasting longer than one hour). For shorter periods, during start-ups or unusual conditions, the limits may be exceeded by 50%.

Table 9.1 lists the harmonic current limits based on the size of the load with respect to the size of the power system to which the load is connected. The ratio  $I_{sc}/I_{Load}$  is the ratio of the short-circuit current available at the point of common coupling (PCC) to the maximum fundamental load current.

All generation systems, whether connected to the distribution, subtransmission, or transmission system, are treated like utility distribution and are therefore held to these recommended practices.

The design of the passive filter is dependent on the attenuation needed in order to reduce the high frequency components of the line currents. Hence, the design inputs for the passive filter are the high frequency spectrum of the three-phase VSC and the harmonic regulation to be fulfilled, for example the IEEE 519 standards on current harmonic emissions into the power grid. The IEEE 519 standards state that the distribution systems current harmonics above the 35th should be less than 0.3 % of the nominal current.

$$I_h \leq 0.3\% \text{ of } I_h \text{ for } h \geq 35 \quad (9.31)$$

The total RMS harmonics current should be less than 5% of the rated current. In practice, different modulation index results in different Total Demand Distortion (TDD)<sup>1</sup>. So the objective is

$$TDD = \frac{I_{harmonics\_rms}}{I_{rate}} < 5\% \quad (9.32)$$

**Table 9.1. Current distortion limits for the three general systems (Maximum harmonic current distortion in percent of  $I_{Load}$ )**  
Individual harmonic order  $h$  (odd harmonics) [5]

	$SCR = I_{sc}/I_{Load}$	$h < 11$	$11 \leq h < 17$	$17 \leq h < 23$	$23 \leq h < 35$	$35 \leq h$	Total demand distortion (TDD)
<b>Distribution Systems</b> (120 V - 69000 V)	< 20*	4.0	2.0	1.5	0.6	0.3	5.0
<b>Subtransmission Systems</b> (69001 V - 161000 V)	< 20*	2.0	1.0	0.75	0.3	0.15	2.5
<b>Transmission Systems</b> ( > 161 kV) Dispersed Generation and Cogeneration	< 50	2.0	1.0	0.75	0.3	0.15	2.5
Even harmonics are limited to 25% of the odd harmonic limits above							
*All power generation equipment is limited to these values of current distortion, regardless of actual $I_{sc}/I_{Load}$ .							
SCR = short circuit ratio at Point of Common Coupling (PCC). $I_{sc}$ = maximum short-circuit current at PCC. $I_{Load}$ = maximum demand load current (fundamental frequency component) at PCC.							

<sup>1</sup> Total Current Demand Distortion is calculated harmonic current distortion against the full load (demand) level of the electrical system rather than fundamental component (uses for calculating THD). At the full load  $TDD(I)=THD(I)$ . So TDD gives us better insight about how big impact of harmonic distortion in our system. For example we could have very high THD but the load of the system is low. In this case the impact on the system is also low.

Maximum Load Current ( $I_L$ ): Is recommended to be the average current of the maximum demand for the preceding 12 months[5]. (Unfortunately, this value is inherently ambiguous making it difficult to derive at the design stage when measured load is not available).

We can characterize current distortion levels with a THD value, but this can be misleading. A small current can have a high THD but not be a significant threat. For example, many adjustable-speed drives will exhibit high THD values for the input current while operating at very light loads. This shouldn't be a concern, because the magnitude of harmonic current would be low in this instance, even though its relative current distortion is quite high.

where  $I_{rate}$  is the rated current (fundamental frequency component) at the PCC and  $I_{harmonics\_rms}$  is given by

$$I_{harmonics\_rms} = \sqrt{\sum_{h=2}^{h=35} I_h^2} \quad (9.33)$$

#### 9.4.2. EN 61000-3-2 Standard

Today, in Europe, compliance to the EN 61000-3-2 (IEC 1000 3-2) is a legal requirement. After many revisions, the standard today applies to all electrical and electronic equipment that has an input current of up to 16A per phase and which is to be connected to the 50Hz, 230V single-phase or 400V three-phase mains network. Depending on the type of equipment and its probable frequency of daily usage, all electrical equipment are categorized into four classes, namely, Class A, B, C and D. Specific maximum limits are set for the harmonic content of the line current drawn by the equipment. Of these, the Class D limits are the most difficult to meet, as the limit depends on the equipment's power rating and applies to equipment that is connected to the utility network for a significant part of its life cycle resulting in the greatest impact on the power supply network. Personal computers and television sets are examples of such equipment. Also, an important waiver is that, other than lighting equipment, limits do not apply for equipment with rated power of 75 W or less (it may be reduced to 50 W in the future) [7].

This standard does not apply to (and has no limits for):

- Non-public networks.
- Non lighting equipment with rated power of 75W or less
- Equipment for rated voltages less than 230 VAC (limit not yet been considered).
- Arc welding equipment intended for professional use.
- Professional equipment (not intended for sale to the general public) with rated power greater than 1kW.
- Heating elements with symmetrical control methods and input power less than or equal to 200W.
- Independent dimmers for incandescent lamps with rated power less than or equal to 1kW.

Thus, any equipment connected to the public utility grid in the European Union is covered by these four classes. Each class has its own set of limits for harmonic currents. Briefly, these different limits are as follows:

##### ***Class A equipment:***

All equipment that does not fit into the other three classes are categorized as Class A equipment; Balanced 3-phase equipment, household appliances excluding equipment identified as class D, tools, excluding portable tools, dimmers for incandescent lamps, audio equipment, and all other equipment, except that stated in one of the following classes. This class set the absolute maximum current values allowed for each harmonic and these are given in table 9.2. Limits do not change with equipment rating.

##### ***Class B equipment:***

All portable tools are categorized as Class B equipment. Harmonic current limits are absolute maximum values. As power tools are used infrequently/for short periods, Class B limits are the least restrictive and set the absolute maximum current allowed for each harmonic to 1.5 times the Class A limits.

##### ***Class C equipment:***

All lighting products, including dimming devices, with an active input power higher than 25 W are categorized as Class C equipment. There are limits on the second harmonics and also on all odd harmonics. The limits are expressed in terms of the fundamental current's percentage. The maximum current percentage allowed for each harmonic, to meet Class C limits, is shown in table 9.3.

**Class D equipment:**

All equipment types that are under 600 W and are considered to have the greatest impact on the power network, like computers and television sets that are frequently used for longer periods, are categorized as Class D equipment. The limits depend on the power rating of the equipment. The current limit for Class D is expressed in terms of mA per Watt of the power consumed. Thus, the acceptable limit of the harmonic current being generated by a load is proportional to its power rating. Hence, low power equipment has a lower absolute limit of harmonic current. These limits are given in table 9.4.

**Table 9.2. Limits for class A equipment**

Harmonic order n	Maximum permissible harmonic current A
Odd harmonics	
3	2.3
5	1.4
7	0.77
9	0.40
11	0.33
13	0.21
$15 \leq n \leq 39$	$0.15 \cdot 8/n$
Even harmonics	
2	1.08
4	0.43
6	0.30
$8 \leq n \leq 40$	$0.23 \cdot 8/n$

**Table 9.3. Limits for class C equipment**

Harmonic order n	Maximum permissible harmonic current expressed as a percentage of the input current at the fundamental frequency %
2	2
3	$30 \cdot \lambda$ *
5	10
7	7
9	5
$15 \leq n \leq 39$ (odd harmonics only)	3

\*  $\lambda$  is the circuit power factor

**Table 9.4. Limits for class D equipment**

Harmonic order n	Maximum permissible harmonic current per watt mA/W	Maximum permissible harmonic current A
3	3.4	2.30
5	1.9	1.14
7	1.0	0.77
9	0.5	0.40
11	0.35	0.33
$13 \leq n \leq 39$ (odd harmonics only)	$3.85/n$	See table 1

The flow chart on Fig. 9.11 is intended as a guideline for the application of EN 61000-3-2 [7]. Based on the specific application conditions it will determine if the standard is applicable or not and which limits apply.

For higher power and higher voltage applications, the IEEE 519-1992 Standard gives recommended practices and requirements for harmonic control in electrical power systems, for both individual consumers and utilities.

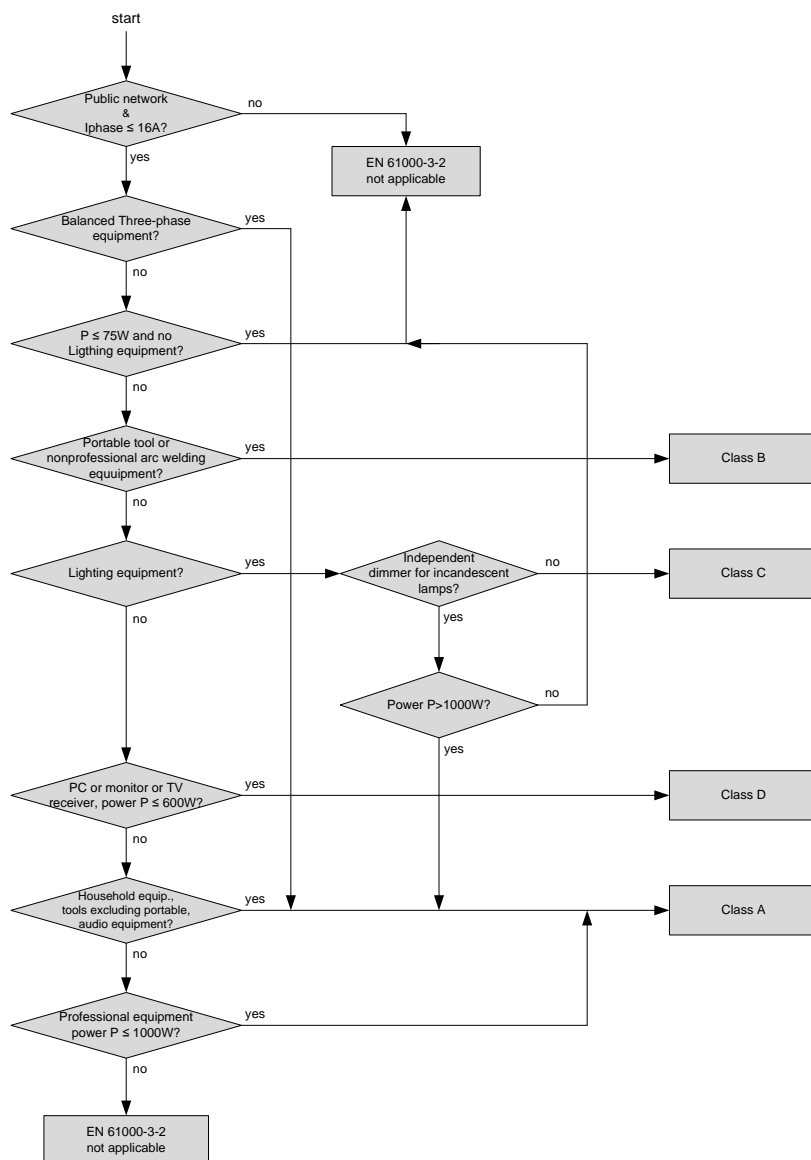


Figure 9.11. Flow chart

## References

- [1] Prasad, V H, "Analysis and comparison of space vector modulation schemes for three-leg voltage source inverters," Master dissertation, 1997, Virginia Polytechnic Institute and State University, Blacksburg, VA.
- [2] K. Ahmed, S. Finney, and B. Williams, "Passive filter design for three phase inverter interfacing in distributed generation," in Proc. CPE, Jun. 2007, pp. 1–9.
- [3] Y. Lang, D. Xu, S. Hadianamrei, and H. Ma, "A novel design method of LCL type utility interface for three-phase voltage source rectifier," in Proc. IEEE 36th Power Electronics Spec. Conf., Jun. 2005, pp. 313–317.
- [4] T. Wang, Z. Ye, G. Sinha, and X. Yuan, "Output filter design for a grid interconnected three-phase inverter," in Proc. IEEE 34th Annual Power Electronics Specialist Conf., Jun. 2003, vol. 2, pp. 779–784.
- [5] IEEE Standards 519-1992, Recommended Practices and Requirements for Harmonic Control in Electric Power Systems, 1992.
- [6] N. Mohan, T. M. Undeland and W. P. Robbins, "Power electronics: converters, applications and design," John Wiley and Sons, 1995.
- [7] Electromagnetic Compatibility, Limits for harmonic current emissions, EN 61000-3-2.

## X. LCL-FILTER DESIGN

A three-phase converter with LCL-filter is illustrated in Fig. 10.1. The LCL-filter reduces the high-order harmonics at the grid side, but a poor design of the filter can cause a lower attenuation compared to that expected or even an increase of the distortion. In fact the current harmonics generated by the converter can cause saturation of the inductors or filter resonance. So the inductors should be correctly designed considering many constraints, such as current ripple through inductors, total impedance of the filter, switching harmonic attenuation, resonance phenomenon and reactive power absorbed by filter capacitors. However, the cost limits the value of the inductors, the losses and the degradation of the performance of the filter limits the damping. A large resistor gives effective damping, but it also increases the losses, so it degrades the performance of the filter. [1]

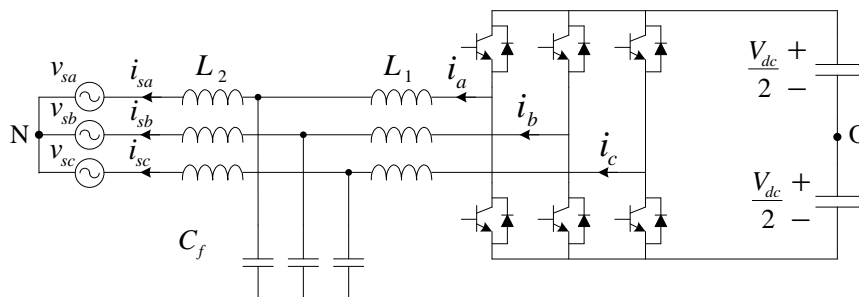


Figure 10.1. Three-phase Voltage Source Rectifier with LCL-filter

Although the harmonic distortion of grid current is usually below 5%, the utility current contains high-frequency components caused by Space Vector Modulation (SVM) switching (2-15 kHz), which can disturb other EMI<sup>1</sup> sensitive loads/equipment. Typically, simple series inductors are used as filter interfaces between the converter and power grid. However, a high value of input inductance should be adopted to reduce the current harmonics around the switching frequency. In high power applications above several kW, like the wind turbine systems, the switching frequency is low, to limit losses. Hence to attenuate the harmonics in the current enough to meet the demands of standard the use of a high value of input inductance could be not enough and it becomes quite expensive to realize larger harmonic reactors. Moreover, the dynamic response of the system becomes poor. In contrast, the LCL-filters offer the potential for improved harmonic performance at lower switching frequencies which is a significant advantage in higher-power applications, with smaller total inductance values. The equivalent single phase LCL-filter configuration for the  $h$ -harmonic is shown in Fig. 10.2, neglecting the resistors. In this figure  $v_h$  and  $i_1 = i_h$  will indicate the  $h$ -harmonic of the voltage and

<sup>1</sup> Electro Magnetic Interference (EMI)

of the current:  $h$  is the order of the switching frequency harmonic. The ripple could be computed, considering that, at high frequencies, the converter is a harmonic generator and the grid can be considered short-circuited. So the converter voltage harmonic, at the switching frequency, is  $v_h \neq 0$  and the grid voltage harmonic, at the switching frequency, is  $v_{s,h} = 0$  [1].

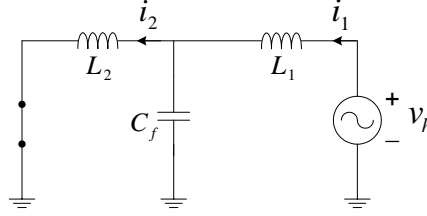


Figure 10.2. Equivalent single phase LCL-filter at the  $h$ -harmonic.

## 10.1. Design Principles

### 10.1.1. Selection of total inductance ( $L = L_1 + L_2$ )

First of all, the AC side inductance ( $L = L_1 + L_2$ ) of converter should meet the requirement of converter output active (reactive) power rating. Considering only fundamental components, the relationship between AC side vectors of converter is shown in Fig. 10.3.

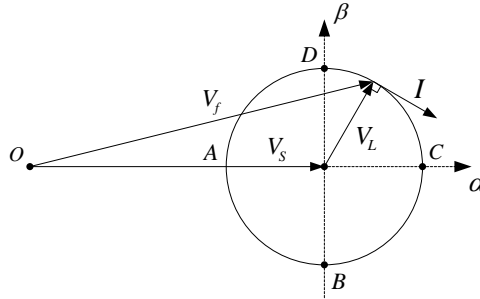


Figure 10.3. Relationship between AC side vectors of converter

where  $V_L$  is the voltage across the inductor. The trajectory of  $V_f$  for a given  $I$  is a circle with radius equal to:

$$|V_L| = \omega L \cdot |I| \quad (10.1)$$

- a) **Maximum Value:** When converter operates at point B or D, which respectively are the unity power factor rectifying and inverting operation points, the constraints on the total inductance:

$$L \leq \frac{\sqrt{V_{dc}^2 - 3\hat{V}_s^2}}{\sqrt{3} \omega \hat{I}} \quad (10.2)$$

where  $\hat{V}_s$  is peak value of grid phase voltage,  $\hat{I}$  is peak value of phase current.

- b) **Minimum Value:** Secondly, the maximum current ripple in one SVM switching (asymmetrical) period can be derived as already demonstrated in previous chapter:

$$\Delta i_{pp,max} = \frac{1}{6} \cdot \frac{V_{dc}}{L \cdot f_s} \quad (10.3)$$

so the total inductance:



$$L \geq \frac{1}{6} \cdot \frac{V_{dc}}{\Delta i_{pp,max} \cdot f_s} \quad (10.4)$$

then  $L$  should fall in the following range:

$$\frac{V_{dc}}{6\Delta i_{pp,max} \cdot f_s} \leq L \leq \frac{\sqrt{V_{dc}^2 - 3\hat{V}_s^2}}{\sqrt{3} \omega \hat{I}} \quad (10.5)$$

Note:  $L$  should be as small as possible to improve the current tracking capability and dynamic response of the system. Therefore as a first estimation to design LCL-filter the minimum constraint is considered; Equation (10.4) is used practically.

### 10.1.2. Selection of inductors $L_1, L_2$ , and capacitor $C_f$

The following analysis is based on equivalent circuit of per-phase of converter. Considering fundamental and switching harmonic components, the equivalent circuit of converter is shown in Fig. 10.4. The function of LCL-filter is to attenuate the switching harmonic components. Only switching harmonic voltage  $v_h$  is considered in the design. The circuit topology becomes as shown in Fig. 10.5. Suppose that the impedances of inductors ( $L_1, L_2$ ) and filter capacitor  $C_f$  at switching frequency have the following relationships:

$$Z_{L_1} = \frac{a}{1+a} Z_L \quad (10.6)$$

$$Z_{L_2} = \frac{1}{1+a} Z_L \quad (10.7)$$

$$Z_{C_f} = -r Z_{L_2} \quad (10.8)$$

and then:

$$L_1 = a L_2 \quad (10.9)$$

$$C_f = \frac{1}{r L_2 \omega_s^2} \quad (10.10)$$

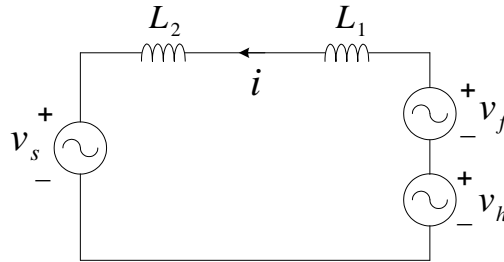


Figure 10.4. Equivalent circuit of converter considering fundamental and switching harmonic components

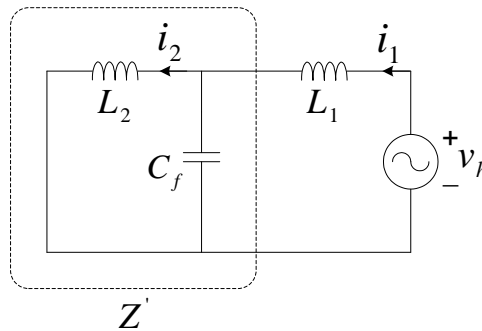


Figure 10.5. Equivalent circuit of converter considering only switching harmonic components

where  $\omega_s$  is switching angular frequency,  $a$  and  $r$  are indexes for the relation between the impedances. Parallel equivalent impedance of  $L_2$  and  $C_f$  (Fig. 10.5) is equal to:

$$Z' = (Z_{C_f} // Z_{L_2}) = \frac{r}{r-1} Z_{L_2} \quad (10.11)$$

### 10.1.2.1. Switching harmonic current attenuation

Using total inductance as  $L$  type filter, switching harmonic current through the total inductor is:

$$I = \frac{V_h}{Z_L} \quad (10.12)$$

After inserting capacitor, currents through  $L_1$  and  $L_2$  respectively become:

$$I_1 = \frac{V_h}{Z_{L_1} + Z'} = \frac{(1+a)(r-1)}{r+a(r-1)} I = \frac{1+a}{1+a+\left(\frac{1}{r-1}\right)} I \quad (10.13)$$

$$I_2 = \frac{Z'}{Z_{L_2}} \cdot \frac{V_h}{Z_{L_1} + Z'} = \frac{1+a}{1+a\left(1-\frac{1}{r}\right)} I = \frac{1+a}{1+a-\left(\frac{a}{r}\right)} I \quad (10.14)$$

switching harmonic current attenuation ratio is defined as:

$$\sigma = \left| \frac{I_2}{I} \right| = \left| \frac{1+a}{1+a\left(1-\frac{1}{r}\right)} \right| \quad (10.15)$$

Parallel equivalent impedance ( $Z'$ ) at switching frequency should be capacitive in order to suppress the switching harmonic current. If  $I_2$  and  $I$  be in same direction, the attenuation ratio becomes:

$$\sigma = \frac{1+a}{1+a\left(1-\frac{1}{r}\right)} \quad (10.16)$$

### 10.1.2.2. Fundamental reactive power absorbed by $C_f$

Generally, fundamental reactive power absorbed by filter capacitors should be less than 5% of rated power  $P$  of converter to avoid excess power factor decrease [1]:

$$Q_{C_f} = \left(\frac{P}{3}\right) \lambda \quad (10.17)$$

where  $Q_{C_f}$  is fundamental reactive power absorbed by filter capacitor for per-phase,  $P$  is total rated power and  $\lambda$  is less than 5%. At fundamental frequency, the equivalent circuit can be simplified as Fig. 10.6.

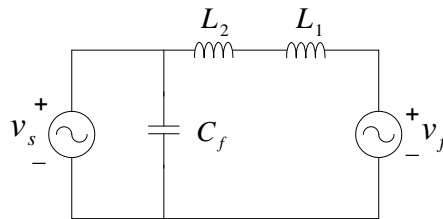


Figure 10.6. The simplified equivalent circuit of grid connected converter so  $Q_{C_f}$  can be calculated by:

$$Q_{C_f} = \frac{V_s^2}{Z_{C_f}} = \omega C_f V_s^2 \quad (10.18)$$

Substituting (10.9), (10.10) and (10.18) into (10.17), one can get:

$$\frac{r}{1+a} = x \quad (10.19)$$

where

$$x = \frac{3\omega V_s^2}{L P \lambda \omega_s^2} \quad (10.20)$$

Considering (10.16) and (10.19), equations for finding  $r$  and  $a$  can be obtained as:

$$\begin{cases} \frac{1+a}{1+a(1-\frac{1}{r})} = \sigma \\ \frac{r}{1+a} = x \end{cases} \quad (10.21)$$

## 10.2. Control System Considerations

In order to tune the LCL-filter the starting point is the current ripple on the converter side of the filter and the harmonic limit imposed on the grid current by the standards. The converter side inductance is designed in order to limit the ripple of the converter side current. Moreover, the inductor should be properly designed so as not to saturate and hence the correct inductor choice is a trade-off between ripple reduction and inductor cost.

On the other side of the filter the grid pollution is evaluated in terms of harmonics rather than in terms of ripple amplitude. Hence the LCL-filter effectiveness in reducing them should be evaluated using a frequency-domain approach. In brief, a time-domain analysis (ripple evaluation) drives the choice of the converter side inductor while a frequency-domain analysis (harmonic evaluation) drives the choice of the LCL-filter resonance frequency and, as a consequence, of some couples of values of grid-side inductor and capacitor that could meet that requirement.

### 10.2.1. Harmonic attenuation of the LCL-filter and choice of the resonance frequency value

The schematic diagram of the power circuit of the VSC connected to the grid through LCL-filter has been shown in Fig. 10.1. Assuming the grid-voltage as a disturbance and neglecting resistances, the transfer function of the filter is then  $i_2(s)/v_f(s)$  and is calculated as

$$\frac{i_1(s)}{v_f(s)} = \frac{1}{z_{eq}(s)} = \frac{1}{sL_1} \cdot \frac{\left(s^2 + \frac{1}{C_f L_2}\right)}{\left(s^2 + \frac{L_1 + L_2}{C_f L_1 L_2}\right)} \quad (10.22)$$

where  $s$  denotes the Laplace operator and  $z_{eq}$  is the equivalent impedance seen from the converter side as shown in Fig. 10.7.

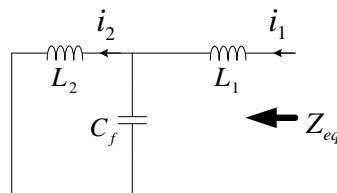


Figure 10.7. Equivalent impedance seen from the converter side  
Using the current divider rule, the grid-side current is:

$$H_I(s) = \frac{i_2(s)}{i_1(s)} = \frac{(1/sC_f)}{\left(sL_2 + \frac{1}{sC_f}\right)} \quad (10.23)$$

Above equation is considered as the ripple attenuation function and is useful for designing and determining harmonic current distortion limit compliance with IEEE-519 limits.

Then the transfer function of the filter becomes:

$$\frac{i_2(s)}{v_f(s)} = \frac{(1/C_f L_1 L_2)}{s \left( s^2 + \frac{L_1 + L_2}{C_f L_1 L_2} \right)} \quad (10.24)$$

The resonance frequency is then:

$$f_{res} = \frac{1}{2\pi} \sqrt{\frac{L_1 + L_2}{C_f L_1 L_2}} \quad (10.25)$$

Figure 10.8 shows the LCL-filter modeled in Laplace domain. All above mentioned transfer functions can be derived from this model. It is possible to control the grid side current  $i_2$  or converter side current  $i_1$ .

Bode plot of  $H_I(s)$ , depicted in Fig. (10.9), can be used to choose the resonance frequency and as a consequence the product  $L_2 C_f$  from (10.23).

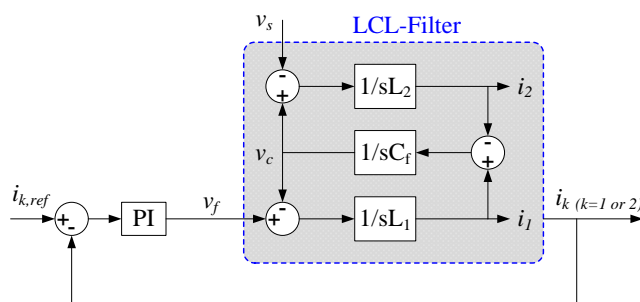


Figure 10.8. Block diagram of LCL-filter

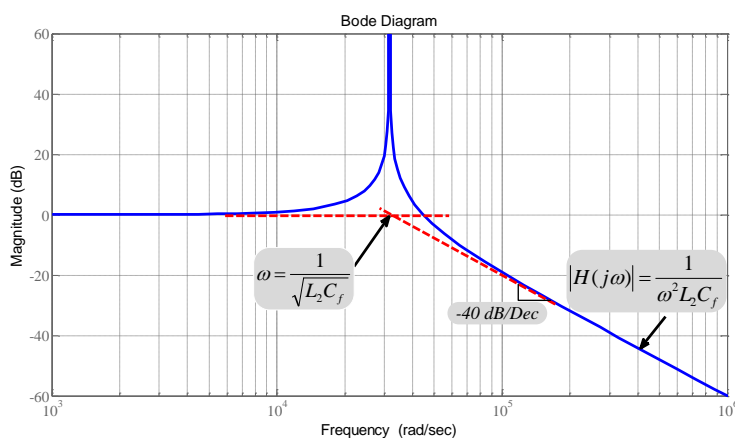


Figure 10.9. Bode plot of Ripple attenuation

For the plot shown in Fig 10.9, the construction of  $H_I(j\omega)$  consists of evaluating the function at both low and high frequencies starting with

$$H_I(j\omega) = \frac{(1/j\omega C_f)}{\left(j\omega L_2 + \frac{1}{j\omega C_f}\right)} \quad (10.26)$$

and considering low frequencies.

$$\lim_{\omega \rightarrow 0} H_I(j\omega) \approx \frac{1}{\frac{j\omega C_f}{1}} = 1 \quad (10.27)$$

For high frequencies,

$$\lim_{\omega \rightarrow \infty} H_I(j\omega) \approx \frac{1}{j\omega L_2} = \frac{-1}{\omega^2 L_2 C_f} \quad (10.28)$$

As shown by (10.28), the roll-off of the high frequency components is  $1/\omega^2$  or -40 dB per decade when (10.26) is expressed in dB form.

**Example:**

A 500 kW system (f.i. Wind Turbine) and a 3 kW system (f.i. Photo Voltaic) with two sets of parameters are given in table 10.1.

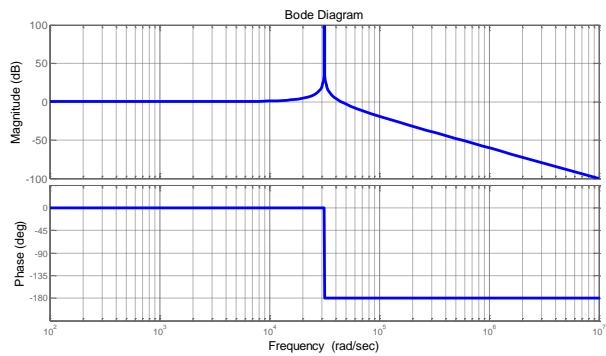
**Table 10.1. Parameters of two systems LCL-filter**

	$L_1$	$L_2$	$C_f$	$f_{res}$ by Eq.(10.25)
3 kW system	0.4 mH	0.2 mH	5 $\mu$ F	6.2 kHz
500 kW system	0.2 mH	0.03 mH	83 $\mu$ F	3.4 kHz

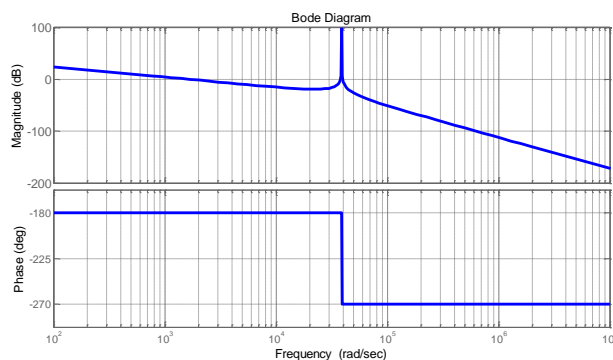
Resonance frequency of two systems as calculated and written in the table I for the higher power converter is lower than the other system. This can be explained by the fact that higher power converters should adopt a lower switching frequency and hence also the LCL-filter resonance should be lower in order to allow a better filtering property. Bode plot of the transfer function of  $i_2/i_1$  and  $i_2/v_f$  for 3 kW and 500 kW systems are plotted in Fig. 10.10 and Fig. 10.11 respectively.

Finally some limits on the parameters values should be introduced [1]:

- The total value of inductance should be lower than 10% to limit the voltage drop during operation.
- The capacitor value is limited by the tolerable decrease of the power factor at rated power (generally less than 5%) [in other word; the maximum reactive power of the capacitor should be 5% of the rated power of converter to avoid excess power factor decrease].
- The resonance frequency should be included in a range between ten times the line frequency and one half of the switching frequency in order not to create resonance problems in the lower and higher parts of the harmonic spectrum.
- The passive damping cannot be too low to avoid oscillation and the losses cannot be too high to not reduce efficiency.

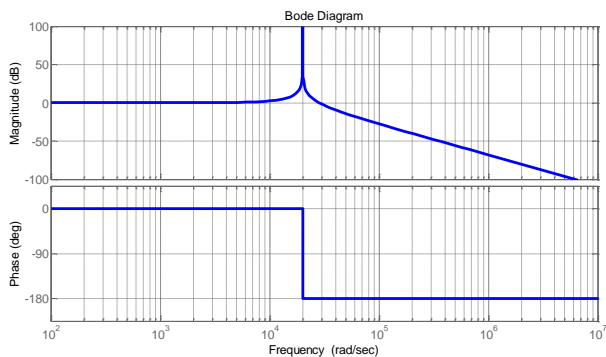


(a)

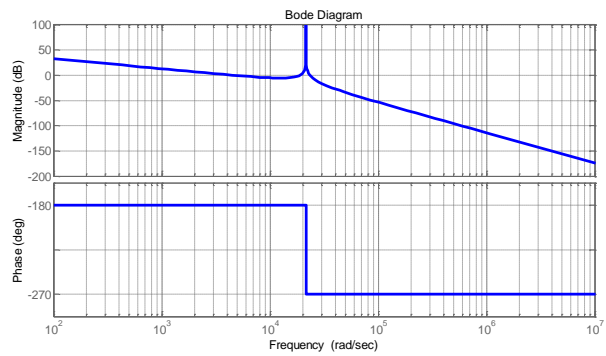


(b)

Figure 10.10. Frequency response of LCL-filter for 3 kW system; a)  $i_2/i_1$  transfer function, b)  $i_2/v_f$  transfer function



(a)



(b)

Figure 10.11. Frequency response of LCL-filter for 500 kW system; a)  $i_2/i_1$  transfer function, b)  $i_2/v_f$  transfer function

## References

- [1] M. Liserre, F. Blaabjerg, and S. Hansen, "Design and Control of an LCL-Filter-Based Three-Phase Active Rectifier", *IEEE Transactions on Industry Applications*, vol. 41, no. 5, Sep./Oct. 2005.
- [2] T. Wang, Z. Ye, G. Sinha, and X. Yuan, "Output filter design for a grid interconnected three-phase inverter," in Proc. IEEE 34th Annual Power Electronics Specialist Conf., Jun. 2003, vol. 2, pp. 779–784.
- [3] Prasad, V H, "Analysis and comparison of space vector modulation schemes for three-leg voltage source inverters," Master dissertation, 1997, Virginia Polytechnic Institute and State University, Blacksburg, VA.
- [4] R. Teodorescu, M. Liserre, and P. Rodriguez, *Grid Converters for Photovoltaic and Wind Power Systems*. Hoboken, NJ: Wiley, 2010.
- [5] K. Ahmed, S. Finney, and B. Williams, "Passive filter design for three phase inverter interfacing in distributed generation," in Proc. CPE, Jun. 2007, pp. 1–9.
- [6] W.A. Hill and S.C. Kapoor, "Effect of two-level PWM sources on plant power system harmonics", Proc. of Industry Applications Conf., vol. 2, pp.1300 – 1306, 1998.
- [7] M. Liserre, F. Blaabjerg, and A. Dell'Aquila, "Step-by-step design procedure for a grid-connected three-phase PWM voltage source converter", *International Journal of Electronics*, vol. 91, no. 8, pp. 445–460, Aug. 2004.
- [8] A. A. Rockhill, M. Liserre, R. Teodorescu, and P. Rodriguez, "Grid Filter Design for a Multi-Megawatt Medium-Voltage Voltage Source Inverter", *IEEE Transactions on Industrial Electronics*, vol. 58, no. 4, April 2011.
- [9] M. Lindgren and J. Svensson, "Control of a voltage-source converter connected to the grid through an LCL-filter-application to active filtering," in Proc. IEEE PESC'98, vol. 1, 1998, pp. 229–235.
- [10] E. Twining and D. G. Holmes, "Grid current regulation of a three-phase voltage source inverter with an LCL input filter," *IEEE Transactions on Power Electronics*, vol. 18, no. 3, May 2003.
- [11] J. Phipps, "A transfer function approach to harmonic filter design," *IEEE Ind. Appl. Mag.*, vol. 3, no. 2, pp. 68–82, Mar./Apr. 1997.
- [12] W. A. Hill, S. C. Kapoor: "Effect of two-level PWM sources on plant power system harmonics", Proc. of IAS 1998 Conference, St. Louis (USA), October 1998, pp. 1300-1306.
- [13] J. Kim, J. Choi, and H. Hong, "Output LC filter design of voltage source inverter considering the performance of controller," in Proc. Int. Conf. Power Syst. Technol., Power Conf., 2000, vol. 3, pp. 1659–1664.
- [14] S. Chandrasekaran, D. Borojevic, D.K. Lindner, "Input filter interaction in three phase AC-DC converters", Proc. of PESC 99, Charleston (USA), June/July 1999, Vol. 2, pp 987-992.
- [15] M. Bojrup, "Advanced control of active filters in a battery charger application", Ph.D. dissertation, Lund Univ. Technol., Lund, Sweden, 1999.
- [16] K. Jalili and S. Bernet, "Design of LCL Filters of Active-Front-End Two-Level Voltage-Source Converters Design of LCL Filters of Active-Front-End Two-Level Voltage-Source Converters", *IEEE Transactions on Industrial Electronics*, vol. 56, no. 5, May 2009.

## XI. RESONANT CONTROLLER

Consider the half-bridge converter of Fig. 11.1 with the closed-loop control block diagram of Fig. 11.2. Depending on the type of the reference signal and the desired performance, different types of controller may be used for the control. For example, if  $i_{ref}$  is a step function and  $V_s$  is a DC voltage, a proportional-integral (PI) controller of the generic form  $G_c(s) = (k_p + k_i/s)$  is sufficient for the control. The integral term of the controller guarantees that  $i$  tracks  $i_{ref}$ , with zero steady-state error. As shown in Fig. 11.2 the open loop transfer function is

$$G_{op}(s) = \left(\frac{k_p}{sL}\right) \left(\frac{s + \frac{k_i}{k_p}}{s + \frac{R}{L}}\right) \quad (11.1)$$

Based on the block diagrams of Fig. 11.2, the open-loop half-bridge converter has a stable pole at  $p = -R/L$ . Typically, this pole is fairly close to the origin and corresponds to a slow natural response. To improve the open-loop frequency response, the pole can be canceled by the zero of the PI controller. Thus, choosing  $k_i/k_p = R/L$  and  $k_p/L = 1/\tau_i$ , where  $\tau_i$  is the desired time constant of the closed-loop system, one obtains the closed-loop transfer function

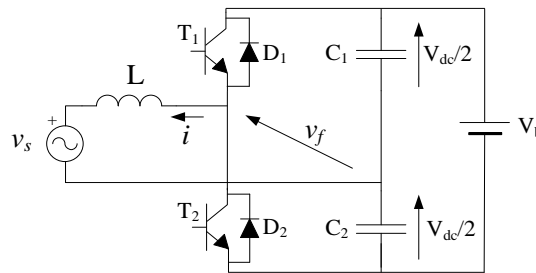


Figure 11.1. Diagram of the half-bridge converter

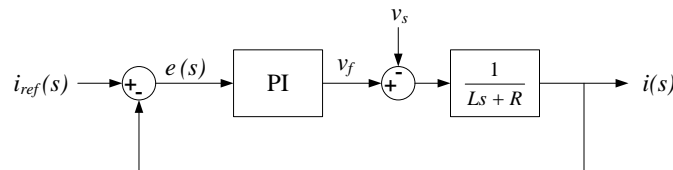


Figure 11.2. Control block diagram of the converter with PI controller.



$$G_i(s) = \frac{i(s)}{i_{ref}(s)} = \frac{1}{\tau_i s + 1} \quad (11.2)$$

which is a first-order transfer function with the unity gain.  $\tau_i$  should be made small for a fast current-control response, but adequately large such that  $1/\tau_i$ , that is, the bandwidth of the closed-loop control system, is considerably smaller, for example, 10 times smaller, than the switching frequency of the half-bridge converter (expressed in rad/s). Depending on the requirements of a specific application and the converter switching frequency,  $\tau_i$  is typically selected in the range of 0.5–5 ms.

### 11.1. Resonant controller

In this section, the half-bridge converter is employed as the main block of three-phase VSC systems, and the sinusoidal current command is a typical requirement. Assume that  $V_s$  is a sinusoidal function of time and also assume that there is a need to track a sinusoidal current command characterized by

$$i_{ref}(t) = \hat{I} \cos(\omega_1 t + \varphi) \cdot U(t) \quad (11.3)$$

where  $\varphi$  is the initial phase angle of the sinusoidal command and  $U(t)$  is the unit step function. Then, if the closed-loop transfer function of the converter system is given by (11.2), the steady-state response of  $i$  to the command has the form

$$i(t) = \frac{\hat{I}}{\sqrt{1 + (\tau_i \omega_1)^2}} \cos(\omega_1 t + \varphi + \delta) \quad (11.4)$$

where the phase shift  $\delta$  is given by

$$\delta = -\tan^{-1}(\tau_i \omega_1) \quad (11.5)$$

Equations (11.4) and (11.5) suggest that if the PI controller is employed,  $i$  tracks  $i_{ref}$  with errors in both the amplitude and the phase angle. According to (11.4), the amplitude of  $i$  is inversely proportional to  $\sqrt{1 + (\tau_i \omega_1)^2}$  and, therefore, smaller than  $\hat{I}$ . In addition, as (11.5) indicates,  $i$  lags  $i_{ref}$  by an angle that can be significant, depending on the product  $\tau_i \omega_1$ .

The capability of the closed-loop system to faithfully track a sinusoidal command depends on the system closed-loop bandwidth. The bandwidth of the closed-loop system of (11.2) is equal to  $1/\tau_i$ . Therefore, a sinusoidal command can be followed with negligible attenuation or phase delay if  $\tau_i$  is adequately small. However, selection of a very small closed-loop time constant may not be possible due to practical limitations/requirements. For example, while a closed-loop current controller with a time constant of  $\tau_i = 2$  ms is considered as being reasonably fast for most high-power converter systems, it tracks a 50 Hz sinusoidal command with an amplitude attenuation of 15% and a phase delay of  $32^\circ$ .

#### Example (11.1)

Consider the half-bridge converter of Fig. 11.1, in conjunction with the control scheme of Fig. 11.2, with the following parameters:  $L = 4.3$  mH,  $R = 3$  m $\Omega$ ,  $V_{dc}/2 = 350$  V, and  $f_s = 3500$  Hz. The controller parameters are  $k_p = 2.15$  and  $k_i = 1.5$ , which correspond to  $\tau_i = 2$  ms.

Let us assume that  $v_s = 220\sqrt{2} \cos(\omega t - \pi/2)$  and that we intend to deliver 3.68 kW to the AC system, at unity power factor. Thus, the current command  $i_{ref} = 16\sqrt{2} \cos(\omega t - \pi/2)$  must be tracked by the closed-loop converter system. Fig. 11.3 shows the system closed-loop response to  $i_{ref}$  when a PI controller is employed. As Fig. 11.3 illustrates,  $i(t)$  is about  $32^\circ$  delayed with respect to  $i_{ref}(t)$  and  $V_s(t)$ . Moreover, the amplitude of  $i$  is only about 85% of peak reference current. Consequently, rather than 3.68 kW at unity power factor, 3.12 kW and 1.95 kVar are delivered to the AC-side source.

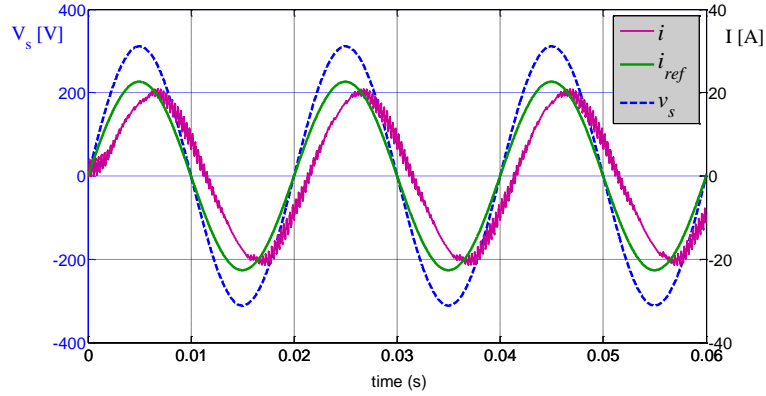


Figure 11.3. Steady-state error for phase and amplitude of the current when PI compensator is employed.

Consider the closed-loop control system of Fig. 11.4 with the following transfer function

$$G_i(s) = \frac{i(s)}{i_{ref}(s)} = \frac{G_{op}(s)}{1 + G_{op}(s)} \quad (11.6)$$

where  $G_{op}(s)$  is defined as

$$G_{op}(s) = K(s)G(s) \quad (11.7)$$

The frequency response of the closed-loop system is

$$G_i(j\omega) = \frac{G_{op}(j\omega)}{1 + G_{op}(j\omega)} \quad (11.8)$$

which can be expressed in polar coordinates as

$$G_i(j\omega) = |G_i(j\omega)|e^{j\delta} \quad (11.9)$$

where  $|G_i(j\omega)|$  and  $\delta$  denote the magnitude and the phase of  $G_i(j\omega)$ , respectively. Based on the definition of the frequency response, the steady-state response of the closed-loop system to a sinusoidal command (with frequency  $\omega_1$ ) is scaled by  $|G_i(j\omega_1)|$  and phase shifted by  $\delta$ , with respect to the command. If the sinusoidal command is to be tracked with zero steady-state error,  $|G_i(j\omega_1)|$  must be equal to unity, and  $\delta$  must be zero. Based on (11.8), this is fulfilled if  $G_{op}(j\omega_1)$ , that is, the loop-gain magnitude, is infinity at the frequency of the command signal. For example, if two of the poles of  $K(s)$  are located at  $s = \pm j\omega_1$ , then  $G_{op}(j\omega_1) = +\infty$ , and the sinusoidal command is tracked with zero steady-state error. In general, to track a command with zero steady-state error, the unstable poles of the Laplace transform of the command must be included in the controller. This not only ensures command tracking with zero steady-state error but also eliminates all disturbances of the same type, in steady state. In a commonly faced scenario, to track a step (DC) command with zero steady-state error, and to reject constant disturbances,  $K(s)$  includes an integral term, that is, it possesses a pole at  $s = 0$ ; the PI controller is a special form of such a controller.

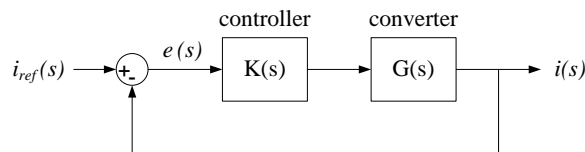


Figure 11.4. A simplified control block diagram of the half-bridge converter.

As an alternative method, the sinusoidal command tracking can be achieved if  $K(s)$  is designed in such a way that the bandwidth of the closed-loop system is adequately larger than the frequency of the command signal. In this approach, no attempt is usually made to include the unstable poles of the command signal in the controller. Consequently, the tracking will not be perfect and a steady-state error, although small, is inevitable.

### Example 2.

Consider the half-bridge converter of previous example and the control block diagram of Fig. 11.4. Let us assume that  $i_{ref}$  is required to be tracked with zero steady-state error.

To satisfy the zero steady-state error requirement, we include a pair of complex-conjugate poles in the controller at  $s = \pm 314j$  rad/s. Thus, a candidate controller is

$$K(s) = k_p + \frac{2k_1s}{s^2 + \omega_1^2} \quad (11.10)$$

which has a frequency and phase response shown in Fig. 11.5.

Figure 11.6 illustrates that  $i(t)$  rapidly reaches and tracks  $i_{ref}$ , without amplitude or phase-angle error.

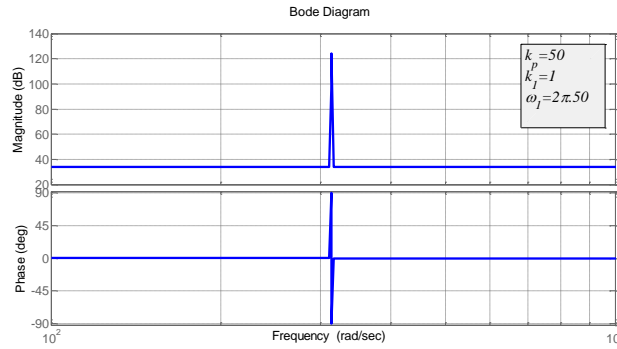


Figure 11.5. Bode plot of PR controller.

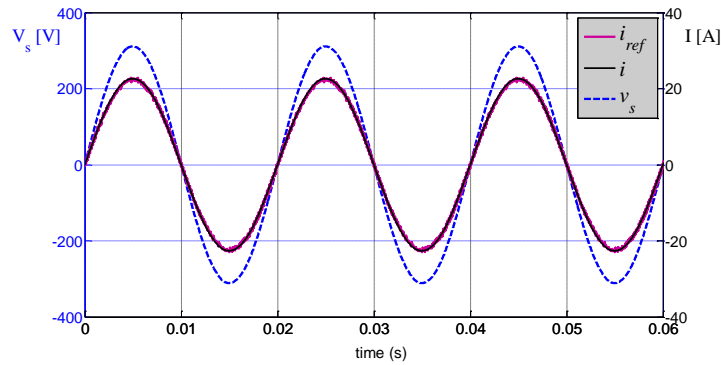


Figure 11.6. Response of the half-bridge converter to a sinusoidal command, based on PR controller.

A more practical controller is given by [1]:

$$K(s) = k_p + \frac{2k_1s}{s^2 + 2\omega_c s + \omega_1^2} \quad (11.11)$$

This controller has a frequency and phase response as shown in Fig. 11.7(a). In order to compare two controllers, Bode response of (11.10) is shown in Fig. 11.7(b) with the same value of  $k_p$  and  $k_1$  used for (11.11). The steady-state output phase and magnitude error achieved by the controller (11.11) will still be approximately zero, provided that it continues to achieve a relatively high gain at the reference frequency.

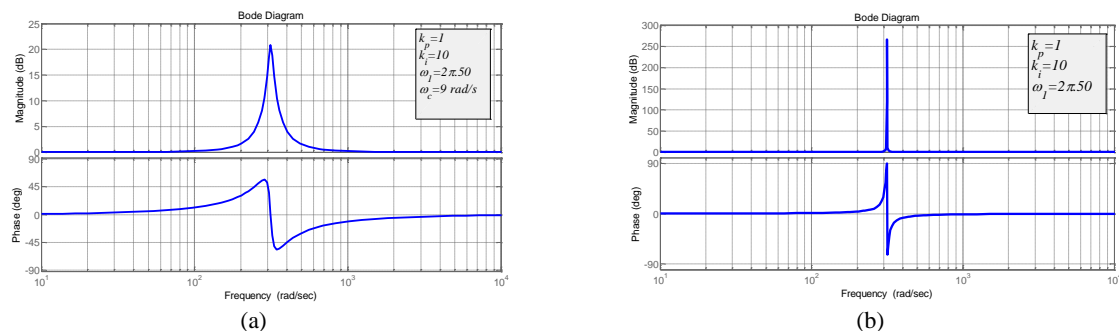
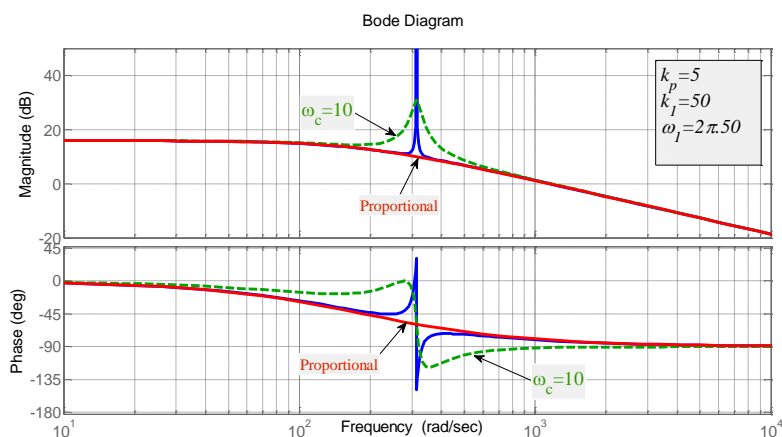


Figure 11.7. Bode plot of resonant controller; a) from Eq. (11.11), b) from Eq. (11.10)

A major benefit of being able to express the frequency response of the regulator in the transfer function form of (11.10) or (11.11), is that linear control theory can be used to investigate the stability of current regulation systems based on this approach.

Using conventional Bode plots, it is straightforward to show that the regulator integral gain can be made sufficiently large to essentially remove all steady-state error (similar to the effect of the finite integral gain that most practical compensators can achieve), without any significant stability limitations. The resonant terms provide very little gain outside their band-pass region due to their narrowband frequency response. Hence, to achieve a reasonable transient response a proportional gain term is also required. Fig. 11.8 shows the magnitude and phase Bode diagrams for a simple proportional regulator and the two regulators described by (11.10) and (11.11).


 Figure 11.8. Open loop Bode plots of proportional and resonant regulators (For  $R=0.8\Omega$ ,  $L=4.3e-3\text{mH}$  as a load).

For the  $k_p = 5$  magnitude crossover frequency (i.e., where the regulator gain becomes less than 1) of the simple proportional regulator occurs at 1 kHz, as indicated in Fig. 11.8. The phase plot shows a phase margin of more than  $100^\circ$  at this frequency so the system is clearly stable.

The introduction of the resonant regulator terms radically changes the Bode plots at the resonant frequency but has little effect at the crossover frequency for the regulator parameters chosen. Hence, both resonant regulators remain stable below the crossover frequency because the phase shift is always less than  $180^\circ$ . Fig. 11.8 also shows that most of the high frequency or transient response of the regulator is determined by the proportional gain since the resonant regulator magnitude responses return to that of a simple proportional system at higher frequencies. So, the larger the proportional gain the faster will be the transient response. This suggests a simple two-step design procedure for the complete regulator. Firstly, choose a proportional gain such that the regulator is stable and gives a good transient response. Then design a resonant component that gives the desired steady-state phase and amplitude error without making the phase margin too small.

The low-pass 3-dB cut-off frequency  $\omega_c$  appears to allow a degree of freedom in the design of the resonant frequency responses. It is often used as a measure of the bandwidth of a filter and therefore increasing its size would appear to broaden the effect of the high gain created by the resonant term

(Fig. 11.9). This in turn would appear to increase the regulator robustness by reducing the sensitivity of the system to variations in the fundamental frequency. For the damped resonant term the gain at the resonant frequency is given by

$$RC(j\omega_0) = \frac{2k_1j\omega_0}{-\omega_0^2 + 2j\omega_c\omega_0 + \omega_0^2} = \frac{k_1}{\omega_c} \quad (11.12)$$

which is clearly inversely dependent on the value of  $\omega_c$ . The Bode response of (11.12) for a range of values of  $\omega_c$  is illustrated in Fig. 11.9. Hence it can be seen that the major difference between the different plots is the increasing peak amplitude at the resonant frequency for smaller values of  $\omega_c$ , without affecting the shoulder frequency gain.

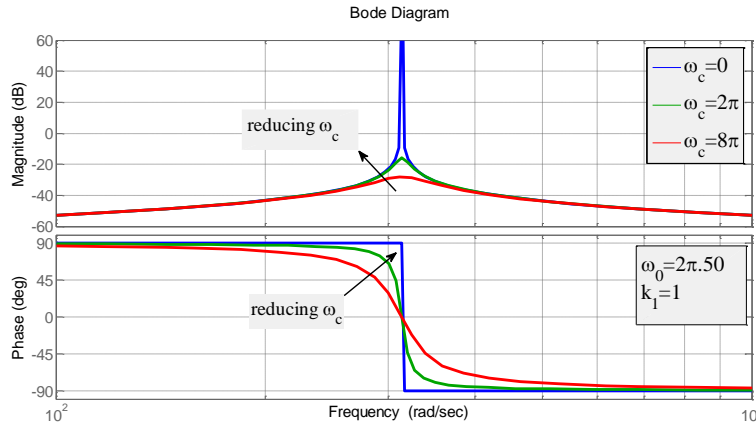


Figure 11.9. Bode response of the resonant term for variation in  $\omega_c$  and  $k_1 = 1$

At frequencies greater than or less than the resonant frequency all the plots converge to the 20 dB per decade asymptotic response regardless of the value of  $\omega_c$ . This illustrates that the infinite gain benefit of the ideal resonant term only occurs at the resonant frequency and any perturbation will lead to a reduction of the generated gain. Hence, the proportional resonant regulator is potentially sensitive to the alignment between the regulator's resonant frequency and the fundamental frequency of the inverter system. The only way of reducing this sensitivity is to increase the regulator gain  $k_1$ , which uniformly increases the gain response but does not affect the shape of the frequency response. For example, if the reference frequency were 48 Hz rather than 50 Hz the loss-less resonant term attenuates the signal by more than 20 dB. Increasing  $\omega_c$  (to supposedly increase the filter bandwidth) actually makes things worse as this flattens the frequency response, further reducing the gain of the resonant term. One major conclusion from this consideration is that there is no benefit to be gained in using the damped resonant implementations. If an ideal resonant term is realizable it is preferable, and if a damped term must be used it should be implemented with as small a value of  $\omega_c$  as possible.

In literatures [1,2] two resonant controllers have been introduced:

$$RC_1(s) = \frac{2 \cdot k_1 s}{s^2 + \omega_1^2} \quad (11.13)$$

$$RC_2(s) = \frac{k_1 \omega_1}{s^2 + \omega_1^2} \quad (11.14)$$

The second controller " $RC_2(s)$ " also has infinite gain at the resonant frequency and hence achieves zero steady-state error when used as a current regulator. But it introduces a phase shift of  $180^\circ$  into the system, compared to the  $90^\circ$  shift of the first controller " $RC_1(s)$ ", as illustrated in Fig. 11.10. In closed loop operation this  $180^\circ$  phase shift results in a poorer phase margin and a poor transient performance for this controller compared to the first one.

It should be noted that the resonant terms provide very little gain outside their band-pass region due to their narrowband frequency response. Hence, to achieve a reasonable transient response a proportional gain term is also required. Fig. 11.10 shows the magnitude and phase Bode diagrams for a simple proportional regulator and the two regulators described by (11.13) and (11.14).

In three-phase VSC systems, we are often interested in tracking a sinusoidal command, rapidly and with small steady-state errors. We also need to guarantee rapid changes in the amplitude and the phase of the commands. Therefore, the control design is noticeably simplified if we can transform the problem of sinusoidal command tracking to a DC command tracking problem in dq-reference frame.

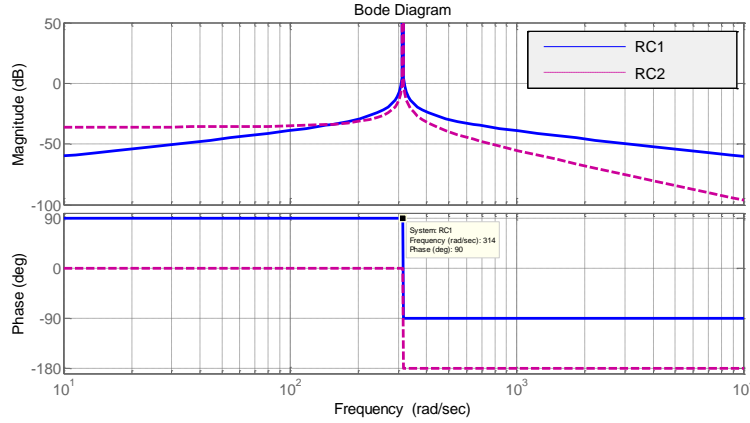


Figure 11.10. Frequency responses of resonant controllers  $RC_1$  and  $RC_2$  for  $k_1 = 5$ .

## 11.2. Improved Control Method by Using Proportional Resonant controller

The bi-directional charger is the interface between the grid and PEV. Here this converter is considered as an active filter and it will control the power factor to unity and regulate the DC bus voltage and control the input current harmonics produced by switching to be low. As shown in Fig. 11.11(a) the conventional control uses the PI controller. In Fig. 11.11(b), the proposed control method is to use Proportional Resonant (PR) and integral controller in dq-reference frame (PR+I). The main goal of a Proportional Resonant (PR) controller is to obtain zero steady-state error for sinusoidal inputs with a specified frequency. Block diagram of the PR is shown in Fig. 11.12 and the transfer function of PR is given by

$$PR = k_p + \frac{2 \cdot k_1 s}{s^2 + \omega_1^2} \quad (11.15)$$

$$PR + I = k_p + \sum_{n=6,12} \frac{2 \cdot k_n s}{s^2 + (n\omega_1)^2} + \frac{k_i}{s} \quad (11.16)$$

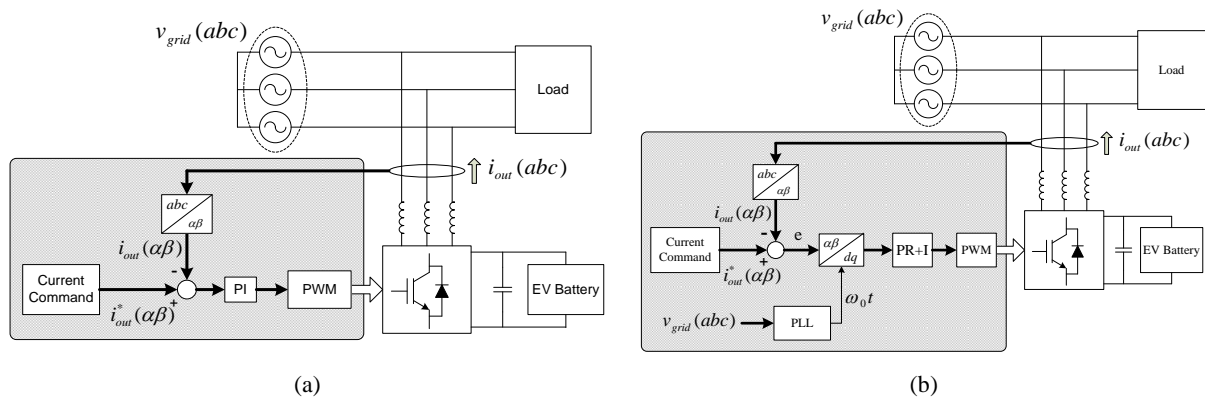


Figure 11.11. BBC control system; a) Conventional PI controller, b) Proposed PR+I controller for V2G in APF mode

where  $k_p$  is the proportional gain,  $k_n$  is the gain of resonant controller, and  $k_i$  is the integral gain. The employment of PR controller, compared with other solutions, gives the following advantages.

- There is zero steady-state error for sinusoidal waveforms having the same frequency as  $\omega_1$ ; this feature can be exploited for Active Power Filters (APF), where the signal frequencies are well defined and practically constant (mains' frequency and its multiples).
- The PR acts as a resonant filter, tuned on  $\omega_1$ ; in this way, multiple PRs with different resonance frequencies can operate in parallel without interfering with each other.
- The PR can operate with both positive and negative sequence signals [3].

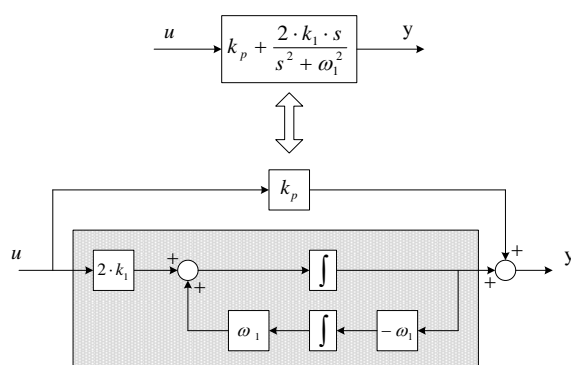


Figure 11.12. Proportional Resonant block diagram

If V2G converter is utilized as APF, the current control must deal with non-sinusoidal reference currents whose harmonic spectrum consists of a fundamental component and of the harmonics drawn by the nonlinear load. For diode or thyristor front-end rectifiers (as a load), these harmonics are of order  $(6k \pm 1)$  ( $k = 1, 2, \dots$ ) of the fundamental frequency  $\omega_1$ . For balance reference waveforms, as explained above, harmonics of order  $(6k - 1)$  are negative sequence and harmonics of order  $(6k + 1)$  are positive sequence that are shown in table I. If we consider the fundamental frequency component as a positive-type sequence, current harmonics and sequences that correspond to balanced waveform, in synchronous reference frame (SRF) are illustrated in table 11.1. The SRF uses a PLL to catch the phase information of the grid voltage.

To better show the advantages of the proposed control method, simulations of both control methods were carried out. Here 5th and 7th current harmonics are considered and their percentages are shown in table 11.2.

Fig. 11.13 and 11.14 show the comparison of the output current and reference current waveform between the improved control method (Fig. 11.11b) and the conventional control method (Fig. 11.11a) clearly demonstrating the improved control method's immunity to grid background harmonics.

Table 11.1. Current harmonics components

Harmonic in $\alpha\beta$ -Frame	Sequences	Harmonic order in dq-frames $\omega_{RF} = +\omega_1$
1 <sup>st</sup>	Positive, fundamental	0
5 <sup>th</sup>	Negative	-6
7 <sup>th</sup>	Positive	+6
11 <sup>th</sup>	Negative	-12
13 <sup>th</sup>	Positive	+12

Table 11.2. Current harmonics components

Harmonic in $\alpha\beta$ stationary reference frame	Percentage
5 <sup>th</sup>	18%
7 <sup>th</sup>	14%

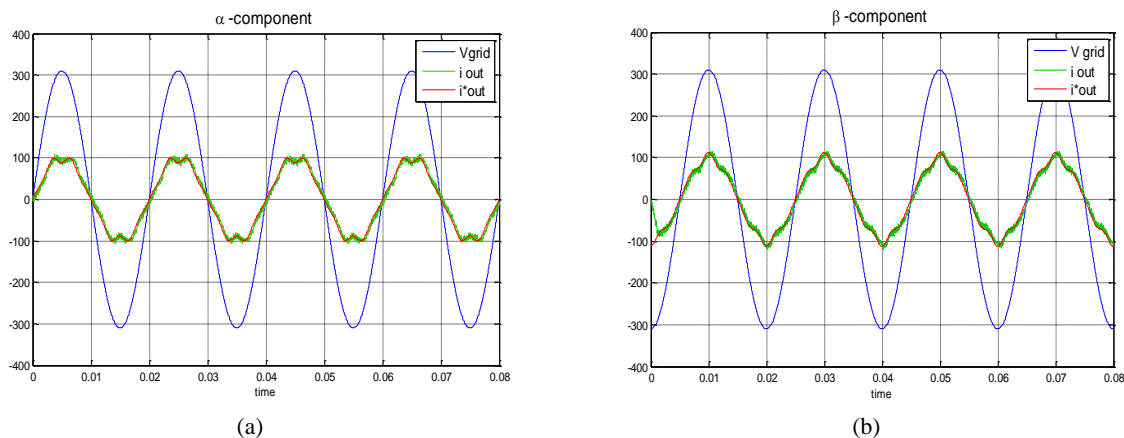


Figure 11.13. Simulation result using conventional PI controller; grid voltage, reference and output current of converter, (a)  $\alpha$ -component (b)  $\beta$ -component

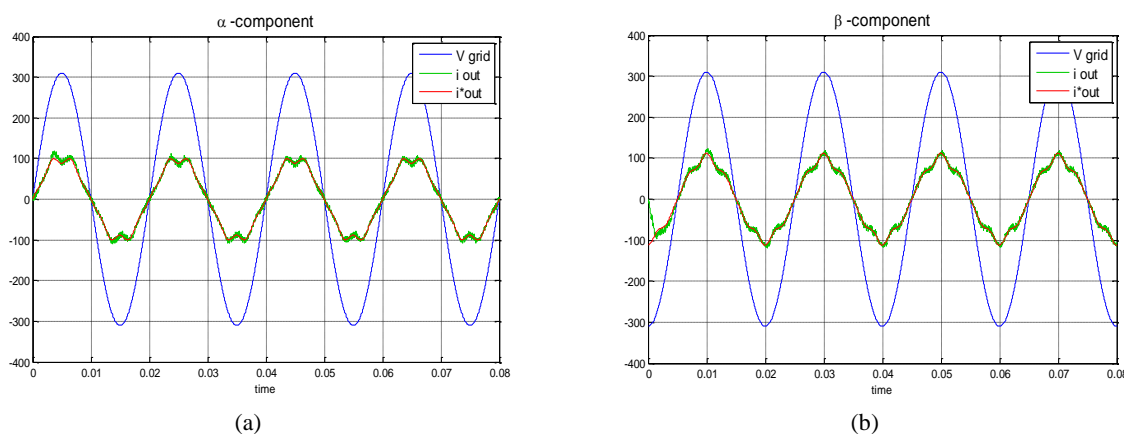


Figure 11.14. Simulation result using proposed PR+I controller; grid voltage, reference and output current of converter, (a)  $\alpha$ -component (b)  $\beta$ -component

There is no much bigger difference between the two methods, even the current generated by the conventional method may be allowed, but this current will be a potential issue to the power quality of the whole power system with a large penetration of the PEVs in the coming future. To better comparison, Fig. 11.15 and 11.16 show the  $\alpha$ -axis error of these two methods. Here both simulation results are extracted from  $\alpha\beta$  frame in order to compare two methods together; however it is possible to apply the proposed configuration just in dq-frame.

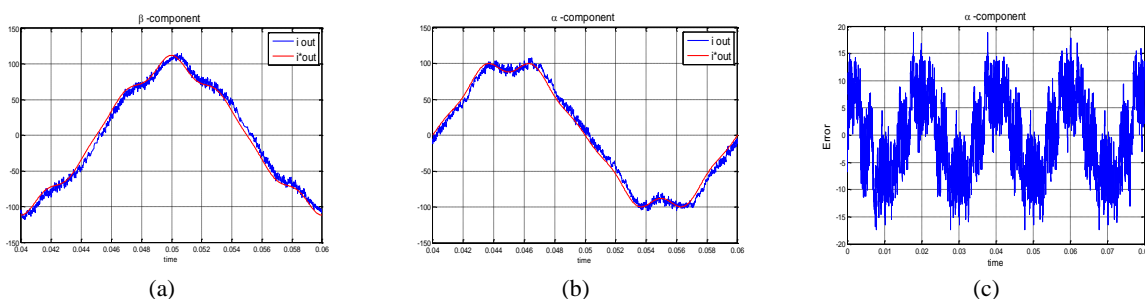


Figure 11.15. Simulation result using conventional PI controller; one period of reference and output current of converter, a)  $\beta$ -component, b)  $\alpha$ -component, and c) error in  $\alpha$ -axis



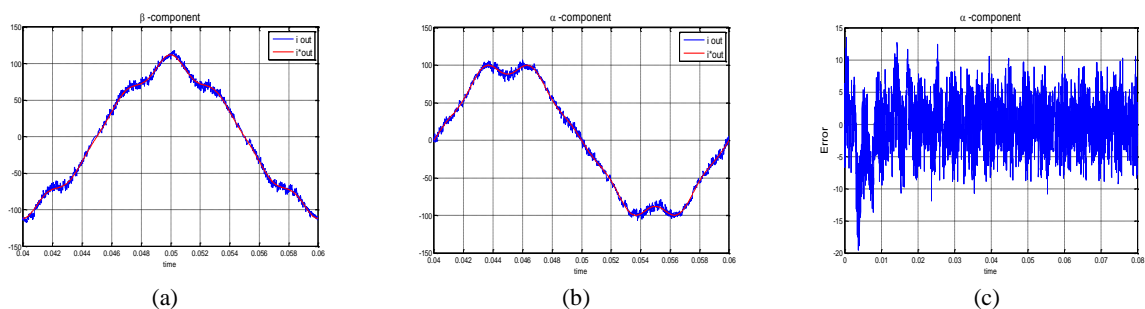


Figure 11.16. Simulation result using proposed PR+I controller; one period of reference and output current of converter; a)  $\beta$ -component, b)  $\alpha$ -component, and c) error in  $\alpha$ -axis

## References

- [1] D. N. Zmood and D. G. Holmes, “Stationary frame current regulation of PWM inverters with zero steady-state error”, *IEEE Transactions on Power Electronics*, vol. 18, no. 3, pp. 814–822, May 2003.
- [2] Y. Sato, T. Ishizuka, K. Nezu, and T. Kataoka, “A new control strategy for voltage-type PWM rectifiers to realize zero steady-state control error in input current,” *IEEE Trans. Ind. Appl.*, vol. 34, pp. 480–486, May/June 1998.
- [3] X. Yuan, W. Merk, H. Stemmler, and J. Allmeling, “Stationary-frame generalized integrators for current control of active power filters with zero steady-state error for current harmonics of concern under unbalanced and distorted operating conditions,” *IEEE Trans. Ind. Appl.*, vol. 38, no. 2, pp. 523–532, Mar./Apr. 2002.

## XII. EV STANDARDS

There are two fundamentally different ways to connect a PEV to the electric power system for charging: one approach is to use a conductive coupling and the other is to use wireless power transfer. For conductive coupling the power flow to the vehicle can be either AC or DC. All PEVs will provide an on-board charger that just needs to be connected to an AC source to charge the vehicle battery. This is called AC charging. There are two approaches for AC transfer: one is to directly connect the PEV to a standard outlet. The other is to connect to Electric Vehicle Supply Equipment (EVSE) which is permanently connected to a branch circuit from a service panel; in other words connecting an EV to AC supply utilizing supply cable and connector permanently attached to the supply equipment. EVSE is the equipment used to deliver electrical energy from an electricity source to a PEV. EVSE communicates with the PEV to ensure that an appropriate and safe flow of electricity is supplied. It is the official term for electric vehicle charging infrastructure; more commonly referred to as charging stations. Most PEVs will also be capable of using an external charger and conductively transferring DC power to the vehicle traction battery. This is called DC charging. DC charging requires closely coordinated communication between the vehicle's battery management system and the external charger to manage the charging session. Figure 12.1 is shown the basic types of charging.

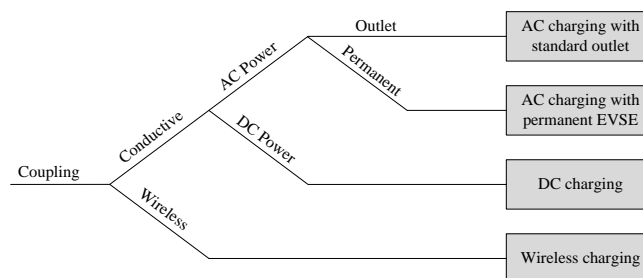


Figure 12.1. Basic Types of Charging

Within each of the four basic types of charging there may be further differentiation based on the power levels that can be supported. This chapter provides standard of electric vehicles and related support infrastructure.

### 12.1. Charging Infrastructure Standards

It is assumed that the primary electric vehicle charging station is located at the residence, business, or fleet facility where the vehicle is parked. Also, it is assumed that there are also a number of public charging sites that are available. In North America, standards for installation, including functional and safety requirements of electric vehicle charging infrastructure, are provided in the National Electrical Code (NEC) “NEC Article 625” [2] and by the Society for Automotive Engineers (SAE) standard J1772 [3]. SAE J1772 defines the electrical rating of charging methods for conductive charger

coupler. Based on the available charging infrastructures, PEVs may be commonly charged by either Level 1 or Level 2 charging method.

Table 12.1 shows the detailed information about the different charging methods specified in North America [2], [3]. The faster charging methods are still under development. No complete standard for the faster charging or connector exists today. Table I shows two typical cases used for faster charging. For smart garage with charging and discharging abilities, level 1 and 2 will be ideal choices, since level 3 charging station will increase the power flow capacity requirement dramatically [1].

Table 12.1. Electrical ratings of different charging methods in North America

Charging method	Nominal Supply Voltage	Maximum Current	power	Typical Charge Time
AC Level 1	120 V, 1-phase	12A or 16A	< 1.92 kW Max	5-8 hours
AC Level 2	208 to 240V, 1-phase	Up to 80A	2.5 - 19.2 kW Max	1-2 hours
AC Level 3	208 to 600V, 3-phase	400A	> 20 kW	10-15 mins
DC Charging	Up to 600V	400A		10-15 mins

The IEC 61851 (International Electrotechnical Commission) standard used in Europe and China was derived from J1772 and has similar requirements, adapted for the European and Asian AC line voltages. Most terminology differences are superficial; where the SAE standard describes “methods” and “levels” the IEC standard talks about “modes” which are virtually the same. For example, like J1772 Level 1, IEC61851 Mode 1 relates to household charging from single-phase 250V (maximum) or three-phase 480V power connections, with a maximum current of 16A. (This is a little higher current than the North American limit.) There are further unique requirements for grounding. Mode 2 uses the same voltages as Mode 1, but doubles the maximum allowable current to 32A (the same as method 2 in North America). Importantly, Mode 2 adds a requirement for a “control pilot function”. Mode 3 supports fast charging with currents up to 250A. Above that, as with J1772, IEC61851 switches to an external DC supply that may supply up to 400A.

Standards SAE and IEC have defined similar but different levels for the different types of charging as explained below.

### 12.1.1. AC charge levels (defined by SAE J1772)

#### 12.1.1.1. AC level 1

Level 1 EVSE provides charging through a 120V plug and requires electrical installation per the NEC. Most, if not all, PEVs will come with a Level 1 EVSE cordset so that no additional charging equipment is required. On one end of the cord there is a standard three-prong household plug (NEMA<sup>1</sup> connector). On the other end there is a J1772 standard connector (see the Connectors and Plugs section), which plugs into the vehicle (Fig. 12.2).

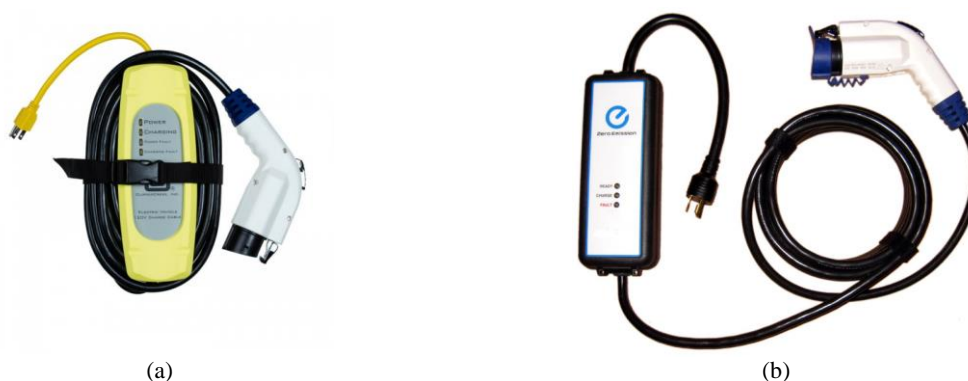


Figure 12.2. Examples of Level 1 EVSE; a) a connector for 120V, 15 amp charging (yellow), b) Improved EVSE to add a versatile Level 1 and Level 2 auto-detect charging option which works on both 120V or 208/240V. Nissan/Panasonic unit pictured, Mitsubishi unit is almost identical and Toyota unit is more compact (blue).

<sup>1</sup> National Electrical Manufacturers Association (NEMA) is the “Association of Electrical Equipment and Medical Imaging Manufacturers” in the United States. Their products are used in utility, industrial, commercial, institutional, and residential applications.

Level 1 typically is used for charging when there is only a 120V outlet available, such as at some residential locations. This is the lowest common voltage level found in both residential and commercial buildings in the United States. Level 1 charging only provides a small amount of power (maximum of up to 1.92 kW), and results in prolonged charging time. Based on the battery type and vehicle, Level 1 charging adds about 3 to 8 km of range to a PEV per hour of charging time.

### 12.1.1.2. AC Level 2

Level 2 EVSE can easily charge a typical EV battery overnight, and it will be a common installation for home, workplace, fleet, and public facilities. Level 2 EVSE offers charging through a 240V (typical in residential applications) or 208V (typical in commercial applications) electrical service. Level 2 EVSE requires installation of charging equipment and a dedicated circuit of 20 to 80A depending on the EVSE requirements (Fig. 12.3). Level 2 equipment uses the same connector on the vehicle as Level 1 equipment. Based on the battery type, charger configuration, and circuit capacity, Level 2 charging adds about 15 to 30 km of range to a PEV per hour of charging time. Since the typical charging time for a 10 kWh battery pack will be 1 to 2h, it is the primary and preferred method for the battery electric vehicle charger for both private and public facilities.

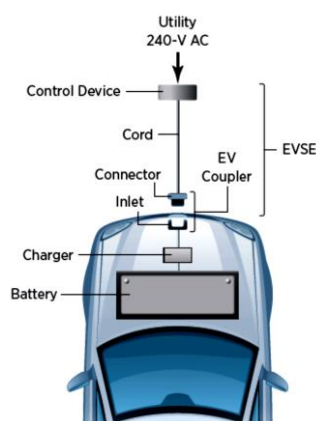


Figure 12.3. Level 2 charging schematic.

### 12.1.1.3. AC Level 3

Accepted standard has not yet been established. It will likely not be used in homes due to costs

### 12.1.2. DC fast charging

Most electric vehicles have on-board charger that uses a rectifier to convert AC current from the electrical grid to DC current suitable for recharging their batteries. Cost and thermal issues limit how much power the rectifier can handle, so beyond around 240 V and 80 Amps it is better for an external charging station to deliver direct current to the vehicle. Such high voltage high-current charging is called DC fast-charging (Fig. 12.4).

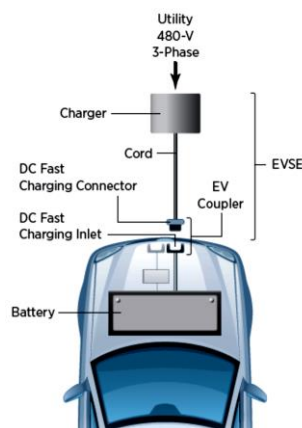


Figure 12.4. DC fast-charging schematic.

DC fast-charging EVSE (480V AC input to the EVSE) enables rapid charging at sites such as heavy traffic corridors and public fueling stations. A DC fast charger can add 90 to 130 km of range to a PEV in 20 minutes.

The Tokyo Electric Power Company (TEPCO) has developed patented technology and a specification for high-voltage (up to 500V DC) high-current (125 A) automotive fast charging via a Japan Automobile Research Institute (JARI) DC fast charge connector. It is the basis for the CHAdeMO protocol. CHAdeMO (sometimes spelled CHAdEMO) is the trade name of a quick charging method for battery electric vehicles delivering up to 62.5 kW of high-voltage direct current via a special electrical connector. It is proposed as a global industry standard by an association of the same name. CHAdeMO was formed by the TEPCO, Nissan, Mitsubishi and Fuji Heavy Industries (the manufacturer of Subaru vehicles). Toyota later joined as its fifth executive member.

Before going to the next section there are some important standards that have to be explained briefly.

### 12.1.3. IEC 60309 standard

IEC 60309 (formerly IEC 309) is an international standard from the International Electrotechnical Commission (IEC) for "plugs, socket-outlets and couplers for industrial purposes". The highest voltage allowed by the standard is 690 V DC or AC; the highest current, 125 A; and the highest frequency, 500 Hz.

#### *Color Identification:*

IEC 60309 plugs and sockets are identified by color. The national mains power around the world is almost always based on a frequency of 50 Hz or 60 Hz, so the color coding refers to the voltage as shown in table 12.2. Effectively the most widespread color codes are yellow 110 V, blue 230 V and red 400 V. The black 500 V color code can often be found on ships.

**Table 12.2. plugs color identification**

Voltage Range	Frequency Range	Color Code
20–25 V	50/60 Hz	Purple
40–50 V	50/60 Hz	White
100–130 V	50/60 Hz	Yellow
200–250 V	50/60 Hz	Blue
380–480 V	50/60 Hz	Red
500–690 V	50/60 Hz	Black

### 12.1.4. IEC 62196 standard

IEC 62196 is an international standard for set of electrical connectors and charging modes for electric vehicles and is maintained by the International Electrotechnical Commission (IEC).

### 12.1.5. IEC/EN 61851-1 standard; recharging modes

The reference standard for EV charging stations is the IEC/EN 61851-1, which envisages four charging modes:

#### 12.1.5.1. Mode 1

Mode 1 charging relates to the connection of the EV to the AC supply network utilizing standardized socket-outlets (domestic connectors) not exceeding 16 A and not exceeding 250 V AC single-phase or 480 V AC three-phase, at the supply side, and using power and protective earth conductors.

Mode 1 connectors do not require any control pins from IEC 61851-1. In many countries there are additional restrictions on household mains being less than 16 A - it is left to the system user to respect the actual charging limits. In some countries like the USA, Mode1 charging is prohibited by national codes. The main reason is that the required earthing is not present in all domestic installations so that Mode 2 was defined as an interim solution.

### 12.1.5.2. Mode 2

Mode 2 charging relates to the connection of the EV to the AC supply network not exceeding 32 A and not exceeding 250 V AC single-phase or 480 V AC three-phase using standard sockets (domestic or industrial connectors). In addition to power conductors and protective earth, these sockets add a control pilot function. An RCD<sup>1</sup> (residual-current device) is required for protection from electric shock. A control box must be in the plug or within 0.3 metres of the plug.

Mode 2 connectors require a control pin from IEC 61851-1 on the electric vehicle. The supply network side of the cable does not need a control pin and the control function is governed by the control box in the cable that is shown in Fig. 12.5b. These provisions allow for charging stations with low complexity while extending the permissible range or charging currents compared to Mode 1 charging. A 1000  $\Omega$  resistor is used between pilot and earthing allowing breaking of the circuit if the current on the pilot-earth loop is lost.

### 12.1.5.3. Mode 3

Mode 3 charging relates connection of the EV to the AC supply network utilizing dedicated EVSE where the control pilot function extends to control equipment in the EVSE, permanently connected to the AC supply as shown in Fig. 12.5c. Mode 3 connectors according to IEC 61851-1 require a range of control and signal pins for both sides of the cable. The charging station socket is dead if no vehicle is present; the pilot pin in the plug on the charger side controls the circuit breaker. For compatibility, the 32 A plugs of IEC 61851-1 Mode 2 connectors (1000  $\Omega$  pilot-earth) may be used, while fast charging with higher currents up to 250 A requires specialized cables satisfying the IEC 61851-1 charging mode. The communication wire between car electronics and charging station allows for integration into smart grid scenarios.

### 12.1.5.4. Mode 4

Mode 4 charging relates to the connection of the EV to the AC supply network utilizing an off-board charger where the control pilot function extends to equipment permanently connected to the AC supply for instance charging station.

In Mode 4 charging the supply network AC power is converted in the charging station to DC. The plug type ensures that only a matching electric vehicle can be connected. Using DC fast charging allows for considerably higher currents, up to 400 A according to IEC 61851-1 Mode 4. Mode 4 connectors according to IEC 61851-1 require a range of control and signal pins to ensure operation for fast charging comparable to Mode 3. The Mode 4 charging station equipment are however much more expensive than Mode 3 EVSE.



Figure 12.5. IEC 61851-1 four charging modes; a) Mode 1, b) Mode 2, c) Mode 3, and d) Mode 4

### 12.1.5.5. Control pilot

As mentioned, the IEC 61851 standard foresees additional protection measures to be provided by so-called control pilot, a device which has the following functions mandated by the standard:

<sup>1</sup> A residual-current device (RCD), or residual-current circuit breaker (RCCB), is an electrical wiring device that disconnects a circuit whenever it detects that the electric current is not balanced between the energized conductor and the return neutral conductor. Such an imbalance may indicate current leakage through the body of a person who is grounded and accidentally touches the energized part of the circuit.

- Verification that the vehicle is properly connected
- Continues verification of the protective earth conductor integrity
- Energization and deenergization of the system
- Selection of the charging rate

An example of control pilot circuit is given in Fig. 12.6 showing the operation of the system. A small current is sent through the control pilot conductor, which is connected to the vehicle body by a resistor. The current returns to the charging station through the earth conductor. When the pilot current flows correctly, the contactor in the charging station is closed and the system is energized.

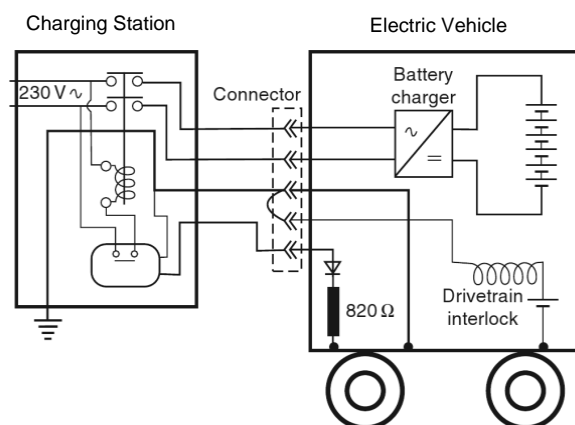


Figure 12.6. Example of control pilot circuit

## 12.2. Connectors and Plugs

Generally there are four plug types:

**Type 1.** The Yazaki connector introduced by Yazaki mainly for North America and Japan (standardized in SAE J1772).

**Type 2.** Mennekes connector introduced by Mennekes in Europe and developed in collaboration with the main German car manufacturers (standardized in VDE-AR-E 2623-2-2).

**Type 3.** EV Plug Alliance introduced by Scame in collaboration with Schneider and Legrand.

**Type 4.** Type 4- The CHAdeMO connector in Japan (using DC charging fast charge).

### 12.2.1. Type 1 (SAE J1772)

In 2001 SAE had proposed a standard for conductive connector which had been approved by the California Air Resources Board for charging stations of electric vehicles. The SAE J1772-2001 plug had a rectangular shape. In 2009 a revision of the SAE J1772 standard was published that included a new design by Yazaki featuring a round housing, being suitable to the North American and Japanese markets. The SAE J1772-2009 connector specifications have been included to IEC 62196-2 standard as an implementation of the Type 1 connector for charging with single-phase AC. As shown in Fig. 12.7 the connector has five pins:



Figure 12.7. SAE J1772 – 2009 plug (Type 1) and its circuit diagram.

- Two pins for AC Line 1 and AC Line 2 (have same size power pins)
- Ground pin
- Two signal pins for proximity detection and control pilot function (have same size pin)  
Proximity detection: Prevents movement of the car while connected to the charger.  
Control pilot: Communication line used to coordinate charging level between the car and the charger as well as other information.

As shown in Fig. 12.8 the J1772 has two charging plugs incorporated into a single design. It's based on the 2009 J1772, which had only an AC charging plug. The current version includes a DC plug underneath the AC plug, which means that not only both options are available, but cars with the older J1772 couplings, such as the 2012 Nissan Leaf and 2013 Chevrolet Volt, can still use the new plug.

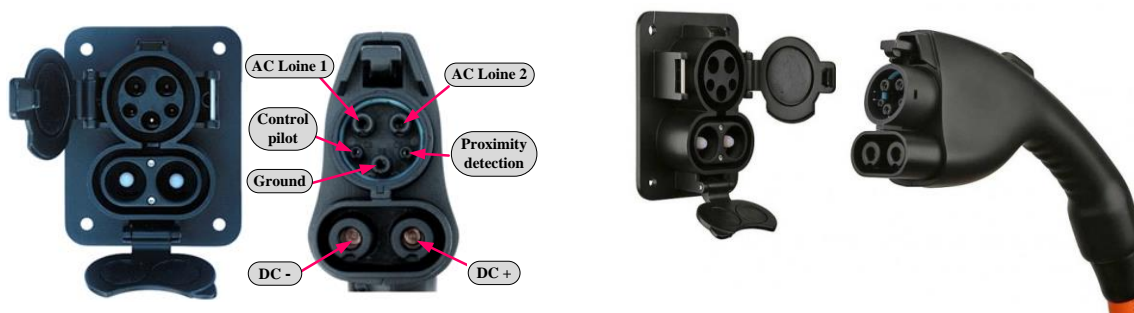


Figure 12.8. The SAE J1772 AC and DC "Combo" plug and receptor

### 12.2.2. Type 2 (Mennekes connector)

Recently, the largest European energy supply companies and vehicle manufacturers agreed on the basic parameters for the charging connection for electric cars. Basis for this agreement is a standard draft developed by Mennekes<sup>1</sup>. Mennekes approaches this topic in an integrated fashion and can cover all sectors ranging from the vehicle socket and the charging cable with plugs up to the charging stations (Fig. 12.9).



Figure 12.9. Vehicle with plug, socket and charging stations

Although being a well known producer in the industrial sector for decades, the Mennekes company became better known to general public for their compliant electric vehicle car recharging connector developed by Mennekes. Mennekes had a background in the design of charging couplers based on the IEC 60309 standard. During the initial presentations in 2009 the new connector had been referenced after its creator and only manufacturer as the "Mennekes design" plug. The actual

<sup>1</sup> Mennekes is a leading manufacturer of industrial plugs and connectors with headquarters in Kirchhundem/Sauerland, Germany.



specification was published formally by VDE in the VDE-AR-E 2623-2-2 publication. Two years later the specification was taken over by the international IEC 62196 as “Type 2” connector but the original nickname is kept in informal conversations. As the term Mennekes connector is ambiguous, Mennekes itself uses the term in press coverage along with a clarification as “Type 2”

With the introduction of the first electric cars in the UK, they were initially able to connect to the electricity grid with using a 3-pin domestic socket or a “Type 1” connection as it was developed in the USA as SAE J1772. The ACEA (organisation of European automobile makers) however settled on the “Type 2” connector that allows access to the three-phase power grid. Many charging point manufacturers are beginning to include a “Type 2 Mode 3” (Mennekes type) socket in addition to a domestic 3-pin socket on their products.

The tasks of the charging plugs are much more complex in this context than one would think at first glance, as they have to cover a large variety of functions. Mennekes managed to develop a charging connector that meets these demands. This connector is no larger than a common 16A plug and suited for both single-phase 230V connection as well as three-phase 400V connection up to a charging current of 63A.

This charging technology also features the required communication interfaces between the charging station and the vehicle. A “proximity” contact for example ensures the activation of the immobiliser and a “control pilot” contact enables communication, meaning data exchange.

In addition, the company is working on system solutions for charging stations in the commercial and the public sector. Demand-conform charging capacities with different charging currents are offered depending on the application field. Time-saving charging stations with charging currents of up to 63A will be available for the commercial and public sector, e.g. on parking places and in parking garages, which reduce the charging times to less than 10 percent compared to charging at home. For the domestic sector, solutions will be developed that allow the recharging of electric cars via common 230V household outlets with earthing contact.

The safety of the charging technology takes top priority. For example, the plugs have to be latched during charging, so that they cannot be pulled out arbitrarily or unintentionally during the charging process. In addition, the vehicle and the charging station must be able to communicate with each other via the charging technology to exchange data (Fig 12.10a). For this purpose, the charging cable developed by Mennekes for the connection between the vehicle socket and the charging station has identical plugs at each end with protection against accidental contact so that the user does not have to wonder which end to plug in and where (Fig 12.10b).



Figure 12.10. Mennekes connector (Type 2); a) plug with lettering b) charging cable

### 12.2.3. Type 3 (EV Plug Alliance)

The EV Plug Alliance was formed on March 28, 2010 by electrical companies in France (Schneider Electric, Legrand) and Italy (Scame). Within the IEC 62196 framework they propose an automotive plug derived from the earlier Scame plugs (the Libera series) that are already in use for light electric vehicles. Gimélec joined the Alliance on May 10 and a number of more companies joined on May 31: Gewiss, Marechal Electric, Radiall, Vimar, Weidmüller France & Yazaki Europe. As of early July 2010 the Alliance has completed the test of products from several partners and the plug and socket-outlet system are made available on the market. The new connector is able to provide three-phase

charging up to 32 A. Limiting the plug to 32 A allows for cheaper plugs and installation costs. Three versions have been developed for type 3:

- Three-phase 500VAC 32A + 2 pilot contacts (in process of being developed and ideal for motor vehicles).
- Single-phase 250VAC 32A + 2 pilot contacts (in process of being developed and ideal for light vehicles).
- Single-phase 250VAC 16A + 1 pilot contact (present version, standardized to safeguard sales).

### 12.2.3.1. Type 3A:

Type 3A connectors were developed in Italy (Scame) in 2000 as the only connection system used to charge electrical vehicles in public areas in Mode 3. Due its small size, it is the preferred connector for small vehicles, such as scooters and motorcycles, with power below 3kW. Thanks to the adaptors, the 3A plug can also be used for charging in environments closed to third parties, such as private garages, using Mode 1 (Fig. 12.11).



Figure 12.11. Type 3A connectors; a) Mode 1: charging in domestic environment (closed to third parties), b) Mode 3: charging in public areas (open to third parties)

### 12.2.3.2. Type 3C

The Type 3C connector is the connection system intended for electric vehicles with rating above 3kW, such as automobiles, promoted by the EV Plug Alliance, an association founded by Scame - Schneider - Legrand, as a single European solution on the infrastructure side (Fig. 12.12). Derived from the Type 3A connector, it has the same protection characteristics against indirect contacts and the additional pole used to verify continuity of the protective conductor. The evolution consists in the possibility to wire in both single-phase and three-phase, in the increased nominal current, and in the introduction of shutters on the plug side (a necessary requirement in case of “Smart Grid”).



Figure 12.12. Type 3C connectors

The connecting solution proposed by EV Plug Alliance allows the installation of recharging infrastructures up to 22 kW equipped with plugs and sockets preventing any accidental contact with live parts. Schneider Electric emphasizes that the “EV Plug” uses shutters over the socket side pins which is required in 12 European countries and that none of the other proposed EV charger plugs (Fig. 12.13). The shutters, imposed by regulations in many European countries, guarantee totally safe usage at home as well as in public areas.

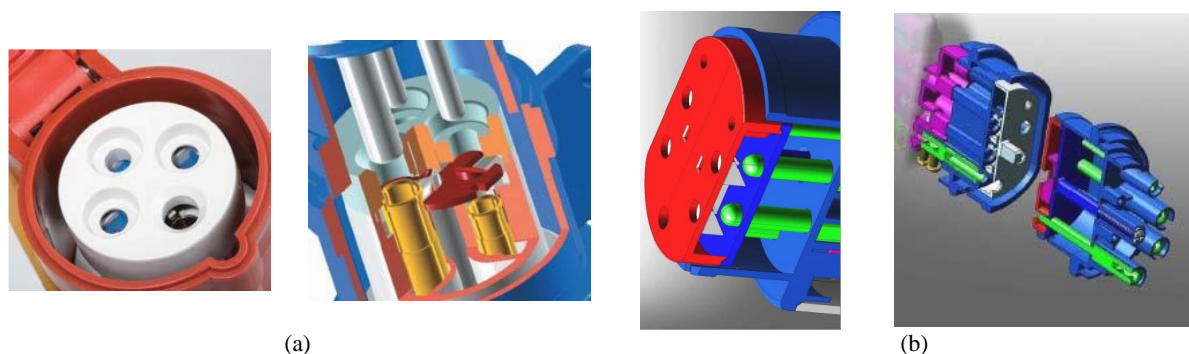





Figure 12.13. EV Plug Alliance; a) Type 3A, Socket with shutter for light vehicles single-phase, 1 pilot contact , b) Type 3C, Plug with shutter for all vehicles single/three-phase, 2 pilot contacts.

The EV Plug Alliance points out that the future IEC 62196 specification will have an annex categorizing electric vehicle charger plugs into three types (Yazaki's proposal is type 1, Mennekes' proposal is type 2, Scame's proposal is type 3) and that instead of having a single plug type at both ends of a charger cable one should choose the best type for each side; The EV Plug (Scame) would be the best option for the charger side / wall box, leaving the choice for the car side open.

Regarding previous subsections, table 12.3 shows the different features of these three types above mentioned connectors.

Table 12.3. Features of three types connectors

Characteristics	Type 1 (SAE J1772)	Type 2 (Mennekes)	Type 3C (EV Plug Alliance)
No. of phases	Single phase	Single phase Three phase	Single phase Three phase
Current	32 A	63 A	32 A
Voltage	250 V	500 V	500 V
No. of pins	5	7	7
Shutters	no	no	Yes
Socket			

#### 12.2.4. Type 4 (CHAdeMO)

CHAdeMO charging system is included in the drafts of international standard at IEC 61851 for charging system and IEC 62196 for connector.

CHAdeMO has mandated the following safety principles to guarantee its safe operation [4].

- Communication is duplicated through the exclusive pilot signals and the data signals via CAN communication. These two communication routes can prevent false operation by defining action by AND condition, and stop order by OR condition.
- The interlocking hardware is structured so that the coupler is never disconnected from the inlet while charging, and no active electricity comes to the exposed terminal parts when disconnected.

- Electricity leakage is prevented through its unique electrical circuit design and the insulation checking procedure. Even if it does ever occur, the impact is limited within the human safety range.

CHAdeMO is featuring connecting devices, consisting of a connector on the charger side and an inlet on the vehicle side. CHAdeMO compatible vehicles utilize Type 1 or Type 2 connector (IEC 62196) for AC normal charging, depending on the local standards.

#### 12.2.4.1. Interlock of connector

- No voltage applied without a vehicle coupler being connected. Control power is supplied to EV contactors via a charger, EV contactors never close and there must be zero voltage unless a vehicle coupler is connected to the vehicle.
- Pre-charge Automatic Safety Check; an insulation test is conducted before charging every time. The circuit insulation and the short circuit between the charger and EV contactors are checked.
- Never release the lock during charging; during charging, the vehicle coupler is locked to the vehicle inlet via a mechanical latch, and the mechanical latch is locked by an electrical lock. Once charging is completed, an electric lock is released after confirming the voltage on a vehicle connector. It is not allowed to release the lock automatically in case the inlet voltage does not drop to a safe level.

#### 12.2.4.2. Protection from electrical shock

- Separation of the power system and battery system via an isolation transformer:  
The isolation transformer inside the charger separates the AC system at the input side and the DC system at the output side, therefore, the output side is a non-earthed system. So the electric shock can be avoided if an earth leakage fault occurs on one of the DC lines.
- Electrical shock protection using a leakage current monitoring device:  
A leakage current monitoring device is installed at the DC side as well as the AC side and it shuts down input power to the charger as soon as leakage current is detected. The electrical shock protection in the DC-2 zone stipulated under IEC60479-1 was realized by combining the leakage current monitoring and immediate automatic disconnection [4].

#### 12.2.4.3. Fail-safe of charging control

- Redundancy of the stop charging:  
The vehicle and charger monitor malfunction during the charging. In addition to this redundant monitoring, two communication lines (CAN signal and Pilot signal) from the vehicle to the charger are prepared to send a signal in case there is a malfunction detected at the vehicle side. This way, charging can be stopped even if one communication line is broken.
- Protection in case the grounding wire and pilot line is disconnected:  
When the vehicle coupler is dropped out, the disconnection of the grounding wire and the pilot wire causes each Pilot signal to turn OFF, which puts a halt to the DC output immediately. So the electrical arcing never continues.

Pins on the CHAdeMO connector are (Fig. 12.14):

- Two Power pins (6, 5)
- Seven control/ communication pins:
  - Two communication pins usually CANbus (8, 9)
  - Two pins for EV relay control (2, 10)
  - One reference Ground for vehicle isolation monitor (1)
  - One proximity or mating detection pin (7)
  - One “ready to charge” pin (4)



Figure 12.14. CHAdeMO pin layout and circuit diagram

Most modern EVSE and PEVs have a standard connector and receptacle based on the SAE J1772 standard. Any vehicle with this receptacle can use any Level 1 or Level 2 EVSE. All major vehicle and charging system manufacturers support this standard, which should eliminate drivers concerns about whether their vehicles are compatible with available charging infrastructure. Most currently available PEVs that are equipped to accept DC fast charging are using the CHAdeMO connector, which is not standard in the United States. As shown in Fig. 12.15 manufacturers may offer the CHAdeMO DC fast charge receptacle (beside the SAE J1772) as an option on fast-charge capable vehicles until a standard is in place. As already mentioned SAE is working on a “hybrid connector” standard for fast charging that adds high-voltage DC power contact pins to the J1772 connector, enabling use of the same receptacle for all levels of charging.



Figure 12.15. The standard J1772 receptacle (right) can receive charge from Level 1 or Level 2 equipment. The CHAdeMO DC fast charge receptacle (left) uses a different type of connector.

## References

- [1] C. Pang, P. Dutta, and M. Kezunovic, “BEVs/PHEVs as Dispersed Energy Storage for V2B Uses in the Smart Grid”, *IEEE Transactions On Smart Grid*, vol. 3, no. 1, March 2012
- [2] M.W. Earley, J. S. Sargent, J. V. Sheehan, and E.W. Buss, *National Electrical Code (NEC) Handbook*, 2008 ed. Quincy, MA: National Fire Protection Association, 2008.
- [3] *SAE Recommended Practice for Electric Vehicle and Plug in Hybrid Electric Vehicle Conductive Charger Coupler*, SAE Standard J1772, Jan. 2010.
- [4] CHAdeMO, Technical Specifications of Quick Charger for the Electric Vehicle, Rev. 0.9.

## Glossary:

SAE	Society for Automotive Engineers
NEC	National Electrical Code
IEC	International Electrotechnical Commission
EVSE	Electric Vehicle Supply Equipment
NEMA	National Electrical Manufacturers Association
JARI	Japan Automobile Research Institute
TEPC	Tokyo Electric Power Company
CHAdeMO	CHArge de MOve

## Appendix A:

### Ideal model of the diode rectifier with DC-side inductance

The idealized model of three-phase diode rectifier with infinite DC-side inductor is presented in Fig. A.1(a).

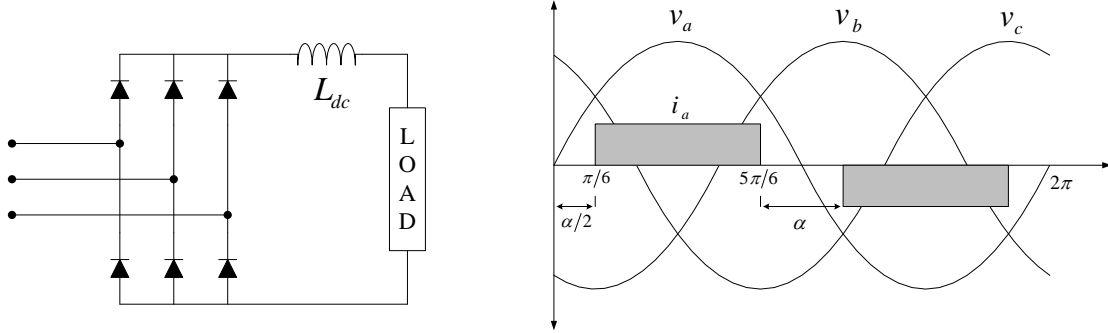


Figure A.1. Ideal three phase rectifier with infinite DC-side inductor  $L_{dc}$  and no grid impedance (a), Voltages and currents of idealized three phase rectifier (b).

The idealized rectifier current is assumed to be smooth on the DC-side (infinite  $L_{dc}$ ) and, for neglected commutation effects ( $L_S = 0$ ), occurs an ideal square. As shown on Fig. A.1b the current changes instantaneously from zero to a finite value. Every phase is conducting only during  $2/3$  of the period. The input diode rectifier current can be described in following form:

$$i_{sa}(t) = \begin{cases} 0 & -\pi < \omega t < -\frac{5}{6}\pi \\ -I_0 & -\frac{5}{6}\pi < \omega t < -\frac{1}{6}\pi \\ 0 & -\frac{1}{6}\pi < \omega t < \frac{1}{6}\pi \\ I_0 & \frac{1}{6}\pi < \omega t < \frac{5}{6}\pi \\ 0 & \frac{5}{6}\pi < \omega t < \pi \end{cases} \quad (\text{A.1})$$

The idealized input current can also be expressed by Fourier series as ( $\alpha$  is considered for the representation of any rectangle waveform by Fourier series.):

$$i_{sa}(t) = \frac{4}{\pi} I_0 \sum_{h=1,3,5,\dots} \sin\left(h\left(\frac{\pi-\alpha}{2}\right)\right) \cdot \frac{1}{h} \sin h\omega t$$

$$i_{sa}(t) = \frac{\sqrt{3}}{2} \frac{4I_0}{\pi} \left( \sin \omega t - \frac{1}{5} \sin 5\omega t + \frac{1}{7} \sin 7\omega t - \frac{1}{11} \sin 11\omega t + \frac{1}{13} \sin 13\omega t - \dots \right) \quad (\text{A.2})$$

As shown in Fig. A.1(b) angle  $\alpha$  is  $\pi/3$  for an ideal diode rectifier. There is no triple harmonics, because considered three-phase system operates without neutral wire. The idealized three-phase diode rectifier has THD=31.1%. Equations (A.2) can be used to determine the order and magnitude of the harmonic currents drawn by a six pulse diode rectifier:

$$h = 6k \pm 1 \quad k = 1, 2, 3 \dots$$

$$\frac{I_h}{I_1} = 1/h \quad (\text{A.3})$$

where  $I_1$  is the fundamental magnitude of current.

Thus, the higher harmonic orders are: 5th, 7th, 11th, 13th etc., with a 50 Hz fundamental frequency, that corresponds to 250, 350, 550 and 650 Hz, respectively. The per unit magnitude of the harmonics of the fundamental is the reciprocal of the harmonic order: 20% for the 5th, 14.3% for the 7th, etc. Eq. (A.1)-(A.2) are calculated from the Fourier series for ideal square wave current (critical assumption for infinite inductance on the input of the converter). Equation (A.2) is fairly good description of the harmonic orders generally encountered. The magnitude of actual harmonic currents often differs from the relationship described in (A.2).